ANL-19/27 Vol.1
ISSN 1931-5007
December 2019

APS Science 2019 Volume 1

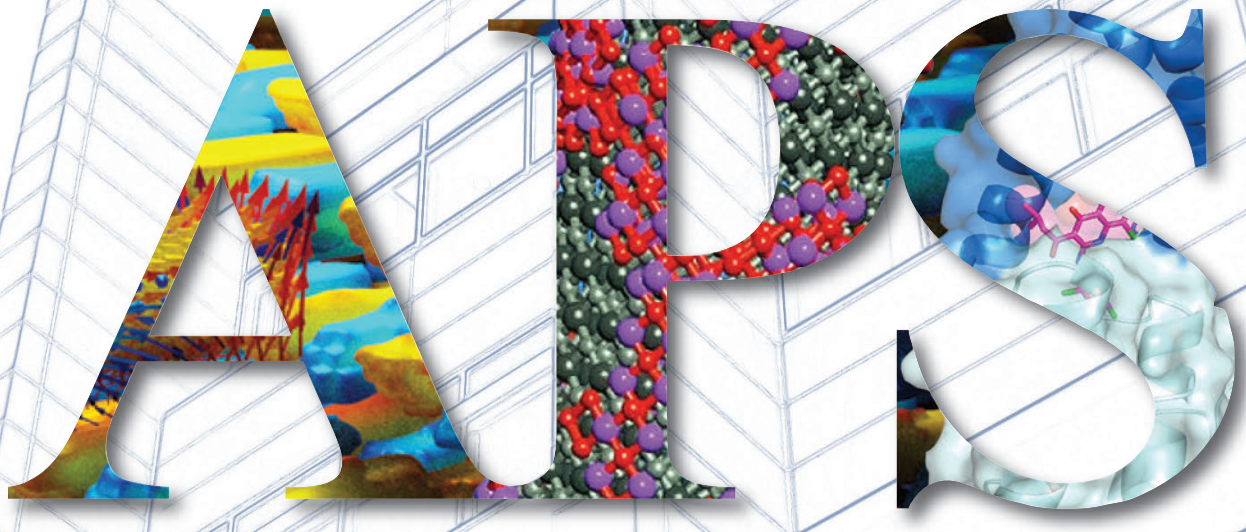

Research and engineering highlights from the Advanced Photon Source at Argonne National Laboratory

Argonne NATIONAL LABORATORY

APS SCIENCE 2019 Volume 1 • December 2019 ANL-19/27 Vol. 1 • Argonne National Laboratory

ANL-19/27 Vol.1 • SSN 1931-5007 • December 2019

About Argonne National Laboratory
Argonne is a U.S. Department of Energy laboratory managed by UChicago Argonne, LLC under contract DE-AC02-06CH11357. The Laboratory's main facility is outside Chicago, at 9700 South Cass Avenue, Lemont, Illinois 60439. For information about Argonne and its pioneering science and technology programs, see www.anl.gov.

DOCUMENT AVAILABILITY
Online Access: U.S. Department of Energy (DOE) reports produced after 1991 and a growing number of pre-1991 documents are available free at OSTI.GOV (http://www.osti.gov/), a service of the US Dept. of Energy's Office of Scientific and Technical Information.

Reports not in digital format may be purchased by the public from the National Technical Information Service (NTIS):U.S. Department of Commerce National Technical Information Service
5301 Shawnee Rd
Alexandria, VA 22312
www.ntis.gov
Phone: (800) 553-NTIS (6847) or (703) 605-6000
Fax: (703) 605-6900
Email: orders@ntis.gov

Reports not in digital format are available to DOE and DOE contractors from the Office of Scientific and Technical Information (OSTI):
U.S. Department of Energy
Office of Scientific and Technical Information
P.O. Box 62
Oak Ridge, TN 37831-0062
www.osti.gov
Phone: (865) 576-8401
Fax: (865) 576-5728
Email: reports@osti.gov

On the cover: Background: the APS central lab/office building.

ANL-19/27 Vol. 1
ISSN 1931-5007
December 2019

APS Science 2019 Volume 1

Research and engineering highlights from the Advanced Photon Source at Argonne National Laboratory

Argonne is a U.S. Department of Energy (DOE) laboratory managed by UChicago Argonne, LLC.
The Advanced Photon Source is a DOE Office of Science user facility
operated for the DOE Office of Science by Argonne National Laboratory under Contract No. DE-AC02-06CH11357.

Table of Contents

Access to Beam Time at the Advanced Photon Source

Five types of beam-time proposals are available at the APS: general user, partner or project user, collaborative access team (CAT) member, CAT staff, and APS staff. All beam time at the APS must be requested each cycle through the web-based Beam Time Request System. Each beam-time request (BTR) must be associated with one of the proposals mentioned above.

GENERAL-USER PROPOSALS AND BTRS Proposals are peer reviewed and scored by a General User Proposal Review Panel, and time is allocated on the basis of scores and feasibility. A new BTR must be submitted each cycle; each cycle, allocation is competitive. Proposals expire in two years or when the number of shifts recommended in the peer review has been utilized, whichever comes first.

PARTNER- OR PROJECT-USER PROPOSALS AND BTRS Proposals are peer reviewed by a General User Proposal Review Panel and reviewed further by a subcommittee of the APS Scientific Advisory Committee and by APS senior management. Although a new BTR must be submitted each cycle, a specific amount of beam time is guaranteed for up to three years.

CAT-MEMBER PROPOSALS from CAT members are typically much shorter and are reviewed by processes developed by individual CATs. Allocation/scheduling is determined by each CAT's management.

CAT AND APS STAFF-MEMBER PROPOSALS AND BTRS These proposals are also very short and are reviewed through processes developed by either the CAT or the APS. Each CAT/beamline determines how beam time is allocated/scheduled. Collaborative access team and/or APS staff may submit general-user proposals, in which case the rules for general-user proposals and BTRs are followed.

In addition to the above, the APS has developed an industrial measurement access mode (MAM) program to provide a way for industrial users to gain rapid access for one-time measurements to investigate specific problems. A MAM proposal expires after one visit. The APS User Information page (www.aps.anl.gov/Users-Information) provides access to comprehensive information for prospective and current APS users.

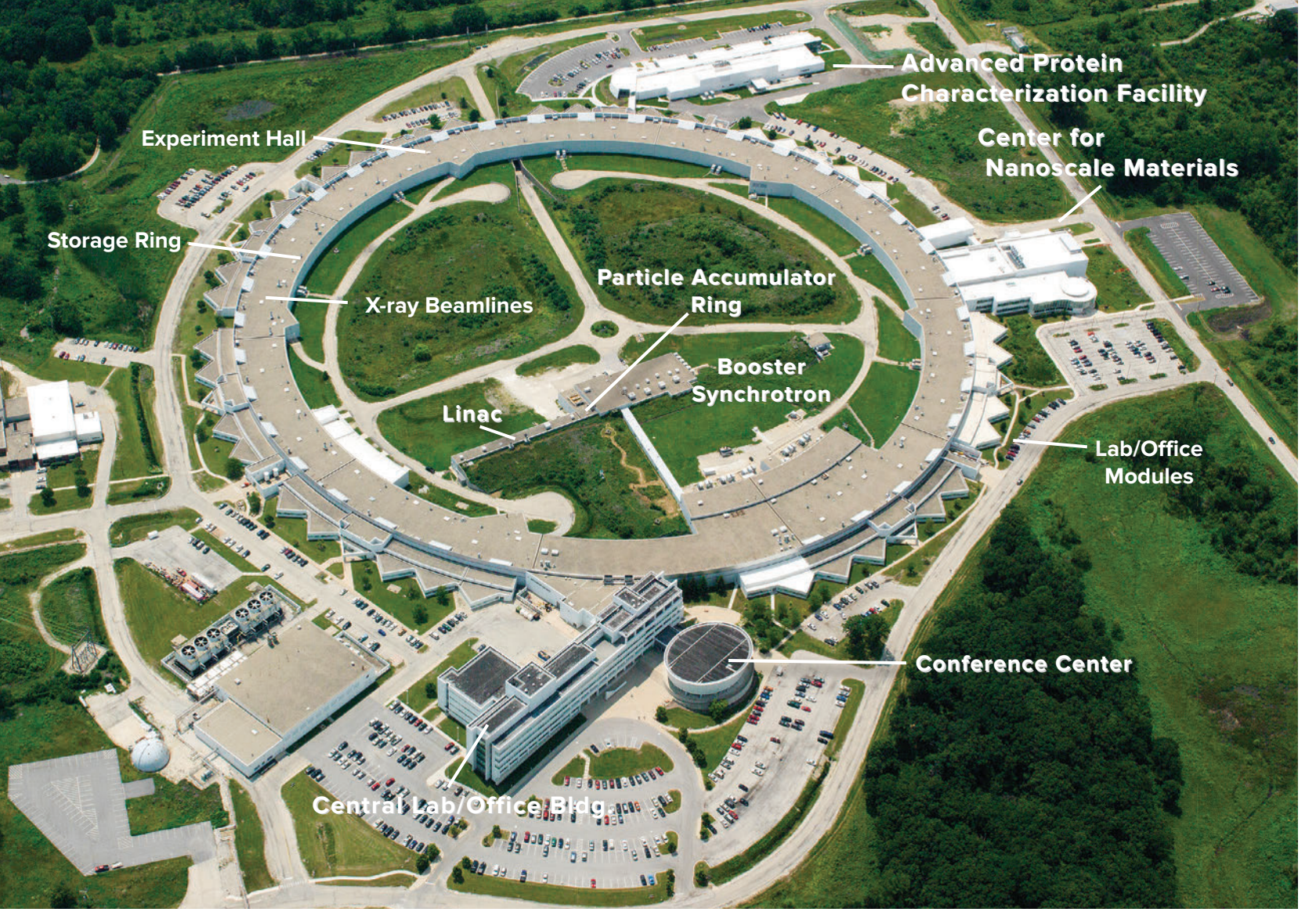

The Advanced Photon Source Facility at Argonne National Laboratory

The APS, a national synchrotron radiation research facility operated by UChicago Argonne, LLC, and Argonne National Laboratory for the U.S. Department of Energy (DOE) Office of Science-Basic Energy Sciences, Scientific User Facilities Division, provides this nation's brightest high-energy x-ray beams for science. Research by APS users extends from the center of the Earth to outer space, from new information on batteries, combustion engines and microcircuits, to new and improved pharmaceuticals, and nanotechnologies whose scale is measured in billionths of a meter. The APS helps researchers illuminate answers to the challenges of our high-tech world, from developing new forms of energy to sustaining our nation's technological and economic competitiveness to pushing back against the ravages of disease. Research at the APS promises to have far-reaching impact on our technology, our economy, our health, and fundamental knowledge of the materials that make up our world.

The APS occupies an 80-acre site on the Argonne campus, about 25 miles from downtown Chicago, Illinois. It shares a site with the Center for Nanoscale Materials and the Advanced Protein Characterization Facility.

For directions to Argonne, see https://www.anl.gov/visiting-argonne.

Contact us

For more information about the APS send an email to apsinfo@aps.anl.gov or write to APS Info, Bldg. 401, Rm. A4113, Argonne National Laboratory, 9700 S. Cass Ave., Lemont, IL 60439.

To order additional copies of this, or previous, issues of *APS Science* send email to apsinfo@aps.anl.gov.

To download PDF versions of *APS Science* back issues go to www.aps.anl.gov/Science/APS-Science

Visit the APS on the Web at www.aps.anl.gov

ARGONNE NATIONAL LABORATORY 400-AREA FACILITIES

ADVANCED PHOTON SOURCE

(Beamlines, Disciplines, and Source Configuration)

ADVANCED PROTEIN CHARACTERIZATION FACILITY

CENTER FOR NANOSCALE MATERIALS

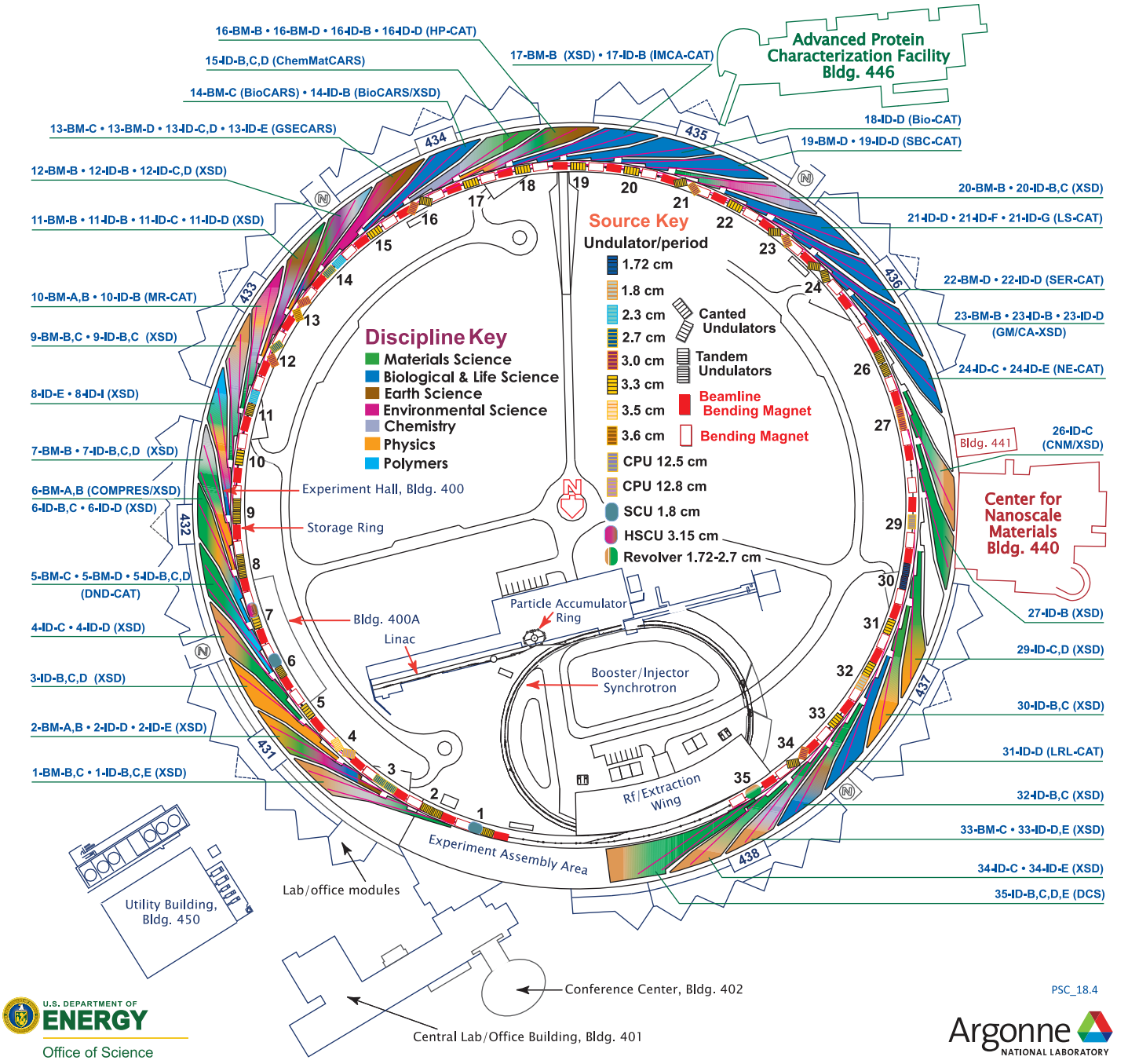

U.S. DEPARTMENT OF ENERGY
Office of Science

Argonne NATIONAL LABORATORY

APS sectors: At the APS, a "sector" comprises the radiation sources (one bending magnet and nominally one insertion device, although the number of insertion devices in the straight sections of the storage ring can vary) and the beamlines, enclosures, and instrumentation that are associated with a particular storage ring sector. The APS has 35 sectors dedicated to user science and experimental apparatus. X-ray Science Division (XSD) sectors comprise those beamlines operated by the APS. Collaborative access team (CAT) sectors comprise beamlines operated by independent groups made up of scientists from universities, industry, and/or research laboratories both federal and private.

APS Beamlines

Key: Beamline designation • Sector operator • Disciplines • Techniques • Radiation source energy • User access mode(s) • General-user status

1-BM-B,C • **X-ray Science Division (XSD)** • Materials science, physics • Optics testing, detector testing, topography, energy dispersive x-ray diffraction, white Laue single-crystal diffraction • 6-30 keV, 50-120 keV • On-site • Accepting general users

1-ID-B,C,E • XSD • Materials science, physics, chemistry • High-energy x-ray diffraction, tomography, small-angle x-ray scattering, fluorescence spectroscopy, pair distribution function, phase contrast imaging • 41-136 keV, 45-116 keV • On-site • Accepting general users

2-BM-A,B • XSD • Physics, life sciences, geoscience, materials science • Tomography, phase contrast imaging • 10-170 keV, 11-35 keV • On-site • Accepting general users

2-ID-D • XSD • Life sciences, materials science, environmental science • Microfluorescence (hard x-ray), micro x-ray absorption fine structure, nanoimaging, ptychography • 5-30 keV • On-site • Accepting general users

2-ID-E • XSD • Life sciences, environmental science, materials science • microfluorescence (hard x-ray), tomography • 7-10.5 keV, 11-17 keV • On-site • Accepting general users

3-ID-B,C,D • XSD • Physics, geoscience, life sciences, chemistry, materials science • Nuclear resonant scattering, inelastic x-ray scattering, high-pressure diamond anvil cell • 7-27 keV, 14.41-14.42 keV • On-site • Accepting general users

4-ID-C • XSD • Physics, materials science • Magnetic circular dichroism (soft x-ray), x-ray magnetic linear dichroism, x-ray photoemission spectroscopy, x-ray photoemission electron microscopy, anomalous and resonant scattering (soft x-ray) • 500-2800 eV • On-site • Accepting general users

4-ID-D • XSD • Physics, materials science • Anomalous and resonant scattering (hard x-ray), magnetic x-ray scattering, magnetic circular dichroism (hard x-ray) • 2.7-40 keV • On-site • Accepting general users

4-ID-E • XSD • Materials science, physics • Synchrotron x-ray scanning tunneling microscopy • 500-1800 eV • On-site • Accepting general users

5-BM-C • **DuPont-Northwestern-Dow Collaborative Access Team (DND-CAT)** • Materials science, polymer science • Powder diffraction, tomography, wide-angle x-ray scattering • 10-42 keV • On-site • Accepting general users

5-BM-D • DND-CAT • Materials science, polymer science, chemistry • X-ray absorption fine structure, high-energy x-ray diffraction, general diffraction • 4.5-25 keV, 4.5-80 keV • On-site • Accepting general users

5-ID-B,C,D • DND-CAT • Materials science, polymer science, chemistry • Powder diffraction, x-ray standing waves, x-ray optics development/techniques, small-angle x-ray scattering, surface diffraction, x-ray reflectivity, wide-angle x-ray scattering • 6-17.5 keV • On-site • Accepting general users

6-BM-A,B • **COMPRES/XSD** • Materials science, geoscience • Energy dispersive x-ray diffraction, high-pressure multi-anvil press • 20-200 keV • On-site • Accepting general users

6-ID-B,C • XSD • Physics, materials science • Magnetic x-ray scattering, anomalous and resonant scattering (hard x-ray), general diffraction, grazing incidence diffraction • 3.2-38 keV • On-site • Accepting general users

6-ID-D • XSD • Physics, materials science • Magnetic x-ray scattering, high-energy x-ray diffraction, powder diffraction, pair distribution function • 50-100 keV, 70-130 keV • On-site • Accepting general users

7-BM-B • XSD • Physics • Radiography, tomography, microfluorescence (hard x-ray) • 5-150 keV, 6-15 keV, 25-55 keV • On-site • Accepting general users

7-ID-B,C,D • XSD • Materials science, atomic physics, chemistry • Time-resolved x-ray scattering, time-resolved x-ray absorption fine structure, phase contrast imaging • 18 keV, 12-26 keV • On-site • Accepting general users

8-ID-E • XSD • Materials science, polymer science, physics • Grazing incidence small-angle scattering, x-ray photon correlation spectroscopy • 7.35-7.35 keV, 11-11 keV • On-site • Accepting general users

8-ID-I • XSD • Polymer science, materials science, physics • X-ray photon correlation spectroscopy, intensity fluctuation spectroscopy, small-angle x-ray scattering • 6-12.5 keV, 10.9-10.9 keV • On-site • Accepting general users

9-BM-B,C • XSD • Materials science, chemistry, environmental science • X-ray absorption fine structure, x-ray absorption near-edge structure • 2.1-25.2 keV • On-site • Accepting general users

9-ID-B,C • XSD • Chemistry, materials science, life sciences • Nano-imaging, microfluorescence (hard x-ray), coherent x-ray scattering (hard x-ray), ultra-small-angle x-ray scattering • 4.5-30 keV • On-site • Accepting general users

10-BM-A,B • **Materials Research (MR)-CAT** • Materials science, chemistry, environmental science, physics • X-ray absorption fine structure • 4-32 keV • On-site • Accepting general users

10-ID-B • MR-CAT • Materials science, environmental science, chemistry • X-ray absorption fine structure, time-resolved x-ray absorption fine structure, microfluorescence (hard x-ray) • 4.3-27 keV, 4.8-32 keV, 15-65 keV • On-site • Accepting general users

11-BM-B • XSD • Chemistry, materials science, physics • Powder diffraction • 22-33 keV • On-site, mail-in • Accepting general users

11-ID-B • XSD • Chemistry, environmental science, materials science • Pair distribution function, high-energy x-ray diffraction • 58.66 keV, 86.7 keV • On-site • Accepting general users

11-ID-C • XSD • Materials science, chemistry, physics • High-energy x-ray diffraction, diffuse x-ray scattering, pair distribution function • 105.6 keV • On-site • Accepting general users

11-ID-D • XSD • Chemistry, environmental science, materials science • Time-resolved x-ray absorption fine structure, time-resolved x-ray scattering • 6-25 keV • On-site • Accepting general users

12-BM-B • XSD • Materials science, polymer science, chemistry, physics, environmental science • X-ray absorption fine structure, small-angle x-ray scattering, wide-angle x-ray scattering • 4.5-30 keV, 10-40 keV • On-site • Accepting general users

12-ID-B • XSD • Chemistry, materials science, life sciences, polymer science, physics • Small-angle x-ray scattering, grazing incidence small-angle scattering, wide-angle x-ray scattering, grazing incidence diffraction • 7.9-14 keV • On-site • Accepting general users

12-ID-C,D • XSD • Chemistry, physics, materials science • Small-angle x-ray scattering, grazing incidence small-angle scattering, wide-angle x-ray scattering, surface diffraction • 4.5-40 keV • On-site • Accepting general users

13-BM-C • **GeoSoilEnviro Center for Advanced Radiation Sources (GSECARS)** • Geoscience, environmental science • Surface diffraction, high-pressure diamond anvil cell, single-crystal diffraction • 15-15 keV, 28.6-28.6 keV • On-site • Accepting general users

13-BM-D • GSECARS • Geoscience, environmental science • Tomography, high-pressure diamond anvil cell, high-pressure multi-anvil press • 4.5-80 keV • On-site • Accepting general users

13-ID-C,D • GSECARS • Geoscience, environmental science • Surface diffraction, microdiffraction, x-ray standing waves, x-ray absorption fine structure, resonant inelastic x-ray scattering, x-ray emission spectroscopy, high-pressure diamond anvil cell, high-pressure multi-anvil press • 4.9-45 keV, 10-75 keV • On-site • Accepting general users

13-ID-E • GSECARS • Geoscience, environmental science • Microfluorescence (hard x-ray), micro x-ray absorption fine structure, microdiffraction, fluorescence spectroscopy • 2.4-28 keV, 5.4-28 keV • On-site • Accepting general users

14-BM-C • **BioCARS** • Life sciences • Macromolecular crystallography, fiber diffraction, biohazards at the BSL2/3 level, subatomic (<0.85 Å) resolution, large unit cell crystallography • 8-14.9 keV • On-site • Accepting general users

14-ID-B • BioCARS • Life sciences, materials science, physics, chemistry • Time-resolved crystallography, time-resolved x-ray scattering, Laue crystallography, wide-angle x-ray scattering, biohazards at the BSL2/3 level, macromolecular crystallography • 7-19 keV • On site • Accepting general users

15-ID-B,C,D • **ChemMatCARS** • Materials science, chemistry • Anomalous and resonant scattering (hard x-ray), microdiffraction, high-pressure diamond anvil cell, single-crystal diffraction, liquid surface diffraction, x-ray reflectivity • 6-32 keV, 10-70 keV • On-site • Accepting general users

16-BM-B • **High Pressure (HP)CAT-XSD** • Materials science, geoscience, chemistry, physics • White Laue single-crystal diffraction, energy dispersive x-ray diffraction, phase contrast imaging, radiography, pair distribution function • 10-120 keV • On-site • Accepting general users

16-BM-D • HPCAT-XSD • Materials science, geoscience, chemistry, physics • Powder angular dispersive x-ray diffraction, single-crystal diffraction, x-ray absorption near-edge structure, x-ray absorption fine structure, tomography • 6-45 keV • On-site • Accepting general users

16-ID-B • HPCAT-XSD • Materials science, geoscience, chemistry, physics • Microdiffraction, single-crystal diffraction, high-pressure diamond anvil cell • 18-60 keV • On-site • Accepting general users

16-ID-D • HPCAT-XSD • Materials science, geoscience, chemistry, physics • Nuclear resonant scattering, inelastic x-ray scattering (1-eV resolution), x-ray emission spectroscopy, high-pressure diamond anvil cell • 5-37 keV, 14.41-14.42 keV • On-site • Accepting general users

17-BM-B • XSD • Chemistry, materials science • Powder diffraction, pair distribution function • 27-51 keV • On-site • Accepting general users

17-ID-B • **Industrial Macromolecular Crystallography Association (IMCA)-CAT** • Life sciences • Macromolecular crystallography, multi-wavelength anomalous dispersion, microbeam, single-wavelength anomalous dispersion, large unit cell crystallography • Subatomic (<0.85 Å) resolution • 6-20 keV • On-site, remote • Accepting general users

18-ID-D • **Biophysics (Bio)-CAT** • Life sciences • Fiber diffraction, microdiffraction, small-angle x-ray scattering, time-resolved x-ray scattering • 3.5-35 keV • On-site • Accepting general users

19-BM-D • **Structural Biology Center (SBC)-XSD** • Life sciences • Multi-wavelength anomalous dispersion, macromolecular crystallography, single-wavelength anomalous dispersion, serial crystallography • 6-13.5 keV • Remote, on-site, mail-in • Accepting general users

19-ID-D • SBC-XSD • Life sciences • Macromolecular crystallography, multi-wavelength anomalous dispersion, subatomic (<0.85 Å) resolution, large unit cell crystallography, single-wavelength anomalous dispersion • 6.5-19.5 keV • On-site, remote, mail-in • Accepting general users

20-BM-B • XSD • Materials science, environmental science, chemistry • X-ray absorption fine structure, microfluorescence (hard x-ray) • 2.7-32 keV, 2.7-35 keV • On-site • Accepting general users

20-ID-B,C • XSD • Materials science, environmental science, chemistry • X-ray absorption fine structure, x-ray Raman scattering, micro x-ray absorption fine structure, microfluorescence (hard x-ray), x-ray emission spectroscopy • 4.3-27 keV, 7-52 keV • On-site • Accepting general users

21-ID-D • **Life Sciences (LS)-CAT** • Life sciences • Macromolecular crystallography • 6.5-20 keV • On-site, remote, mail-in • Accepting general users

21-ID-F • LS-CAT • Life sciences • Macromolecular crystallography • 12.7 keV • Remote, on-site, mail-in • Accepting general users

21-ID-G • LS-CAT • Life sciences • Macromolecular crystallography • 12.7 keV • Remote, on-site, mail-in • Accepting general users

22-BM-D • **Southeast Regional (SER)-CAT** • Life sciences • Macromolecular crystallography, single-wavelength anomalous dispersion, multi-wavelength anomalous dispersion • 8-20 keV • On-site, remote • Accepting general users

22-ID-D • SER-CAT • Life sciences • Macromolecular crystallography, multi-wavelength anomalous dispersion, single-wavelength anomalous dispersion, microbeam • 6-20 keV • On-site, remote • Accepting general users

23-ID-B • **National Institute of General Medical Sciences and National Cancer Institute (GM/CA)-XSD** • Life sciences • Macromolecular crystallography, microbeam, large unit cell crystallography, subatomic (<0.85 Å) resolution, multi-wavelength anomalous dispersion, single-wavelength anomalous dispersion • 3.5-20 keV • On-site, remote • Accepting general users

23-ID-D • GM/CA-XSD • Life sciences • Macromolecular crystallography, microbeam, large unit cell crystallography, subatomic (<0.85 Å) resolution, multi-wavelength anomalous dispersion, single-wavelength anomalous dispersion, serial crystallography • 5-20 keV • On-site, remote • Accepting general users

24-ID-C • **Northeastern (NE)-CAT** • Life sciences • Macromolecular crystallography, microdiffraction, single-wavelength anomalous dispersion, single-crystal diffraction, microbeam, multi-wavelength anomalous dispersion, subatomic (<0.85 Å) resolution • 6.5-20 keV • On-site, remote • Accepting general users

24-ID-E • NE-CAT • Life sciences • Macromolecular crystallography, microbeam, microdiffraction, single-wavelength anomalous dispersion, single-crystal diffraction • 12.68 keV • On-site, remote • Accepting general users

26-ID-C • **Center for Nanoscale Materials (CNM)/XSD** • Physics, materials science • Nanodiffraction, nano-imaging, coherent x-ray scattering, synchrotron x-ray scanning tunneling microscopy • 6-12 keV • On-site • Accepting general users

27-ID-B • XSD • Physics • Resonant inelastic x-ray scattering • 5-14 keV, 5-30 keV • On-site • Accepting general users

29-ID-C,D • XSD • Physics, materials science • Resonant soft x-ray scattering, angle-resolved photoemission spectroscopy • 250-2200 eV, 2200-3000 eV • On-site • Accepting general users

30-ID-B,C • XSD • Physics, materials science • Inelastic x-ray scattering • 23.7-23.9 keV • On-site • Accepting general users

31-ID-D • **Lily Research Laboratories (LRL)-CAT** • Life sciences • Macromolecular crystallography, single-wavelength anomalous dispersion • 9-13.5 keV • Mail-in • Accepting general users

32-ID-B,C • XSD • Materials science, life sciences, geoscience • Phase contrast imaging, radiography, transmission x-ray microscopy, tomography • 7-40 keV • On-site • Accepting general users

33-BM-C • XSD • Materials science, physics, chemistry • Diffuse x-ray scattering, general diffraction, powder diffraction, x-ray reflectivity, grazing incidence diffraction, anomalous and resonant scattering (hard x-ray) • 5-35 keV • On-site • Accepting general users

33-ID-D,E • XSD • Materials science, physics, chemistry, environmental science • Anomalous and resonant scattering (hard x-ray), diffuse x-ray scattering, general diffraction, surface diffraction, surface diffraction (UHV), x-ray reflectivity • 4-40 keV, 6-25 keV • On-site • Accepting general users

34-ID-C • XSD • Materials science, physics • Coherent x-ray scattering • 5-15 keV • On-site • Accepting general users

34-ID-E • XSD • Materials science, physics, environmental science, geoscience • Microdiffraction, Laue crystallography, microbeam, microfluorescence (hard x-ray) • 7-30 keV • On-site • Accepting general users

35-ID-B,C,D,E • **Dynamic Compression Sector (DCS)** • Physics, materials science, geoscience • Time-resolved x-ray scattering, phase contrast imaging, radiography • 7-35 keV, 7-100 keV, 24-24 keV • On-site • Accepting general users

Welcome

Stephen Streiffer

At times it seems that the speed of change at the Advanced Photon Source (APS) can mirror the speed of the electrons in our storage ring: not exactly the speed of light, but close. Here are just a few examples.

The APS Upgrade Project (APS-U) represents the greatest change (for the better), not only for the quality of our x-rays but also for the new and enhanced beamlines that will be available to our users. Better photons plus revolutionary instrumentation will propel our outstanding user community to even more impactful discoveries.

On July 25, 2019, following a rigorous review, our sponsor, the Basic Energy Sciences Program Scientific User Facilities Division in the Office of Science, granted the APS-U Critical Decision 3, giving us full budget authority as we continue to execute the project (www.aps.anl.gov/APS-Upgrade). The pace of acquiring new storage ring components has accelerated (no pun intended), with new magnets, diagnostics, power supplies, and vacuum systems in various stages of fabrication, procurement, and acceptance.

On the Operations side, we're delivering new capabilities for our users and replace aging systems. For instance, the XTIP beamline at 4-ID-E has been commissioned and has started taking general users; and an initiative to replace aging storage ring klystrons with solid-state power supplies is being led by the RF Group in the Accelerator Systems Division headed by Division Director John Byrd.

The High Pressure and Structural Biology Center collaborative access teams are now part of the X-ray Science Division (XSD) under Division Director Jonathan Lang, as HPCAT-XSD and SBC-XSD, respectively, broadening and deepening the XSD portfolio. Andrzej Joachimiak, the long-time leader of SBC-CAT, continues as SBC-XSD Group Leader. Nenad Velisavljevic (Lawrence Livermore National Laboratory) is now the HPCAT-XSD Director, and Maddury Somayazulu (aka Zulu) is the new HPCAT-XSD Group Leader.

We strengthened the Photon Sciences Directorate organization with some key moves and appointments. George Srajer has assumed a new role as Deputy Associate Laboratory Director (DALD) for Planning and Integration. John Connolly is now DALD for Operations, while continuing as APS Engineering Support Division (AES) Director. Alec Sandy is now the XSD Associate Division Director for Beamline Technologies, and Dean Haeffner is the XSD Associate Division Director for Beamline Development. Nena Moonier is now Group Leader of the Experimental Facilities Operation Group in AES, replacing the estimable and retired Bruce Glagola.

Our facility infrastructure is being rejuvenated. New LED lighting in the experiment hall; sector-by-sector installation of a new experiment hall roof; new and improved signage around the exterior of the experiment hall; a completely re-designed plaza in front of the Central Lab/Office Building; even the addition of LED lighting for the iconic APS sign next to the plaza – all of these projects, under the watchful eye of Site Operations Group Leader Ron Tollner, are being or have been undertaken by the Argonne Facilities Division on our behalf.

Meanwhile the excellence of our users and staff is unchanged, as you can see from the list of awards and honors later in this newsletter.

And the fascinating, impactful, potentially world-changing discoveries by our users just keep coming; their results are too plentiful to cover in this “Welcome,” but this first volume of our annual highlights book for 2019 gives a sample (there’s much more on our website at https://www.aps.anl.gov/APS-Science-Highlight/All):

We hope you will enjoy reading about the science carried out on your behalf at the APS.

Stephen Streiffer

Argonne Associate Laboratory Director for Photon Sciences and Director, Advanced Photon Source

Electronic and Magnetic Materials

Supercrystal Freezes an Exotic State of Matter

Materials scientists are fascinated by so-called “non-equilibrium” materials, which develop new electronic or magnetic states when struck with a laser beam. Unfortunately, those states often disappear quickly; the energy from the photons excites the materials into a higher state, but when the energy is gone, the material returns to its ground state. Now, researchers have found they can create a supercrystal, which locks a new state into place, and used the APS to dig into how that works.

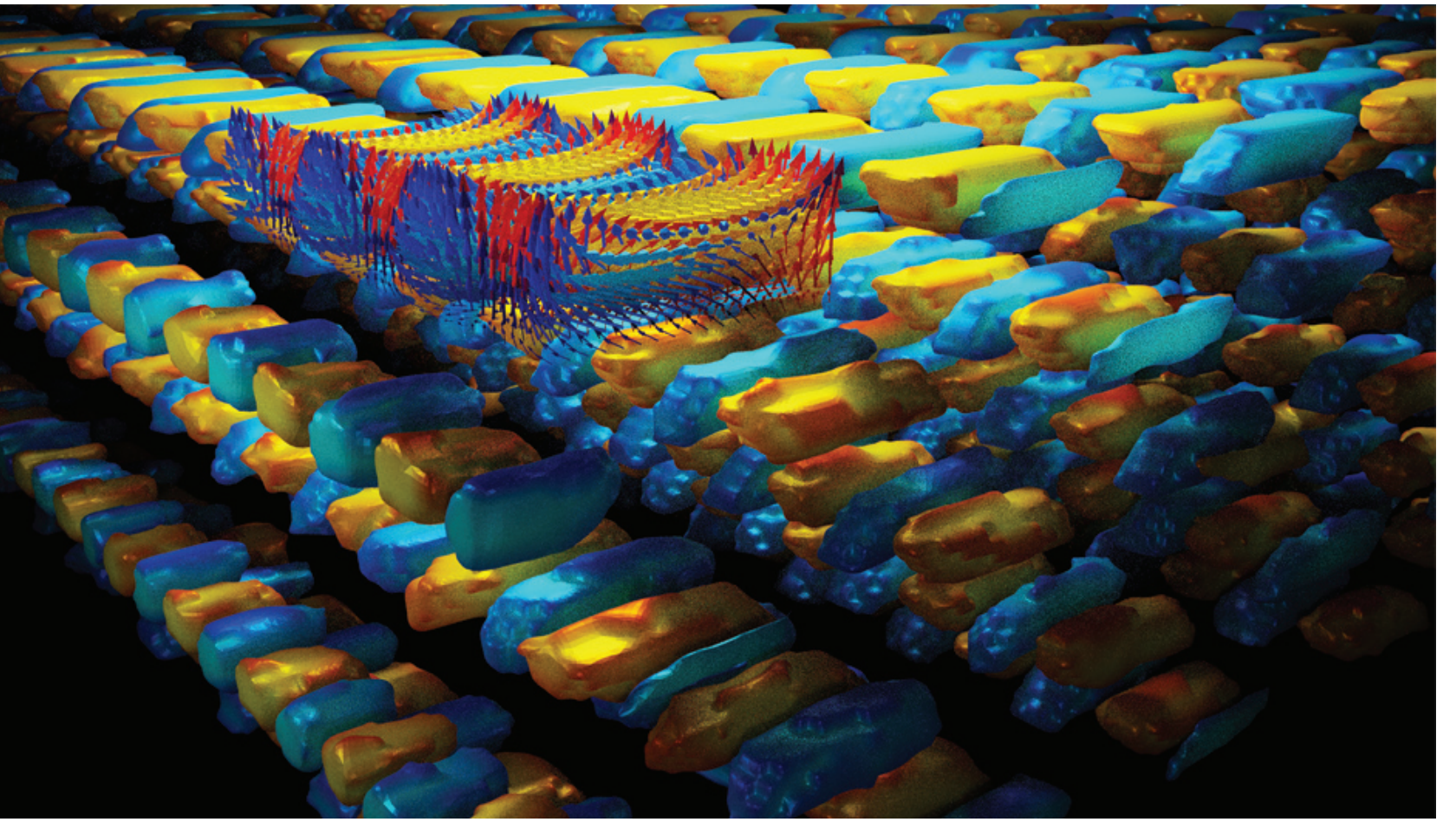

Fig. 1. A software-created rendition shows a supercrystal formed by striking the material with a sub-picosecond burst of laser light.

The material they built consists of alternating layers of lead titanate and strontium titanate. Lead titanate is ferroelectric, so it contains positive and negative electrical poles. Strontium titanate is not ferroelectric and therefore not polar. When the two are placed in alternating layers, the mismatch creates whirling vortices of electrical polarization in the material. Also contributing to this state is a mismatch between the crystal lattices of the two materials and the substrate on which they sit. The substrate, dysprosium scandium oxide, has structures smaller than the lead titanate and larger than the strontium titanate, causing those compounds to be either squeezed or stretched, respectively.

When the researchers in this study from Pennsylvania State University, Oak Ridge National Laboratory, Argonne, the University of California, Berkeley, and Lawrence Berkeley National Laboratory struck their sample with a laser beam that lasted less than a picosecond, the atoms in the material reordered themselves in such a way that original mixture of two structures dissolve and give rise to a new structure that is not seen by any other means (Fig. 1). They dubbed the resulting structure a "supercrystal," because it had repeating unit cells on tens of nanometer scale, much larger than those in an ordinary crystal with repeat units of a tenth of a nanometer. The supercrystal retained its state indefinitely, but that state could be erased by heating the material above approximately 430 K. Such a switchable material might be of interest as a new type of non-volatile memory, though the researchers were more interested in understanding the how the new state arises than in practical applications.

To figure out the origin of the new state, they performed x-ray diffraction (XRD) on their material at XSD beamlines 7-ID-C and 11-ID-D at the APS. Both of those beamlines have lasers. The team used the XRD to map the location of the atoms in the material, then struck the atoms with lasers and looked again to see how they had changed. When they examined the pristine sample, the diffraction pattern showed periodic order only in one direction, due to the stacking of the layers. After they excited the sample with the laser, a more complex, three-dimensional diffraction pattern appeared, showing that the material had become ordered in all three directions. By varying the power of the laser, the length of the pulse, and the wavelength of the light, they learned about the effects the photons were having.

For instance, they discovered they needed to reach a certain intensity of light to achieve the state they were looking for. That supports the idea that it is an accumulation of charge carriers created when the material absorbs photons that causes the phase change, and that the change does not happen until the carriers reach a particular density. The measurements they made matched a theoretical model their colleagues had developed. They also determined that the laser pulse had to be less than a picosecond for the switch to work.

They also performed XRD at XSD beamlines 33-BM-C and 33-ID-D,E, where they heated the material and saw at which temperatures the new state decayed. X-ray diffraction microscopy at beamline 33-ID-D,E allowed them to see variations in the crystal structure before and after the laser pulses. Their next step is to try and measure how long it takes the new states to form, with the hope that information will allow them uncover the changing dynamics of the charge carriers and figure out the physics of how the supercrystal is created. — Neil Savage

See: V. A. Stoica[1]*, N. Laanait[2], C. Dai[1], Z. Hong[1], Y. Yuan[1], Z. Zhang[3], S. Lei[1], M. R. McCarter[4], A. Yadav[4], A. R. Damodaran[4], S. Das[4], G. A. Stone[1], J. Karapetrova[3], D. A. Walko[3], X. Zhang[3], L. W. Martin[4,5], R. Ramesh[4,5], L.-Q. Chen[1], H. Wen[3], V. Gopalan[1]*, and J. W. Freeland[3]**, "Optical creation of a supercrystal with three-dimensional nanoscale periodicity," Nat. Mater. **18**, 377 (April 2019). DOI: 10.1038/s41563-019-0311-x
Author affiliations: [1]Pennsylvania State University, [2]Oak Ridge National Laboratory, [3]Argonne National Laboratory, [4]University of California, Berkeley, [5]Lawrence Berkeley National Laboratory
Correspondence: * vxg8@psu.edu, ** freeland@anl.gov

V.A.S., Y.Y., L.W.M., C.D., L.-Q.C., H.W., V.G., and J.W.F. acknowledge support from the U.S. Department of Energy (DOE) Office of Science-Basic Energy Sciences, under Award Number DE-SC-0012375 for the development of the materials and ultrafast experiments. Z.H., S.L., and G.A.S acknowledge support from the National Science Foundation (NSF) DMR-1210588 and the NSF Center for Nanoscale Science grant number DMR-1420620. L.-Q. C. also acknowledges support from NSF DMR-1744213. PFM data were collected at PSU, University of California, Berkeley, and at the Center for Nanophase Materials Sciences, a DOE Office of Science User Facility at Oak Ridge National Laboratory. N.L. acknowledges support from the Eugene P. Wigner Fellowship at Oak Ridge National Laboratory, a U.S. DOE facility managed by UT-Battelle, LLC, for the U.S. DOE Office of Science under contract no. DE-AC05–00OR22725. R.R. and L.W.M. acknowledge funding from the Gordon and Betty Moore Foundation's EPiQS Initiative, under grant GBMF5307. N.L. acknowledges use of the Compute and Data Environment for Science (CADES) at Oak Ridge National Laboratory. This research used resources of the Advanced Photon Source, a U.S. DOE Office of Science User Facility operated for the DOE Office of Science by Argonne National Laboratory under Contract DE-AC02-06CH11357.

Layer-By-Layer Crystals: Creating Memories as They Grow

Modern microelectronics, such as high-efficiency lighting or solid-state lasers, rely on crystals with precisely controlled structure and composition for their useful properties. Thus, it is important to understand and control crystal growth processes at the atomic scale. In one proposed process, called "layer-by-layer growth," atoms skate on a surface to find each other, nucleating into flat, island-like clusters that steadily expand until they merge and eventually coalesce into a complete layer. This cycle repeats itself as new layers subsequently form and stack upon the first one. Although the basic ideas of layer-by-layer growth have been verified in many systems, it is not clear whether they accurately describe the growth of modern materials—gallium nitride (GaN), for instance—by synthesis methods such as metalorganic vapor-phase epitaxy (MOVPE) used in industry. Previous synchrotron studies of GaN MOVPE used incoherent x-rays to follow the surface structure during growth—a technique that provides information only on average island size and orientation. To provide a more detailed view, researchers used the APS to characterize the exact arrangement of the islands nucleating in each layer of crystal. Their research demonstrates a powerful new technique for characterizing atomic-scale surface processes and could eventually help scientists optimize crystal growth or develop new types of crystals for electronics and other applications.

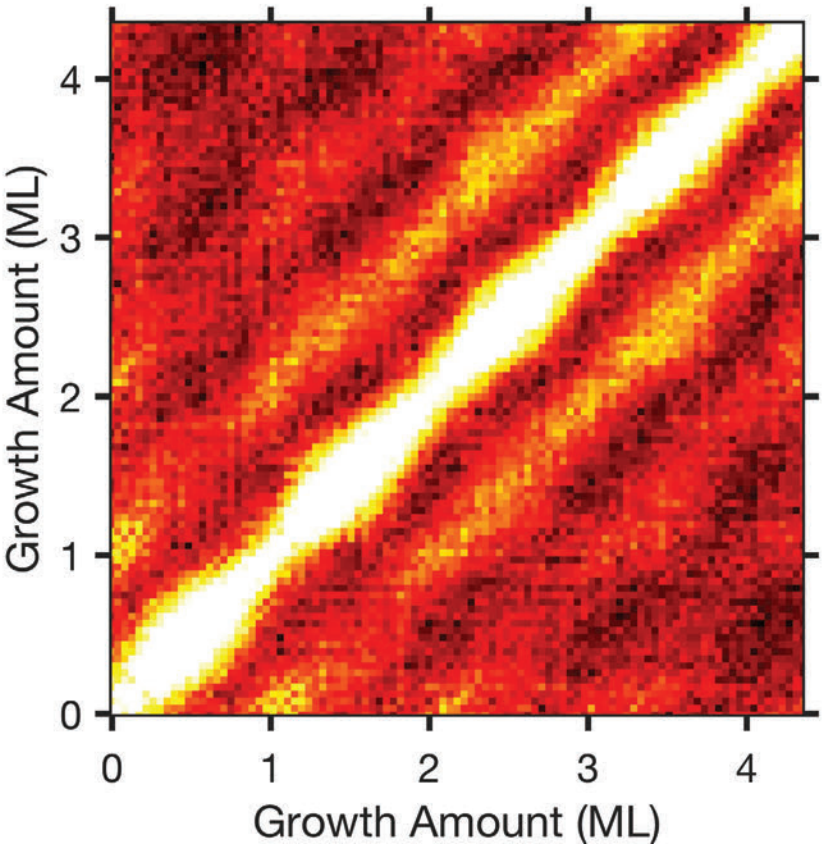

The team of researchers from Argonne, Northern Illinois University, and Sogang University (Korea) employed a coherent x-ray beam at XSD beamline 12-ID-D at the APS. Unlike the incoherent beams used in previous experiments, the coherent beam allowed the researchers to characterize the exact arrangement of the islands nucleating in each layer of crystal. Their findings showed that, rather than displaying a different random pattern in each layer, the islands forming in a new layer nearly mirror the placement of those in previous layers (Fig. 1).

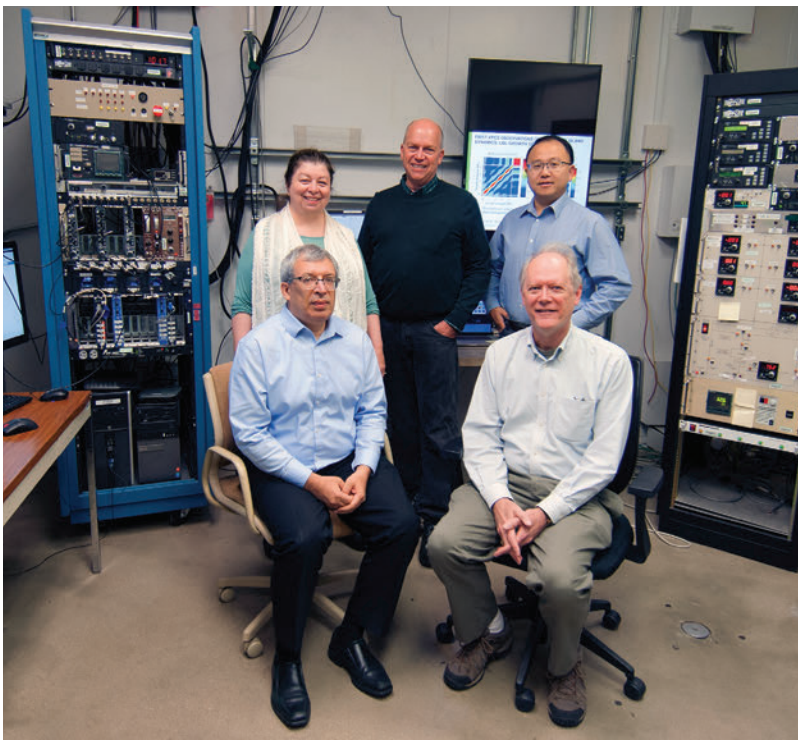

Members of the research team in the APS 12-ID-D control room: Back row, left to right: Carol Thompson, Jeffrey Eastman, and Hua Zhou. Front row, left to right: Peter Zapol and Brian Stephenson. Not pictured are team members Guangxu Ju, Dongwei Xu, Matthew Highland, Paul Fuoss, and Hyunjung Kim.

The researchers used a relatively high-energy (26 keV) coherent x-ray beam to penetrate the growth environment and minimize disturbance by the beam, monitoring the MOVPE process as it occurred. Passing through the chamber walls, the x-rays deflected off the growing islands, producing a coherent "speckle" pattern picked up by an imaging detector.

After statistically analyzing these patterns, the researchers made a surprising finding: The islands forming on each layer after the first layer "remembered" the original island placement. Although it is unknown exactly why the island arrangement persists between layers, computer simulations suggest that island nucleation on top of an almost complete layer is most likely to occur at locations far away from the remaining holes in the layer. Because the holes themselves tend to be at locations far away from the original nucleation sites of that layer, the new island arrangement can mimic the previous one.

This represents a type of chemical communication between layers, the authors say. Importantly, the persistent arrangement is not due to defects in the crystal structure (such as dislocations) producing static preferred sites for island nucleation.

The authors add that such a discovery was only possible with a coherent x-ray source. This shows the new type of analysis that will be widely available in the future with the APS Upgrade, when high-intensity coherent x-ray beams will be available at many beamlines.

— Christen Brownlee

< Fig. 1. Two-time correlations in the measured speckle from two-dimensional islands during growth of 4.5 monolayers (ML). The pattern indicates that the arrangement of islands in successive layers is correlated with that in previous layers.

See: Guangxu Ju[1‡*], Dongwei Xu[1‡‡], Matthew J. Highland[1], Carol Thompson[2], Hua Zhou[1], Jeffrey A. Eastman[1], Paul H. Fuoss[1‡‡‡], Peter Zapol[1], Hyunjung Kim[3], and G. Brian Stephenson[1**], "Coherent X-ray spectroscopy reveals the persistence of island arrangements during layer-by-layer growth," Nat. Phys. **15**, 589 (2019). DOI: 10.1038/s41567-019-0448-1

Author affiliations: [1]Argonne National Laboratory, [2]Northern Illinois University, [3]Sogang University Present address: ‡Arizona State University, ‡‡Huazhong University of Science and Technology, ‡‡‡SLAC National Accelerator Laboratory
Correspondence: * gju@anl.gov, ** stephenson@anl.gov

Support was provided by the U.S. Department of Energy (DOE) Office of Science-Basic Energy Sciences, Materials Sciences and Engineering (XPCS measurements and analysis) and Scientific User Facilities (KMC model development). Computing resources were provided on Blues and Fusion, high-performance computing clusters operated by the Laboratory Computing Resource Center at Argonne National Laboratory. This research used resources of the Advanced Photon Source, a U.S. DOE Office of Science User Facility operated for the DOE Office of Science by Argonne National Laboratory under Contract No. DE-AC02-06CH11357.

Probing Conductivity in a Newly-Synthesized Liquid Crystal

Liquid crystals are most familiar as the compounds used in the displays of smart phones, laptops, and other electronic devices. But liquid crystals can possess additional attributes, such as the ability to efficiently conduct ions. Researchers now report the synthesis of a new liquid-crystal compound, 4T/PEO4, that features excellent conductivity of ions over a considerable temperature range. Like many other liquid crystals, 4T/PEO4 can self-assemble to form a large-scale, semi-ordered structure. In a first for this class of materials, the research team used molecular dynamics (MD) modeling to help guide the compound's synthesis and to gain insight about its self-assembly behavior. The structure of the new compound was corroborated by x-ray experiments at the APS. Complimentary simulation and experimental data have revealed several technologically-relevant features of 4T/PEO4. Perhaps even more importantly, the researchers anticipate that their early-stage reliance on computer modeling will be applied to the development of other liquid crystals and soft materials for a host of applications, such as flexible and inexpensive organic semiconductors, as battery electrolytes, and in solar cells.

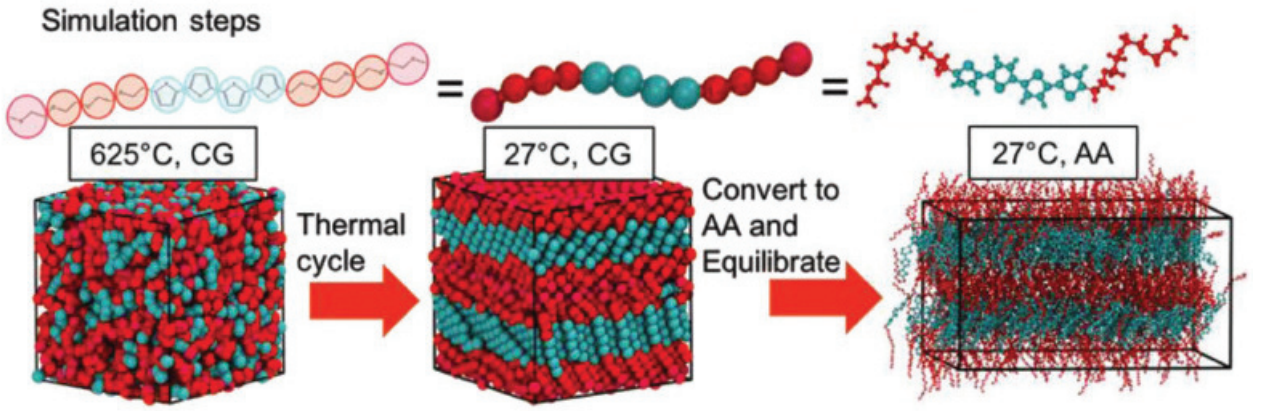

4T/PEO4 is an abbreviated term for quarterthiophene/poly(ethylene oxide). The basic structure of this liquid crystal molecule is four linked thiophene rings (the 4T part of 4T/PEO4), which together form a central core, or rod, that is connected at either end to a molecular coil. Thiophenes are small molecular rings made of carbon and hydrogen atoms bound to one another, along with a single sulfur atom. The pair of coils (the PEO4 part) are composed of ethylene oxide molecules. The central molecular rod was chosen for its electron conductivity, while the flexible coils promote ion conduction. Individual 4T/PEO4 molecules were arranged in stacks via chemical bonds known as p-bonds, which promoted conductivity in two dimensions.

The researchers from Cornell University and The University of Chicago used grazing-incidence wide-angle x-ray scattering (GIWAXS) carried out at XSD beamline 8-ID-E of the APS to observe the self-assembly behavior of 4T/PEO4. This technique involves scattering x-rays at a very shallow (grazing) angle, allowing the topology of thin films to be mapped precisely. The GIWAXS data indicated the 4T/PEO4 molecules formed an ordered structure known as the smectic phase, which occurs in many liquid crystals. The smectic phase was retained even after 4T/PEO4 was combined with the compound LiTFSI, which was employed for its ability to donate lithium ions. LiTFSI stands for lithium bis(trifluoro-methanesulfonyl)imide.

The GIWAXS measurements were performed over temperatures ranging from 25° C to 123° C. Above 100° C, the smectic ordering of 4T/PEO4 dissipated, which reduced the compound's ionic conductivity. When the 4T/PEO4 was cooled, the ordering was restored, but the ionic conductivity did not fully return to its original level.

The x-ray measurements were compared to results obtained using a MD simulation of 4T/PEO4 behavior. The type of modeling the researchers preferred is known as all-atom (AA) molecular dynamics. In an AA simulation, the electric forces and potentials of all the atoms involved are used to precisely calculate overall molecular behavior. Due to the slow dynamics of this particular molecular system, a simplified approach called coarse-grained (CG) modeling was initially utilized. In the CG model, for instance, each thiophene ring in the 4T/PEO4 compound was represented as a sphere instead of as a ring of individual atoms.

The simplified CG simulation was initiated at sufficiently high temperature (625° C) to ensure a completely disordered state of 4T/PEO4. Simulating a rapid cool-down to 27° C resulted in an ordered, smectic phase of 4T/PEO4, which was in agreement with the GIWAXS observations. The results of the simplified CG simulation were subsequently converted to the AA method to obtain a more highly refined view of the dynamic process, as illustrated in Fig. 1.

Both the experimental data and the MD simulation reveal that the newly-synthesized 4T/PEO4 liquid crystal is an excellent ion conductor that also possesses an ability to conduct electrons. This dual capability may prove useful in different technological applications. Simulation and experiment also demonstrated that 4T/PEO4 retains its smectic structure even after mixing with LiTFSI.

The success of the MD simulation in both synthesizing and predicting the behavior of 4T/PEO4 gives the researchers confidence that these same techniques will prove useful for creating new types of liquid crystals. More broadly, these same modeling techniques should also prove applicable to other soft materials. — Philip Koth

< Fig. 1. Steps involved in modeling the behavior of 4T/PEO4 molecules at 27° C. The molecule's thiophene rings are indicated by cyan, while its PEO units are shown in red. Starting at left, the first step utilizes CG modeling of 4T/PEO4 behavior at high temperature (625° C). CG modeling of the molecular system continues (middle panel) as the temperature is lowered to 27° C. Finally, the right-hand panel depicts translation from CG to AA modeling in order to produce the highest fidelity simulation of 4T/PEO4 molecules at 27° C. From Z. Liu et al., Adv. Funct. Mater. **29**, 180522 (2019). © 2018 WILEY-VCH Verlag GmbH & Co. KGaA, Weinheim

See: Ziwei Liu[1], Ban Xuan Dong[2], Mayank Misra[1], Yangyang Sun[1], Joseph Strzalka[3], Shrayesh N. Patel[2], Fernando A. Escobedo[1], Paul F. Nealey[2]**, and Christopher K. Ober[1]*, "Self-Assembly Behavior of an Oligothiophene-Based Conjugated Liquid Crystal and Its Implication for Ionic Conductivity Characteristics," Adv. Funct. Mater. **29**, 1805220 (2019). DOI: 10.1002/adfm.201805220
Author affiliations: [1]Cornell University, [2]The University of Chicago, [3]Argonne National Laboratory
Correspondence: * cko3@cornell.edu, ** nealey@uchicago.edu

This work was supported by the National Science Foundation (NSF) (DMREF-1629369). This work made use of the Cornell Center for Materials Research Shared Facilities which are supported through the NSF MRSEC program (DMR-1719875). This research used resources of the Advanced Photon Source, a U.S. Department of Energy (DOE) Office of Science User Facility operated for the DOE Office of Science by Argonne National Laboratory under Contract DE-AC02-06CH11357.

Single-Molecule Magnets for Data Storage

Researchers are investigating the potential storage capacity of single-molecule magnets (SMMs) in an effort to push the boundaries of magnetic data storage systems. In this work, a research team used a novel spectroscopic tool at the APS to study magnetic properties in molecular compounds incorporating dysprosium (Dy), a lanthanide, giving rise to the compound's single-molecule magnet behavior. Eventual success in this field will lead to single-molecule magnets that can store massive amounts of data at or close to room temperature.

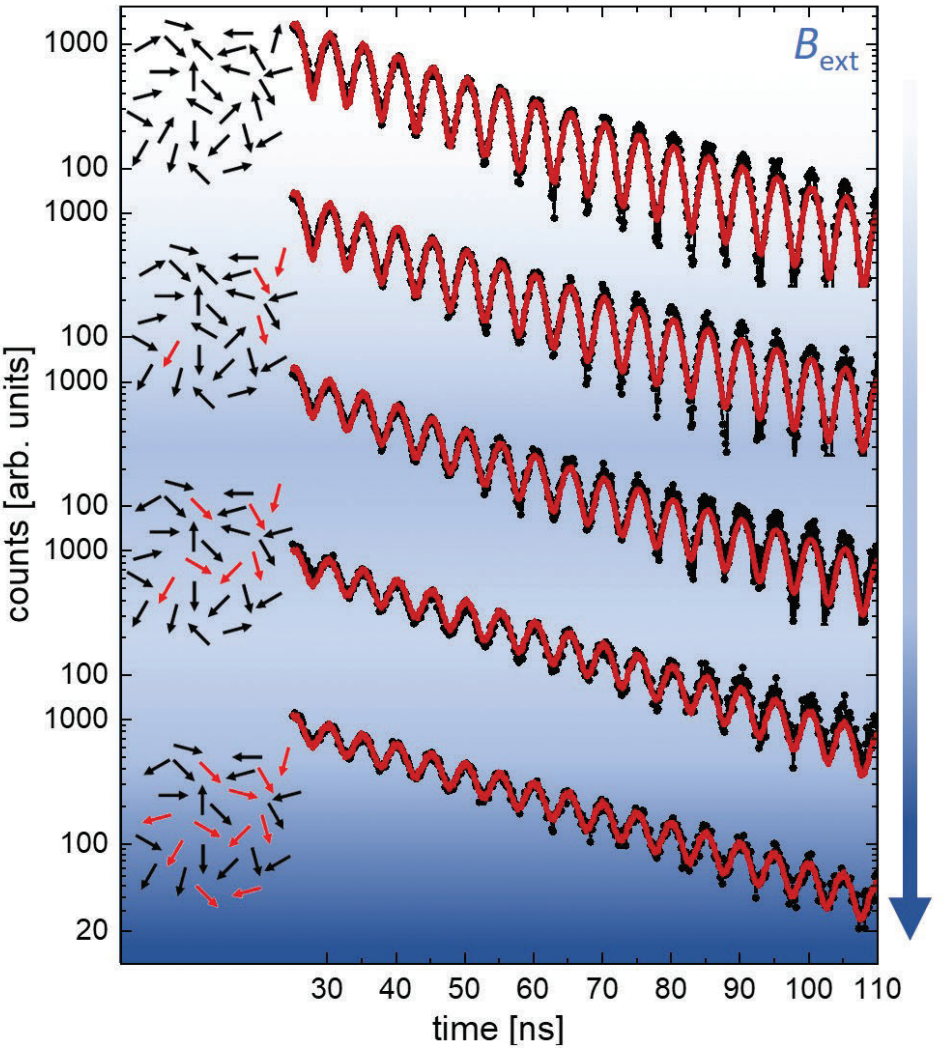

Magnetism, which results from electron spin, is used to store data; specifically, data is encoded by different patterns of magnetization on a magnetically coated surface. Magnetic storage is currently found in hard disks, memory chips, and sensors. As we near the time when current methods of data storage are no longer able to increase, researchers must pursue multiple paths for increasing data storage capacity.

One promising way to increase magnetic data storage is with a new form of magnet. In SMMs, the metal center of the molecule connects to organic ligands to form a molecule with magnetic characteristics. Such a SMM could be capable of storing much more data in the future. Only a few metals are capable of being SMMs. Iron and the lanthanide group of rare-earth elements (atomic numbers 57 to 71) are the most promising metal ions. Dysprosium, element 66, is currently thought to be one of the best metal centers for SMMs because it can generate a relatively large magnetic moment (magnetic strength and orientation), strong magnetic anisotropy, blocking temperatures up to 80 K, and magnetic hysteresis.

For this work, the research team from Technische Universität Kaiserslautern (Germany), the Karlsruhe Institute of Technology (Germany), Argonne, Northern Illinois University, and the University of Illinois at Urbana-Champaign used time-domain synchrotron Mössbauer spectroscopy (SMS), an analytical method in which atomic nuclei absorb high-energy x-rays, to investigate the magnetic properties of a DyIII-based SMM (Fig. 1). The researchers measured the influence of the coordinating ligands on the strength of the magnetic hyperfine interactions found between the Dy electron shell and the 161Dy nucleus. The technique revealed the properties of the metal center in a way similar to slow motion, allowing researchers to gain additional information such as how quickly the system returns to its original state and how long the molecule's storage time might be.

The research used the XSD x-ray beamline 3-ID-D at the APS to perform the ^{161}Dy time-domain SMS experiments. The experiments were carried out in liquid helium at -269° C because to date, SMMs only exhibit magnetic properties under these conditions. This work shows that ^{161}Dy SMS can successfully probe Dy magnetization and reveal the impact of the coordinating ligands on the magnetic hyperfine field at the Dy ion. The new technique reveals phenomena on a nanosecond time scale, such as the influence of the crystal field, magnetic characteristics, and relaxation phenomena. It will further elucidate the influence of intramolecular interactions and cooperative effects in both polynuclear Dy systems and heterometallic molecular clusters.

Fig. 1. Time-domain SMS spectra on a SMM incorporating dysprosium demonstrate the correlation of the magnetic hyperfine field at the ^{161}Dy nucleus and the increasing average magnetization induced by external fields.

The results of the current study show that ^{161}Dy SMS is an effective local probe for understanding the influence of coordinating ligands on the magnetic structure of Dy-containing molecular compounds. Its goal is to understand the properties of SMMs that will eventually lead to the development of better magnetic storage systems.

— Dana Desonie

(Note: The work was done in close cooperation with the chemists' group of Professor Dr. A. K. Powell from Karlsruher Institut of Technology, working on the development of novel molecular systems with new properties and functions. This research is part of a larger project in which teams of chemists and physicists are working on molecular systems to develop novel properties and functions. In this Transregio Collaborative Research Centre "Cooperative Effects in Homo and Heterometallic Complexes' [SFB/TRR 88 3MET], the researchers focus on molecular systems with two or more metal centers, searching for efficient materials for magnetic storage or more effective catalysts for chemical reactions.)

See: Lena Scherthan[1]*, Sebastian F. M. Schmidt[2], Hendrik Auerbach[1], Tim Hochdörffer[1], Juliusz A. Wolny[1], Wenli Bi,[3,5], Jiyong Zhao[3], Michael Y. Hu[3], Tom Toellner[3], E. Ercan Alp[3], Dennis E. Brown[4], Christopher E. Anson[2], Annie K. Powell[2]***, and Volker Schünemann[1]**, "^{161}Dy Time-Domain Synchrotron Mössbauer Spectroscopy for Investigating Single-Molecule Magnets Incorporating Dy Ions," Angew. Chem. **131**, 3482 (2019).
DOI: 10.1002/anie.201810505
Author affiliations: [1]Technische Universität Kaiserslautern, [2]Karlsruhe Institute of Technology, [3]Argonne National Laboratory, [4]Northern Illinois University, [5]University of Illinois at Urbana-Champaign
Correspondence: *schertha@rhrk.uni-kl.de,
**schuene@physik.uni-kl.de,
***annie.powell@kit.edu

This work was supported by the Deutsche Forschungsgemeinschaft (DFG) through SFB/TRR 88 3MET. W.B. would like to acknowledge the partial support by COMPRES, the Consortium for Materials Properties Research in Earth Sciences under National Science Foundation Cooperative Agreement EAR 1606856. This research used resources of the Advanced Photon Source, a U.S.Department of Energy (DOE) Office of Science User Facility operated for the DOE Office of Science by Argonne National Laboratory under Contract No.DE-AC02-06CH11357.

An Exciting Candidate for Spintronics Applications

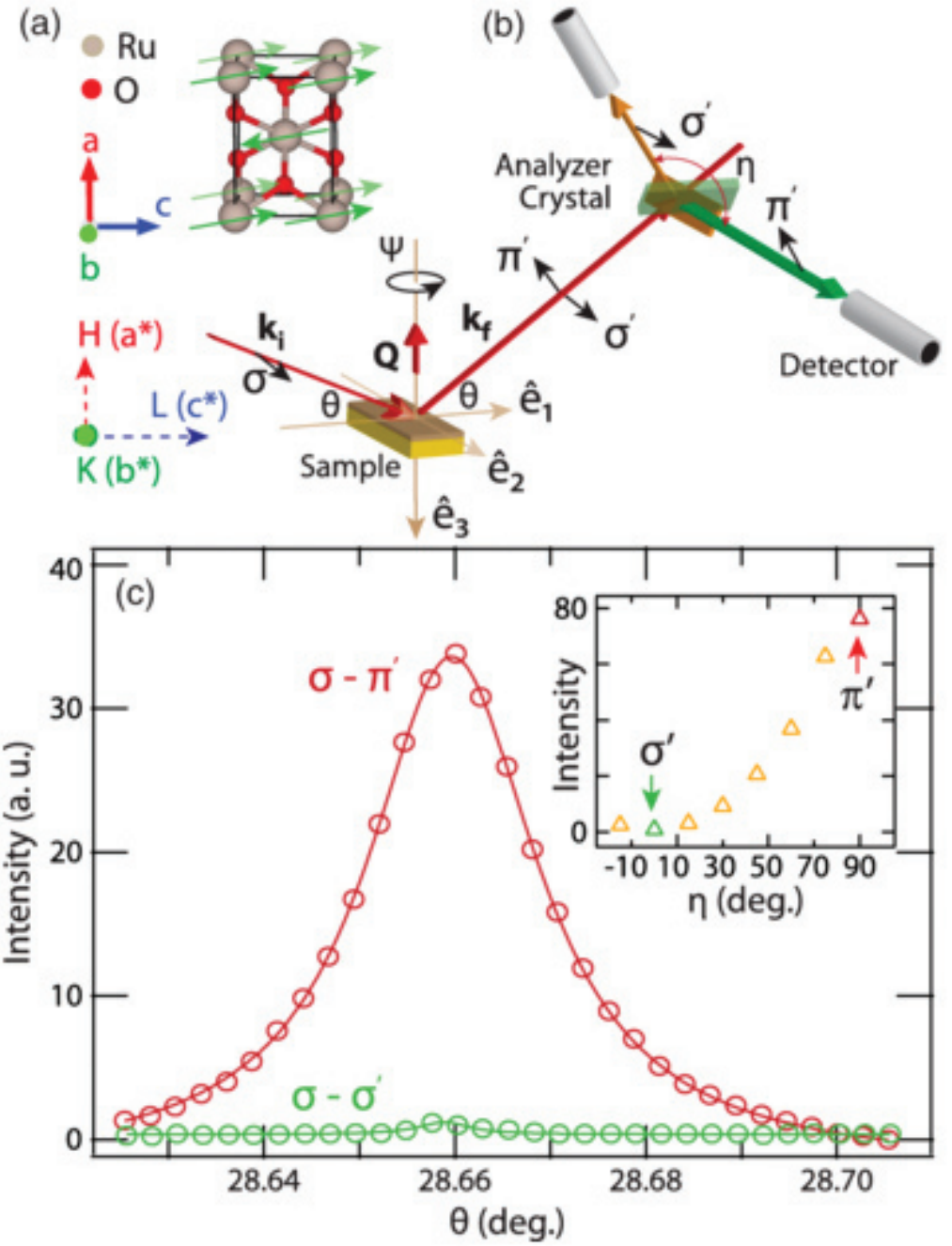

Fig. 1. Results showing (a) the authors' proposed magnetic structure for rutile RuO_2 (Ru: light gray; O: red); (b) the experimental configuration of the scattering geometry; and (c) the polarization dependence of the scattered intensity. From Z. H. Zhu et al., Phys. Rev. Lett. **122**, 017202 (2019). © 2019 American Physical Society

The next evolution for data storage may come from spintronic devices. Unlike traditional electronics, which solely take into consideration an electron's charge, the new field of spintronics controls electrons by acting on their intrinsic spin. The importance of this field is highlighted by the fact that the 2007 Nobel Prize in Physics was awarded for the discovery of giant magnetoresistance, which paved the way for spintronics research. Although a fairly nascent field, spintronics have already considerably enhanced data storage technology, including hard drive capacity. Spintronics electronics can store data in a way that is less susceptible to damage from outside forces, require less energy to operate, and can transmit information much more rapidly. Researchers carrying out studies at the APS used high-brightness x-rays to determine that metallic ruthenium oxide (RuO_2) harbors a unique type of magnetism that makes it an exciting potential candidate for novel spintronics applications.

RuO_2, a parent compound of several highly superconductive and antiferromagnetic materials, has recently shown promise in the field of electronics. It was previously thought to be only weakly magnetic, but that information came from studies using a bulk quantity of the crystal. However, new data from experiments using a single crystal of RuO_2 suggest that the ruthenium crystal story is incomplete. This discovery was of particular interest to those involved in spintronics research, as an ideal spintronic material would be superconductive, antiferromagnetic, and active in a thin layer of crystals. Researchers from the Massachusetts Institute of Technology and Argonne were eager to investigate this potentially valuable material further in the hopes of making progress in this new, exciting field.

Resonant elastic x-ray scattering (REXS) experiments were conducted at the XSD 4-ID-D x-ray beamline at the APS. Because REXS is a technique that carefully selects the properties of the beam of light used to excite the crystal being analyzed and observes the changes in the light that are caused by interaction with the crystal after scattering, it is particularly useful when trying to detect magnetism in metals, as it can distinguish spin order of the material. The team performed all measurements on both thin RuO_2 films, which are of significant use to applications, and bulk single crystals. Using the powerful REXS technique, they were able to confirm that the thin-film crystal exhibited the antiferromagnetism that was suggested previously. They also observed what is called a "collinear antiferromagnetism," meaning the individual magnetic moments of the atoms tended to lie along a fixed axis within the crystal. This is significant because this linearity in magnetism allows for easier manipulation by spintronic devices. Figure 1 displays the resulting proposed magnetic structure for rutile RuO_2 as well as the experimental geometry used and the polarization dependence of the scattered intensity, displaying the hallmark signature of x-ray scattering from magnetism.

Previous research had suggested that RuO_2 exhibits antiferromagnetic tendencies at elevated temperatures, which is highly unusual in this type of conductive material. To test this further, the team studied crystals that were held at a range of temperatures, from 200 K to 400 K (about -100° F, or 38° C, to 260° F, or 127° C). They were able to produce evidence for antiferromagnetism, even at temperatures as high as 320 K. This is an important finding, as spintronic devices would likely be operating at room temperature.

Given how rare it is to find all of these unique properties in a single material, it is reasonable to predict that we may see the use of RuO_2 in spintronic devices in the near future. — Alicia Surrao

See: Z. H. Zhu[1]*, J. Strempfer[2], R. R. Rao[1], C. A. Occhialini[1], J. Pelliciari[1], Y. Choi[2], T. Kawaguchi[2], H. You[2], J. F. Mitchell[2], Y. Shao-Horn[1], and R. Comin[1]**, "Anomalous Antiferromagnetism in Metallic RuO_2 Determined by Resonant X-ray Scattering," Phys. Rev. Lett. **122**, 017202 (2019).
DOI: 10.1103/PhysRevLett.122.017202
Author affiliations: [1]Massachusetts Institute of Technology, [2]Argonne National Laboratory
Correspondence: * zzh@mit.edu, ** rcomin@mit.edu

This research was supported by the National Science Foundation through the Massachusetts Institute of Technology Materials Research Science and Engineering Center, DMR-1419807. R. C. acknowledges support from the Alfred P. Sloan Foundation. J. P. acknowledges financial support by the Swiss National Science Foundation Early Postdoc.Mobility Fellowship Project No. P2FRP2_171824. The work in the Materials Science Division of Argonne National Laboratory (bulk crystal synthesis) was supported by the U.S. Department of Energy (DOE) Office of Science-Basic Energy Sciences, Materials Science and Engineering Division. This research used resources of the Advanced Photon Source, a U.S. DOE Office of Science User Facility operated for the DOE Office of Science by Argonne National Laboratory under Contract DE-AC02-06CH11357.

Disorder in the Cuprate Superconductors

The mechanisms underlying high-temperature superconductivity (T_c) remain poorly understood. However, it is becoming apparent that the coexistence/competition of superconductivity with other ordered states, most notably magnetism and charge density order, plays an important role in cuprate, as well as iron-based, superconductors. Now, researchers using the APS have shown that the interplay between superconductivity and charge density order in a cuprate superconductor can be tuned by disorder. Atomic-scale disorder created by particle irradiation strongly suppressed charge order while at the same time enhancing the superconducting transition temperature by 50%. Developing materials that exhibit superconductivity at room temperature for widespread commercial use would allow a significant reduction in energy consumption throughout the power grid. While this is a dream today, fundamental research advances our understanding of the physics underlying superconductivity and helps pave the way for important new materials.

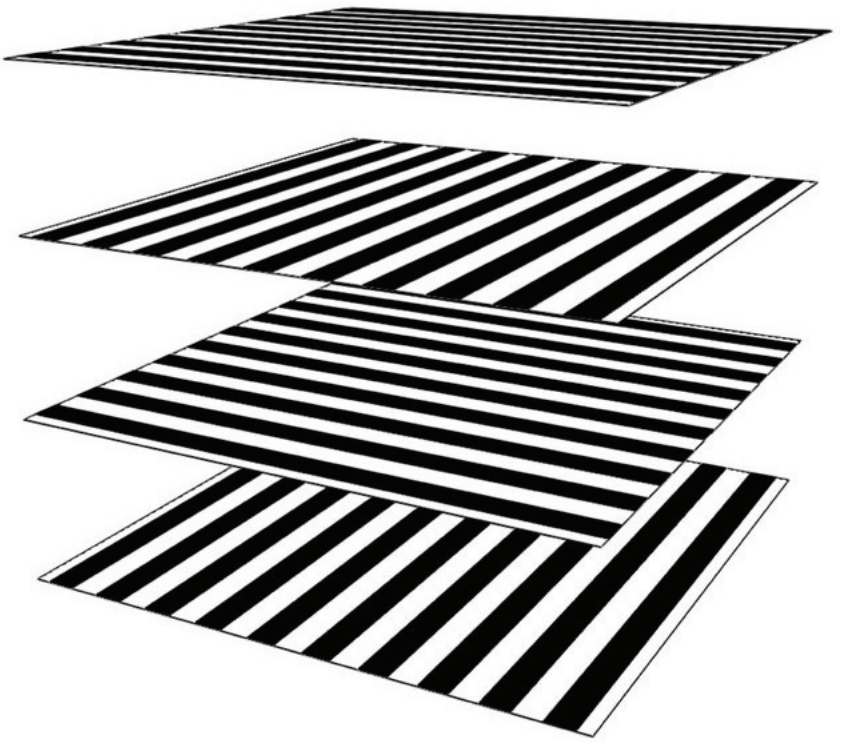

Fig. 1. Schematic of the charge-ordered state in LBCO in the pristine state (this page) and after introduction of defects (next page). The layers represent the superconducting CuO_2 panes and the white and black stripes represent the modulated pattern of high and low charge density. An atomic-scale defect (the sphere on the next page) causes deformation and suppression of the charge stripe order. As a consequence, superconducting correlations in the perpendicular direction, which are completely cancelled in the pristine state, re-emerge, causing an increase in T_c. From M. Leroux et al., Proc. Natl. Acad. Sci. U.S.A. **116**(22), 10691. (May 28, 2019). © 2019 National Academy of Sciences

Superconductivity is based on the quantum-mechanical behavior of electrons in solids and involves pair-wise correlations between electrons with opposite velocity and spin, so-called “Cooper pairing.” The stronger this paring interaction is and the more electrons it involves, the higher the superconducting transition temperature will be. The most dramatic consequence is that the electrical resistance drops to zero when the sample is cooled to Tc. This property lies at the heart of all envisioned or actual large-scale applications of superconductors, for in-

stance in high-field magnets or the electric power grid; the magnets in all magnetic resonant imaging machines are wound from superconducting wires.

It is not clear what specific attributes make a material a high-temperature superconductor; currently, a superconducting material cannot be predicted. Furthermore, as high-temperature superconductors are complicated materials, other ordered states, such as magnetism or charge density order, may coexist or compete with superconductivity. In a charge density wave, the electron density in a solid undergoes a periodic spatial modulation. Electrons involved in a charge-ordered state generally do not participate in superconductivity .

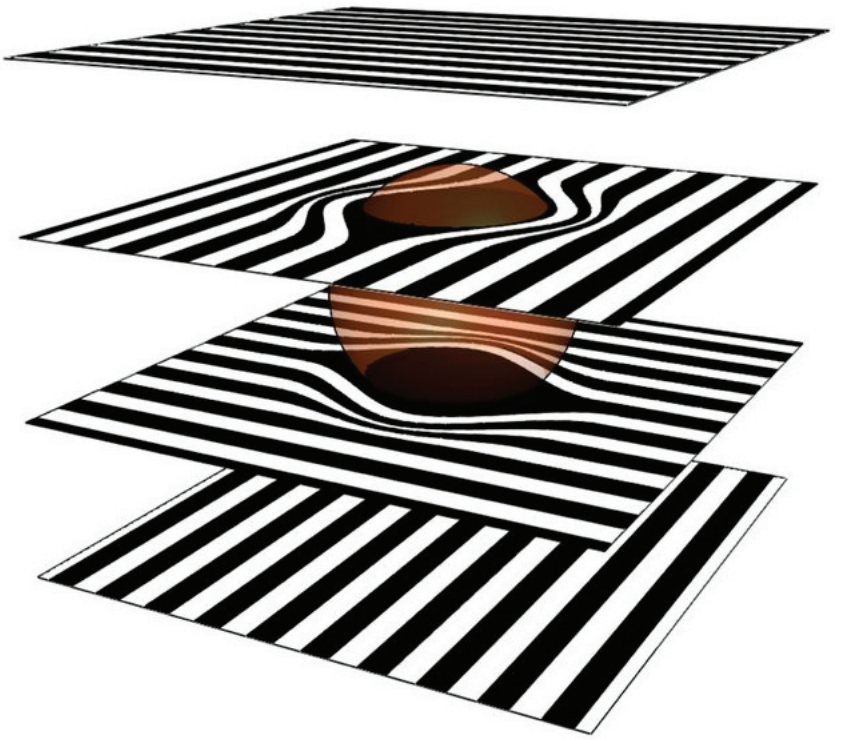

In the past decade, charge order has been found to be ubiquitous in cuprate high-temperature superconductors, although the debate on whether charge order helps or hinders superconductivity is still ongoing. In this work, researchers from Argonne, Cornell University, Universite´ Grenoble Alpes (France), Western Michigan University, and Brookhaven National Laboratory used atomic-scale disorder induced by proton-irradiation to tune the balance between superconductivity and charge order in the cuprate $La_{1.875}Ba_{0.125}CuO_4$ (LBCO, Fig. 1). Since charge order is a modulation in real space, it is expected to be highly sensitive to disorder. In contrast, superconductivity arises from order in the motion of electrons and only weak suppression is expected. Surprisingly, T_c increased by up to 50% upon irradiation. Detailed x-ray scattering experiments over a wide range of temperatures were carried out at the XSD 6-ID-B,C x-ray beamline at the APS, and also at the Cornell High Energy Synchrotron Source (CHESS) at Cornell University. The results were instrumental in establishing that upon irradiation, the charge order amplitude is indeed strongly suppressed while the period of the charge modulation does not change. The latter demonstrates that there is no irradiation-induced charge doping that could falsify results.

This work revealed strong competition between charge order and bulk superconductivity in LBCO. The microscopic mechanism may be related to the structure of the charge ordered state, which consists of a criss-cross pattern of stripes. This pattern induces a pair-density wave in which the modulations of the normal electron density and of superconducting Cooper pairs are coupled. As a result, the 90° turns from layer to layer induce a frustration of superconducting correlations along the perpendicular direction leading to quasi-two-dimensional behavior and low T_c. Defects perturb and suppress this pattern of nearly perfect cancellation and thereby lead to three-dimensional-correlations and an increase in T_c. — Dana Desonie

See: Maxime Leroux[1]*, Vivek Mishra[1], Jacob P. C. Ruff[2], Helmut Claus[1], Matthew P. Smylie[1], Christine Opagiste[3], Pierre Rodière[3], Asghar Kayani[4], G. D. Gu[5], John M. Tranquada[5], Wai-Kwong Kwok[1], Zahirul Islam[1], and Ulrich Welp[1]**, "Disorder raises the critical temperature of a cuprate superconductor," Proc. Natl. Acad. Sci. U.S.A. **116**(22), 10691. (May 28, 2019).
DOI: 10.1073/pnas.1817134116
Author affiliations: [1]Argonne National Laboratory, [2]Cornell University, [3]Université Grenoble Alpes, [4]Western Michigan University, [5]Brookhaven National Laboratory
Correspondence: * maxime@lanl.gov, ** welp@anl.gov

The experimental study at Argonne National Laboratory was supported by the U.S. Department of Energy (DOE) Office of Science-Basic Energy Science, Materials Sciences and Engineering Division. V.M. was supported by the Center for Emergent Superconductivity, an Energy Frontier Research Center, funded by the U.S. DOE Office of Science-Basic Energy Sciences. The work at Brookhaven National Laboratory was supported by the U.S. DOE Office of Science-Basic Energy Sciences, Division of Materials Sciences and Engineering, under Contract DE-SC0012704. Proton irradiation was performed at Western Michigan University. Beamline A2 at CHESS is supported by the National Science Foundation (NSF) and the National Institutes of Health/National Institute of General Medical Sciences under NSF Award DMR-1332208. This research used resources of the Advanced Photon Source, a U.S. DOE Office of Science User Facility operated for the DOE Office of Science by Argonne National Laboratory under Contract DE-AC02-06CH11357.

How Pressure Affects the 4f Electronic Structure of Light Lanthanides

The physics and chemistry of lanthanides are critically important to fields ranging from catalysis and the separations chemistry of nuclear waste, to cuprate superconductivity and bioscience, yet theoretical treatment of these materials remains a fundamental challenge. The difficulty stems primarily from the underlying nature of their f-electron states. In materials with partially filled f shells, the electrons occupy narrow, strongly correlated energy bands whose electronic interactions give rise to myriad exotic behaviors. An important example of the challenges involved in modeling emergent f-electron phenomena is the first-order phase transition that several lanthanides undergo at high pressures, resulting in a volume collapse (VC). Previous research at the APS demonstrated that controversies concerning the f-state changes underlying the VC of cerium (Ce) (Lipp et al. 2012) could be resolved by studying the pressure evolution of nonresonant x-ray emission spectroscopy (NXES) $L\gamma_1$ emission spectra both experimentally and theoretically. A team of researchers extended the applicability of this integrated methodology to the high-pressure, room temperature behavior of other early lanthanides: lanthanum (La), praseodymium (Pr), and neodymium (Nd). The experimental portions of both investigations were conducted at the APS.

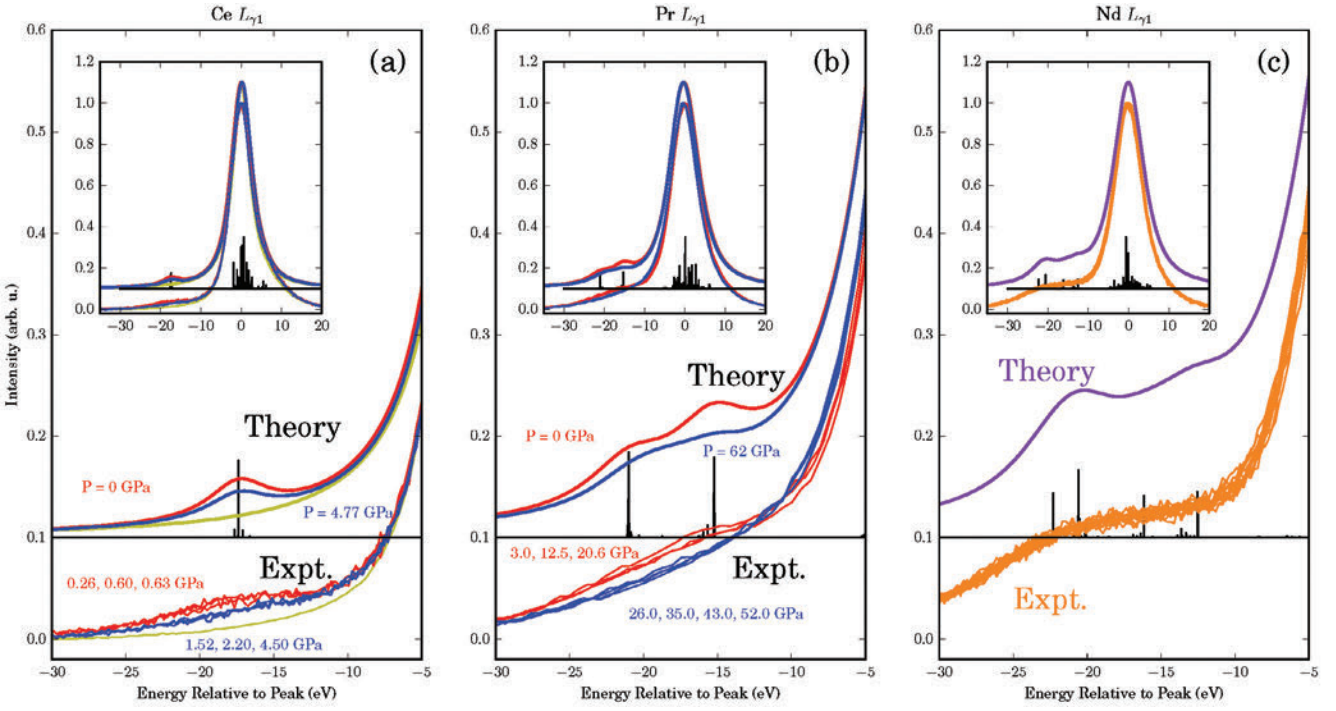

When subjected to high pressure, lanthanide crystal structures at room temperature usually pass through several high-symmetry transformations before transitioning to low-symmetry phases indicative of f-electron bonding. Neodymium, for example, reaches its low-symmetry structure entirely through smooth transformations, and therefore does not exhibit a VC transition. In contrast, Pr's low-symmetry transition is accompanied by a large VC (~10%). Ce is a unique case in that it exhibits an isostructural ($\gamma \rightarrow \alpha$) VC (15%) unassociated with a high-to-low symmetry transition.

Cerium's VC became controversial nearly as soon as it was discovered. The Hubbard-Mott (HM) and Kondo volume collapse (KVC) theories strongly disagree in their expectations of the behavior of the local $4f$ magnetic moment across the VC. The HM model theorizes that the localized $4f$ state of the γ phase transforms into a weakly correlated $4f$ band in the α phase, resulting in a quenching of the intrinsic $4f$ moment. By contrast, the KVC model predicts the onset of dynamic screening of a stable $4f$ moment with decreasing volume. Lipp et al. presented key new evidence directly validating the KVC model by combining data relating to the low-energy satellite feature of Ce's high-pressure NXES $L\gamma_1$ emission line with calculations based on an extended local atomic model of the physics responsible for the deep core-hole spectra. The close correspondence between theory and experiment allowed Lipp et al. to conclude that the VC begins with the sudden onset of $4f$-to-conduction band hybridization and that the magnetic moment per $4f$ electron largely persists in the collapsed phase, both of which are consistent with the Kondo hypothesis.

By way of extending the work of Lipp et al., researchers from the University of California, Davis, the University of Washington, Stanford University, SLAC National Accelerator Laboratory, and Lawrence Livermore National Laboratory compared the effects of increased pressure on the low-energy satellite features of the NXES $L\gamma_1$ emission lines of La, Ce, Pr, and Nd at ambient temperature, again both experimentally at the HPCAT-XSD x-ray beamline 16-ID-D at the APS and theoretically (Fig. 1).

The researchers found that the satellite peaks for Ce and Pr experienced sudden reductions concurrent with their respective VC transitions. These experimental results were supported by state-of-the-art modified atomic calculations which extended previous work performed on Ce alone to Pr and Nd.

The results suggest that changes to $4f$ occupation in early lanthanides are more consistently associated with the evolution of the satellite feature than the reduction of the $4f$ moment. The calculations provide crucial evidence of a clear relationship between the intensity of the satellite feature of the NXES $L\gamma_1$ emission line and $4f$-conduction band hybridization. Thus, despite the importance of Kondo screening of the moments in the volume collapse of Ce and Pr, the interpretation of their NXES spectra appears also to fit in a broader, common picture focused on $4f$ occupation. — Vic Comello

< Fig. 1. The shoulder peak (satellite) region of the experimental and calculated x-ray emission spectra for light lanthanide metals. The red (blue) curves in (a) for Ce and (b) for Pr are at low (high) pressure. In the theory spectra, low pressure is modeled using parameters at $P = 0$ GPa, and the blue curves are obtained using high-pressure parameters (4.77 GPa for Ce and 62 GPa for Pr). The yellow curves in (a) are results of lanthanum for a zero shoulder peak reference. (c) The Nd $L\gamma_1$ spectra do not change with pressure up to 43 GPa. Here, experimental and theoretical results are shown as orange and purple, respectively. The calculated spectra are shifted by +0.1. Insets show the full $L\gamma_1$ spectra. The vertical black lines are the calculated transition probabilities before broadening at zero pressure. From W.-T. Chiu et al., Phys. Rev. Lett. **122**, 066401 (2019). © 2019 American Physical Society

See: W.-T. Chiu[1], D. R. Mortensen[2], M. J. Lipp[3*], G. Resta[1], C. J. Jia[4], B. Moritz[4], T. P. Devereaux[4,5], S. Y. Savrasov[1], G. T. Seidler[2], and R. T. Scalettar[1], "Pressure Effects on the $4f$ Electronic Structure of Light Lanthanides," Phys. Rev. Lett. **122**, 066401 (2019). DOI: 10.1103/PhysRevLett.122.066401
Author affiliations: [1]University of California, Davis, [2]University of Washington, [3]Lawrence Livermore National Laboratory, [4]SLAC National Accelerator Laboratory, [5]Stanford University
Correspondence: * lipp1@llnl.gov

C. J. J., B. M., and T. P. D. at SLAC are supported by the U.S. Department of Energy (DOE) Office Science-Basic Energy Sciences, Materials Sciences and Engineering Division, under Contract No. DE-AC02-76SF00515 for the atomic multiplet calculations and interpretation. D. R. M. and G. T. S. acknowledge support from the DOE Office of Science-Basic Energy Sciences under Grant No. DE-SC0002194 and also by the Office of Science, Fusion Energy Sciences, under Grant No. DE-SC0016251. G. R. and S. Y. S. were supported by National Science Foundation Grant No. DMR-1411336 (S. Y. S). NXES studies were performed under the auspices of the U.S. DOE by Lawrence Livermore National Laboratory under Contract No. DE-AC52-07NA27344; and at HPCAT-XSD, whose operations are supported by the DOE-National Nuclear Security Administration under Award No. DE-NA0001974 and DOE-Basic Energy Sciences under Award No. DE-FG02-99ER45775, with partial instrumentation funding by the U.S. National Science Foundation. The theoretical work of W.-T. C. and R. T. S. was supported by the Stewardship Sciences Academic Alliance program under Grant No. DE-NA0002908. Portions of the computational work were performed using the resources of the National Energy Research Scientific Computing Center supported by the DOE Office of Science under Contract No. DE-AC02-05CH11231. This research used resources of the Advanced Photon Source, a U.S. DOE Office of Science User Facility operated for the DOE Office of Science by Argonne National Laboratory under Contract DE-AC02-06CH11357.

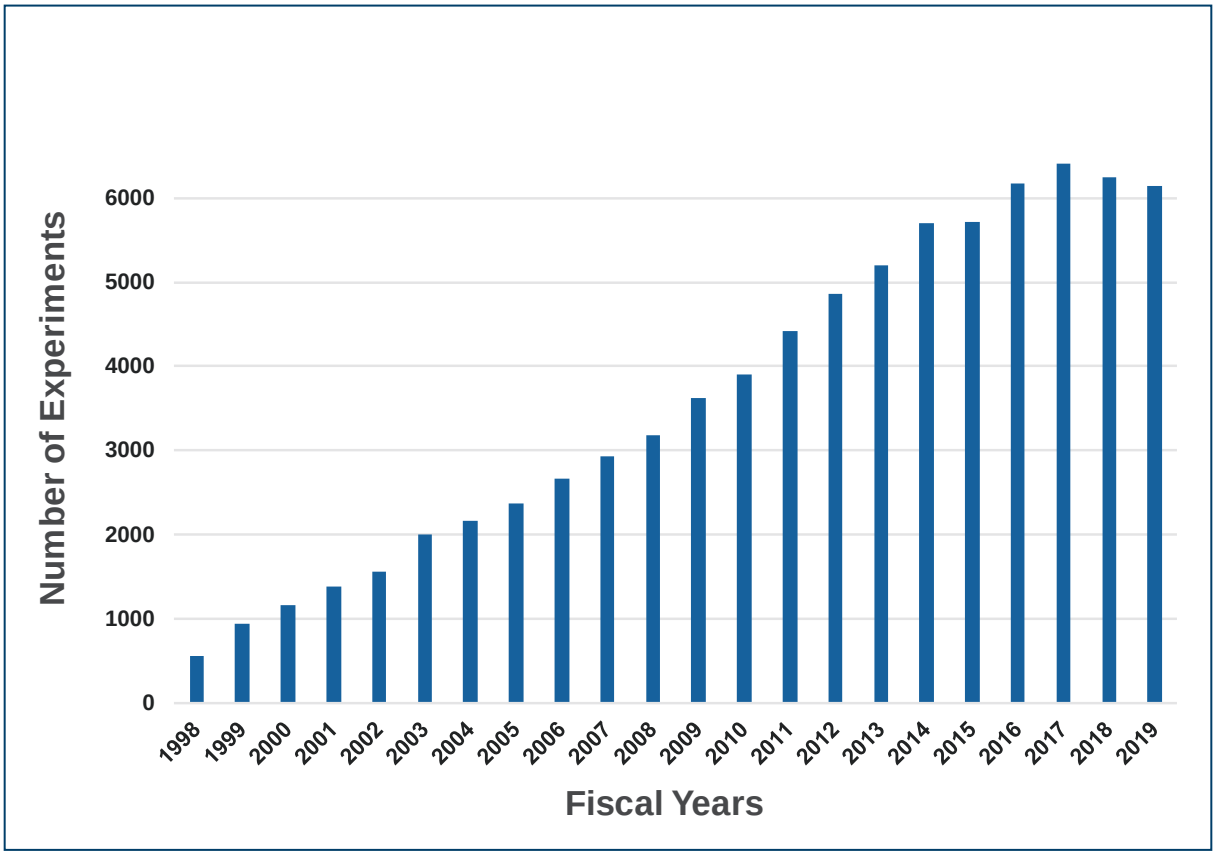
Number of Experiments
6000
5000
4000
3000
2000
1000
0
1998
1999
2000
2001
2002
2003
2004
2005
2006
2007
2008
2009
2010
2011
2012
2013
2014
2015
2016
2017
2018
2019
Fiscal Years

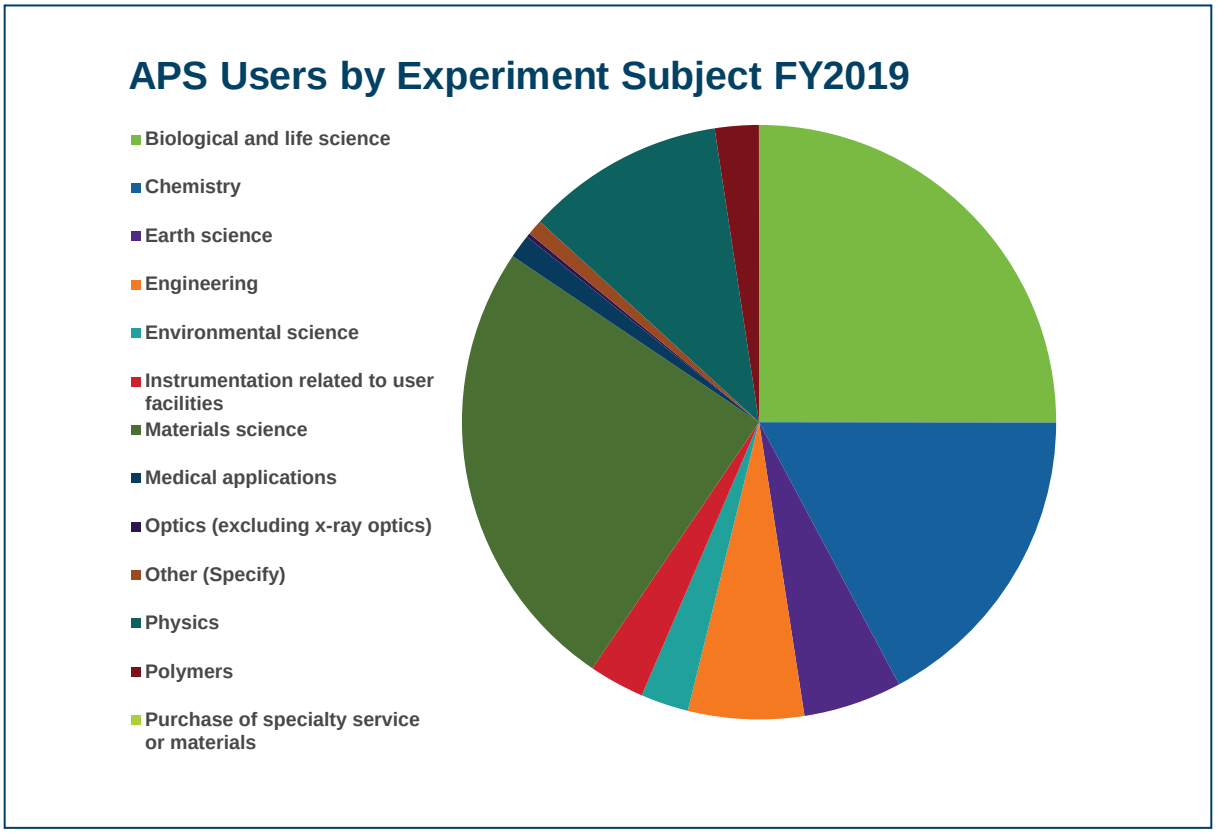
APS Users by Experiment Subject FY2019
Biological and life science
Chemistry
Earth science
Engineering
Environmental science
Instrumentation related to user facilities
Materials science
Medical applications
Optics (excluding x-ray optics)
Other (Specify)
Physics
Polymers
Purchase of specialty service or materials

Engineering Materials and Applications

Superionic Crystals Can Make Better Rechargeable Batteries

There is a great need for rechargeable batteries that are safer and more efficient than the current standard, lithium-ion batteries. One promising area of research is in solid-state electrolytes such as superionic crystals, in which part of the material is solid and part is liquid at the same time, which allows electrical flow. These superionic crystals can also help harvest waste heat to produce electricity with thermoelectric modules. In this work, a superionic crystalline material, $CuCrSe_2$, was bombarded with x-rays at the APS, and with neutrons at the Spallation Neutron Source (SNS), to reveal how the copper ions could behave as a liquid. With a better understanding of superionic materials, researchers can get closer to developing better and safer personal electronics.

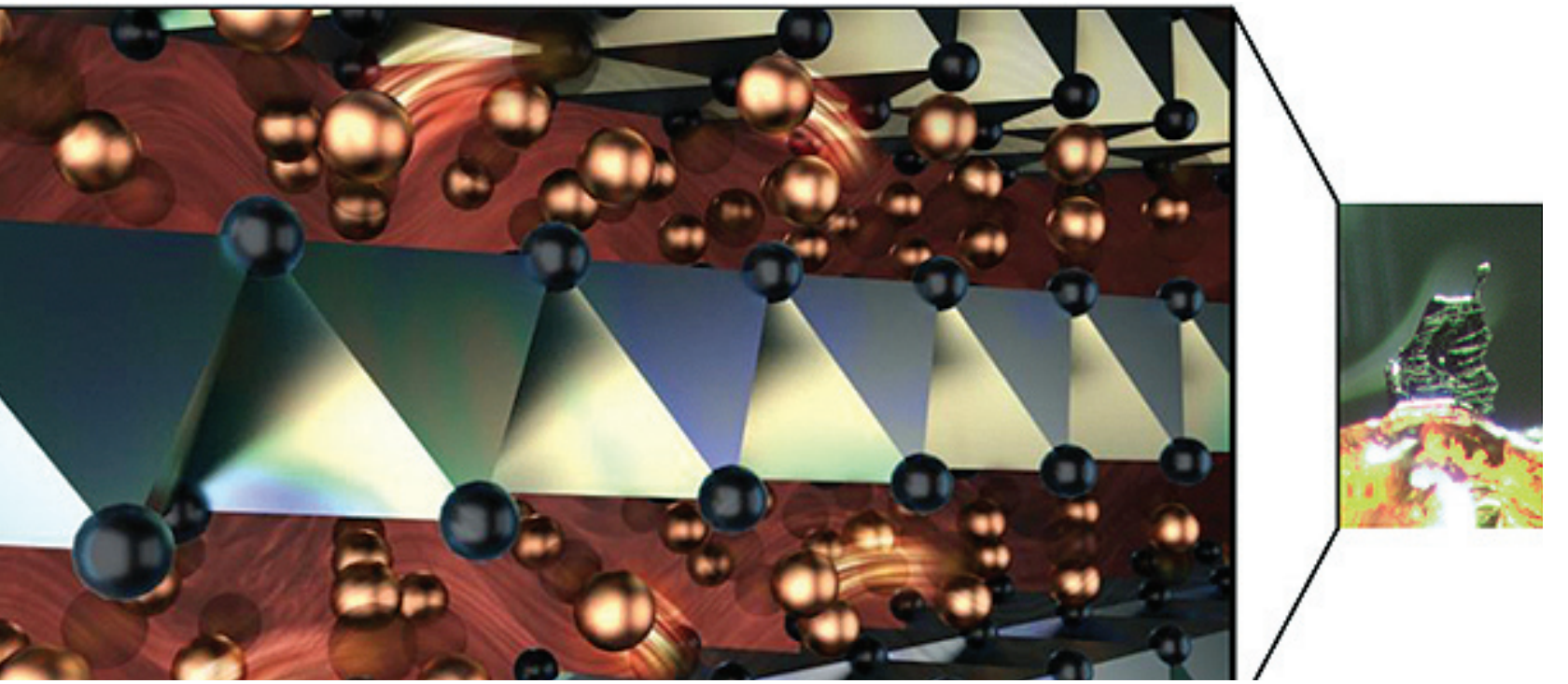

Fig. 1. An artist's rendition of the intriguing superionic crystalline structure of $CuCrSe_2$, which has copper ions that flow like a liquid between solid atomic layers of chromium and selenium. To the right is a photograph of the tiny $CuCrSe_2$ single crystal used for IXS studies. The sample is a thin flake approximately 25-µm thick, and less than 1-mm wide. Credit: Oak Ridge National Laboratory/Jill Hemman

Rechargeable lithium-ion batteries are currently the best option for use in portable electronics, from phones to laptops. In these batteries, liquid lithium electrolyte flows from the negative to the positive electrode during discharge and from the positive to the negative during charging. While these batteries are essential for modern electronics, they are not perfect for their job. Lithium-ion batteries have difficulty retaining a charge and operating at high and low temperatures, and they have been known to catch fire or explode. As a result, researchers are continually looking for better electrolytic materials that are safer, less expensive, longer-lived, more energy dense, and faster charging.

One substance of great interest are superionic crystals, a rare class of materials that is a cross between a liquid and a solid. At a given temperature, some of the atoms in these materials retain a rigid crystalline structure, while others liquify and can flow through the solid crystalline structure. These materials show differences in atomic dynamics; the atoms that flow in a liquid follow stochastic diffusive dynamics, while remaining affixed to well-defined lattice sites in a crystalline solid.

In this study, researchers employed DOE Office of Science user facilities to conduct experiments and simulations to better understand the atomic dynamics of one superionic material, $CuCrSe_2$. The researchers powdered samples of the material and heated it to above 190° F. The researchers then performed inelastic neutron scattering experiments on an 8-g sample with the CNCS and ARCS time-of-flight spectrometers at the SNS at Oak Ridge National Laboratory. The powerful neutrons revealed a wide-scale view, in which solid chromium (Cr) and selenium (Se) vibrated in the atomic structure and Cu ions jumped randomly within the Cr and Se structure. This flow appears to occur at about the same speed as liquid water molecules move.

Inelastic x-ray measurements were performed on minute single crystals of $CuCrSe_2$ (Fig. 1) at the HERIX spectrometer at the XSD 30-ID-C beamline of the APS. The high-resolution x-rays depicted a narrower but more detailed view of the structure. Scaffolded vibrations enabled shear waves to propagate, revealing that the structure was solid, even in the presence of the liquid sublayer.

Subsequent simulations at the National Energy Research Scientific Computing Center at Lawrence Berkeley National Laboratory allowed the researchers to directly compare the results of the neutron and x-ray spectroscopy experiments. The simulations showed that below 190° F, the Cu was trapped, vibrating in pockets of the scaffold structure. Above 190° F, the Cu hopped randomly between available sites, allowing it to flow through the solid crystal. Additional research is needed to reveal the interactions of the Cu ions as the scaffold sites become occupied.

These findings will allow researchers to better understand the atomic dynamics that occur in matter in the intermediate state between liquid and solid and guide them in their quest to create high-performance solid-state electrolytes. Superionic compounds with ultralow conductivities will be useful for both thermoelectric applications and in rechargeable batteries that are safer and more efficient for use in personal electronics. — Dana Desonie

See: Jennifer L. Niedziela[1,2‡*], Dipanshu Bansal[2**], Andrew F. May[1], Jingxuan Ding[2], Tyson Lanigan-Atkins[2], Georg Ehlers[1], Douglas L. Abernathy[1], Ayman Said[3], and Olivier Delaire[2***], "Selective breakdown of phonon quasiparticles across superionic transition in $CuCrSe_2$," Nat. Phys. **15**, 73 (January 2019). DOI: 10.1038/s41567-018-0298-2
Author affiliations: [1]Oak Ridge National Laboratory, [2]Duke University, [3]Argonne National Laboratory ‡Present address: Oak Ridge National Laboratory
Correspondence: * niedzielajl@ornl.gov, ** dipanshu.bansal@duke.edu, *** olivier.delaire@duke.edu

We are grateful to J. Z. Tischler (APS) for algorithms enabling deconvolution of the energy resolution from the inelastic x-ray phonon scattering data. We would also like to acknowledge technical support from D. Dunning, T. Russell, and S. Elorfi at the SNS. JJ.L.N., J.D., and T.L.-A. were supported as part of the S3TEC EFRC, an Energy Frontier Research Center funded by the U.S. Department of Energy (DOE) Office of Science-Basic Energy Sciences under award no. DE-SC0001299. D.B. and O.D. were supported by the U.S. DOE Office of Science-Basic Energy Sciences, Materials Sciences and Engineering Division, under the Early Career Award no. DE-SC0016166 (principal investigator O.D.). A.F.M. was supported by the U.S. DOE Office of Science-Basic Energy Sciences, Materials Sciences and Engineering Division. The research at Oak Ridge National Laboratory's Spallation Neutron Source was sponsored by the Scientific User Facilities Division, Basic Energy Sciences, U.S. DOE. *Ab initio* molecular dynamics calculations were performed using resources of the National Energy Research Scientific Computing Center, a U.S. DOE Office of Science User Facility supported by the Office of Science of the U.S. DOE under Contract no. DE-AC02-05CH11231. Density functional theory simulations for this research used resources of the Oak Ridge Leadership Computing Facility at the Oak Ridge National Laboratory, which is supported by the Office of Science of the U.S. DOE under Contract no. DE-AC05-00OR22725. This research used resources of the Advanced Photon Source, a U.S. DOE Office of Science User Facility operated for the DOE Office of Science by Argonne National Laboratory under contract no. DE-AC02-06CH11357.

A Touch of Salt Stabilizes Silicon Anodes in Li-Ion Batteries

One way of improving the energy density of lithium-ion (Li-ion) batteries is to replace the standard graphite-based anodes with silicon (Si). Advances in performance are vitally important because Li-ion batteries are increasingly used for powering consumer electronics, all-electric and hybrid vehicles, and for industrial energy storage. Though highly promising, silicon anodes degrade markedly over a short number of battery charge/discharge cycles. In this study, researchers demonstrated that adding tiny amounts of salts containing magnesium (Mg) or certain other doubly or triply charged elements can greatly reduce silicon anode degradation over a large number of charge/discharge cycles. To gain insight into the mechanisms promoting the observed silicon anode stabilization, a number of experimental techniques were applied to samples at Argonne including nuclear magnetic resonance, electron microscopy, and x-ray diffraction. High-resolution x-ray diffraction (HRXRD) data gathered at the APS revealed key nanoscale changes within Si anodes due to the added salts. The research team's findings are essential in the effort to incorporate more silicon into practical Li-ion batteries, which would permit greater energy storage in lighter batteries.

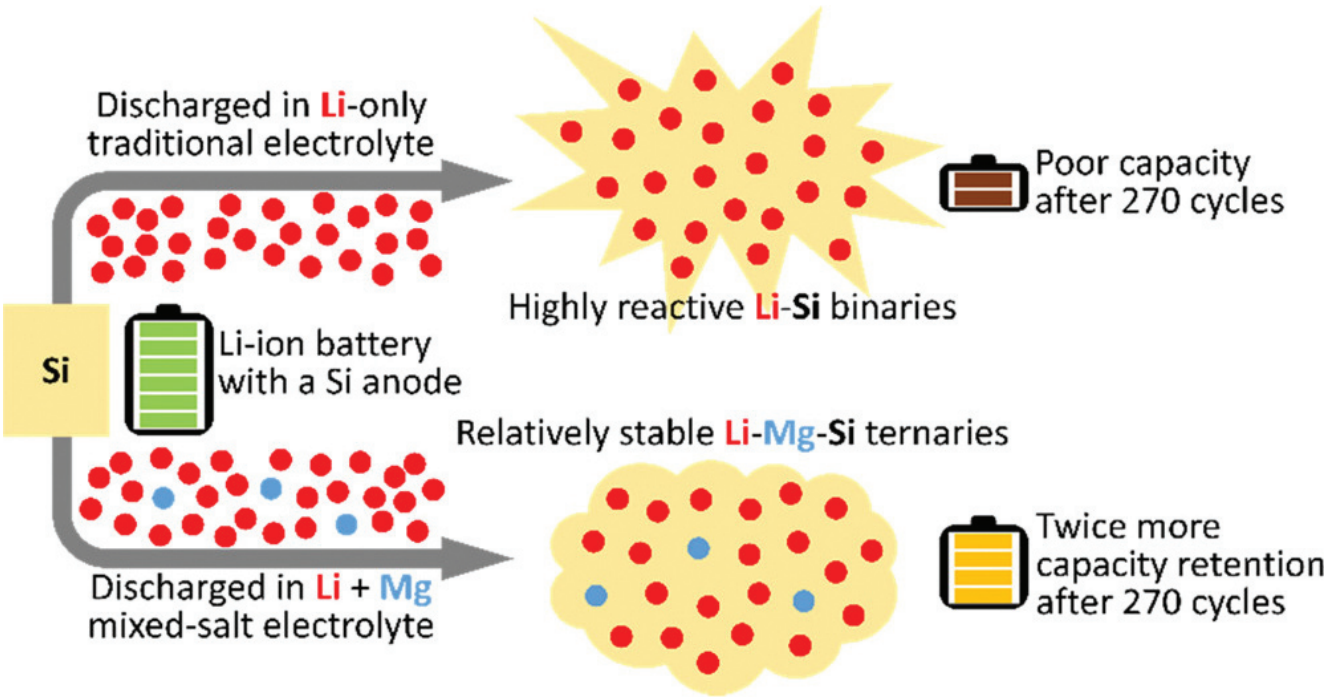

Today's sophisticated Li-ion batteries all share three fundamental components: a negative and positive electrode (the anode and cathode, respectively) and an electrolyte. While many different anode materials are available, graphite is by far the most commonly used. In a fully charged Li-ion battery, the maximum amount of lithium ions reside between layers within the graphite anode. As power is drawn a chemical reaction releases lithium ions from the anode into the electrolyte and toward the cathode. Simultaneously, electrons from the anode power an external circuit, such as a light or motor. During recharging, the process reverses and lithium ions incorporate back into the anode.

In comparison to graphite, silicon has around a 10-fold greater capacity for incorporating lithium ions, making it a highly desirable anode material. Unfortunately, two major obstacles exist. First, as silicon absorbs and releases lithium ions, it swells and shrinks dramatically, causing its lattice to crack and disintegrate. This disintegration greatly reduces battery performance. However, considerable progress is being made in producing silicon anodes that are less susceptible to disintegration. This technology is still being developed for commercialization.

The other major issue for silicon anodes stems from contamination by molecules within the electrolyte. Most Li-ion electrolytes consist of lithium salts and organic compounds. Repeated charge/discharge cycles lead to reactions between the silicon anode and the lithium salts that result in compounds of lithium and silicon. These lithium silicides are highly reactive and continually reduce the electrolyte's organic components and consume key battery ingredients, which over time significantly reduces battery performance. Resolving this reactivity problem was the main focus of this research.

In the first stage of the study, researchers added a small proportion of Mg salt to a common Li-ion electrolyte. After numerous charge/discharge cycles, the magnesium salt was shown to significantly reduce the detrimental reactions between lithium silicides and the electrolyte's organic components. The researchers also examined the effect of other salts (composed of calcium, aluminum, or zinc) on battery performance. With the exception of the zinc salt, the battery cells incorporating a secondary salt performed dramatically better as compared to a test cell using an ordinary electrolyte. The stark difference in electrolyte reactivity and battery cell performance is illustrated in Fig. 1.

< Fig. 1. Schematic depicting the impact of adding a secondary salt of Mg to a lithium-ion battery with a Si anode. Lithium ions are represented as red dots, while magnesium ions are blue. The upper half shows that a battery with only lithium ions forms more reactive lithium-silicon (Li-Si) compounds, while the lower half reveals that adding a small number of magnesium ions in the electrolyte results in ternary (three-part) compounds of lithium-magnesium-silicon (Li-Mg-Si) that are far less reactive, enabling the battery to successfully withstand many more charge/discharge cycles.

Adding a secondary salt also dramatically reduced anode degradation. X-ray tests were performed during charging using an electrolyte with magnesium salt added. A formation of a significantly less reactive magnesium doped lithium silicide as ternary phase was identified using HRXRD at the XSD 11-BM-B beamline at the APS. Furthermore, the magnesium also helped reduce the reactions of the new surfaces generated during the large swings between expansion and contraction that typically occurs in silicon anodes during cycling. Supportive scanning electron microscopy and transmission electron microscopy studies were performed at the Argonne Center for Nanoscale Materials.

Overall, this study demonstrated that adding salt, as a magnesium or calcium salt, can reduce the formation and detrimental effects of highly reactive lithium silicides in both the electrolyte and silicon anode. These beneficial effects were obtained with only a negligible decrease in battery performance. Tests also demonstrated that no harmful compounds formed during the experiments. The two highest-performing salts in this study, magnesium and calcium, are plentiful, inexpensive, and environmentally safe. Moreover, it is straightforward to incorporate these secondary salts into electrolytes for industrial-level battery production. — Philip Koth

See: Binghong Han*, Chen Liao, Fulya Dogan, Stephen E. Trask, Saul H. Lapidus, John T. Vaughey**, and Baris Key***, "Using Mixed Salt Electrolytes to Stabilize Silicon Anodes for Lithium-Ion Batteries via in Situ Formation of Li–M–Si Ternaries (M = Mg, Zn, Al, Ca)," ACS Appl. Mater. Inter. **11**, 29780 (2019).
DOI: 10.1021/acsami.9b07270
Author affiliation: Argonne National Laboratory
Correspondence: * hbhtiancai@gmail.com,
** vaughey@anl.gov, *** bkey@anl.gov

The authors would like to thank Brian Cunningham and David Howell from the Vehicle Technologies Program, at the U.S. Department of Energy, Office of Energy Efficiency and Renewable Energy for their support. The work at Argonne National Laboratory was supported by the U.S. Department of Energy (DOE) Office of Vehicle Technologies, under Contract No. DE-AC02-06CH11357. The electrodes in this article were fabricated at the Argonne Cell Analysis, Modeling, and Prototyping (CAMP) Facility. The Center for Nanoscale Materials and the Advanced Photon Source are supported by the U.S. DOE Office of Science-Basic Energy Sciences, under Contract No. DE-AC02-06CH11357.

Observing Li-Ion Gradients to Help Batteries Make the Grade

Lithium-ion (Li-ion) batteries have become the dominant energy source for modern electronic devices. They are also used to power electric cars. While gasoline-fueled cars can refill in a matter of minutes, electric vehicles require anywhere from 30 min to 12 h to charge. For wider adoption in electric vehicles, Li-ion batteries will need to have shorter charging times closer to consumers' expectations. However, charge rates higher than 1C (a full charge in 1 h) can quickly degrade performance, reducing capacity, cycle life, and thermal stability. Research at the APS is providing new information about the root cause of this degradation and, thus, clues to a remedy.

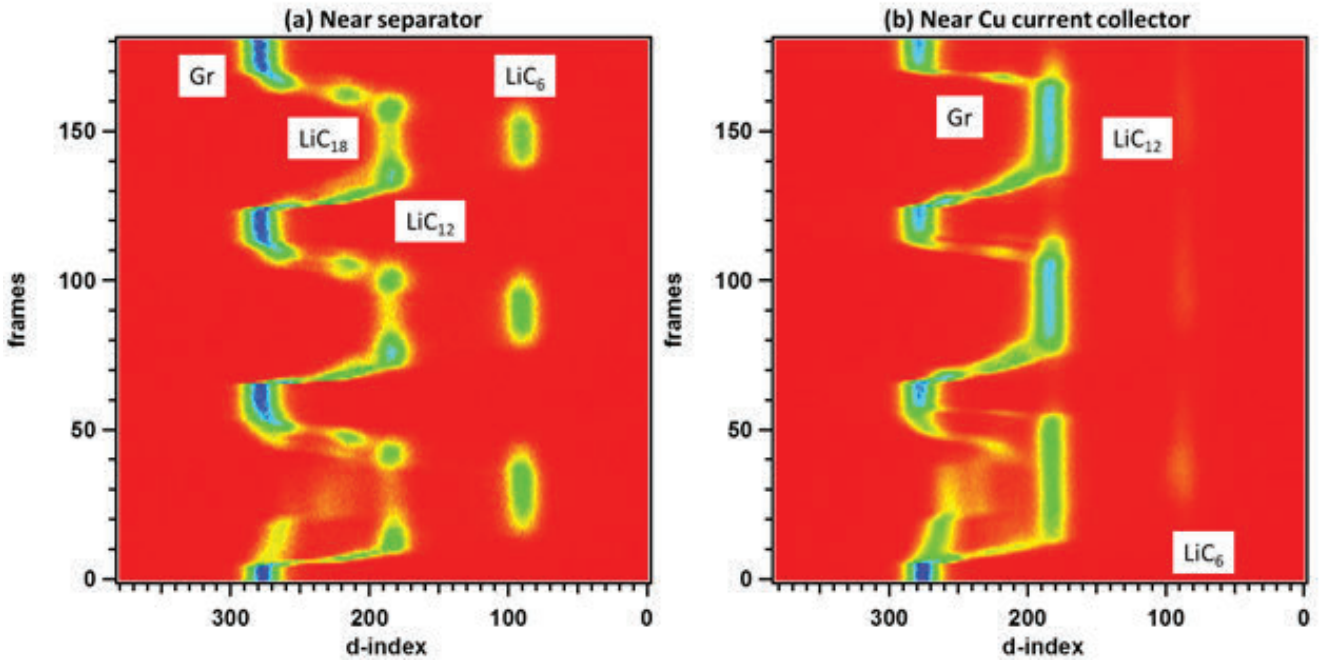

Fig. 1. False-color representation of charge and discharge in a graphite electrode near the microporous separator (a) and near the copper current collector (b). Three cycles of charge and discharge are stacked up vertically from the bottom to the top (frames), while the x-axis shows d-spacing indices. Greater lithiation corresponds to a smaller d-index. Initially only graphite (Gr) peaks are observed; as the cell is charged, the graphite electrode goes through a succession of dilute phases until LiC_{12} is formed (one can see a distinct "blot"); further charge yields the LiC_6 phase. Observe the asymmetry between charge and discharge and considerable difference across the cell [panel (a) vs. panel (b)], suggesting phase oversaturation and rapid spinodal decomposition during discharge.

During charging in these batteries, lithium ions are extracted (deintercalated) from a lithiated transition metal oxide in the cathode, where these cations form sheets of positive charge between the oxide layers, and inserted (intercalated) between carbon layers in graphite (Gr) in the anode. During discharge, this process reverses. The Gr and oxide are contained in porous electrode matrices infused with liquid electrolyte. This matrix holds the electrochemically active particles and also provides a conductive path for the electrons to reach current collectors.

Theoretical studies attribute the detrimental effects of high rate charge to lithium metal plating on the Gr, kinetic losses, and lithium ion concentration gradients that develop in both the electrolyte filling the matrix pores and in the porous electrodes. The concentration gradients are problematic for a number of reasons. First, they polarize the cell, lowering capacity by causing the cell to reach its cut-off voltage before all the lithium is fully extracted from the cathode. Second, heterogenous lithiation can lower the anode's potential, creating conditions that cause lithium plating. Finally, these gradients can facilitate structural stresses within the particles of the active material, causing fracture, and in the electrode matrix at large, causing the coating to peel off the current collector.

The higher the current flowing through the cell, the steeper the lithium-ion gradients, and the greater their detrimental effect on battery performance and life. Although studies have used many means to model these concentration gradients, few have directly measured them within a working battery.

To fill this knowledge gap, researchers from Argonne and the University of Delaware used the XSD 6-BM-A beamline at the APS to peer into a working Li-ion battery using the energy dispersive x-ray diffraction (EDXRD) technique. The team created "movies" of lithiation and delithiation in different sections of the cell. The EDXRD technique allowed them to quantify the lithium gradients that formed in the battery's porous graphite electrode during cycling at a 1C rate, showing that the conditions for polarization and plating occur even at this modest rate.

The researchers performed their experiments using a standard Li-ion coin cell. Before and during cell operation, the team carried out EDXRD to observe the pristine electrodes and compare them with the conditions that developed during cycling. The x-ray photons from the beamline penetrated through the stainless-steel casing of the coin cell, forming diffraction patterns that identified ordered phases in the Gr layers.

Their results (Fig. 1) show that in the initial stages of charging, the Li content is nearly uniform across the anode. However, as the cell is charged further, a concentration gradient develops, with more lithium present near the electrode surface than at the back. This negative gradient remains the entire time the cell is charging, with lithiation taking time to reach the back of the electrode matrix. During discharge, Li depletion occurs near the surface and gradually spreads into the back of the cell. However, this process does not exactly mirror that of lithiation—during the majority of the cycle, the Li content remains significantly higher in the surface of the electrode. These conditions make Li plating and structural stresses difficult to avoid, even when charging is relatively slow.

The authors note that better knowledge of this imbalance between inhomogeneity in Li insertion and depletion adds insight to why these batteries quickly fail over time at higher charging rates. Eventually, they suggest, researchers may be able to find ways to better design Li-ion cells to protect them from this inherent vulnerability.

— Christen Brownlee

See: Koffi P. C. Yao[1,2], John S. Okasinski[1], Kaushik Kalaga[1], Ilya A. Shkrob[1], and Daniel P. Abraham[1]*, "Quantifying lithium concentration gradients in the graphite electrode of Li-ion cells using *operando* energy dispersive X-ray diffraction," Energy Environ. Sci. **12**,656 (2019). DOI: 10.1039/c8ee02373e
Author affiliations: [1]Argonne National Laboratory, [2]University of Delaware
Correspondence: * abraham@anl.gov

Support from the U.S. Department of Energy (DOE) Office of Vehicle Technologies, is gratefully acknowledged. The electrodes used in this article are from Argonne's Cell Analysis, Modeling and Proto-typing (CAMP) Facility, which is supported within the core funding of the Applied Battery Research (ABR) for Transportation Program. We are grateful to our many colleagues (Stephen Trask, Bryant Polzin, Andrew Jansen, Dennis Dees, Jonathan Almer and Andrew Chuang) for their support and guidance during this eS̆ort. This research used resources of the Advanced Photon Source, a U.S. DOE Office of Science User Facility operated for the DOE Office of Science by Argonne National Laboratory under Contract DE-AC02-06CH11357.

The Prohibitive Structural and Voltage Effects Associated with Oxygen-Anion Redox

As society has continued to trend toward a more sustainable future, the use of rechargeable batteries has concomitantly increased over time. However, as this technology has become more widespread, its demands have also grown. Compared to contemporary batteries, an ideal, next-generation rechargeable battery would hold a charge for an even longer period of time, have an overall greater lifespan, and be able to power much larger equipment. Anionic oxygen redox of lithium-based crystals is one potential strategy that could meet these pressing demands. Using the APS, researchers were able to carefully map out the steps involved in oxygen-anion redox. Moreover, the team deduced why known, prohibitive issues regarding this application have historically occurred. Shedding light on this important energy system helps make the future of rechargeable batteries seem even brighter.

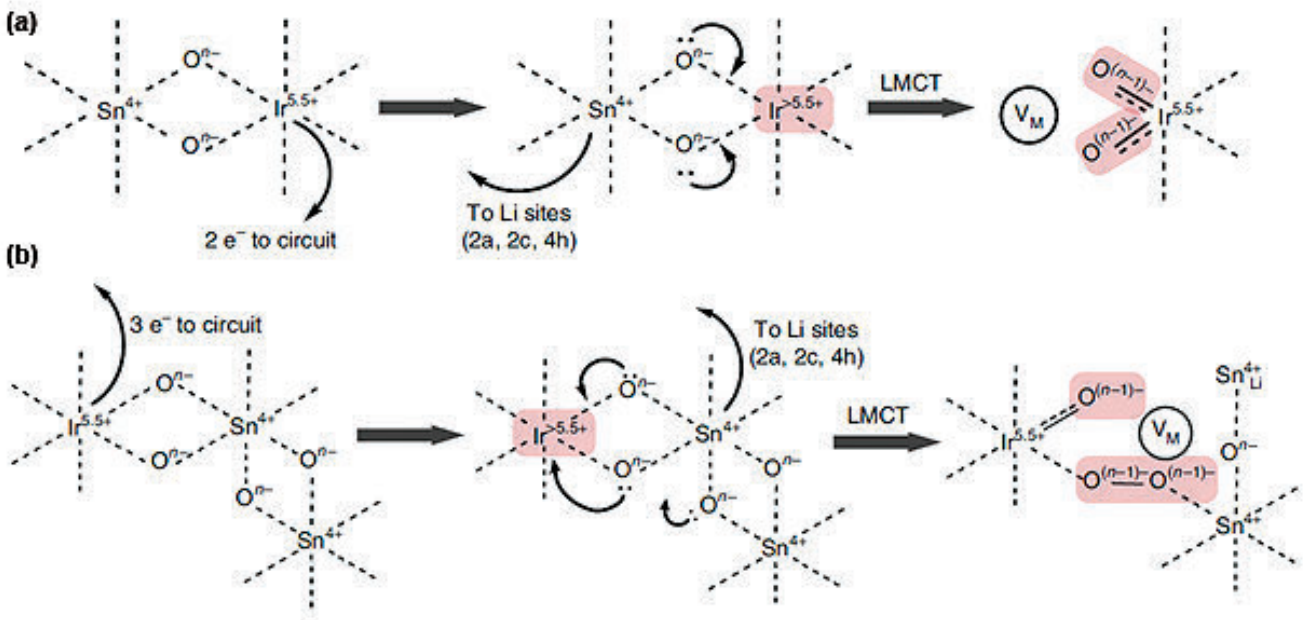

Fig. 1. The proposed stepwise electronic mechanism of cation migration and ligan-to-metal charge transfer-mediated anion redox in $Li_2Ir_{1-y}Sn_yO_3$. From J. Hong et al., Nat. Mater **18**, 256 (March 2019). © 2019 Springer Nature Limited

While anionic oxygen redox has shown considerable promise in the development of materials that would provide significantly increased power capacity, this application faces several challenges. Two electrochemical phenomena, voltage hysteresis and voltage fade, are associated with this type of reaction and currently preclude its widespread use. In addition, the oxidation of oxygen is highly correlated with local structural transformations. Previous research suggests that the surface lattice structure of the conductive material is mostly responsible for these shortcomings. To learn more about this process and its potential to revamp rechargeable batteries, scientists from Stanford University, the University of California, Berkeley, SLAC National Accelerator Laboratory, Lawrence Berkeley National Laboratory, and Argonne worked together to perform cutting edge-research using lithium iridate (Li_2IrO_3), a model compound in which the anion redox properties can be tuned by tin substitution.

Using this system, the team conducted a series of experiments. This included synchrotron x-ray diffraction of crystal powders before and after experiencing an electrochemical charging cycle, which is similar to what a rechargeable battery would be subjected to. These experiments were performed at XSD beamline 11-1D-B at the APS, and at beamline 2-1 at the Stanford Synchrotron Radiation Lightsource at the SLAC National Accelerator Laboratory. These measurements involved using specialized computer programs to fit the diffractions created when hitting a crystalline powder with an x-ray in order to build an atomic model of a compound. The researchers were able to show how disorder in the crystal evolved as oxygen is oxidized.

X-ray total scattering studies were also conducted at beamline 11-1D-B at the APS. Following this data collection, and in order to measure the relative distances between atoms, an atomic pair distribution function analysis was conducted. This revealed that the distances between Ir-O and O-O were short and were able to influence their local environment. The Ir L_3 edge was also measured using x-ray absorption near edge structure at XSD beamline 20-BM-B at the APS. This is a powerful technique that can measure precise details in x-ray absorption spectra, including elements, coordination sites, valence electrons, and structural distortions. Yet another technique utilized was resonant inelastic x-ray scattering, which was conducted at the Advanced Light Source at Lawrence Berkeley National Laboratory. This is an x-ray spectroscopy tool that can analyze the types of specific bonds that transition metals, like Ir, form. More broadly, this technique can probe the molecular electronic structure of a given material.

Using these methods, the authors discovered the specific pathway in which the crystal disorders during anion redox. This is due to the types of interactions that were found to occur, such as the de-coordination of oxygen. With the combined suite of experimental techniques, the team concluded by proposing the stepwise electronic mechanism shown in Fig. 1.

Looking forward to the future, the authors concluded that the development of an oxygen redox system that could avoid these undesirable properties has exciting, beneficial implications for a variety of applications, including rechargeable batteries. — Alicia Surrao

See: Jihyun Hong[1,2‡], William E. Gent[1,3], Penghao Xiao[3], Kipil Lim[1,2], Dong-Hwa Seo[4], Jinpeng Wu[2,3], Peter M. Csernica[1], Christopher J. Takacs[2], Dennis Nordlund[2], Cheng-Jun Sun[5], Kevin H. Stone[2], Donata Passarello[2], Wanli Yang[3], David Prendergast[3], Gerbrand Ceder[3,4*], Michael F. Toney[2**], and William C. Chueh[1,2***], "Metal–oxygen decoordination stabilizes anion redox in Li-rich oxides," Nat. Mater. **18**, 256 (March 2019).
DOI: 10.1038/s41563-018-0276-1
Author affiliations: [1]Stanford University, [2]SLAC National Accelerator Laboratory, [3]Lawrence Berkeley National Laboratory, [4]University of California, Berkeley, [5]Argonne National Laboratory
[‡]Present address: Korea Institute of Science and Technology (KIST)
Correspondence: * gceder@berkeley.edu,
** mftoney@slac.stanford.edu,
*** wchueh@stanford.edu

This research was supported by the Assistant Secretary for Energy Efficiency and Renewable Energy, Office of Vehicle Technologies, Battery Materials Research Program, U.S. Department of Energy (DOE). W.E.G. was supported additionally by the Advanced Light Source Doctoral Fellowship and the Siebel Scholars programme. K.L. was supported additionally by the Kwanjeong Education Foundation Fellowship. Use of the Advanced Light Source was supported by the DOE Office of Science-Basic Energy Sciences under contract no. DE-AC02-05CH11231. Use of the Stanford Synchrotron Radiation Lightsource was supported by the U.S. DOE Office of Science-Basic Energy Sciences under contract no. DE-AC02-76SF00515. Work at the Molecular Foundry was supported by the U.S. DOE Office of Science-Basic Energy Sciences under contract no. DE-AC02-05CH11231. Part of this work was performed at the Stanford Nano Shared Facilities, supported by the National Science Foundation under award ECCS-1542152. The computational work was funded by the NorthEast Center for Chemical Energy Storage, an Energy Frontier Research Center, supported by the U.S. DOE Office of Science-Basic Energy Sciences under award no. DE-SC0012583. G.C. also thanks the China Automotive Battery Research Institute and the General Research Institute for NonFerrous Metals for financial support on oxygen redox in cathode materials. This research used resources of the Advanced Photon Source, a U.S. DOE Office of Science User Facility operated for the DOE Office of Science by Argonne National Laboratory under Contract DE-AC02-06CH11357, and the Canadian Light Source and its funding partners.

Going Under the Surface of Laser-Induced Spattering

Researchers using the APS have elucidated in detail the laser-induced spattering behavior in the common titanium alloy Ti-6Al-4V. Combining image analysis with numerical simulations, they were, for the first time, able to connect the visible spattering above the metal surface with the previously-unseen keyhole dynamics below and inside the metal that cause the phenomenon, providing a substantial step forward in our understanding of laser-induced spattering.

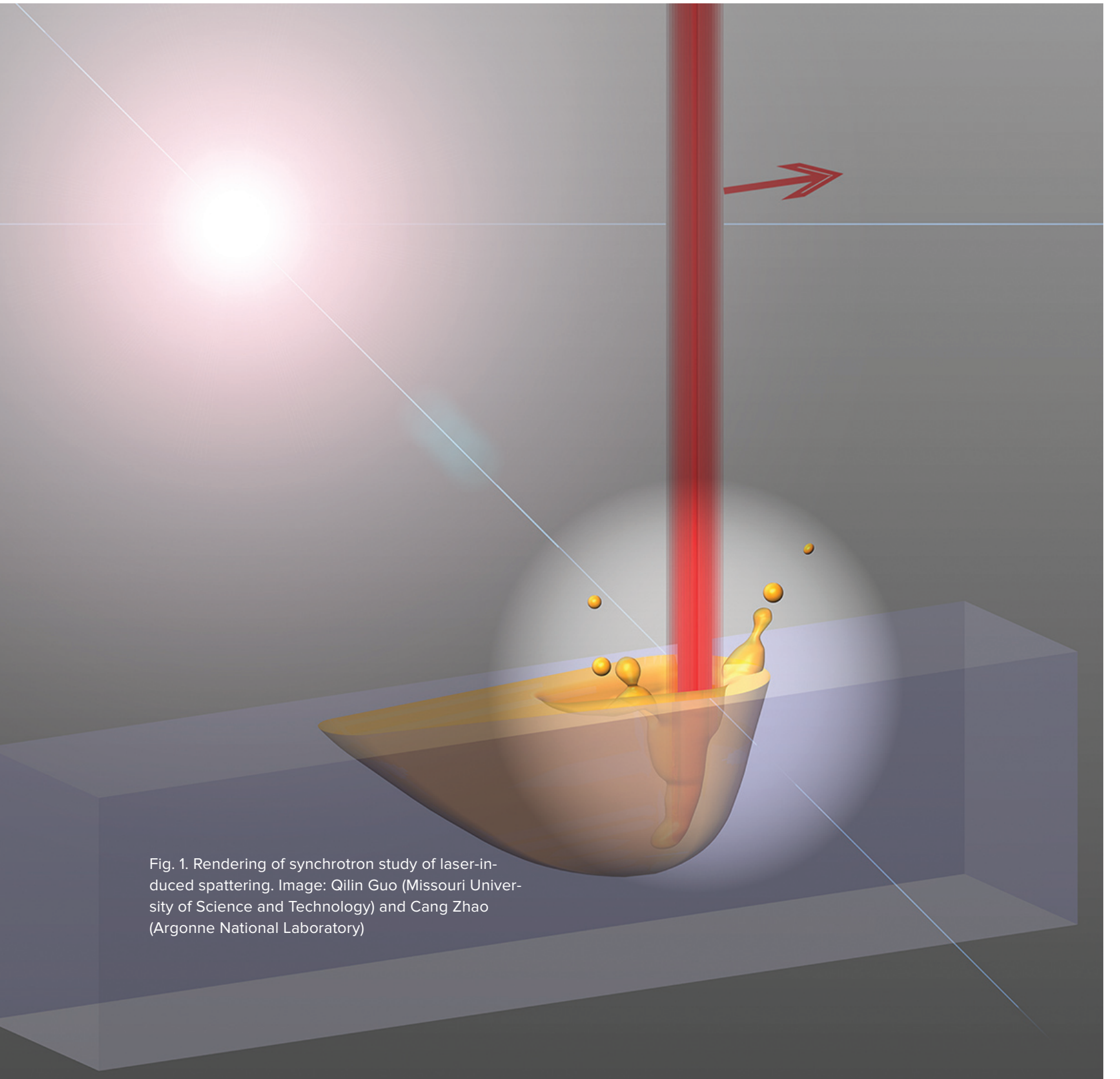

Fig. 1. Rendering of synchrotron study of laser-induced spattering. Image: Qilin Guo (Missouri University of Science and Technology) and Cang Zhao (Argonne National Laboratory)

The power, versatility, and exquisite precision of lasers have made them an indispensable tool for a diverse range of manufacturing processes, including welding, machining, and more recently, additive manufacturing (AM) or three-dimensional (3-D) printing techniques. But sometimes even the most sophisticated techniques can introduce new problems that can impair their effectiveness. In laser manufacturing and processing, such a problem is spattering, in which hot liquid metal droplets from the beam's path are strewn from the melt pool (Fig. 1). These droplets, or spatters, might be pretty to observe but are a headache to manufacturers; they solidify along the metal surface, creating agglomerations and impurities that must be removed, not to mention craters and defects that compromise the material's structural integrity and properties. Yet despite years of research, a complete understanding of the mechanisms of laser-induced spattering and how to control it has remained elusive, mostly because of the difficulty of adequately probing the process in real time with only optical and infrared imaging.

The advantages of micrometer spatial resolution, sub-nanosecond temporal resolution, an ultra-high millions-per-second frame rate, and the penetrating power of the extremely bright x-rays allowed the experimental team working at the XSD 32-ID-B x-ray beamline of the APS to visualize unprecedented details in subsurface processes. The team, from Argonne, the Missouri University of Science and Technology, and the University of Utah defined the laser-induced spattering phenomenon as consisting of four separate events, all of which occur over a span of several microseconds.

At first, the initial J-shaped keyhole under the laser changes to a reverse-triangle-like shape as several small protrusions form near the rim of the front keyhole wall, then flow downward. In the second event, a following protrusion rapidly grows into a tongue-like one, with a miniature keyhole forming on top, driven by directional vapor plume collisions toward the front wall. This tongue-like protrusion suddenly disappears in a small apparent bulk explosion, leading to the third and fourth identified events, which occur simultaneously: rapid curvature changes and cratering on the keyhole walls and the emergence of thin melt ligaments along the keyhole rims. As the melt ligaments rise from the keyhole rims, they eventually break up into spatters. Those flying ahead of the laser scanning direction tend to travel in nearly-straight trajectories at a constant speed, but backward-flying spatters exhibit curved trajectories at varying speeds near the keyhole.

The investigators find that these behaviors are directly related to the relationship between the local laser absorption and the changing keyhole morphology, as different areas are rapidly heated or cooled and effects such as melt and vapor flow, pressures, and evaporation come into play. The team's numerical analyses based on the current experiments cannot yet completely characterize the specific mechanisms of the bulk explosion leading to the spattering, but note that it displays signs of a phase and/or a vapor explosion. Further description will require more direct thermal measurements and faster imaging at the nanoscale.

The research team's work also provides enough new details to begin considering possible solutions to mitigate or even eliminate it in certain laser processing and AM techniques. In laser powder bed fusion, for example, possibilities could include pre-sintering to make the powder bed more rigid and thus less susceptible to spattering, or the use of a high-velocity laminar gas flow.

The current findings confirm that the most effective ways to reduce and eliminate laser-induced spattering will involve controlling melt and vapor flow, especially within the keyhole. New laser techniques and control systems might be a practical approach. For the price of some pretty fireworks, manufacturers will gain a new confidence in the reliability and durability of their laser-processed products. — Mark Wolverton

See: Cang Zhao[1], Qilin Guo[2], Xuxiao Li[3], Niranjan Parab[1], Kamel Fezzaa[1], Wenda Tan[3]*, Lianyi Chen[2]**, and Tao Sun[1]***, "Bulk-Explosion-Induced Metal Spattering During Laser Processing," Phys. Rev. X **9**, 021052 (2019). DOI: 10.1103/PhysRevX.9.021052
Author affiliations: [1]Argonne National Laboratory, [2]Missouri University of Science and Technology, [3]University of Utah
Correspondence: * wenda.tan@mech.utah.edu,
** chenliany@mst.edu, *** taosun@aps.anl.gov

The authors would like to thank Alex Deriy at the APS, and Zherui Guo and Wayne Chen at Purdue University for their assistance with the x-ray experiments. T. S., C. Z., N. P., and K. F. acknowledge the support from Laboratory Directed Research and Development funding from Argonne National Laboratory provided by the Director, Office of Science of the U.S. Department of Energy (DOE) under Contract No. DE-AC02-06CH11357. L. C. would like to thank the National Science Foundation (NSF) for their support (Grant No. 1762477). W. T. would like to thank the NSF for their support (Grant No. 1752218). This research uses resources of the Advanced Photon Source, a U.S. DOE Office of Science User Facility operated for the DOE Office of Science by Argonne National Laboratory under Contract No. DE-AC02-06CH11357.

Putting the Squeeze on AM Lattices

One of the many advantages resulting from the advent of three-dimensional (3-D) printing, otherwise known as additive manufacturing (AM), is that it makes possible the fabrication of highly complex structures that were not possible with traditional techniques. For example, lattices for use as waveguides or similar functions can be created with customized properties. However, a good understanding of the dynamic wave propagation behavior in these novel and complex structures is necessary for their optimal use in practical applications. A quartet of researchers conducted a series of *in situ* experimental observations of wave propagation in AM-fabricated polymer lattice structures using high-speed phase contrast x-ray imaging at the APS, complemented by direct numerical simulations. Further similar work should open the path to practical applications of these unconventional materials.

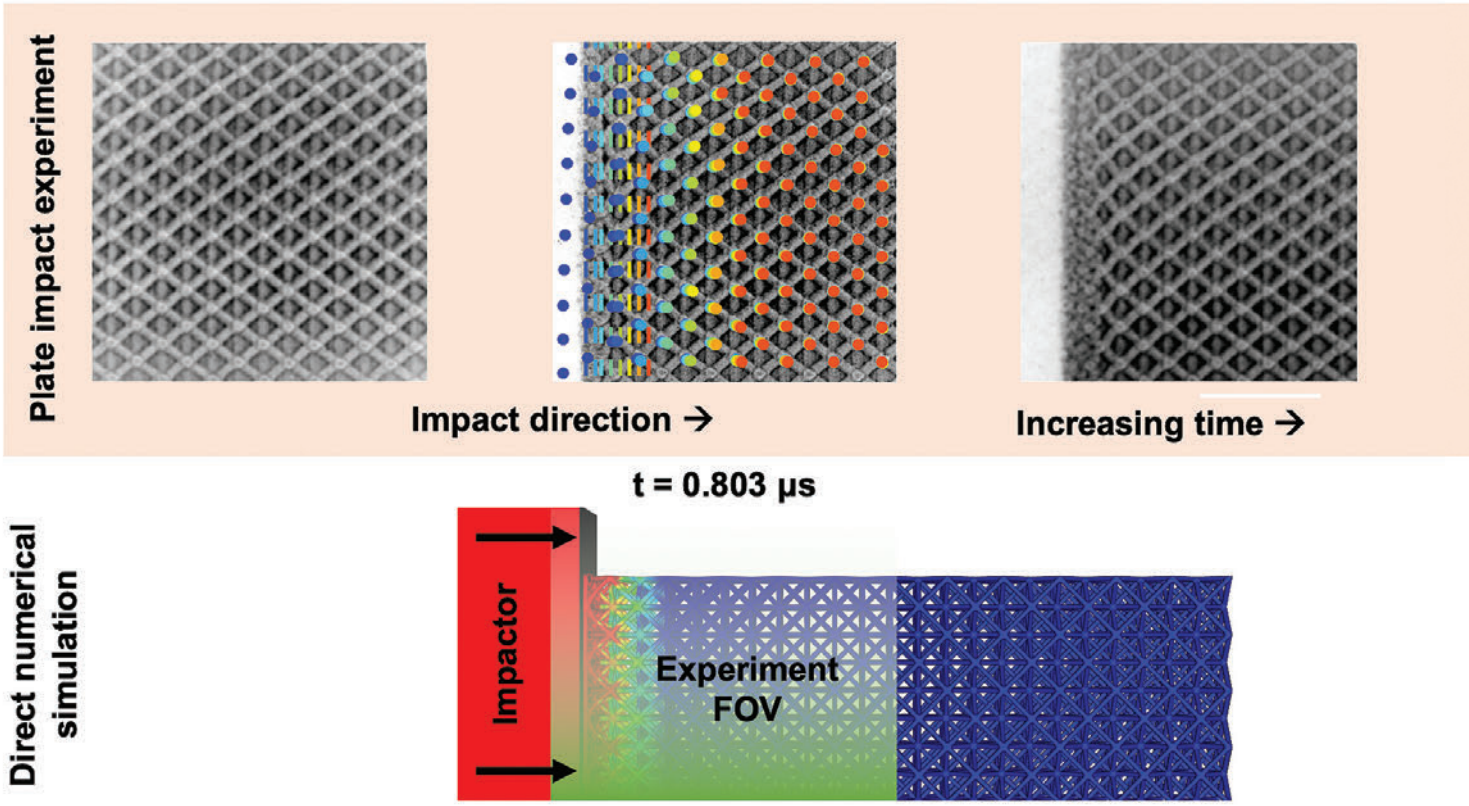

Fig. 1. Top row: Experimental images from a plate-impact experiment with *in situ* x-ray imaging showing the elastic compression and plastic compaction of the polymer lattice. The field-of-view (FOV) is 1.7 mm x 1.7 mm. Colored dots represent the location of the lattice nodes throughout the sequence of experimental images, which track the effect of the elastic precursor wave on the material movement. Bottom row: Direct numerical simulation mimicking the above experiment. The impactor and lattice are colored by the local material velocity at each specific snapshot in time. One notes evidence of material movement running ahead of the compaction front, which is indicative of an elastic precursor. Snapshots of the simulation are shown below the experimental images at the identical instant in time.

Recent work revealed that when subjected to dynamic compression, which creates mechanical shock waves that propagate throughout the material, polymer lattices display an elastic precursor wave in addition to plastic waves. Because of the complex structure of such lattices, including the presence of free surfaces within them, this mechanical shock wave behavior cannot easily be compared to waves in bulk solids. These complicating factors led to additional questions regarding the behavior of the elastic precursor wave under various impact conditions, including its speed, decay, and propagation distance.

To investigate these issues more closely, the research team from the Lawrence Livermore and Los Alamos na-

tional laboratories tracked the evolution of the elastic precursor wave in a 4 x 8 x 12 octet AM-fabricated polymer lattice using x-ray phase contrast imaging at the DCS 35-ID x-ray beamline at the APS. To induce dynamic compression of the samples, two types of gas-gun driven flyers were used: PMMA and Al-6061. The researchers compared their experimental results with direct numerical simulations.

Elastic precursor waves are transmitted atom by atom through a lattice, and although they can travel faster overall than plastic waves, the pressure they transmit is much lower than plastic waves evidenced by their low particle speeds. If dynamic compression is very strong, elastic waves may be overtaken by plastic waves (which are pressure dependent), a condition known as "overdriving." The elastic precursor wave is usually seen to decay significantly in bulk materials over a propagation distance of several millimeters, even with far higher pressure and amplitude in metals compared to polymers. This can make the characterization of elastic precursor waves quite challenging, especially when comparing to polymer lattices.

Nevertheless, the experimenters managed to measure the movement of lattice nodes with sufficient resolution to visualize the elastic precursor wave as it moved through the sample. They utilized five different impact conditions, with one condition close to the point of overdriving. The researchers observed an elastic precursor wave under four of the conditions (Fig. 1). This wave propagated through more than 10 unit cells without fully dissipating, contrary to behaviors seen in bulk solids or in granular and porous materials. No elastic precursor was seen under the near-overdriving condition, but the investigators note that this may be due to the resolution limits of the experimental setup.

Numerical simulations compared quite well with the experimental data and made it possible to substantiate the speed of the elastic precursor. The elastic wave was shown to be essentially independent of the impact conditions or the material properties of the lattice, and as in a bulk solid, is considered to travel at the sound speed in the material.

The research team notes that the presence of elastic and plastic waves at the same time in a particular material is a complex phenomenon to study, particularly in a unique structure such as the octet lattice examined in these experiments. However, the fact that this work demonstrated these kinds of classical mechanical phenomena in a novel AM structure was interesting and unexpected, and promises that a better understanding of the dynamic behavior of these unique materials is within reach. — Mark Wolverton

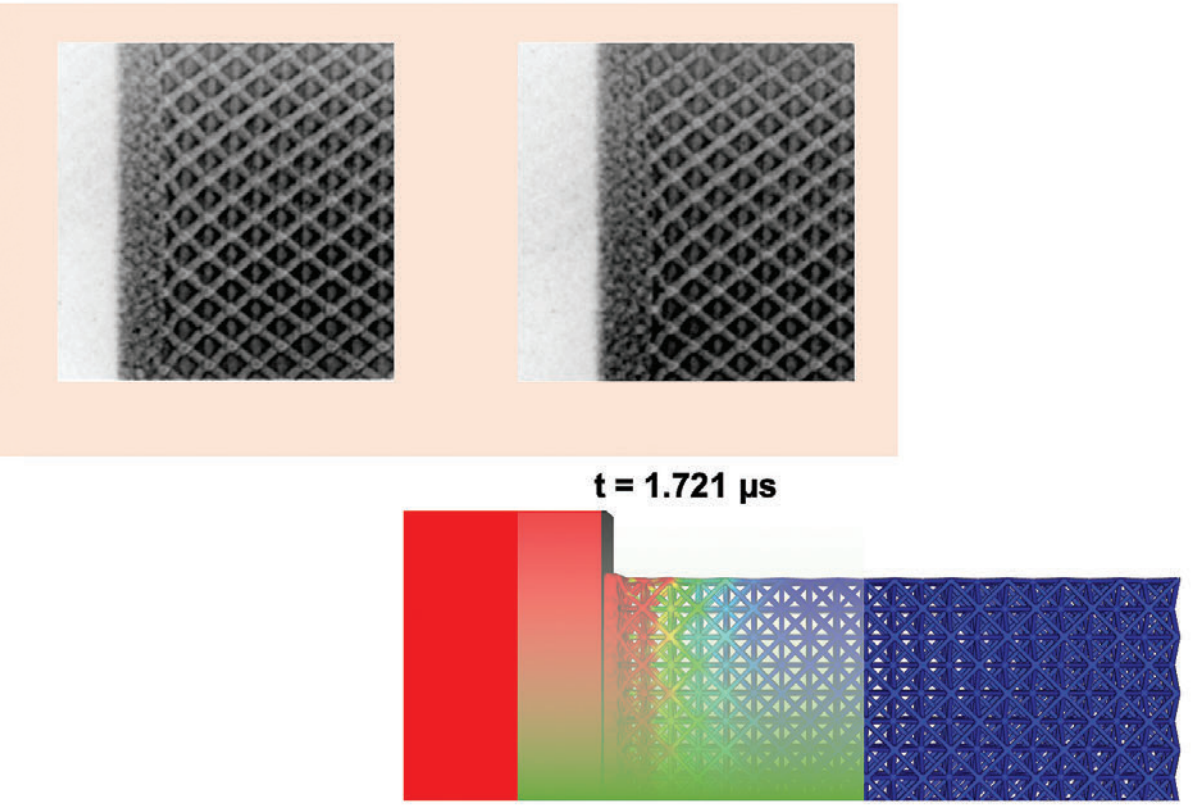

See: Jonathan Lind[1]*, Brian J. Jensen[2], Matthew Barham[1], and Mukul Kumar[1], "In situ dynamic compression wave behavior in additively manufactured lattice materials," J. Mater. Res. **34**(1), 2 (January 14, 2019). DOI: 10.1557/jmr.2018.351
Author affiliations: [1]Lawrence Livermore National Laboratory, [2]Los Alamos National Laboratory
Correspondence: * lind9@llnl.gov

This work was performed under the auspices of the U.S. Department of Energy (DOE) by Lawrence Livermore National Laboratory under Contract DE-AC52-07NA27344 and by Los Alamos National Laboratory under contract DE-AC52-06NA25396. This publication is based in part upon work performed at the Dynamic Compression Sector, which is operated by Washington State University under the DOE/National Nuclear Security Administration Award No. DE-NA0002442. This research used resources of the Advanced Photon Source, a U.S. DOE Office of Science User Facility operated for the DOE Office of Science by Argonne National Laboratory under Contract No. DE-AC02-06CH11357.

3-D Metal Printing without Pores

Porosity is a major unwanted byproduct of the prominent additive manufacturing (AM) technique of laser powder bed fusion (LPBF) of metals. The presence of myriad pores of varying sizes in the finished metal pieces seriously compromises their strength and durability. Understanding precisely what creates pores during the LPBF process is critical to finding ways to reduce and eliminate them. Using advanced high-speed, hard x-ray imaging techniques at the APS, a team of researchers has penetrated the dynamics and mechanisms of pore formation and elimination during LPBF fabrication. The team expects that the methods demonstrated in this work could be perfected and extended not just in LPBF printing but across other AM techniques and other fabrication technologies.

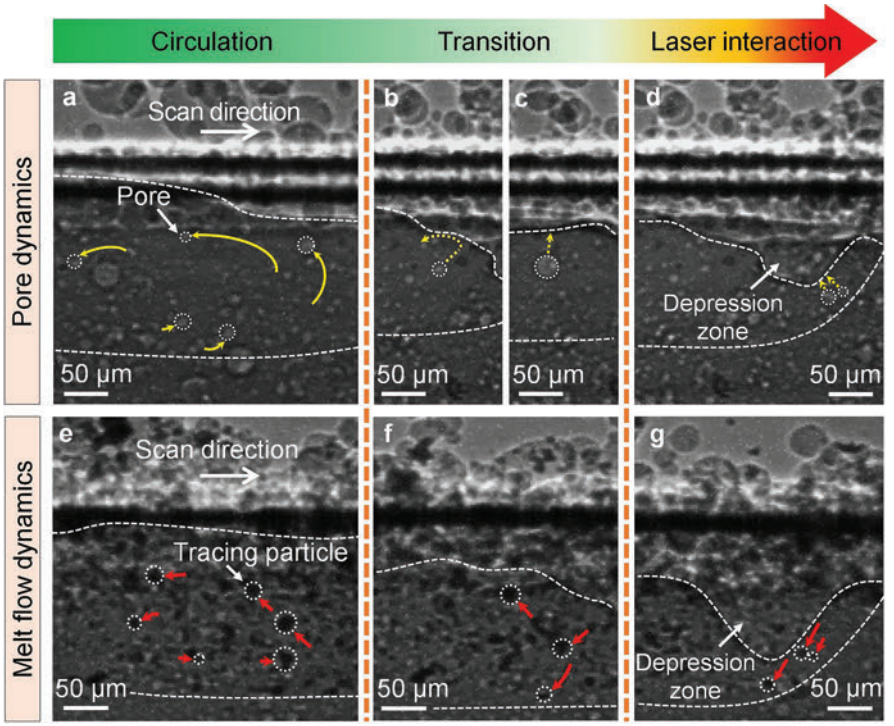

Fig. 1. Pore and melt flow dynamics during the laser powder bed fusion additive manufacturing process. (a)-(d): X-ray images showing pore dynamics inside the melt pool during the LPBF process. Dotted arrows indicate the future trajectories of the pores, while solid arrows mark the history of pore trajectories. Pores exhibit circular patterns at the circulation domain (a), while pores in the laser interaction domain move toward depression zone and escape from the melt pool (d). In the transition domain, (b) and (c), pores exhibit irregular moving behavior, sometimes moving toward the melt pool surface and escaping (c), and sometimes circulating in the melt pool. (e)-(g): X-ray images showing melt flow dynamics inside the melt pool during the LPBF process. Red arrows indicate the trajectories of tracing particles (tungsten microparticles) at the circulation domain (e), transition domain (f), and laser interaction domain (g). The dotted white lines indicate melt pool boundaries. From S.M.H. Hojjatzadeh et al., Nat. Commun. **10**, 3088 (2019). © 2019 Springer Nature Limited

One of the challenging aspects of understanding pore formation in LPBF is that various factors can be responsible, either individually or acting in combination, including pore transfer from feedstock, vaporization of volatile elements, and other causes. The buoyant forces that normally help to eliminate pores from other liquids are not effective in the LPBF melt pool because of high drag forces, so post-processing techniques, an imperfect solution at best, are usually the only option to eliminate pores in finished pieces. A better option would be to prevent or at least reduce pores during printing, which requires a deeper and more detailed understanding of how they form.

Previous efforts to achieve such understanding have been hampered by the high velocities and tiny sizes of pores in the LPBF melt pool, along with the opacity of the metallic substances involved. The team from the Missouri University of Science and Technology, the National University of Singapore, Argonne, and the U.S. DOE Kansas City National Security Campus overcame those obstacles by using the extreme brightness x-rays available at the XSD 32-ID-B beamline of the APS, which enabled high-speed, high-resolution, *in situ* imaging in real time during the actual LPBF process. The team studied samples of AlSi10Mg alloys to first characterize pore behavior and then to examine possible elimination techniques.

The high speed and resolution attainable afforded by the APS x-rays allowed the details of individual pore movement to be seen (Fig. 1). This revealed the variations in pore dynamics in different regions of the melt pool, which the experimenters delineated as (1) a laser interaction domain nearest to the laser beam, (2) a circulation domain farther away from the beam in which pores circulated at various speeds, and (3) a transition domain between the two, where some pores simply circulated and others moved toward the melt pool surface and escaped.

The researchers first considered the pore movements they observed in these domains in light of the mechanisms usually reported in the literature, chiefly buoyancy and melt-induced drag. They found that at these pore sizes, the drag force is far greater than the buoyant force, preventing pores from escaping at the pool surface in the circulation domain. However, even with the high melt flow velocity in the laser interaction domain, pores tend to move in a direction almost perpendicular to the melt flow direction and quickly escape, despite the influence of buoyant and drag forces.

The experimenters hypothesize that this phenomenon is driven by a high-temperature gradient that creates an elevated thermocapillary force driving the melt from hot to cold regions, resulting in pore movement from cold to hot regions. They simulated this mechanism using a multiphysics model to study the melt pool temperature gradient, which showed that pores in the laser interaction domain accelerated via the thermocapillary force as they moved toward the depression zone and exited the melt pool, confirming the behavior seen in the actual experiments. A force map showing the ratio of thermocapillary force to drag force confirmed that the thermocapillary force dominates pore movement in the laser interaction domain, while drag force is prevalent in the circulation domain, and the buoyant force is too small to exert any appreciable effect except at very large pore sizes that are not seen in the LPBF process. Contrary to previous hypotheses, then, the thermocapillary force appears to be the main driver for pore elimination during LPBF.

The research team next investigated how the thermocapillary force could be used to eliminate pores in the midst of the LPBF process, experimenting on both AlSi10Mg and Ti6Al4V to demonstrate effectiveness over multiple alloys. By inducing specific thermocapillary force through laser rescanning at the proper parameters, involving a temperature gradient high enough to overcome the melt induced drag force over a large enough domain, the experimenters were able to achieve effective pore elimination in the samples. — Mark Wolverton

See: S. Mohammad H. Hojjatzadeh[1], Niranjan D. Parab[2], Wentao Yan[3], Qilin Guo[1], Lianghua Xiong[1], Cang Zhao[2], Minglei Qu[1], Luis I. Escano[1], Xianghui Xiao[2], Kamel Fezzaa[2], Wes Everhart[4], Tao Sun[2]*, and Lianyi Chen[1]**, "Pore elimination mechanisms during 3D printing of metals," Nat. Commun. **10**, 3088 (2019).
DOI: 038/s41467-019-10973-9
Author affiliations: [1]Missouri University of Science and Technology, [2]Argonne National Laboratory, [3]National University of Singapore, [4]U.S. Department of Energy Kansas City National Security Campus
Correspondence: * taosun@aps.anl.gov, ** chenliany@mst.edu

The authors would like to thank Alex Deriy at the APS for his help on the beamline experiments. This work is funded by the U.S. Departmrnt of Energy (DOE) Kansas City National Security Campus Managed by Honeywell Federal Manufacturing & Technologies (FM&T), the National Science Foundation, the Intelligent Systems Center at Missouri S&T, and partially by Laboratory Directed Research and Development funds from Argonne National Laboratory provided by the Director, Office of Science, of the U.S. DOE under Contract No. DE-AC02-06CH11357. W.Y. would like to thank the support from Singapore Ministry of Education Academic Research Fund Tier 1. The journal article was authored by Honeywell Federal Manufacturing & Technologies under Contract No. DE-NA0002839 with the U.S. DOE. This research used resources of the Advanced Photon Source, a U.S. DOE Office of Science User Facility operated for the DOE Office of Science by Argonne National Laboratory under Contract No. DE-AC02-06CH11357.

Capturing Anions for Better Desalination

One method for desalinating salt water is a process called "capacitive deionization." An electrical potential difference is applied across two electrodes, and negatively charged anions are pulled to the positive anode while positively charged cations flow to the negative cathode. Such electrodes are usually made of carbon, but their efficiency is relatively low. Researchers are looking for better electrode materials, but while good materials that capture cations have been developed by people who make them for batteries, anion-capturing materials technology is not as far along. Because the lower-efficiency electrode determines the performance of the whole system, it's important to improve anion capture. Now researchers using the APS have shown a promising way to insert anions into electrodes.

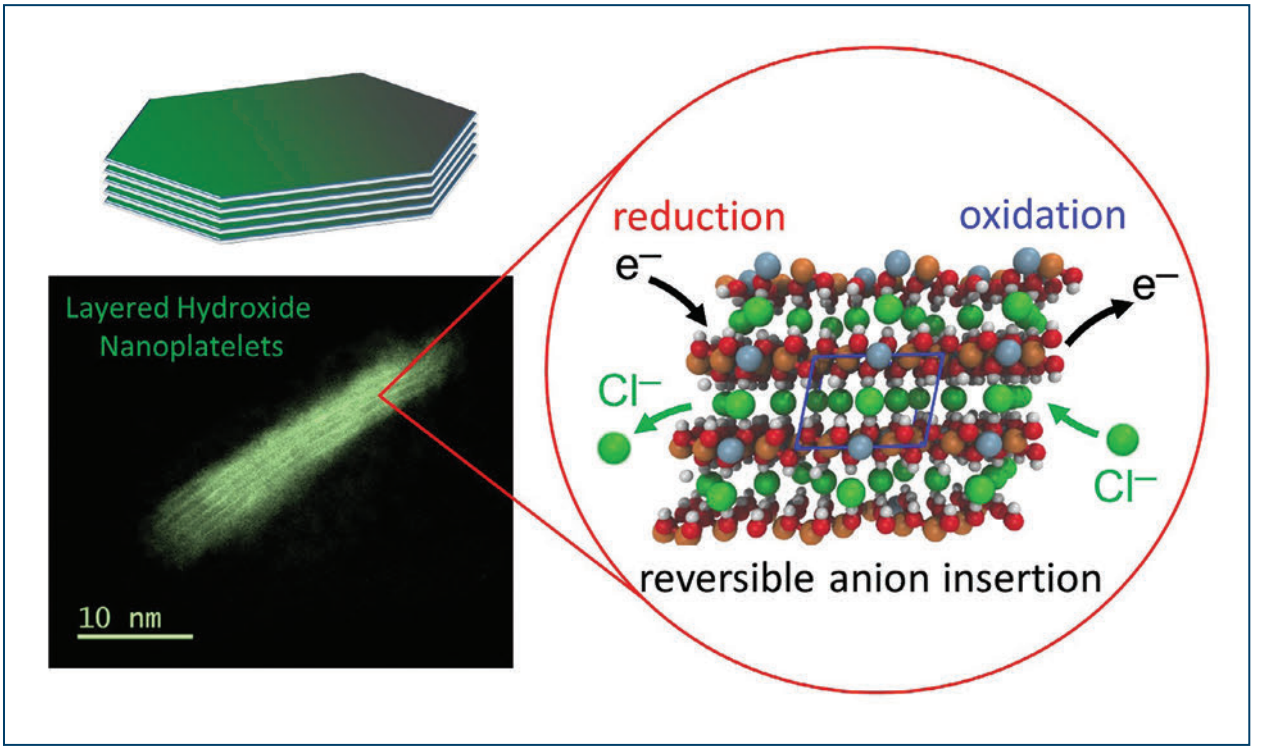

Fig. 1. Layered hydroxide nanoplatelets (upper left) are stacked together. As a potential is applied, anions are drawn out of water into the structure (right).

The process uses a layered hydroxide containing cobalt. Cobalt atoms in the hydroxide structure are surrounded by six oxygen atoms, each bridging to another cobalt or other metal atom, or "center," to form a flat plate. Such metal centers not only give structure to the hydroxide, they also participate in oxidation-reduction (redox) reactions. The hydroxide structure is stacked in layers that anions fit between, and applying a positive charge to the layers pulls the anions out of the water to the electrode (Fig. 1). The process can also be reversed to release the anions.

The team from Argonne, the National Institute of Standards and Technology, the University of Missouri, the University of New South Wales (Australia), the University of Maryland, and the Illinois Institute of Technology first performed computational modeling to predict which metals could be used in the layered hydroxide to produce the electrical properties they needed. One of the hydroxides their model predicted contained both cobalt and vanadium metal centers, so they synthesized that and subjected it to tests. As it turned out, the vanadium did not play a role; the cobalt alone was responsible for the reaction.

To examine their hydroxides, the researchers first carried out high-energy x-ray diffraction (HEXRD) studies at XSD beamlines 11-ID-B and 11-ID-C at the APS to confirm that they did indeed have layered hydroxide structures in various samples they'd made. The measurements allowed them to compare the atomic structures of several material systems, including manganese-aluminum, cobalt-aluminum, cobalt-chromium, and cobalt-vanadium. Previous studies of such structures have been based on manganese-aluminum, so the researchers used that as a reference point, although they do not expect it to be useful for deionization; neither manganese nor aluminum undergo redox reactions in water at workable voltages.

They next performed HEXRD with pair distribution function analysis at XSD beamline 6-ID-D as they charged and discharged the material. That allowed them to watch the structure changing and observe anions in the space between layers moving in and out as they altered the electrical potential. The changes were rather subtle, the researchers said, and would have been impossible to observe without the advanced instrumentation available at the APS. The test allowed the researchers to see what happened as they increased or decreased the potential, and they were surprised to learn that the anion insertion happened at a different potential level than their model had predicted.

Further studies, using x-ray absorption spectroscopy at the MR-CAT beamline 10-BM-B, also at the APS, revealed how the environment around the cobalt changed during anion insertion. Such measurements give information including the number of atoms around the cobalt and where they're positioned, which shows that the cobalt's oxidation state is changing during anion insertion. These studies showed that the cobalt was responsible for the anion insertion behavior.

While this was the first demonstration of anion insertion in layered hydroxides and thus serves as a proof of concept, cobalt is not an ideal material for this application. It's toxic, for one thing, and it degrades in water over time. Layered hydroxides can be built with other metal centers, however, and the researchers are studying other materials that may prove to be more stable and environmentally friendly. — Neil Savage

See: Matthias J. Young[1,2,3]*, Tatyana Kiryutina[2], Nicholas M. Bedford[2,4]**, Taylor J. Woehl[2], and Carlo U. Segre[6], "Discovery of Anion Insertion Electrochemistry in Layered Hydroxide Nanomaterials," Sci. Rep. **9**, 2462 (2019). DOI:10.1038/s41598-019-39052-1

Author affiliations: [1]Argonne National Laboratory, [2]National Institute of Standards and Technology, [3]University of Missouri, [4]University of New South Wales, [5]University of Maryland, [6]Illinois Institute of Technology

Correspondence: * matthias.young@missouri.edu, **n.bedford@unsw.edu.au

M.J.Y. acknowledges the National Research Council for a Research Associateship award at the National Institute of Standards and Technology (NIST), partial support as part of the Joint Center for Energy Storage Research (JCESR), an Energy Innovation Hub funded by the U.S. Department of Energy (DOE) Office of Science-Basic Energy Sciences, and partial support from faculty start-up funds provided by the University of Missouri. T.J.W. acknowledges partial support from a National Research Council Research Associateship award at NIST and partial support from faculty start-up funds provided by University of Maryland. MR-CAT operations are supported by the Department of Energy and the MR-CAT member institutions. We would like to thank Yang Ren for assistance with experiments at 11-ID-C, Karena Chapman and Kevin Beyer for assistance with experiments at 11-ID-B, Chris Benmore and Douglas Robinson for assistance with experiments at 6-ID-D, and John Katsoudas for assistance with experiments at 10-BM. This research used resources of the Advanced Photon Source, a U.S. DOE Office of Science User Facility operated for the DOE Office of Science by Argonne National Laboratory under Contract DE-AC02-06CH11357.

Toward a Strong, Lightweight, and Ductile Aluminum Alloy

Inexpensive, abundant, and useful—pure aluminum metal is soft and ductile and perfect for end uses such as soda cans and aluminum foil. But add just a little bit of copper, magnesium, or zinc, and aluminum transforms into a super-strong yet lightweight material, stiff and resilient enough to be used in aircraft and automobile frames. Although we discovered how to alloy aluminum with other metals 60 years ago, we still don't entirely understand how these small additions cause such dramatic changes in aluminum properties. Now, researchers have used the unique capabilities of the APS to detail for the first time how these metals change the nanoscale structure of aluminum, and to explore how we might control the metallurgy to design even better aluminum alloys with even more desirable properties.

Metallurgists make aluminum alloys by dissolving a small amount of one or more metals—say 1% of copper by weight—into a larger body of aluminum. Once the addition is completely dissolved, the mixture is quenched, that is, cooled quickly so that it stays evenly mixed. Then the mix is slowly reheated just enough that tiny particles of Al_2Cu precipitate out.

These particles are shaped like tiny needles or plates. Just a few tens of nanometers long, they give aluminum alloys their strength and stiffness. Material scientists knew the particles did this, but until now they didn't know exactly how.

A team of researchers from Arizona State University used the APS to find out. They took a sample of aluminum copper alloy and heated it slowly to allow the copper to precipitate into nanoparticles of Al_2Cu. The researchers, with colleagues from XSD, then milled pillars, using a focused ion beam, down to about 50 µm at the tip, and imaged these at the XSD x-ray beamline 32-ID-C at the APS. They used the transmission x-ray microscope at that beamline to perform absorption full-field hard x-ray nano-computed tomography. Similar to a medical computed tomography scan, the transmission x-ray microscope was used to take a series of two-dimensional images of the interior nanostructure of the wire, and then, using tomoPy, an open-source, Python-based toolbox developed at the APS, those images were reconstructed into a three-dimensional picture (Fig. 1) .

Once they had imaged the starting structure of the alloy, the team carefully applied pressure to the wire with a diamond tip until the wire indented. Then they again used the transmission x-ray microscope to image the wire to see how the internal structure had deformed.

When they examined the deformation, the researchers found something intriguing: the larger nanoparticles, thicker than ~80 nm, tended to buckle and kink when stressed. This buckling gave the alloy ductility as it allowed energy to dissipate. Meanwhile, the smaller nanoparticles of Al_2Cu were what gave the material strength by serving as obstacles for slip in the material. Without these obstacles, stressing the aluminum caused the metal to separate into regions that slide against each other, eventually shearing apart. But the small, needle-like nanoparticles blocked those movements and prevented the shearing.

Typically, materials that are strong are also brittle, while ductile materials tend to be soft. It was thought that ductility and strength were mutually exclusive, but the results of this study suggest that aluminum alloys might be able to have both strength and ductility—if the distribution of small and large nanoparticles can be tuned just right. With clever metallurgy, we might be able to have aluminum alloys that are both super strong and ductile, the researchers suggest.

The next steps in this research will use the same beamline at the APS to examine how even smaller nanoparticles, as small as 20-nm in diameter, affect deformation in aluminum alloys. The researchers also plan to

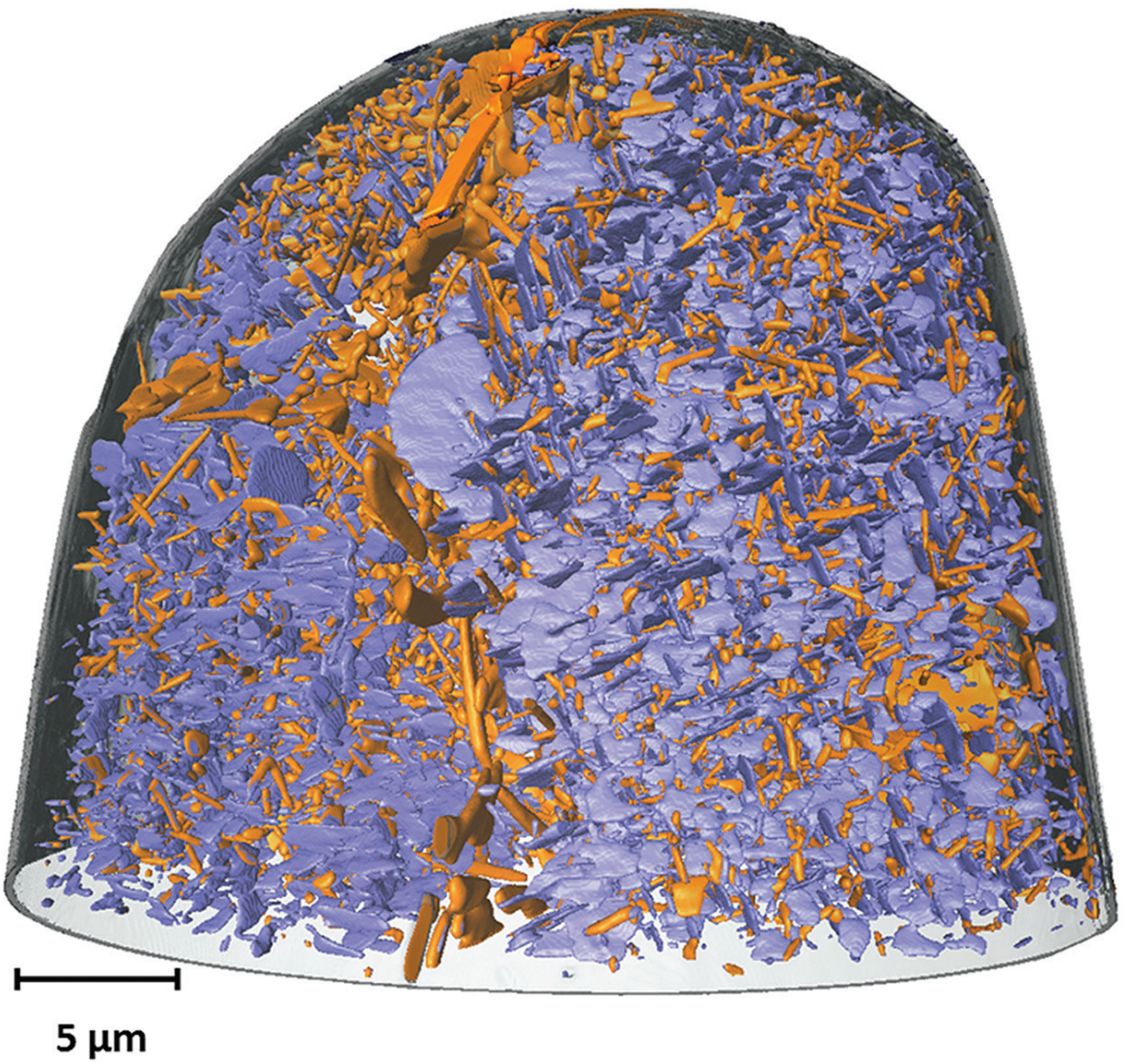

Fig. 1. This transmission x-ray microscope image shows the interior nanostructure of the aluminum copper alloy. The blue areas are aluminum, while the orange shows the needle- and plate-like AL_2Cu nanoparticles that precipitate out of the mix and are responsible for the alloy's strength.

see if other elements such as magnesium and zinc form nanoparticles and affect aluminum alloy properties in ways similar to copper. The ultimate goal will be to understand the alloys' behavior at the nanoscale well enough to design materials that are stronger and more durable than anything currently available. — Kim Krieger

See: C. Shashank Kaira[1], Tyler J. Stannard[1], Vincent De Andrade[2], Francesco De Carlo[2], and Nikhilesh Chawla[1]*, "Exploring novel deformation mechanisms in aluminum-copper alloys using *in situ* 4D nanomechanical testing," Acta Mater. **176**, 242 (2019). DOI: 10.1016/j.actamat.2019.07.016

Author affiliations: [1]Arizona State University, [2]Argonne National Laboratory
Correspondence: * nchawla@asu.edu

The authors are grateful for financial support from the Army Research Office under Contract No. W911NF1410550 (Dr. Michael Bakas and Dr. David Stepp, Program Managers). We acknowledge the use of facilities within the Center for 4D Materials Science and the Leroy Eyring Center for Solid State Science at Arizona State University. This research used resources of the Advanced Photon Source, a U.S. Department of Energy (DOE) Office of Science User Facility operated for the DOE Office of Science by Argonne National Laboratory under Contract No. DE-AC02-06CH11357.

Good Vibrations

Materials science tends to divide solids into two basic types: conductors and insulators. Conductors transport energy efficiently in the form of heat or electricity. Insulators do not. And the higher the temperature, the worse an insulator is at transporting energy. But not all materials fall neatly into one of these two categories, and those exceptions can sometimes be useful. For example, materials that conduct electricity but insulate heat can be used for converting heat into electricity and are called thermoelectrics. A team of researchers used the APS to study one such promising class of materials, lead chalcogenides, and confirmed what their simulations predicted: As the temperature rose, certain frequencies of vibration (heat) moved through the material more efficiently, while others shut down. Their work could help materials scientists better understand why some substances have unusual properties, and eventually identify or design materials that can gather waste heat and put it to work elsewhere. Ultimately, such materials could convert waste heat into electricity, or replace mechanical cooling systems that rely on fossil fuels with more environmentally friendly solid-state devices.

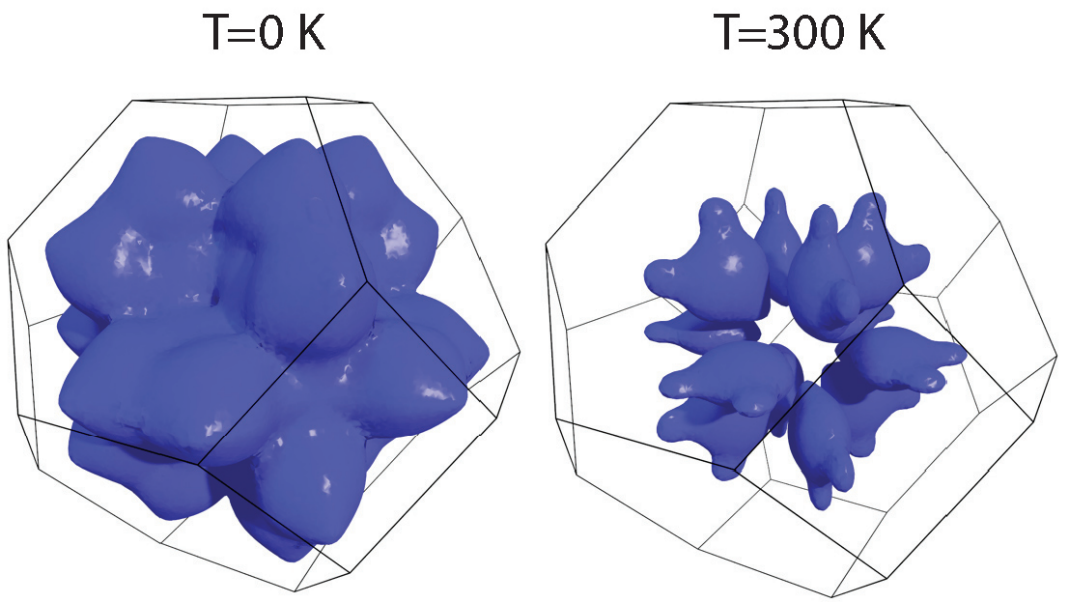

Fig. 1. The image shows the calculated phase space (the notional "area" available for movement) of a three-phonon scattering process in the transverse optical mode of lead selenide (PbSe). The phase space shrinks as the temperature rises. The researchers' data from the APS HERIX instrument confirmed this calculation. From M. E. Manley et al., Nat. Commun. **10**, 1928 (2019). © 2019 Springer Nature Limited

Lead selenide (PbSe) transports heat badly because its crystalline structure doesn't vibrate in a typical harmonic way. Instead, the crystals vibrate in complicated modes that interact in unexpected ways and sometimes localize, i.e., they stop moving heat through the crystal.

Researchers from Caltech simulated the molecular dynamics of PbSe, explicitly accounting for the anharmonic behavior of the material, to see if they could get some insight into its heat transport. In a typical insulator, the modes of vibration interact more and more as the material gets warmer and warmer. These interactions interfere with heat transport. But surprisingly, the simulation did not find this to be entirely true for PbSe. Instead, the simulation showed that at high temperature one of the modes of vibration split off from the others, not propagating at all, while another traveled more freely.

The Caltech group teamed up with a researcher from Oak Ridge National Laboratory (ORNL) who heated a sample of PbSe while passing a beam of neutrons through it at the NIST Center for Neutron Research. At room temperature, the researchers saw several different modes of vibration, indicated by how the energy and direction of the neutrons changed after passing through the sample. But as the PbSe warmed, they not only observed the trans-

verse optical (TO) phonon mode flatten out and stop propagating just as the simulation predicted, they also observed sharpening of the longutudinal acoustic (LA) phonon mode. On the other hand, instrumental resolution prevented qualitative analysis of the predicted splitting of TO mode from intrinsic localized mode (ILM) and made determination of the energy linewidth of LA mode challenging. High-energy-resolution measurements were later performed on the same crystal using the HYSPEC time-of-flight cold neutron spectrometer at the Spallation Neutron Source at ORNL in order to look for any fine-energy structure. These measurements revealed an additional sharp but weak dispersionless feature matching the in-band ILM feature and shows a flatter, more fragmented TO phonon, as predicted in their simulation, meaning a transition into the anharmonic dynamics upon heating.

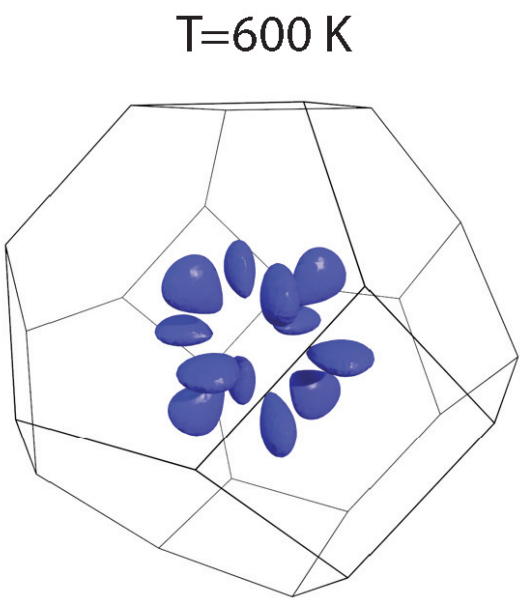

The team wanted to take a closer look at those modes that disappeared, so to view the vibrational modes of interest as the PbSe was slowly warmed, they and a colleague from Argonne carried out inelastic x-ray scattering studies at the HERIX spectrometer on the XSD 30-ID-C beamline of the APS, the only synchrotron in North America that will work for this kind of experiment because it has the highest flux, the brightest x-rays, very little noise from randomly scattered rays, and better control over the energy of the x-rays than any other facility. What the researchers saw at the APS confirmed their simulation results and the neutron beam analysis: The velocity of certain vibrational modes shrank, gradually slowing to a stop as the temperature rose (Fig. 1). At room temperature (about 294 K) certain vibration modes interacted with other nearby modes fairly normally. But as the temperature rose to 770 K, these modes sharpened, interacting with other modes less and persisting for long periods of time. The reason this happens is that when one mode localized its movement in energy-momentum space, this reduced the number of possible scattering paths, allowing the other mode to pass more freely through the crystal. It is surprising because normally with increasing temperature, the thermal population of more vibrations increases the scattering, and it is usually assumed that the available scattering channels do not change.

The measurements at the APS confirmed what the neutron beam experiment had shown: The flattening out wasn't just of certain isolated modes, but of whole swaths of vibrations in the material. Understanding how vibrations can be induced to stop propagating in a pristine crystal opens new avenues to control thermal transport without disrupting the crystal regularity needed for favorable electric properties in thermoelectric applications. The trick is dealing with the compensating effects that come with localization from changes in the phase space for scattering other vibrations.

These results tell us that materials can be more complex than researchers had thought. It also gives theorists an idea of which characteristics unusual thermoelectrics like PbSe should have, allowing scientists to seek out materials with even better properties, or design them from scratch. — Kim Krieger

See: M.E. Manley[1]*, O. Hellman[2], N. Shulumba[2], A.F. May[1], P.J. Stonaha[1], J.W. Lynn[3], V.O. Garlea[1], A. Alatas[4], R.P. Hermann[1], J.D. Budai[1], H. Wang[1], B.C. Sales[1], and A.J. Minnich[2]**, "Intrinsic anharmonic localization in thermoelectric PbSe," Nat. Commun. **10**, 1928 (2019). DOI: 10.1038/s41467-019-09921-4
Author affiliations: [1]Oak Ridge National Laboratory, [2]California Institute of Technology, [3]National Institute of Standards and Technology, [4]Argonne National Laboratory
Correspondence: * manleyme@ornl.gov,
** aminnich@caltech.edu

This work was supported by the U.S. Department of Energy (DOE) Office of Science-Basic Energy Sciences, Materials Sciences and Engineering Division under Contract Number DE-AC05-00OR22725. A portion of this research performed at the Oak Ridge National Laboratory's Spallation Neutron Source was sponsored by the U.S. DOE Office of Science-Basic Energy Sciences. The authors acknowledge the support of the National Institute of Standards and Technology, U.S. Department of Commerce, in providing the neutron research facilities used in this work. H. Wang's effort was sponsored by the DOE Energy Efficiency and Renewable Energy, Office of Vehicle Technologies Materials program. N.S. and A.J.M. acknowledge the support of the DARPA MATRIX program under Grant No. HR0011-15-2-0039. This work used the Extreme Science and Engineering Discovery Environment (XSEDE), which is supported by National Science Foundation Grant No. ACI-1053575. This research used resources of the Advanced Photon Source, a U.S. DOE Office of Science User Facility operated for the DOE Office of Science by Argonne National Laboratory under Contract No. DE-AC02-06CH11357.

Finding the Right Recipe for Efficient Solar Cells

Researchers continually strive to improve the efficiency of solar cells. The greater the percentage of sunlight that a cell transforms into electricity, the more power that photovoltaic provides. One type of solar cell that has shown promise for higher efficiencies is based on a crystalline structure known as a perovskite, a calcium titanium oxide mineral, with the chemical formula $CaTiO_3$. Lead halide perovskite solar cells that contain bromine or iodine have reached the highest known power conversion efficiencies—approximately 25.2%—when alkali metals such cesium iodide or rubidium (Rb) iodide are added. But the role these materials play in improving the solar cells has not been understood. Now researchers using the APS have shown just how the alkali metals contribute.

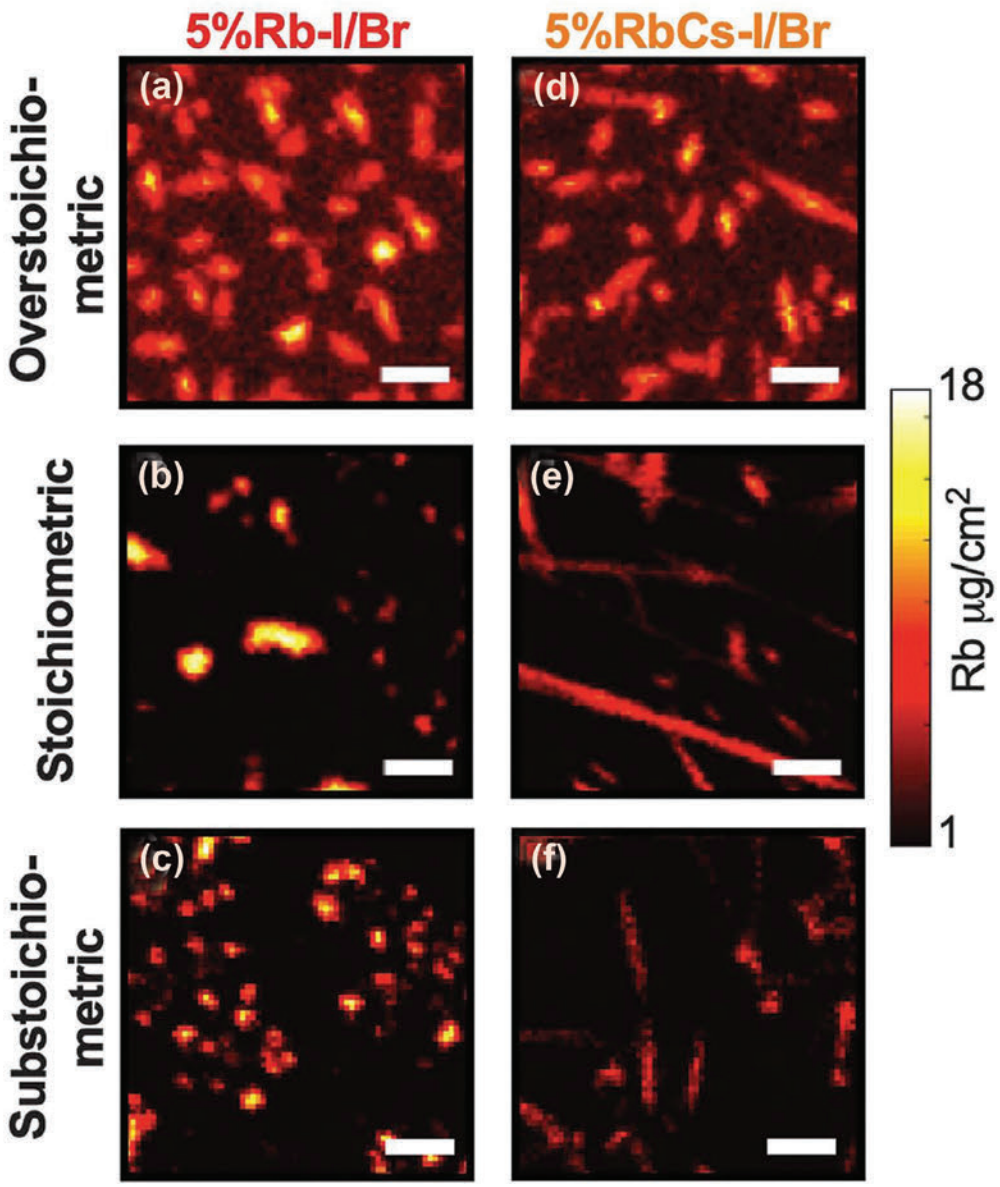

Halides in the perovskites—bromine and iodine—tend to form clusters, which have a negative effect on the electronic properties of the solar cell. The individual halides each have conduction bands with different energy levels. Where different clusters meet, cascades of electrons can flow from one conduction band to the other, and some get lost in the process before reaching the electrodes that take electricity out of the solar cell. Adding small amounts of alkali metals causes the halides to be more evenly distributed, reducing clusters and making the perovskites more homogeneous, so cascades are less likely.

But adding too much of the alkali metals has its own consequences. When the concentration of the metals is greater than about 1% of the solution used to create the perovskite thin film, the alkali metals—particularly the rubidium—start to agglomerate together, leading to "dead zones." In these zones, the separate charge carriers created when the photons were absorbed—the negative electrons and positive holes—recombine and thus fail to produce electrical current.

The researchers from the Massachusetts Institute of Technology, the Georgia Institute of Technology, the University of California, San Diego, and Purdue University, with colleagues from Argonne, performed x-ray fluorescence (XRF mapping) measurements at the XSD 2-ID-D beamline at the APS. The technique allowed them to identify the elements in the perovskite thin film (Fig. 1). A 200-nm-diameter probe provided high resolution, and moving their sample around the probe in a helium atmosphere allowed them to build up a map of the location of the various elements. They could see pockets of bromine or of rubidium very clearly. Cesium was harder to identify than rubidium, because its signal overlaps that of iodine, making it difficult to distinguish the two.

They also used current induced by the x-ray beam-induced current mapping to measure the flow of electricity at the same time they mapped the distribution of the elements, to see what effect the concentration of rubidium or bromine in a given area had. The signal-to-noise ratio was poor, so they repeated that step elsewhere with an electron beam-indiced current.

Having identified areas in the thin film where the beam produced either high or low current, the researchers performed scanning x-ray diffraction microscopy of those areas at the CNM/XSD nanoprobe beamline 26-ID-C. That allowed them to look at the crystallographic orientation of the rubidium. Areas with low current had a large amount of rubidium in a perovskite structure; areas with high current did not. The APS Upgrade will enable these measurements at the 2-ID and 26-ID beamlines to be performed much faster while much larger areas can be imaged than are possible today.

As it turns out, the benefits of homogenizing the halides outweighs the loss from the clumping of alkali metals until the concentration of the metals passes 5%. And using cesium iodide and rubidium iodide together worked better than using either of them separately. The researchers also examined the use of potassium iodine, but that showed little benefit. Other work has shown that the best-case scenario for efficiency is a mixture that contains both cesium and rubidium at 5% each. Future work will look for ways to get the beneficial effect of the homogenization while reducing the clumping of the alkali metals. — Neil Savage

< Fig. 1. Elemental distribution of Rb in perovskites of different compositions. (a) to (c) Rb XRF maps of the 5% Rb–added samples with different stoichiometries. (d) to (f) Rb XRF maps of the 5% Rb and 5% Cs–added samples with different stoichiometries. Scale bar: 5 µm. From J.-P. Correa-Baena et al., Science **363**, 627 (8 February 2019).

See: Juan-Pablo Correa-Baena[1,2*], Yanqi Luo[3], Thomas M. Brenner[3‡], Jordan Snaider[4], Shijing Sun[1], Xueying Li[3], Mallory A. Jensen[1], Noor Titan Putri Hartono[1], Lea Nienhaus[1], Sarah Wieghold[1], Jeremy R. Poindexter[1], Shen Wang[3], Ying Shirley Meng[3], Ti Wang[4], Barry Lai[5], Martin V. Holt[5], Zhonghou Cai[5], Moungi G. Bawendi[1], Libai Huang[4], Tonio Buonassisi[1**], David P. Fenning[3***], "Homogenized halides and alkali cation segregation in alloyed organic-inorganic perovskites," Science **363**, 627 (8 February 2019). DOI: 10.1126/science.aah5065
Author affiliations: [1]Massachusetts Institute of Technology, [2]Georgia Institute of Technology, [3]University of California, San Diego, [4]Purdue University, [5]Argonne National Laboratory ‡Present address: Weizmann Institute of Science
Correspondence: * jpcorrea@gatech.edu, ** buonassisi@mit.edu, *** dfenning@eng.ucsd.edu

This research was supported by the U.S. Department of Energy (DOE) EERE Postdoctoral Research Award (J.-P.C.-B); National Science Foundation (NSF) grant CBET-1605495 (T.B.); Skoltech grant 1913/R as part of the Skoltech NGP Program (T.B., J.-P.C.-B., N.T.P.H., and S.W.); NSF grant DMR-1507803 (J.S., T.W., and L.H.); NSF grant GRFP 1122374 (M.A.J.); DOE grant DE-SC0001088 (L.N. and M.G.B.); California Energy Commission Advance Breakthrough EPC-16-050 (Y.L., S.W., Y.S.M., and D.P.F.); Hellman Fellowship (X.L. and D.P.F.); NSF grant CHE-1338173 (TEM work at UC, Irvine, IMRI); and San Diego Nanotechnology Infrastructure with NSF grant ECCS-1542148 (FIB and EBIC). Use of the Center for Nanoscale Materials, an Office of Science user facility, was supported by the U.S. DOE Office of Science-Basic Energy Sciences, under Contract No. DE-AC02-06CH11357. This research used resources of the Advanced Photon Source, a U.S. DOE Office of Science User Facility operated for the DOE Office of Science by Argonne National Laboratory under Contract No. DE-AC02-06CH11357.

Light Source Protein Structures Deposited in the Protein Data Bank*

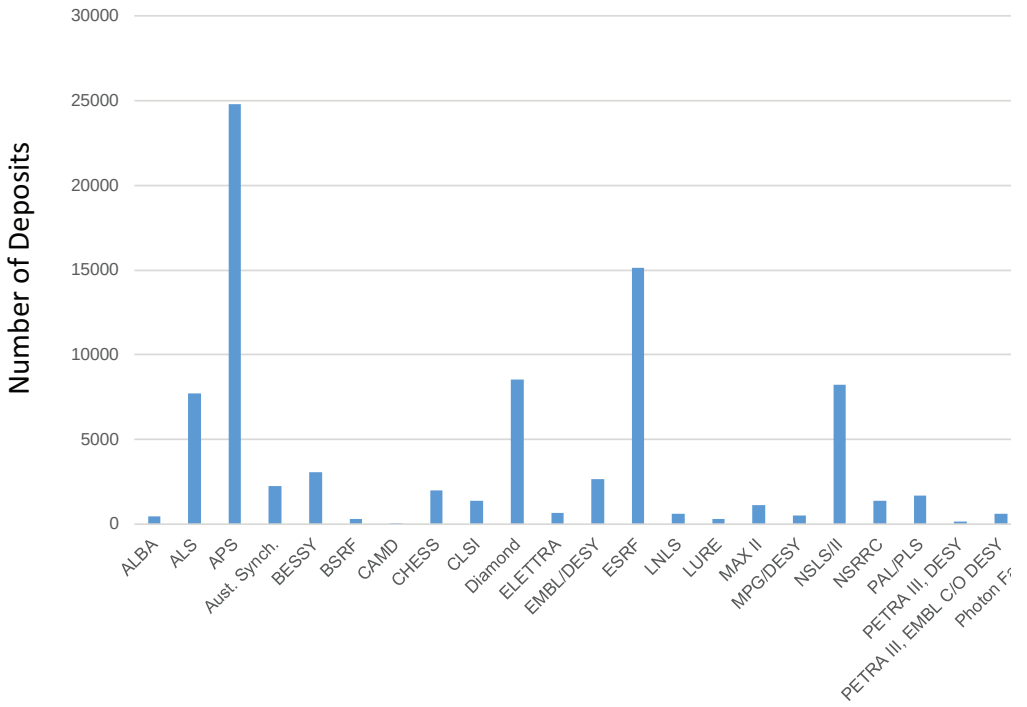

*As of 12.31.19

APS Journal Articles Recorded to Date (calendar years)*

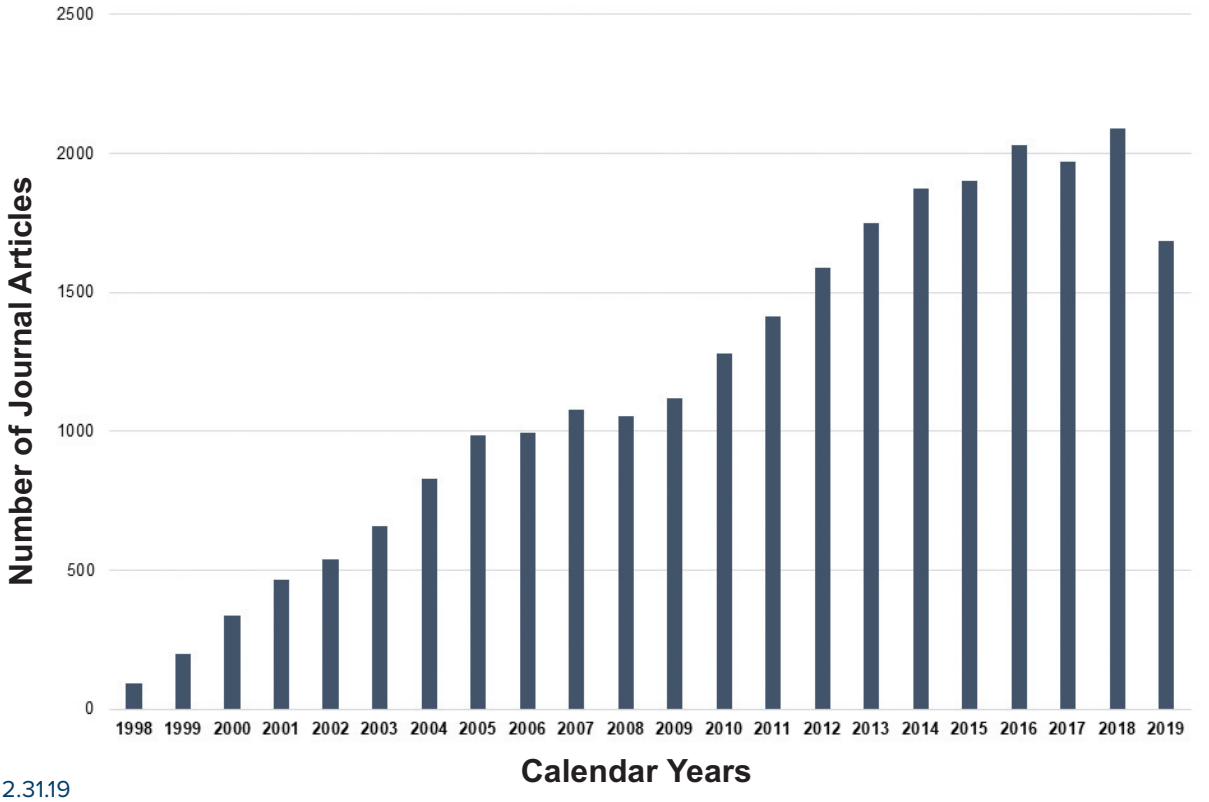

*As of 12.31.19

Soft Materials and Liquids

Why Z Phase Matters

Deep down on the inside, at the level of atoms, most solid pieces of matter are crystalline. Pure metals like iron often have simple crystal structures, while others can be more complex. Some are even quasicrystals, which have their atoms in complicated, crystal-like patterns that never quite repeat. Studies of the structure of crystalline materials show that many factors influence that atomic geometry, but the size and shape of an atom or molecule is the most important. And that can help solve real-world problems. Famously, British engineer Lord Kelvin in 1887 asked how space could be most efficiently partitioned into cells of equal volume with the least area of surface between them. Kelvin's problem has never been definitively solved, but in 1994 mathematicians demonstrated that a crystal structure, the Frank Kasper A15 phase, was more efficient than any previous solution. Frank Kasper structures are ordered approximations of quasicrystals. The A15 phase was the inspiration for the Beijing National Aquatics Center water cube for the 2008 Olympics because it allowed for the construction of a space with cells of equal volume using the least amount of material. Another Frank Kasper structure, the Z phase, could theoretically construct the same space with even less material—if the cells are allowed to be unequal. Now, a team of scientists has used the APS to show that the Z phase can exist in a soft, self-assembling material. Their work provides insight into potential special properties of Z phase matter, and shows how other, more complex Frank Kasper phases could be constructed.

In order to build a material with a Frank Kasper Z phase structure, researchers from the University of Akron in Ohio, the South China Institute of Technology, Northern Illinois University, The University of Tokyo (Japan), and the Riken Center for Emergent Matter Science (Japan) had to build a nano-sized, multipart molecule. They attached six identical polyhedral silesquioxane cages (six-sided polygons made of silicon and oxygen) to a central triphenylene core using covalent links with adjustable lengths. By tuning the lengths of the links just right, the researchers could persuade the complex molecules to self-assemble into spherical motifs, which then squish together to form polyhedra in Frank Kasper patterns (Fig. 1).

The resulting material, a white powdery solid, initially arranged itself in a Frank Kasper A15 phase. The team then annealed the material at 170 ° Celsius, and the material went through a structural phase transition to become a Frank Kasper Z phase. The researchers used ultraviolet spectroscopy to check that the phase transition occurred. But to really know for sure, the team, with colleagues from Argonne, imaged the atomic arrangement with small- and wide-angle x-ray scattering at XSD beamlines 12-ID-B and 12-ID-C of the APS.

X-ray scattering creates patterns as the x-rays bounce off atoms in a repeating arrangement in a crystalline solid. The regularly spaced atoms in the crystal can be described as being in planes; the patterns and difference in x-ray scatters between the planes can differentiate even between solids with the same chemical composition but different phase arrangements. The SAXS analysis clearly showed the difference between the Frank Kasper A15 formation and the Frank Kaspar Z.

The high energy and resolution of the APS x-ray beams make it possible to characterize different phases of a complex material clearly and efficiently. Beamline 12-ID-B contains two detectors to detect a wide range of scattered x-rays, and 12-ID-C can change the wavelength of the incoming x-rays by adjusting the source energies. Together, these Sector 12 beamlines allowed the researchers to study many different length scales in the material, and completely characterize the atomic arrangement of the structures.

Now that the researchers have shown a Frank Kasper Z phase in a soft material, they have the tools to assemble all 27 possible Frank Kaspar phases. In their future work, they plan to design other self-assembling molecules to demonstrate other unconventional structures in soft matter, such as bicontinuous P phase and the icosahedral quasicrystal phase. — Kim Krieger

See: Zebin Su[1,2], Chih-Hao Hsu[2], Zihao Gong[2], Xueyan Feng[2], Jiahao Huang[2], Ruimeng Zhang[2], Yu Wang[2], Jialin Mao[2], Chrys

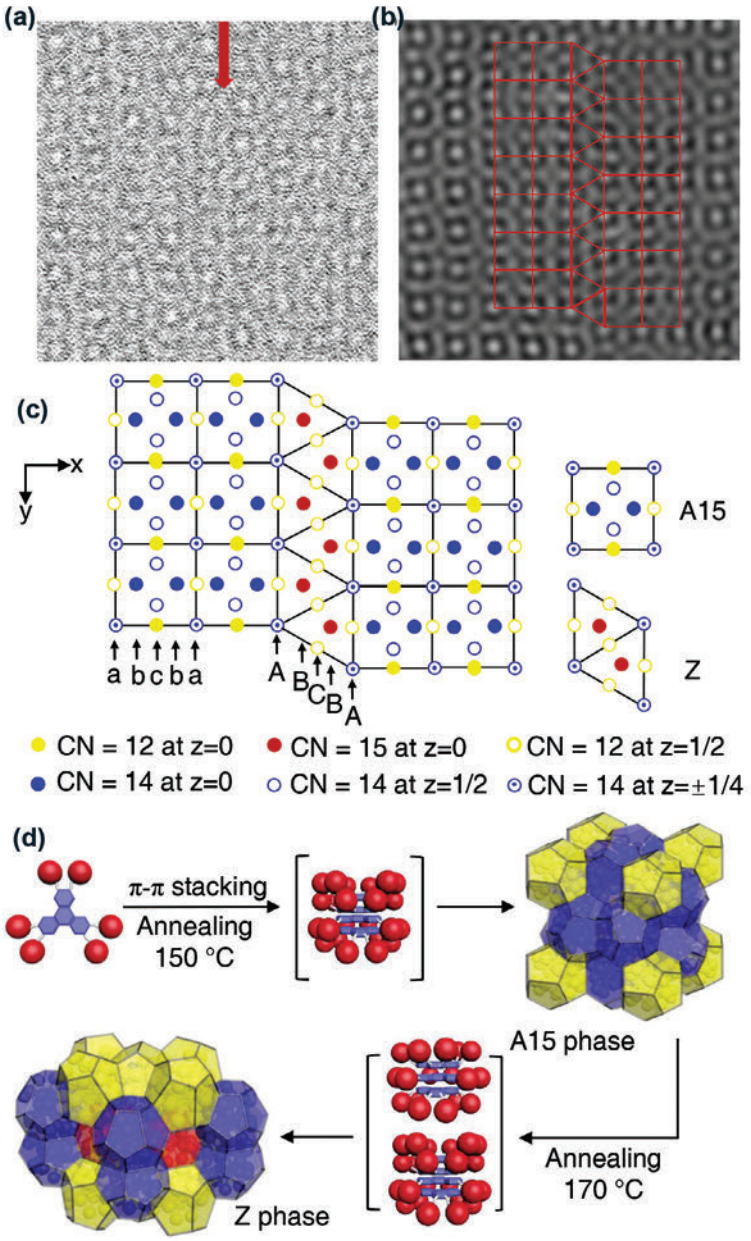

Fig. 1. The mechanism of phase transformation. Starting at top, first the silesquioxane (red) cages attach to the triphenylene core (blue). Then those units fit together to form a Frank Kasper A15 structure. In the structure they squish into polyhedra with either 12 faces (yellow) or 14 faces (blue). After annealing, some of the polyhedra squish even more to have 15 faces (red). This is the Frank Kasper Z phase. From Z. Su et al., Nat. Chem. **11**, 899 (October 2019). © 2019 Springer Nature Limited

Wesdemiotis[2], Tao Li[3,4], Soenke Seifert[3], Wei Zhang[1], Takuzo Aida[5,6], Mingjun Huang[1]*, and Stephen Z. D. Cheng[1,2]**, "Identification of a Frank–Kasper Z phase from shape amphiphile self-assembly," Nat. Chem. **11**, 899 (October 2019).
DOI: 10.1038/s41557-019-0330-x
Author affiliations: [1]South China University of Technology, [2]University of Akron, [3]Northern Illinois University, [5]The University of Tokyo, [6]Riken Center for Emergent Matter Science
Correspondence: * huangmj25@scut.edu.cn,
** scheng@uakron.edu

This work was supported by the National Science Foundation (DMR-1408872 to S.Z.D.C. and CHE-1808115 to C.W.) and the Program for Guangdong introducing Innovative and Entrepreneurial Teams (no. 2016ZT06C322). T. L. is grateful to the support by the Northern Illinois University start-up funds. This research used resources of the Advanced Photon Source, a U.S. Department of Energy (DOE) Office of Science User Facility operated for the DOE Office of Science by Argonne National Laboratory under contract no. DE-AC02-06CH11357.

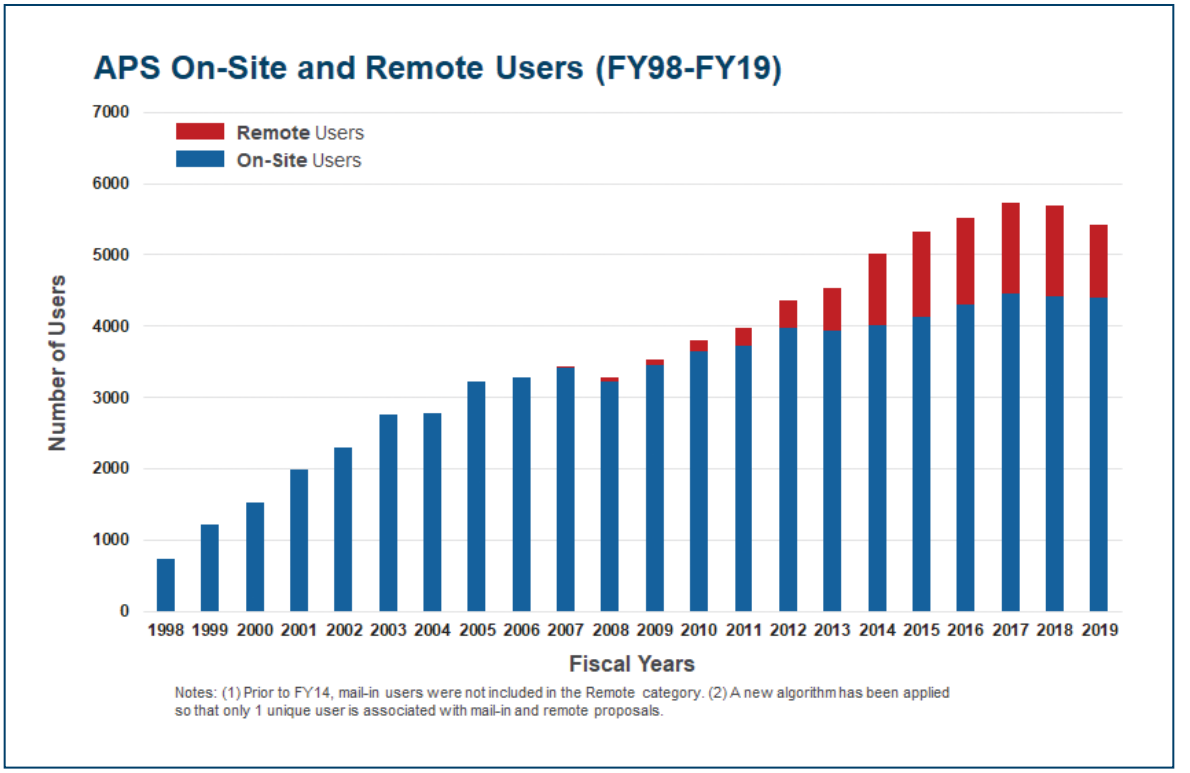
APS On-Site and Remote Users (FY98-FY19)
Remote Users
On-Site Users
Number of Users
7000
6000
5000
4000
3000
2000
1000
0
1998 1999 2000 2001 2002 2003 2004 2005 2006 2007 2008 2009 2010 2011 2012 2013 2014 2015 2016 2017 2018 2019
Fiscal Years
Notes: (1) Prior to FY14, mail-in users were not included in the Remote category. (2) A new algorithm has been applied so that only 1 unique user is associated with mail-in and remote proposals.

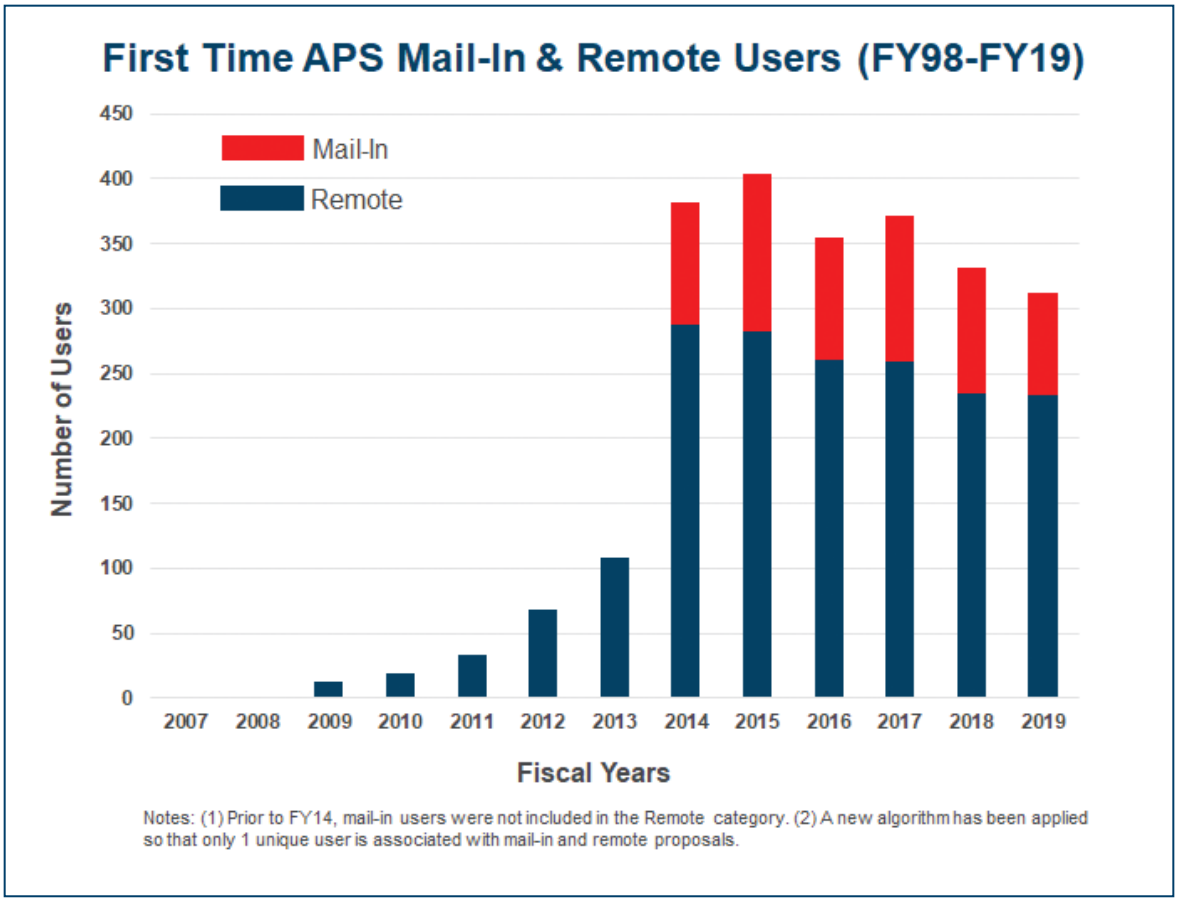
First Time APS Mail-In & Remote Users (FY98-FY19)
Mail-In
Remote
Number of Users
450
400
350
300
250
200
150
100
50
0
2007 2008 2009 2010 2011 2012 2013 2014 2015 2016 2017 2018 2019
Fiscal Years
Notes: (1) Prior to FY14, mail-in users were not included in the Remote category. (2) A new algorithm has been applied so that only 1 unique user is associated with mail-in and remote proposals.

Chemical Science

Revealing Porous Materials' Behavior under Pressure

Chemists rely on metal organic frameworks (MOFs) for a number of applications including catalyzing reactions, separating molecules, and trapping gases. Yet when exposed to pressure, for example in manufacturing processes, these porous materials are prone to unpredictable structural changes. Scientists have struggled to understand these shifts, which can impact a material's mechanical stability. Using x-ray experiments carried out at the APS, researchers investigated the compressibility of a select group of MOFs. The team discovered that the materials' ability to resist compression depends on particular structural properties such as linker length and the amount of internal empty space it contains. These insights could help researchers design valuable porous materials for high-pressure applications.

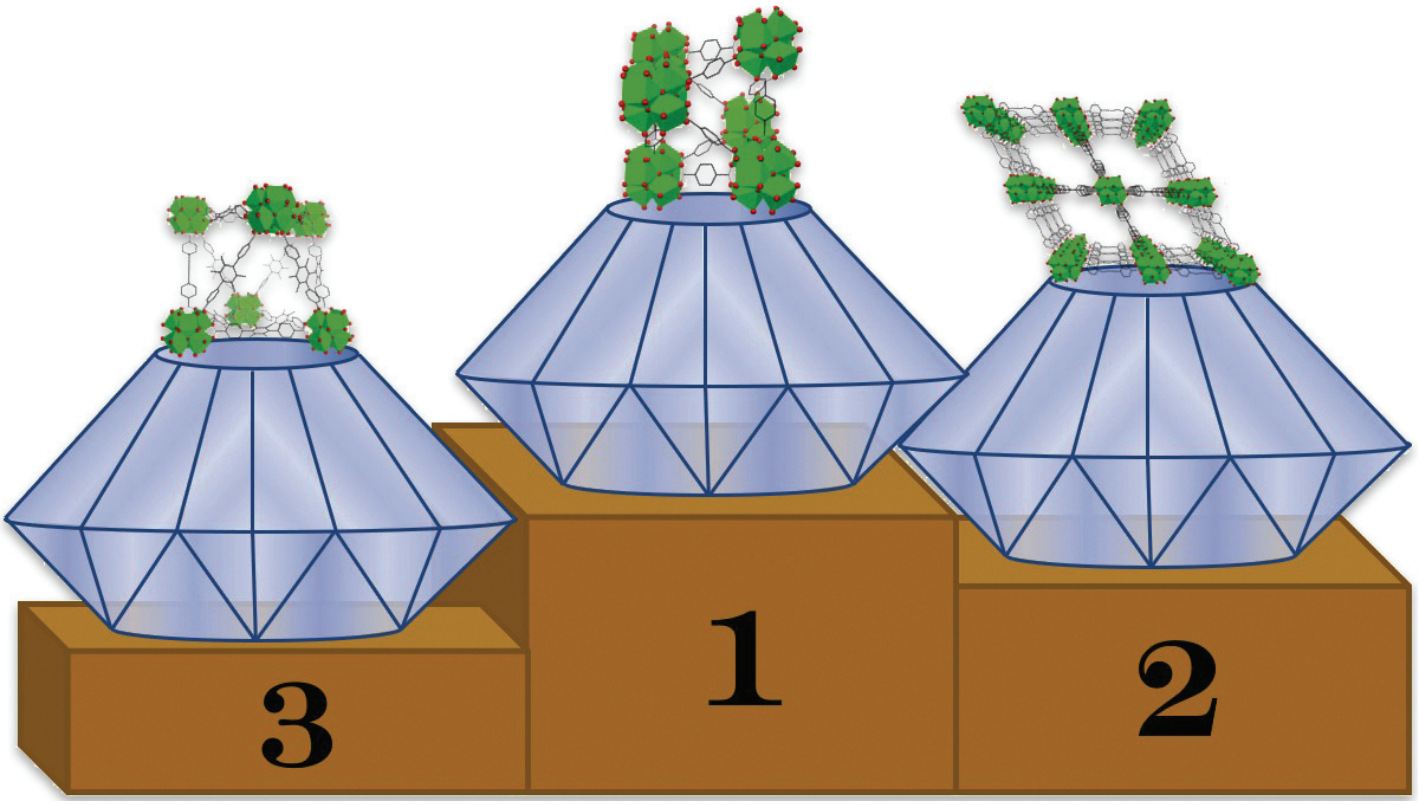

Fig. 1. Researchers evaluated the compressibility of seven MOFs, finding that UiO-66 (1) was the best at resisting compression while PCN-57 (3) was the worst; NU-903's (2) compressibility fell in between the two.

In recent years, MOF development has proliferated as researchers find more uses for these open structures. The enormous diversity of their architecture, however, has made it hard to systematically study the relationship between compression and structure, which includes numerous related and complicating aspects.

The present study offers the most extensive experimental investigation of compression in MOFs to date, according to the authors. The research team from Northwestern University, Stony Brook University, and Argonne evaluated seven zirconium (Zr)-based MOFs from two MOF families with distinct topologies: UiO MOFs that assemble into tetrahedral and octahedral cages, and NU-900 MOFs that form diamond-shaped channels interspersed with miniature windows.

First, the researchers synthesized the MOFs, taking extra precautions to minimize material defects, which can influence the measurement of a material's properties. MOFs were placed in a diamond anvil cell, a device in which samples are squeezed at intense pressure between two diamond tips. In the cell, the materials were subjected to pressures up to 0.5 GPa which are typically used in manufacturing processes such as pelletization or extrusion. The team probed the sample's properties through x-ray diffraction experiments using synchrotron radiation at the XSD 17-BM beamline of the APS.

While known for their chemical and thermal stability, the Zr MOFs readily buckled under pressure. The team measured each material's resistance to compression, known as its bulk modulus, and observed that the bulk moduli of the structurally similar MOFs spanned almost an order of magnitude—a range comparable to that of the malleable metal sodium and the stone quartz.

The researchers also investigated the MOFs key structural features to examine how each property impacts the materials' compressibility. These features include linker length, nearest node distance, ambient pressure node-node contraction, and void fraction, a measure of the empty space within the material.

Their analysis revealed several correlations between bulk modulus and structure. The team found that the void fraction and bulk modulus is inversely related for both MOF classes, meaning that as a material contains less empty space, it becomes more resistant to compression. Nearest node distance and linker length are also inversely related to bulk modulus, but to different degrees depending on the class of MOF.

Based on these observations, the authors propose that compression in all seven cases happens mostly through the distortion of the linker—essentially bending at an angle—and thus depends on the linker's flexibility. The team found that MOFs with pre-distorted structures had larger compression than those with undistorted structures. Notably, two MOFs, DUT-52 and PCN-57, which possess distorted linkers at ambient pressure, demonstrated much lower bulk moduli than other materials with very similar structures (Fig. 1). This compression mechanism requires empty space for the linker to bend, which supports the team's observation that as void fraction increases, bulk modulus decreases.

The authors propose that these relationships can be extended to other types of MOFs and porous materials as well. While further studies are needed, the researchers' findings provide the foundation for a predictive model of the compressibility of MOFs under pressure.

— Tien Nguyen

See: Louis R. Redfern[1,2], Lee Robison[1], Megan C. Wasson[1], Subhadip Goswami[1], Jiafei Lyu[1], Timur Islamoglu[1], Karena W. Chapman[2,3*], and Omar K. Farha[1**], "Porosity Dependence of Compression and Lattice Rigidity in Metal-Organic Framework Series," J. Am. Chem. Soc. **141**, 4365 (2019).
DOI: 10.1021/jacs.8b13009
Author affiliations: [1]Northwestern University, [2]Argonne National Laboratory, [3]Stony Brook University
Correspondence: * karena.chapman@stonybrook.edu,
** o-farha@northwestern.edu

O.K.F. gratefully acknowledges support from the Defense Threat Reduction Agency (HDTRA1-18-1-0003). This material is based on work supported in part by the U.S. Department of Energy (DOE) Office of Science, Office of Workforce Development for Teachers and Scientists, Office of Science Graduate Student Research (SCGSR) program. The SCGSR program is administered by the Oak Ridge Institute for Science and Education (ORISE) for the DOE. ORISE is managed by ORAU under contract DE-SC0014664. Use was made of the IMSERC x-ray facility at Northwestern University, which has received support from the Soft and Hybrid Nanotechnology Experimental (SHyNE) Resource (NSF ECCS-1542205), the State of Illinois, and the International Institute for Nanotechnology (IIN). This research used resources of the Advanced Photon Source, a U.S. DOE Office of Science User Facility operated for the DOE Office of Science by Argonne National Laboratory under contract no. DE-AC02-06CH11357.

Ultraviolet Light Makes a Polymer Run Hot or Cold

Plastic materials that can be switched from their normal character as heat insulating materials to ones that can conduct heat well by simply turning the lights on could have a wide range of applications in engineering. Applications might be found in carrying and releasing drug molecules to disease sites in the body, or controlling the way in which components in a device stick together. Or perhaps more obviously, in allowing heat to be channeled through a building or vehicle in a controlled way without the need for louvers and fans. Toward that end, researchers used the APS to investigate a plastic, polymeric material with a view to modifying it to change properties reversibly when light shines on it.

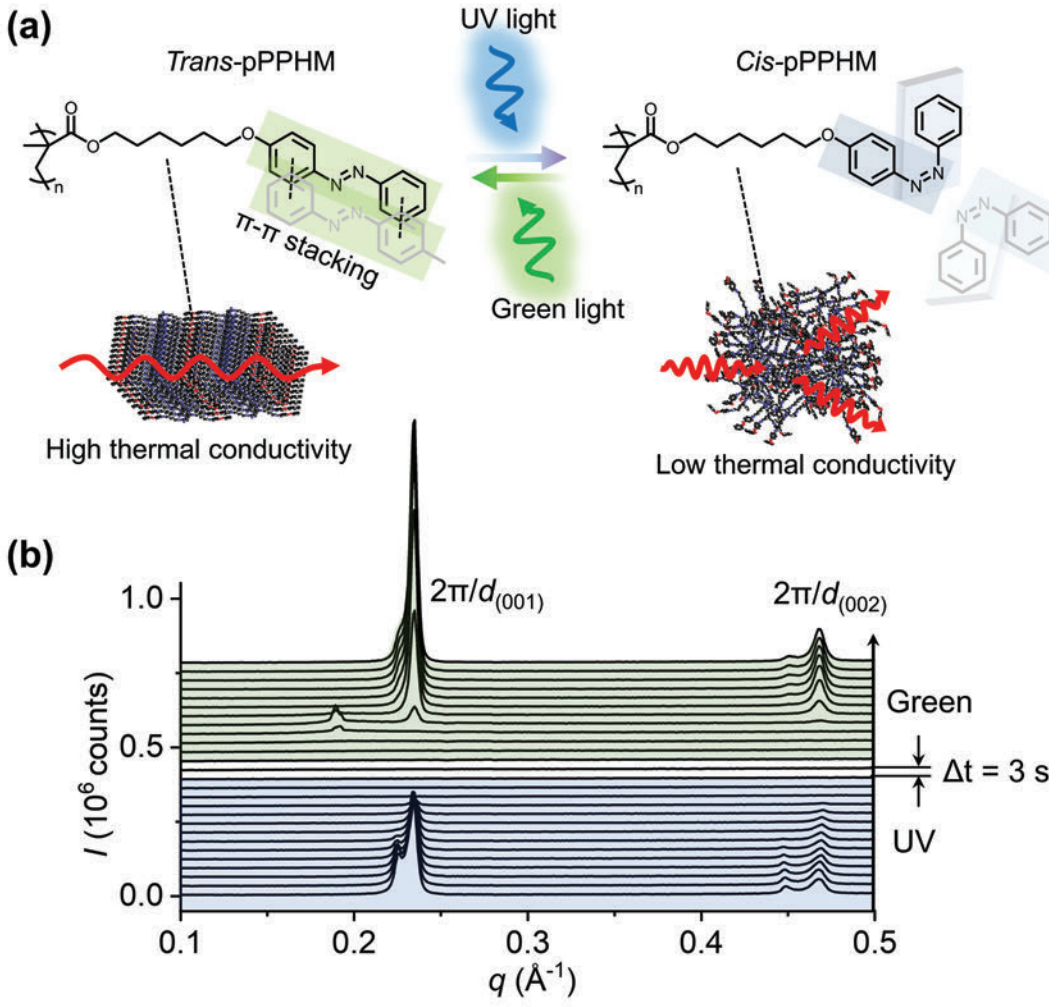

The properties of countless materials can be changed by heating them, adding acid or alkali, or in the case of so-called "photoresponsive materials," by bathing them in light. Such materials have found utility in diverse areas of modern technology for controlled drug delivery, in diagnostic and environmental sensors, in self-healing devices, and in the development of artificial muscles for robotics and other types of actuators. One aspect of such control that has been a prime target for research is the development of materials that can be switched from heat insulators to conductors and back again with a simple external stimulus.

The research team from the University of Illinois at Urbana-Champaign, Argonne, and the Air Force Research Laboratory modified their polymer with organic chemical groups containing a nitrogen atom known as azobenzene groups. These units exist in a flat, *trans*, form and a non-planar, *cis*, form. When they illuminate their azopolymer with ultraviolet light, the azobenzene side chains in the *trans* state flip to the *cis* state. This change in conformation is reversed by bathing the material with green light to reconfigure the azobenzenes once more to the trans state.

Critically, in the planar, or *trans*, form, the azobenzene groups stack together; this means that the polymer is quite solid; it is a semi-crystalline thermal conductor. However, when ultraviolet light shines on the material, the planar trans groups, in flipping to the non-planar *cis* state, can no longer stack neatly together. This makes the polymer chains lose their crystalline form and enter a liquid state. It is in this liquid state that the transport of heat is suppressed.

The material thus switches from a thermal conductor to a thermal insulator. The team's experiments show that the difference in conductivity between the two states is large – a more than threefold change. The transition takes place at room temperature within a matter of seconds. Green illumination causes recrystallization to take place and the azopolymer reverts to its solid, thermally conducting condition.

The researchers used synchrotron x-ray scattering to investigate in detail the structural changes that occur in their polymer modified with azobenzene groups and observe exactly how the change from *trans* to *cis* affects the material (Fig. 1). They looked at the azopolymer supported on an aluminum, polyimide, and sapphire support platform using XSD beamlines 12-ID-B and 12-ID-C at the APS. Specifically, the synchrotron x-ray research techniques of GIWAXS (grazing-incidence wide-angle x-ray scattering), transmission WAXS (wide-angle x-ray scattering), GISAXS (grazing-incidence small-angle x-ray scattering), and transmission SAXS (small-angle x-ray scattering) were key to unlocking the secrets of the azopolymer on the short- and long-range macromolecular scales. The samples were probed using 13.3 keV (12-ID-B) and 18 keV (12-ID-C) x-rays.

Thus, the team has demonstrated a fast transition induced by light; this represents powerful control of the thermophysical properties of a polymer. — David Bradley

< Fig. 1. (a) Schematic illustration of *trans* and *cis*-poly[6-(4-(phenyldiazenyl) phenoxy)hexyl methacrylate] (pPPHM) during light-triggered crystal-to-liquid transition. Ultraviolet light changes the shape of light-sensitive azobenzene groups in the polymer, driving melting and a reduction in thermal conductivity. (b) WAXS data of pPPHM. Under ambient condition or visible light (left side), the polymer exhibits sharp diffraction peaks indicating a highly ordered crystalline structure. Once exposed to UV light it transforms to a disordered liquid. Visible light reverses the transition and recovers the crystalline structure with high thermal conductivity.

See: Jungwoo Shin[1], Jaeuk Sung[1], Minjee Kang[1,] Xu Xie[1], Byeongdu Lee[2], Kyung Min Lee[3], Timothy J. White[3], Cecilia Leal[1], Nancy R. Sottos[1], Paul V. Braun[1]*, and David G. Cahill[1]**, "Light-triggered thermal conductivity switching in azobenzene polymers," Proc. Natl. Acad. Sci. U.S.A. **116**(13), 5973 (March 26, 2019). DOI: 110.1073/pnas.1817082116
Author affiliations: [1]University of Illinois at Urbana–Champaign, [2]Argonne National Laboratory, [3]Air Force Research Laboratory
Correspondence: * pbraun@illinois.edu, ** d-cahill@illinois.edu

Sample preparation and characterization were performed at the Materials Research Laboratory and the Beckman Institute for Science and Technology at the University of Illinois at Urbana–Champaign. This work was supported by the National Science Foundation (NSF) Engineering Research Center for Power Optimization of Electro-Thermal Systems, with Cooperative Agreement EEC-1449548, and Air Force Office of Scientific Research Grant FA9550-16-1-0017. This work was also supported by NSF Grant DMR 1554435. This research used resources of the Advanced Photon Source, a U.S. Department of Energy (DOE) Office of Science User Facility operated for the DOE Office of Science by Argonne National Laboratory under Contract DE-AC02-06CH11357.

Metal Centers Cooperate to Catalyze Controlled Carbene Polymerization

Polyolefins are pervasive materials found in products such as shoes, toys, and piping systems. They're made mostly by polymerizing olefin monomers, although this approach has its limits. A complementary synthetic strategy, known as carbene polymerization, generates polyolefins that can't be constructed from olefin monomers. Chemists have struggled to achieve a practical carbene polymerization method that proceeds in a controlled or living manner, desirable features that would allow researchers to promote growth at a constant rate and suppress chain termination to extend the polymer chain as desired. Now, scientists have developed a new class of initiators, called (π-allyl)palladium carboxylate dimers, that polymerizes carbene precursors in a controlled, quasi-living fashion. Based on experimental data obtained at the APS, as well as theoretical data, the research team suggests that the reaction occurs through a dinuclear mechanism previously unreported for carbene polymerization. These new mechanistic insights may help researchers design better initiators for carbene polymerization and other catalytic reactions as well.

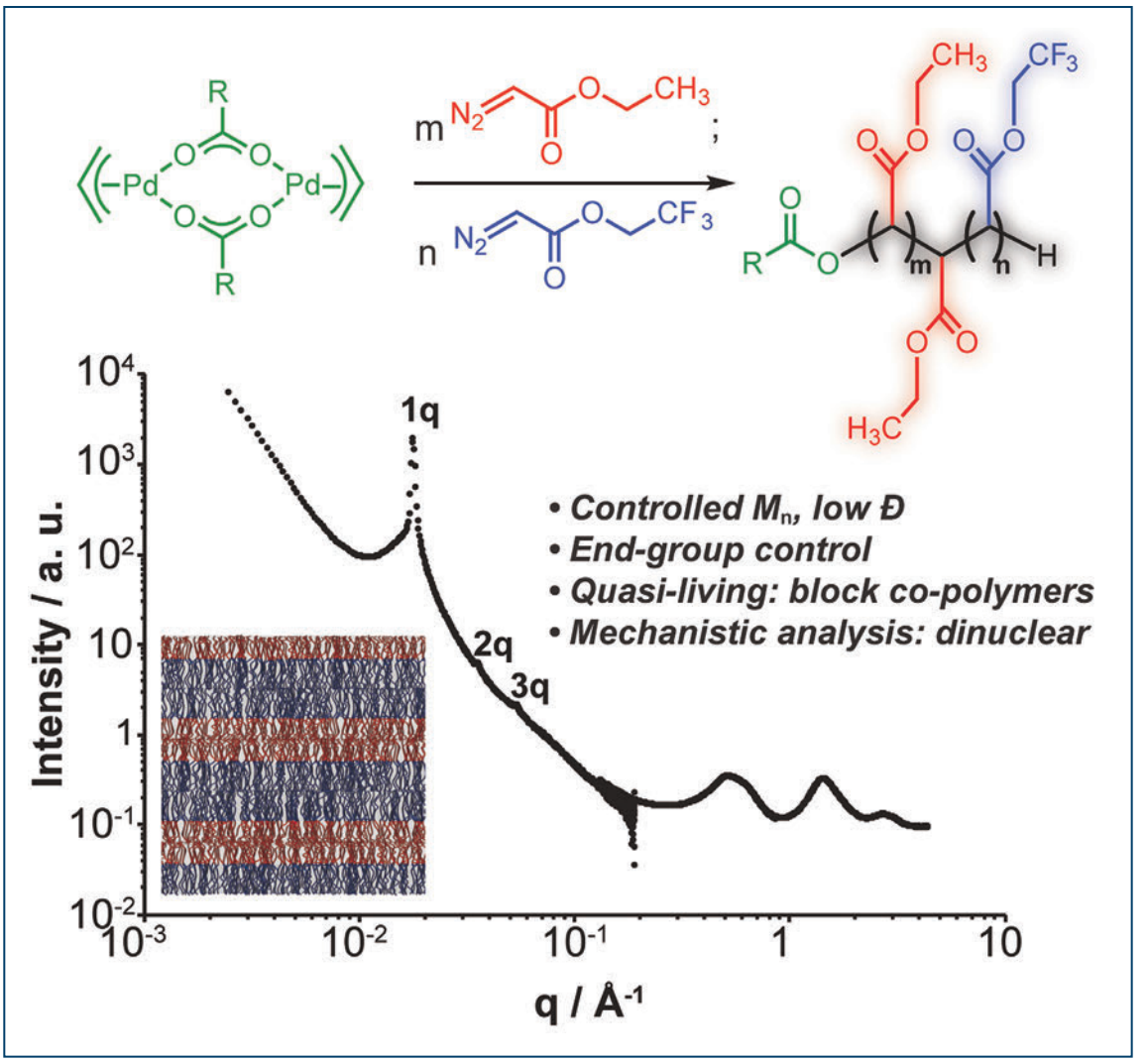

To carry out challenging reactions, enzymes often rely on multinuclear catalysis, which involves the cooperative action of more than one of the enzymes' metal centers. While chemists have admired this powerful tactic found in nature, multinuclear catalysis is a relatively underexplored area outside of enzymatic contexts compared to single-site catalysis. Researchers from the University of California, Berkeley, the University of Illinois at Urbana-Champaign, and Northwestern University reported a carbene polymerization reaction that appears to operate through multinuclear catalysis. Although previous studies have demonstrated carbene polymerization, these examples are limited and suffer from the formation of unwanted byproducts and lower polymer yields. In the new method, the polymerization occurs in close to quantitative yields and was also used to synthesize block copolycarbenes.

The team began their studies by evaluating the polymerization of ethyl diazoacetate (EDA) using a known (π-allyl)palladium chloride dimer initiator. This initiator affords polymerization in low to moderate yield, which researchers suspected was due to the chloride ligand's low nucleophilicity as well as Lewis basicity. To address this issue, the team switched chloride for the more nucleophilic and Lewis basic carboxylate. They observed that the (π-allyl)palladium carboxylate dimer led to a dramatically increased polymer yield of 87%, up from 13% yield with the chloride ligand initiator.

Polymerization of EDA using the improved carboxylate initiator produced high average molecular weight polymers (Mn ~25,000) and high degrees of polymerization (DP ~290). The average molecular weight values obtained indicated that half of the available Pd sites initiated chain growth, which supports a dinuclear mechanistic pathway. While initiator decomposition or partial consumption could have been responsible for this observation, a variable temperature proton nuclear magnetic resonance experiment reveal that wasn't the case.

The authors propose that, in a dinuclear mechanism, one of the acetate ligands initiates polymer growth through migratory insertion while the other acetate acts as a bridge between the two palladium centers, which was supported by experimental reaction kinetics data. They found additional evidence of the polymerization's dinuclear mechanism in density functional theory calculations.

< Fig. 1. Small-angle x-ray scattering profile (obtained at DND-CAT) of a diblock copolymer synthesized using the novel initiators. The lamellar morphology is illustrated at the bottom right. From A.V. Zhukhovitskiy et al., J. Am. Chem. Soc. **141**, 6474 (2019). © 2019 American Chemical Society

To evaluate the "livingness" of their method, the researchers subjected it to a chain lifetime test, in which EDA was added to the reaction in two batches, with progressively more time between the two batch additions. Fewer than 10% of the chains were terminated in 15 min, and extension proceeded effectively; thus, the authors characterized their method as quasi-living. Taking advantage of this feature, the researchers also carried out polymerization of EDA, followed by 2,2,2-trifluoroethyl diazoacetate to form diblock copolymers.

X-ray scattering analysis (Fig. 1) of these block copolymers at the DND-CAT 5-ID-B,C,D beamline at the APS revealed that the polymer films were well-ordered in a lamellar morphology, and the chains were highly extended.

These results describe a previously unseen dinuclear mechanism for carbene polymerization and offers mechanistic insights that could improve initiator design in the future. — Tien Nguyen

See: Aleksandr V. Zhukhovitskiy[1], Ilia J. Kobylianskii[1], Andy A. Thomas[2], Austin M. Evans[3], Connor P. Delaney[2], Nathan C. Flanders[3], Scott E. Denmark[2], William R. Dichtel[3], and F. Dean Toste[1]*, "A Dinuclear Mechanism Implicated in Controlled Carbene Polymerization," J. Am. Chem. Soc. **141**, 6474 (2019). DOI: 10.1021/jacs.9b01532
Author affiliations: [1]University of California, Berkeley, [2]University of Illinois Urbana-Champaign, [3]Northwestern University
Correspondence: * fdtoste@berkeley.edu

We thank the National Institute of Health (NIH) (R35 GM118190) for support of this work. A.V.Z. is a Merck Fellow of the Life Sciences Research Foundation. I.J.K. is a Swiss National Science Foundation (NSF) postdoctoral fellow. A.A.T. is a NIH National Research Service Award fellow (1F32GM125163). A.M.E. is supported by the NSF Graduate Research Fellowship under grant DGE-1324585, the Ryan Fellowship, and the Northwestern University International Institute for Nanotechnology. This work made use of the UC Berkeley Catalysis Center, managed by M. Zhang, the College of Chemistry and QB-3 Institute NMR facilities, the Stanford University Mass Spectrometry facility, and DND-CAT, which is supported by Northwestern University, The Dow Chemical Company, and DuPont de Nemours, Inc. Data was collected using an instrument funded by the NSF under award no. 0960140. Work at the Molecular Foundry was supported by the Office of Science-Basic Energy Sciences, of the U.S. Department of Energy (DOE) under contract DE-AC02-05CH11231. DFT studies were conducted at the Molecular Graphics and Computation Facility, funded by NIH grant S10OD023532. This research used resources of the Advanced Photon Source, a U.S. Department of Energy (DOE) Office of Science User Facility operated for the DOE Office of Science by Argonne National Laboratory under contract DE-AC02-06CH11357.

Meeting a Carbon Dioxide Reduction Challenge

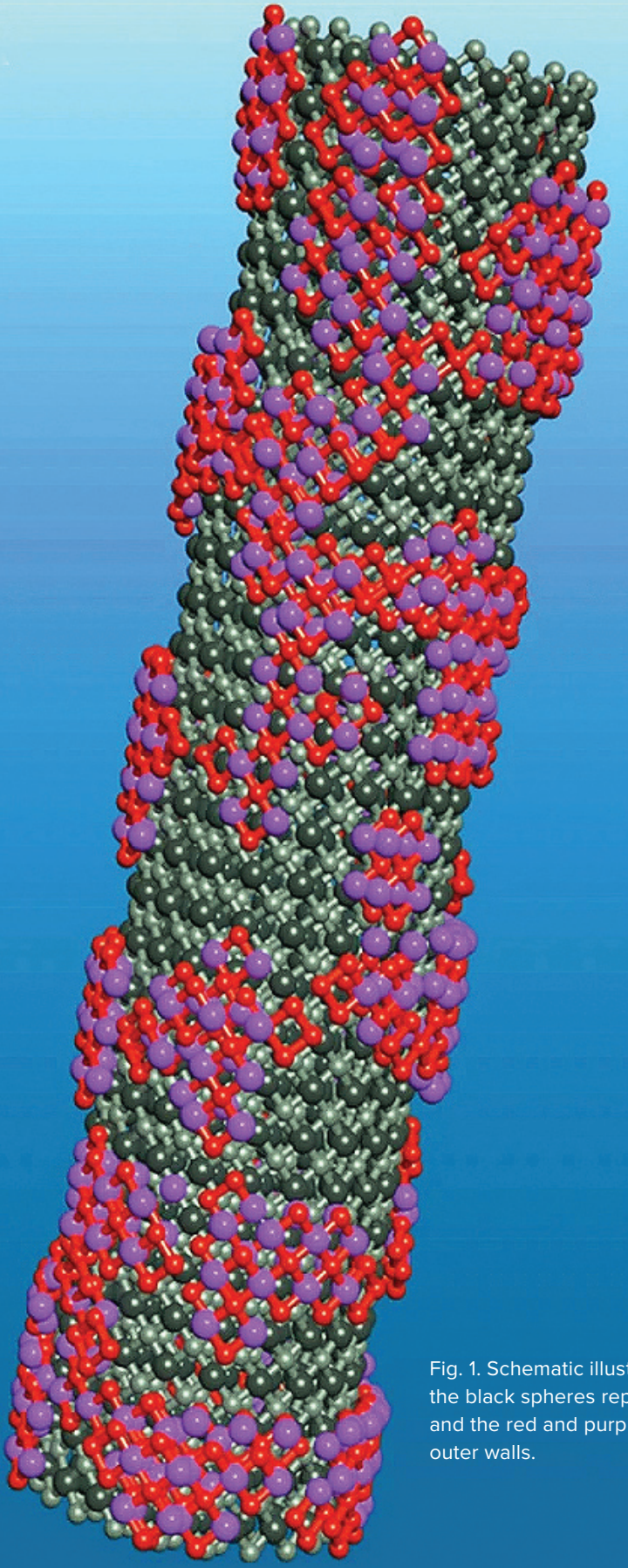

Fig. 1. Schematic illustration of the structure of Bi_2O_3 NTs; the black spheres represent the crystalline inner walls, and the red and purple spheres represent the fragmented outer walls.

Electrochemical carbon dioxide (CO_2) reduction (CDR) provides an efficient strategy for solving energy and environmental problems. It uses the electricity generated by renewable energy sources to drive the electrochemical immobilization of CO_2 and convert it into high value-added chemical products. But electrochemical CDR currently faces many challenges, including slow reaction kinetics, low selectivity of target products, and competitive hydrogen evolution reactions. Therefore, the development of cost-effective, stable and highly efficient CDR electrocatalyst is the key to the large-scale application of electrochemical CDR technology. Using a simple solvothermal method, a multi-institution international research team synthesized a bismuth oxide nanotube precursor with a one-dimensional tubular structure that exhibits very good catalytic activity in electrochemical carbon dioxide reduction. *In situ* synchrotron radiation characterization carried out at the APS showed that the bismuth oxide catalyst precursor had a large number of structural defects after it was converted into a metal phase at the cathode side. The theoretical calculations show that the existence of defects is very helpful to improving CDR catalytic activity. The test results of both the H-type electrolytic cell and the flow cell confirm its excellent electrochemical performance. This work provides a viable guide for materials design applied to the large-scale implementation of electrochemical CO_2 fixation.

The authors first prepared a Bi_2O_3 nanotube (Fig. 1) with a fragmented outer surface and then converted it into a highly deficient metal NTD-Bi by a cathodic conversion method. In the H-type electrolytic cell, the Faraday efficiency of formic acid can remain between 98% and 100% with a current density achieving 36 mA/cm^2 during the 48-h tests in a CO_2 saturated 0.5M $KHCO_3$ electrolyte. In the self-designed flow cell, the NTD-Bi catalytic performance of CDR to produce formate can achieve a current density up to 210 mA/cm^2, and Faraday efficiency of 98%, which can last for 11-13 h in 1M KOH electrolyte. This is the first time the technical requirements of commercial applications have been met, in which the current density should be greater than 200 mA/cm^2, the productivity of formic acid should be over 95%, and the stability should reach 1000 h. In addition, the combining of NTD-Bi with silicon demonstrates the good photo-electrocatalytic performance of CDR in producing formate.

In order to explore the fine structure and chemical environment of the catalyst during the electrochemical reduction of CO_2, the authors conducted synchrotron *in situ* and *operando* x-ray absorption spectroscopy (XAS) measurements at the DND-CAT x-ray beamline 5-BM-D at the APS. The XAS results confirmed that Bi_2O_3 nanotubes had been reduced to NTD-Bi before the CO_2 reduction reaction (-0.24 V), in which the coordination number of Bi-Bi is 2.6±1.8, significantly smaller than the coordination number of the standard bismuth metal (CN = 6). Although the authors were unable to accurately determine the atomic configuration of these low coordination sites, the EXAFS results provide reliable evidence that NTD-Bi has a large number of defects or voids under actual operating conditions. The authors also used density functional theory (DFT) for simulation analysis to compare the CO_2 reduction pathways on the ideal and defective Bi surfaces, which show that the presence of abundant defect sites in NTD-Bi can stabilize the *OCHO (intermediate to formate) and greatly enhance the kinetics of the reaction.

See: Qiufang Gong[1], Pan Ding[1], Mingquan Xu[2], Xiaorong Zhu[3], Maoyu Wang[4], Jun Deng[1], Qing Ma[5], Na Han[1], Yong Zhu[2], Jun Lu[6], Zhenxing Feng[4]*, Yafei Li[3]**, Wu Zhou[2]***, and Yanguang Li[1]****, "Structural defects on converted bismuth oxide nanotubes enable highly active electrocatalysis of carbon dioxide reduction," Nat. Commun. **10**, 2807 (2019).
DOI: 10.1038/s41467-019-10819-4
Author affiliations: [1]Soochow University, [2]University of Chinese Academy of Sciences, [3]Nanjing Normal University, [4]Oregon State University, [5]Northwestern University, [6]Argonne National Laboratory
Correspondence: **** yanguang@suda.edu.cn,
*** wuzhou@ucas.ac.cn, ** liyafei@njnu.edu.cn,
* zhenxing.feng@oregonstate.edu

Y.G.L. acknowledges the support from the Ministry of Science and Technology of China (2017YFA0204800), the Priority Academic Program Development of Jiangsu Higher Education Institutions, and Collaborative Innovation Center of Suzhou Nano Science and Technology. Y.F.L. acknowledges the support from the National Natural Science Foundation of China (21873050). W.Z. thanks the financial support from the Ministry of Science and Technology of China (2018YFA0305800) and the National Natural Science Foundation of China (51622211). Z.F. thanks the start-up funding from Oregon State University. Q.F.G. thanks the support from the Postgraduate Research & Practice Innovation Program of Jiangsu Province (KYCX17_2045). DND-CAT, which is supported by Northwestern University, The Dow Chemical Company, and DuPont de Nemours, Inc. This research used resources of the Advanced Photon Source, a U.S. Department of Energy (DOE) Office of Science User Facility operated for the DOE Office of Science by Argonne National Laboratory under Contract No. DE-AC02-06CH11357.

A Highly Active Single-Atom Electrocatalyst for Oxygen Evolution Reaction

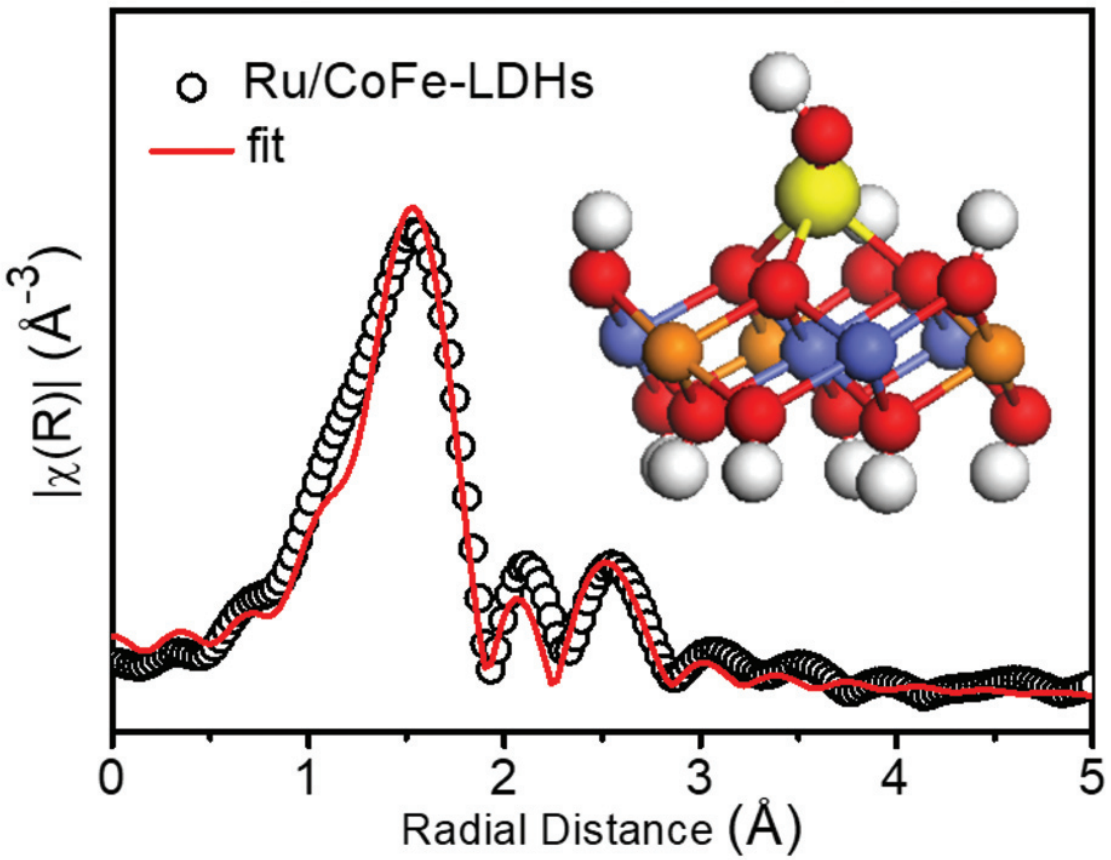

Fig. 1. Corresponding model-based fittings of Ru EXAFS for Ru/CoFe-LDHs and simulated EXAFS spectra from Ru–O and Ru–O–M (M = Co or Fe) bonds (the inset is the magnifying local structure of Ru/CoFe-LDHs), showing the exclusive existence of Ru–O–M bonds in Ru/CoFe-LDHs sample

A highly active and stable single-atomic ruthenium (Ru) catalyst has been engineered to exhibit lower overpotential and better stability than commercial benchmark RuO_2 catalyst. The mechanism of its record-high activity has been studied using high-brightness synchrotron x-rays by a research team carrying out structural and valence characterization of the material at the APS. This work has provided a new guideline for materials design and also demonstrated potential applications in the industrialization of cost-effective and efficient energy conversion devices.

High-energy, dense, and environmentally benign hydrogen has attracted much attention as a new sustainable energy resource. The water electrolyzer, an electrochemical energy conversion device to split water, is one of the promising methods for producing hydrogen. However, it requires stable and highly active electrocatalysts, since the key half-reaction, oxygen evolution reaction (OER), suffers from sluggish kinetics. This is because total four-electron transfer is needed to convert OH^- in water to oxygen (O_2) in this reaction, thus slowing down the process compared to fast and effective one-electron transfer reaction (e.g., H^+ to H atom). The research team in this work, led by Beijing University of Chemical Technology and Oregon State University, has developed a single-atom Ru catalyst by using the transition metal layered double hydroxide (LDH) as support to fix the single Ru atom and act as co-active sites. This method largely reduces the usage of precious metal (Ru) and relies on the earth-abundant materials, which not only lowers the cost of catalysts but also improves the energy conversion efficiency.

Most single atom catalysts are unstable and so can form significant agglomerates under reaction conditions. This restructuring can be caused by various conditions and lead to less than desirable catalytic performance. However, the new Ru single-atom catalyst developed by the team shows opposite properties: super stable and hightly efficient. By using the *in situ* and *operando* x-ray absorption spectroscopy (XAS) at the DND-CAT x-ray beamline 5-BM-D at the APS, the team was able to find out why by the direct observation of the structure and oxidization state change of each element in the complex catalyst (Fig. 1) under OER condition. *Ex situ* XAS spectra were collected at the 1W1B end station of the Beijing Synchrotron Radiation Facility.

The team correlated the catalytic performance with the oxidization state and catalyst structures determined from the *in situ* XAS. Comparing with several different Ru catalysts that are anchored on different LDH substrates, the LDH with cobalt (Co) and iron (Fe) elements show the lowest OER overpotential (198 mV at 10 mA/cm^2). This extremely positive catalytic performance was the result of the strong synergetic electron coupling between Ru and CoFe atoms, which was also confirmed by theoretical calculations. The reversible structure change of Ru and irreversible structure change of CoFe suggests that the Ru atoms is the active site for OER, and the shorter Ru-O-Metal bonding formation under reaction condition is the key to further stabilize the Ru single atom. This special arrangement confines the Ru oxidization state to be lower than 4+ (Ru^{4+}), which explains the stability mechanism of the engineered catalyst.

The authors also applied the solubility test on RuO_2 and Ru single atoms, further demostrating the better stability of Ru/CoFe-LDHS compared to RuO_2. Moreover, the density function theory calculations on Ru anchored on different LDHs confirms the strongest synergetic electron coupling results in the lowest activation energy barrier.

See: Pengsong Li[1, 2], Maoyu Wang[3], Xinxuan Duan[1], Lirong Zheng[4], Xiaopeng Cheng[5], Yuefei Zhang[5], Yun Kuang[1], Yaping Li[1], Qing Ma[6], Zhenxing Feng[3]*, Wen Liu[1]**, and Xiaoming Sun[1]***, "Boosting oxygen evolution of single-atomic ruthenium through electronic coupling with cobalt-iron layered double hydroxides," Nat. Commun. **10**, 1711 (2019). DOI: 10.1038/s41467-019-09666-0
Author affiliations: [1]Beijing University of Chemical Technology, [2]Yale University, [3]Oregon State University, [4]Institute of High Energy Physics of the Chinese Academy of Sciences, [5]Beijing University of Technology, [6]Northwestern University
Correspondence: *** sunxm@mail.buct.edu.cn,
* zhenxing.feng@oregonstate.edu, ** wenliu@mail.buct.edu.cn

This work was financially supported by the National Natural Science Foundation of China (NSFC), the National Key Research and Development Project(Grant No. 2016YFF0204402), the Program for Changjiang Scholars and Innovative Research Team in the University (Grant No. IRT1205), the Fundamental Research Funds for the Central Universities, the Long-Term Subsidy Mechanism from the Ministry of Finance and the Ministry of Education of PRC. P.L. thanks financial support from the China Scholarships Council (CSC). Z.F. thanks the startup financial support from Oregon State University. DND-CAT is supported by Northwestern University, E.I. DuPont de Nemours & Co., and The Dow Chemical Company. This research used resources of the Advanced Photon Source, a U.S. Department of Energy (DOE) Office of Science User Facility operated for the DOE Office of Science by Argonne National Laboratory under Contract No. DE-AC02-06CH11357.

Making Methane More Malleable with Metal-Organic Frameworks

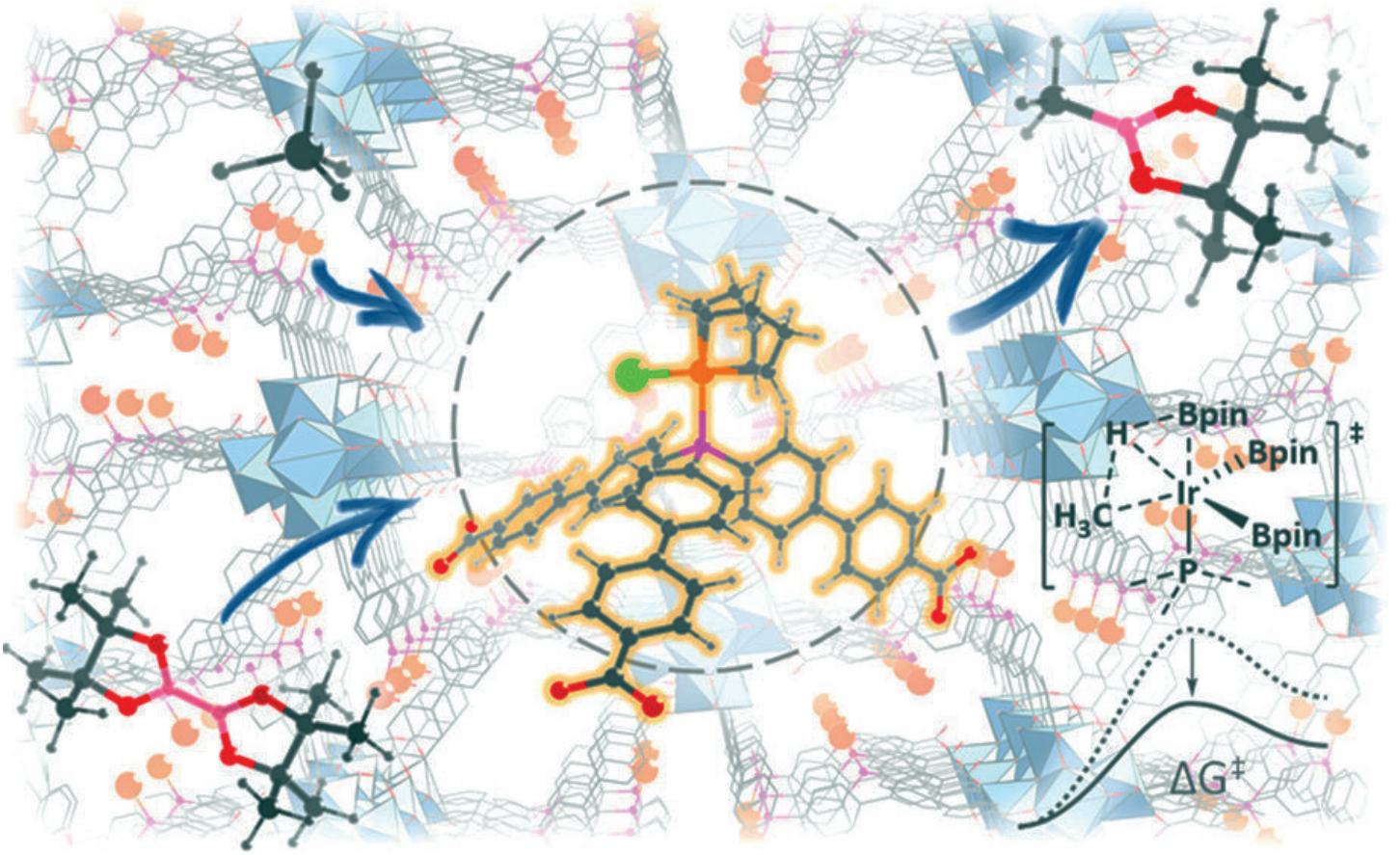

Fig. 1. A MOF stabilizes a four-coordinated iridium (Ir) catalytic site and lowers the activation barrier for methane borylation.

Just because a molecule is small and simple does not make it easy to manipulate. Methane, a single carbon bonded to four hydrogen atoms, is the simplest hydrocarbon molecule. Due to its abundance in shale gas and other sources, methane has extraordinary potential as a building block for a wide range of useful chemicals, from fuels to polymers. However, converting methane to these chemicals is difficult because of chemistry challenges, limiting methane's potential. In this work, researchers describe a novel approach to methane activation: borylation with catalytic help from a metal-organic framework (MOF). Using the APS, the team characterized the MOF and demonstrated how to jumpstart methane borylation, offering a promising strategy for getting more out of methane.

Methane's chemical stubbornness has two main causes. First, methane's carbon-hydrogen bonds are extremely strong, making the molecule resistant to chemical reactions. Second, selectivity issues can lead to the production of unwanted side products. Lengthy and energy-intensive high-temperature reaction conditions can overcome these challenges, but chemists for obvious reasons would prefer a simpler way to activate methane under mild conditions.

Borylation is a common strategy for activating otherwise inert molecules, such as methane. The reaction creates an easily cleavable carbon-boron bond that is primed for downstream reactions. Yet, previous attempts to borylate methane have met with mixed results, often resulting in products with multiple boron atoms, which is problematic for downstream reactions. Moderate progress has come from homogenous reaction conditions using phenanthroline- and diphosphine-iridium complexes to promote methane borylation under mild conditions, but catalytic activity and selectivity remain less than ideal.

In this study, the research team turned toward MOFs to solve their catalytic and selectivity challenges. MOFs are a class of compounds that include a metal or metal cluster, in this case zirconium, coordinated by organic ligands to form, again in this case, a three-dimensional structure. The coordinated iridium serves as the catalytic center, while the surrounding framework can be carefully selected and formed to optimize a reaction. Rather than homogenous conditions, MOFs can, by virtue of their rigid structure, offer greater control over a chemical reaction by exerting the spatial arrangement of atoms and directional control over the reaction.

The researchers studied a series of mono(phosphine)-Ir-based MOFs, and found one, Zr-P1-Ir, that outperformed other complexes for catalyzing the mono-borylation of methane, providing an impressive turnover number of 127 at a relatively mild temperature of 110° C. To better understand the mechanism of the highly performing MOF, which may help the researchers improve performance further, the researchers collected x-ray absorption spectra of the MOFs at the MR-CAT 10-BM-B x-ray beamline of the APS. The data revealed that Zr-P1-IR adopts a distorted tetrahedral geometry with one chloride, one bidentate COD (1,5-cyclooctadiene), and one mono(phosphosphine) from the MOF ligand.

Additional x-ray absorption near edge structure data, also collected at the MR-CAT beamline, uncovered the metal center oxidation states. This structural data, combined with density functional theory calculations, suggested that MOFs stabilize highly active and low-coordinate Ir complexes that are key for promoting catalytic methane borylation (Fig. 1). The authors say that this strategy may be generally applied, beyond methane, for the activation of inert compounds. — Erika Gebel Berg

See: Xuanyu Feng[1], Yang Song[1], Zhe Li[1,2], Michael Kaufmann[1], Yunhong Pi[1,3], Justin S. Chen[1], Ziwan Xu[1], Zhong Li[3], Cheng Wang[2], and Wenbin Lin[1]*, "Metal–Organic Framework Stabilizes a Low-Coordinate Iridium Complex for Catalytic Methane Borylation," J. Am. Chem. Soc. **141**(28), 11196 (2019).
DOI: 10.1021/jacs.9b04285
Author affiliations: [1]The University of Chicago, [2]State Key Laboratory of Physical Chemistry of Solid Surface, [3]South China University of Technology
Correspondence: * wenbinlin@uchicago.edu

This work was supported by the National Science Foundation (Grant CHE-1464941). Z. Li and Y. Pi acknowledge financial support from the China Scholarship Council. We thank Mr. Wenbo Han and Mr. Taokun Luo for experimental help. MR-CAT operations are supported by the U.S. Department of Energy (DOE) and the MR-CAT member institutions. This research used resources of the Advanced Photon Source, a U.S. DOE Office of Science User Facility operated for the DOE Office of Science by Argonne National Laboratory under Contract No. DE-AC02-06CH11357.

A Compound that Can Switch Between Single- or Multi-Site Reactivity

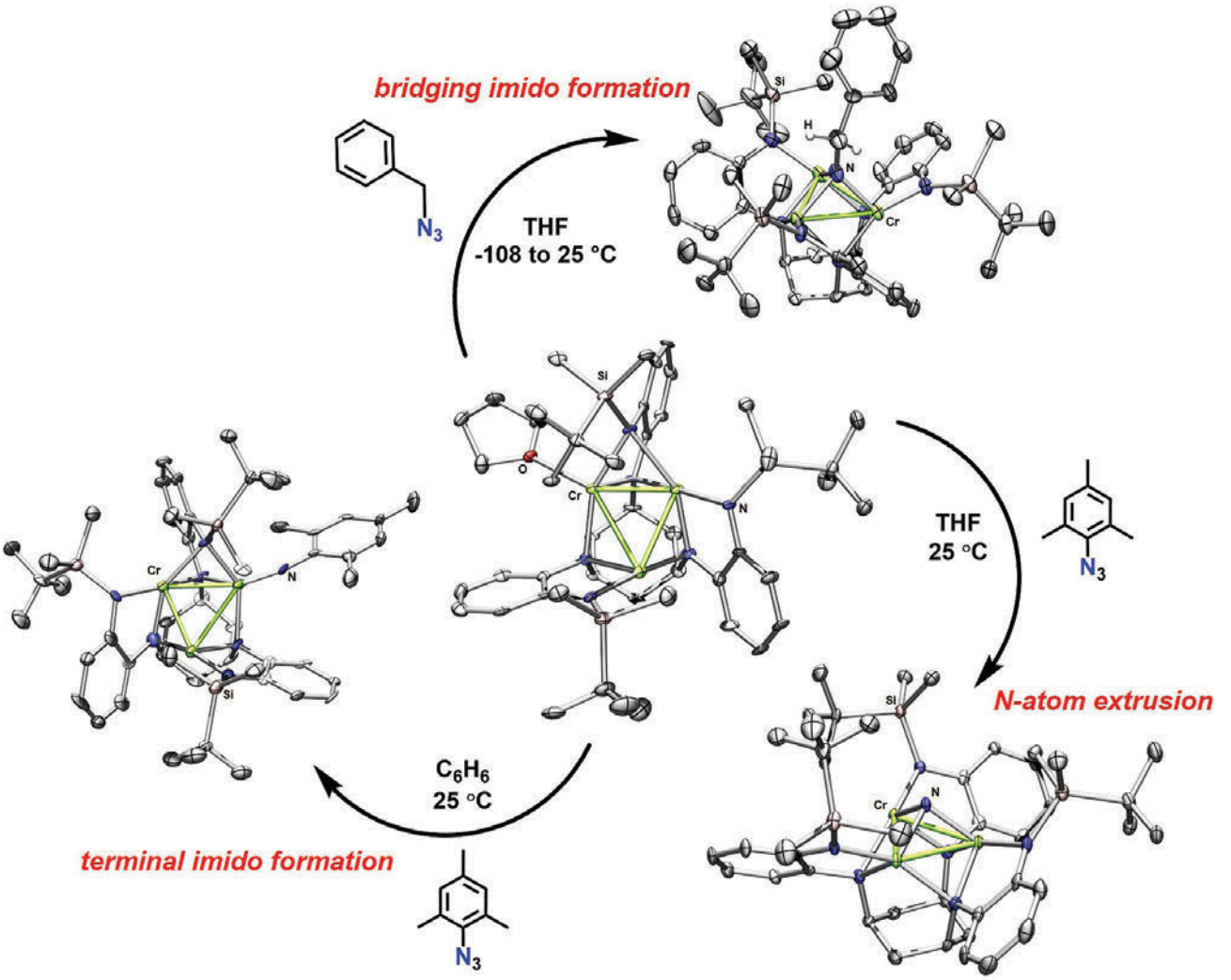

Fig. 1. The ligand-templated trichromium complex (center) undergoes three distinct modes of reactivity with organic azides: single-site reactivity to form a terminal imido (left), cooperative azide activation to form a bridging imido (top right), and cooperative terminal N-atom extrusion from the azide to form a bridging nitride (bottom right).

Over millennia, many enzymes have evolved the ability to catalyze extremely challenging chemical reactions. These enzymes derive this enviable ability from their polynuclear reactivity, which involves multiple active metal sites in the compound cooperatively reacting with small molecules substrates depending on their size and the surrounding environment. However, exactly how this happens is poorly understood. In hopes of harnessing this powerful reactivity, synthetic chemists have designed reactive polynuclear cluster compounds to mimic this chemistry, although they've struggled to control how the compounds react with substrates. Now, a team of researchers, supported by data obtained at the APS, has developed a trichromium cluster that demonstrates distinct single- or multi-site reactivity depending on the solvent and size of the reaction substrate. By taking advantage of this molecular strategy found in nature, scientists may be able to explore new reactivity for small-molecule substrates.

In nature, the bacterial enzyme carbon monoxide dehydrogenase (CODH) converts carbon dioxide to carbon monoxide and back again, and is crucial to the global carbon cycle. To perform this transformation, CODH's complex protein environment controls small-molecule access to the enzyme's polynuclear reaction sites. Researchers are attempting to recreate this type of chemistry in the lab by designing polynuclear metal cluster compounds.

To this end, a team of scientists from Harvard University and The University of Chicago developed a novel trichromium cluster compound, (^{tbs}L)Cr_3(thf), that exhibits single- and multi-site reactivity (Fig. 1).

The team synthesized the trinuclear cluster compound starting from a bulky hexadentate templating ligand (*ortho*-phenylenediamine-based) and three equivalents of a chromium precursor compound. They previously attached the same ligand to a triiron cluster that also exhibited cooperative reactivity. X-ray diffraction experiments revealed that each chromium atom has a distinct molecular environment: Cr1 is bound to three anilide molecules and a molecule of tetrahydrofuran; Cr2 is surrounded by four anilide molecules; and Cr3 sits at a three-coordinate site.

The scientists exposed the trichromium cluster to azide compounds under various reaction conditions and observed three distinct reaction products (Fig. 1). First, the team reacted the trichromium compound with benzyl azide at low temperature to produce a symmetric, bridged imido complex (^{tbs}L)Cr_3(μ^3-NBn). They moved to a larger mesityl azide substrate dissolved in benzene which gave the terminally-bound imido complex (^{tbs}L)Cr_3(μ^1-NMes). Finally, the researchers observed that reacting the trichromium cluster with mesityl azide and switching to tetrahydrofuran as the solvent resulted in a bond cleavage to give the nitride complex (^{tbs}L)Cr_3-(μ^3-N). The researchers confirmed the product structures through single-crystal x-ray diffraction data obtained using the ChemMatCARS 15-ID-B,C,D x-ray beamline at the APS.

Using proton nuclear magnetic resonance spectroscopy experiments, the researchers investigated how the substrate size and solvent affected the reaction pathway. In the reaction between the trichromium cluster and the benzyl azide substrate, the authors suggest that the small molecule can easily access the cluster's trinuclear face and form the bridging product. However, when trichromium is in the presence of azide substrates that are bulkier, like mesityl azide, these molecules react faster at the tetrahydrofuran site, which is the most accessible site in the cluster. In the case of the larger azide substrates, the reaction solvent dictates what product will form. When benzene is the solvent, the tetrahydrofuran ligand dissociates to help form terminal imido products. When the solvent is tetrahydrofuran, this ligand dissociation is minimized, encouraging reaction on the trinuclear face, which is followed by N-N bond cleavage to produce a nitride compound because of the substrates' bulkiness.

The researchers' results demonstrate that their novel trichromium complex can react with organic azide compounds with controlled single- or multi-site reactivity. They plan to conduct further experiments to investigate where oxidation is occurring within the cluster's chromium core.

— Tien Nguyen

See: Amymarie K. Bartholomew[2], Cristin E. Juda[1], Jonathon N. Nessralla[3], Benjamin Lin[1], Su Yin Grass Wang[4], Yu-Sheng Chen[4], and Theodore A. Betley[1]*, "Ligand-Based Control of Single-Site vs. Multi-Site Reactivity by a Trichromium Cluster," Angew. Chem. Int. Ed. **58**, 5687 (2019). DOI: 10.1002/anie.201901599.
Author affiliations: [1]Harvard University, [2]Columbia University, [3]University of California, Berkeley, [4]The University of Chicago
Correspondence: * betley@chemistry.harvard.edu

This work was supported by grants from the National Institutes of Health (GM 098395), the U.S. Department of Energy (DOE) (DE-SC0008313), and Harvard University. ChemMatCARS is supported by the National Science Foundation under grant number NSF/CHE-1834750. This research used resources of the Advanced Photon Source, a U.S. DOE Office of Science User Facility operated for the DOE Office of Science by Argonne National Laboratory under Contract No.DE-AC02-06CH11357.

APS Users by Source of Support FY2019

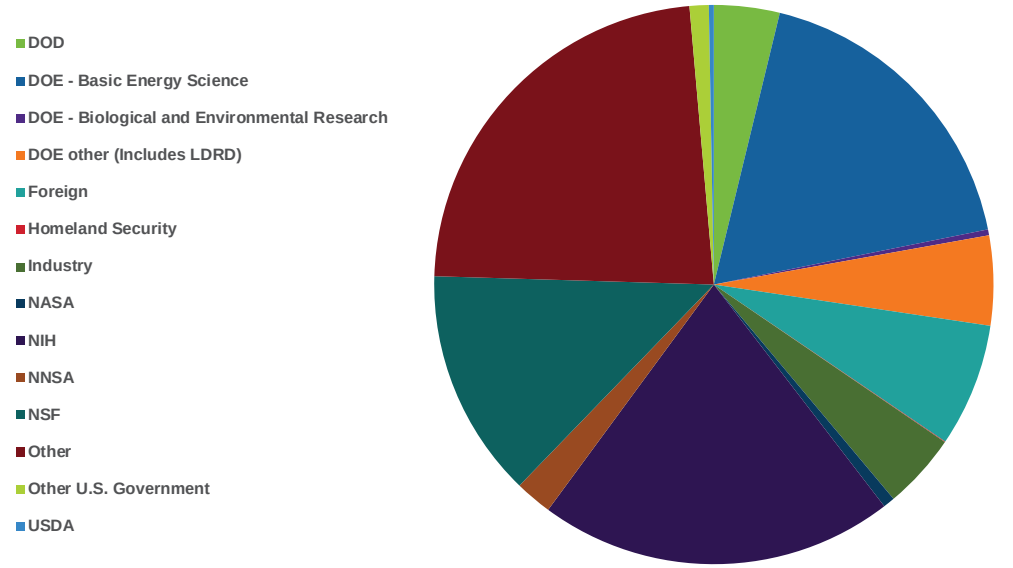

APS Users by Employer FY2019

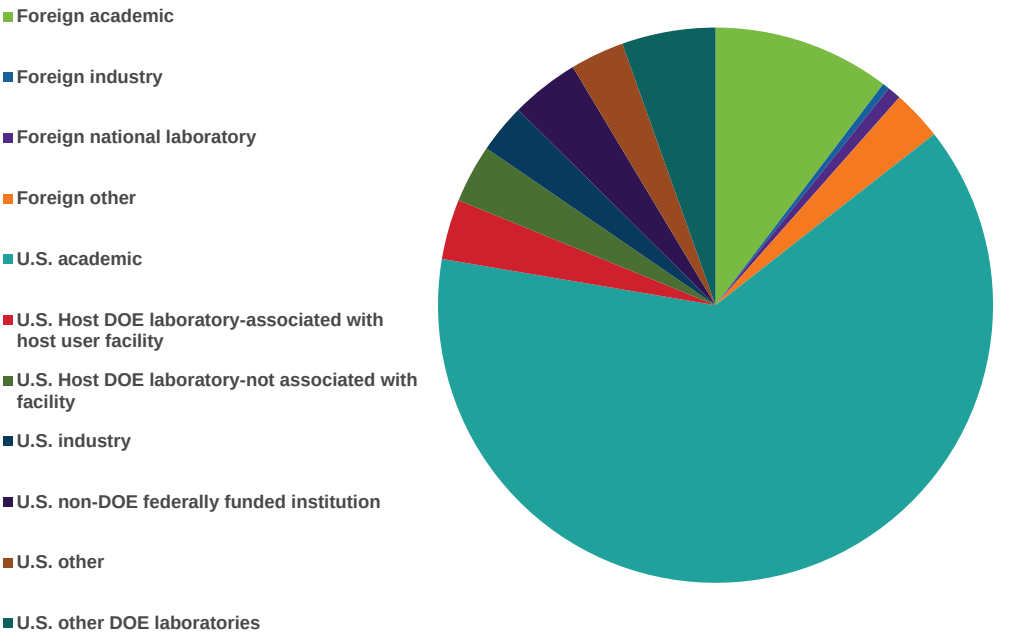

Life Science

Buffing Up Your Skeleton:
The Active Role of Collagen in Building Bones

We use our skeleton every day, but our mental model of our bones may look more like a glow-in-the-dark Halloween costume, or a teaching skeleton hanging on a sitcom set, than true anatomy. While these common representations of skeletons focus on the sturdy aspects of bones, the structural frames of actual bones are built by a soft organic portion. To create bones, the human body precipitates calcium phosphate minerals using collagen, a long protein, as scaffolding. Our bodies mineralize calcium phosphate both inside and outside collagen-confined spaces, and scientists are still working to understand how the two types of mineralization occur. Research at the APS (Fig. 1) investigated mineralization rates and shown that collagen structures reduce the energy barriers to mineralization by providing a substrate on which the calcium phosphate can precipitate. Since common bone diseases, such as osteoporosis, hinge on an abnormal calcium phosphate precipitation process, this improved understanding of the role of collagen in precipitation could lead to insight into the treatment of these diseases.

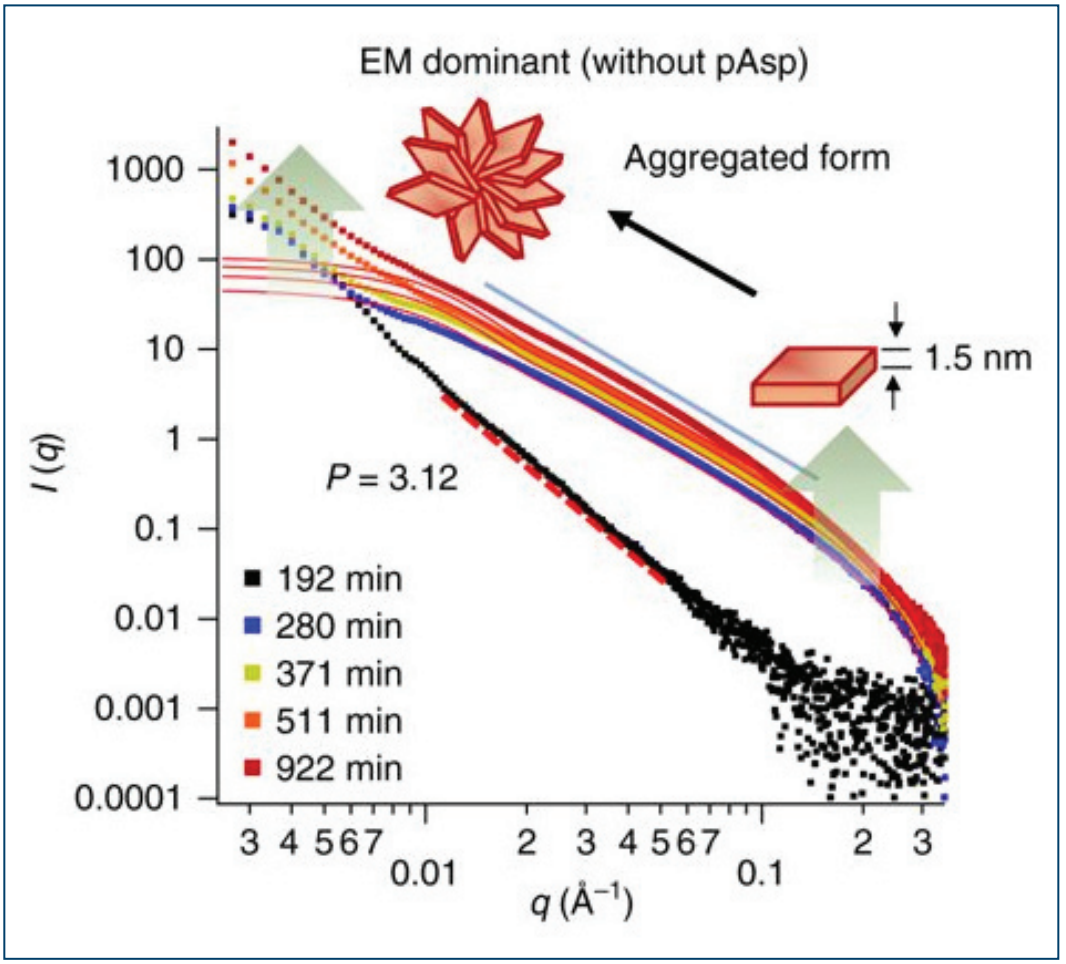

The mineralization of calcium phosphate into bioapatite crystals happens in two environments within the human body. Calcium phosphate precipitates in unconfined spaces (extrafibrillar mineralization) and confined spaces (intrafibrillar mineralization) within the collagen scaffolding, or matrix. These confined, nanosized spaces for mineralization are created within bones as collagen molecules naturally assemble into fibrils. Both types of mineralization begin with nucleation, a process of changing phase from soluble ions to a solid, followed by growth and crystallization. Figure 2 shows scanning electron microscopy images of nucleation in both environments; nucleation in unconfined spaces occurs in the top half and nucleation in confined spaces in the bottom half. Although both mineralization types produce bioapatite crystals, each uses a different series of reaction kinetics and thermodynamics.

Studies in the chemical literature suggest that forming clusters during a pre-nucleation step (which then act as seeds during nucleation itself) is an effective way to reduce the nucleation energy barrier in unconfined environments. However, this mechanism cannot explain how nucleation occurs in confined environments where the presence of nucleation inhibitors and confined space size keep pre-nucleation clusters from forming. A team comprising members from Washington University in St. Louis, Argonne, and Columbia University used a combination of scanning electron microscopy, x-ray techniques (which can investigate the reactions in real time and without destroying samples), and modified classical nucleation theory to investigate the discrepancy between these ideas.

First, the team created samples representative of both environments using simulated body fluids; a matrix of collagen fibrils was used to evaluate the effects of nanoscale confined spaces on calcium phosphate nucleation. The team also tested the effect of the presence of polyaspartic acid, which is commonly used to simulate nucleation inhibitors within the body known as non-collagenous proteins. The team used *in situ* small-angle x-ray scattering analysis at the XSD 12-ID-B beamline at the APS to probe the nucleation processes in both confined and unconfined spaces within collagen matrices, with and without polyaspartic acid. They took wide-angle x-ray diffraction data of their samples during nucleation using the XSD 11-ID-B beamline at the APS to identify the crystal phases.

< Fig. 1. Small-angle x-ray scattering pattern collected during mineralization without pAsp for extrafibrillar mineralization. From D. Kim et al., Nat. Commun. **9**, 962 (2019). © 2019 Springer Nature Publishing AG

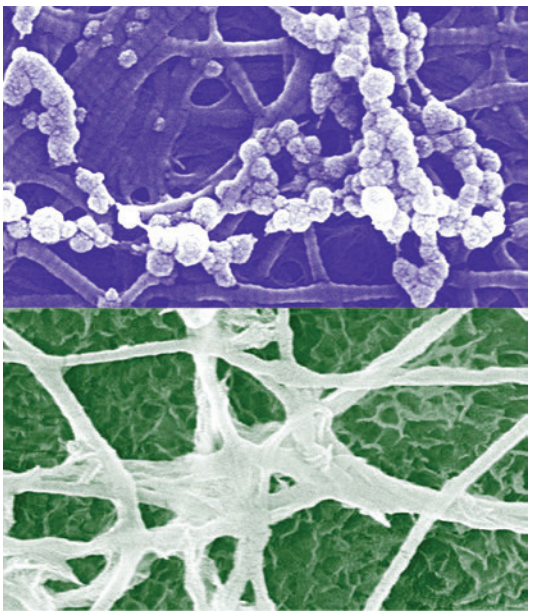

Fig. 2. This scanning electron microscopy image shows calcium phosphate minerals nucleation in both extrafibrillar (purple colored image) and intrafibrillar (green colored image) spaces of collagen matrices. Without polyaspartic acid, extrafibrillar nucleation of calcium phosphate is dominant while with polyaspartic acid, intrafibrillar nucleation mainly occurs.

The team found that in the absence of polyaspartic acid, nucleation occurred mainly in unconfined spaces, and concluded that the presence of the polyaspartic acid, a nucleation inhibitor, shunted the majority of nucleation to the nanoscale collagen-confined spaces. In these confined, two-dimensional spaces within collagen matrices, the effective surface area for nucleation is limited, which decreases the surface energy penalty for nucleation.

Although our bones may benefit us by being strong and static, collage fibrils are not simply a passive substrate in the process by which our body builds bones. Instead, the generation of bone depends on the active control of collagen fibrils. — Mary Alexandra Agner

See: Doyoon Kim[1], Byeongdu Lee[2], Stavros Thomopoulos[3], and Young-Shin Jun[1]*, "The role of confined collagen geometry in decreasing nucleation energy barriers to intrafibrillar mineralization," Nat. Commun. **9**, 962 (2018).
DOI: 10.1038/s41467-018-03041-1
Author affiliations: [1]Washington University in St. Louis, [2]Argonne National Laboratory, [3]Columbia University
Correspondence: * ysjun@seas.wustl.edu

The project was supported by the National Science Foundation (DMR-1608545 and DMR-1608554). The Nano Research Facility and the Institute of Materials Science & Engineering at Washington University in St. Louis provided their facilities for the experiments. This research used resources of the Advanced Photon Source, a U.S. Department of Energy (DOE) Office of Science User Facility operated for the DOE Office of Science by Argonne National Laboratory under Contract No. DE-AC02-06CH11357.

Enhancing the Power Stroke of Cardiac Muscle Could Help Those with Heart Failure

The molecular interactions that drive muscle contraction have been investigated for decades. Basically, force is generated when the thick-filament motor protein, myosin, breaks down adenosine triphosphate (ATP) to adenosine diphosphate (ADP) and inorganic phosphate (Pi) and uses the released energy to move filaments of the thin-filament structural protein, actin. Cardiac muscle can use an alternative form of ATP, 2-deoxy-ATP (dATP), which has been shown to generate even more contractile force than standard ATP. Interestingly, this is true in both healthy heart muscle and in heart muscle with diminished function, such as that seen in people with heart failure. This has led to the intriguing possibility that dATP, or molecules that act in a similar manner, might be used as a therapy to improve cardiac muscle function in people with heart failure. Recently, researchers used data from studies at the APS and other experiments to try to understand the structural basis for dATP's remarkable effect. The work may help in the design of therapeutics that are urgently needed to enhance contraction of failing hearts.

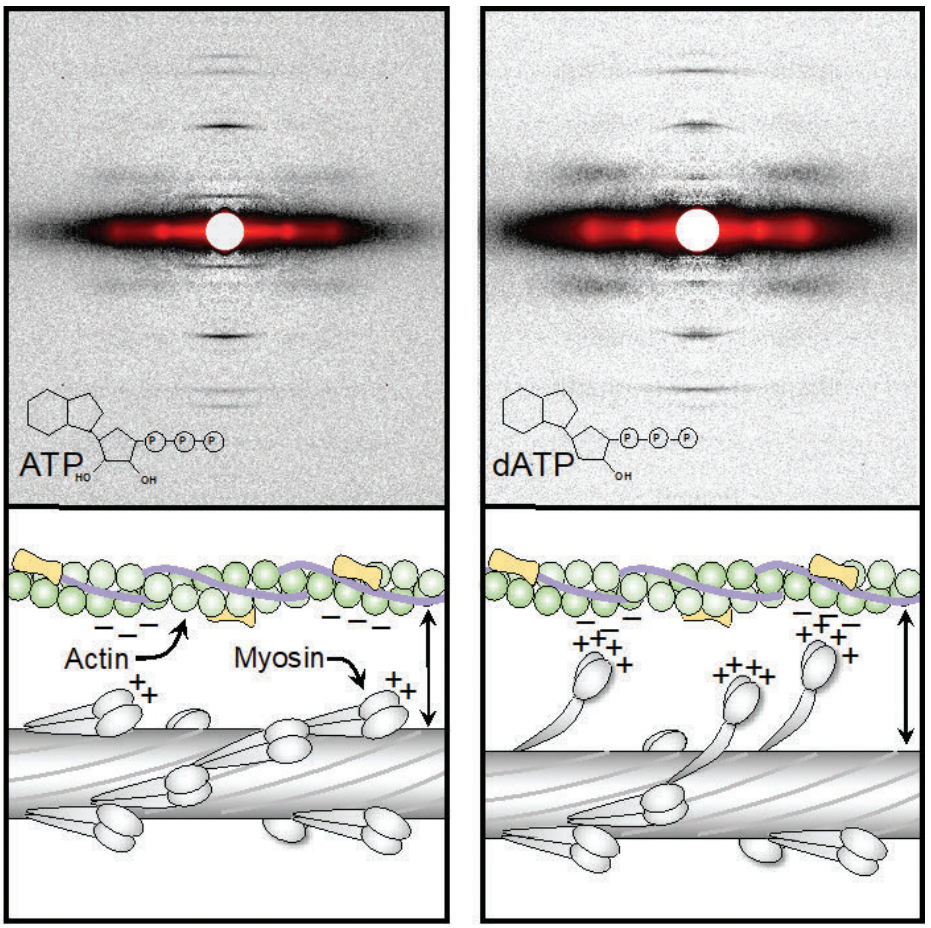

The research team, from the University of Washington, the University of California at San Diego, and the Illinois Institute of Technology had previously shown that dATP could improve contractility in heart muscle and were interested in learning more about why it worked. However, the very fast time frame of the weak interactions between myosin and actin makes it difficult to these study small changes. The first approach they used was a computational structural analysis in which they compared the atomically detailed structures of actin and myosin in the presence of ADP + Pi and dADP + Pi. After analysis of the effects of small changes created by the different molecules, predictions from this analysis suggested that dADP + Pi would increase the number of polar (i.e., charged) interactions between actin and myosin and enhance their affinity. This, they hypothesized, would increase the association kinetics of the actin-myosin interaction. They were able to confirm this using Brownian dynamics simulations that showed that the greater electrostatic interactions between actin and myosin result in faster association kinetics between the two proteins.

Next, these differences were confirmed in an in vitro motility assay in which the fraction of sliding actin filaments is measured on a myosin-coated surface over a range of ionic strengths. Previous work with fast skeletal muscle myosin had shown that the fraction of sliding filaments decreases with increasing ionic strength but that this decrease is slower with dATP than ATP, consistent with the increased electrostatic interactions idea. However, the map of surface charges on cardiac myosin and fast skeletal myosin differ somewhat, so the team felt it was important to demonstrate that cardiac muscle myosin also exhibited this behavior in the motility assay. As they had hypothesized, they observed significantly greater actin sliding with dATP than with ATP over a range of ionic strengths.

To assess effects of dATP on the structure of myosin, the team turned to small-angle x-ray scattering. Using rat cardiac muscle preparations observed under physiological conditions that would maintain the muscle in a resting conformation, the team used the Bio-CAT 18-ID-D beamline at the APS to measure x-ray diffraction patterns from ATP- and dATP-treated muscles. The two-dimensional x-ray diffraction pattern images allowed them to measure the periodicity of myosin along the thick filaments and the orientation of the myosin heads with regard to both thick and thin filaments. The x-ray diffraction data suggested that the myosin heads were shifted away from the thick myosin filaments and leaned more toward the actin filaments with dATP compared to ATP, decreasing the pre-power stroke distance between the myosin head and actin filament (Fig. 1).

A number of myosin-targeted therapies are currently under development and these results provide important clues to how small changes in molecular interactions may translate into therapeutically valuable changes in muscle contraction. — Sandy Field

< Fig. 1. Quantitative image analysis of x-ray diffraction patterns from cardiac muscle treated with ATP (top left panel) and dATP (top right panel) reveals a structural basis for the enhancement of cardiac contraction with dATP. The bottom panels illustrate the difference between resting myosin motors in the presence of ATP (bottom left) and dATP (bottom right) and their interaction with the actin filament. In the presence of dATP, myosin motors have a slightly altered conformation that increases their electrostatic interaction with actin, bringing them closer to the actin filaments and improving the likelihood that they will be available to generate force during cardiac contraction.

See: Joseph D. Powers[1,2]*, Chen-Ching Yuan[1], Kimberly J. McCabe[2], Jason D. Murray[1], Matthew Carter Childers[1], Galina V. Flint[1], Farid Moussavi-Harami[1], Saffie Mohran[1], Romi Castillo[1], Carla Zuzek[1], Weikang Ma[3], Valerie Daggett[1], Andrew D. McCulloch[2], Thomas C. Irving[3], and Michael Regnier[1]**, "Cardiac myosin activation with 2-deoxy-ATP via increased electrostatic interactions with actin," Proc. Natl. Acad. Sci. U.S.A. **116**(23), 11502 (June 4, 2019). DOI: 10.1073/pnas.1905028116
Author affiliations: [1]University of Washington, [2]University of California, San Diego, [3]Illinois Institute of Technology
Correspondence: * j2powers@ucsd.edu,
** mregnier@uw.edu.

This work was supported by National Institutes of Health (NIH) Grants R01 HL128368 and R56 AG055594 (to M.R.), NIH Grant U01 HL122199 (to M.R. and A.D.M.), NIH Grant T32-HL007312 (to J.D.P.), a Sackler Scholars Program Fellowship in Integrative Biophysics (to C.-C.Y.), NIH Grant T32-HL105373 (to K.J.M.), NIH Grant K08 HL128826 (to F.M.-H.), and NIH Grant T32-EB1650 (to J.D.M.). This project was supported by Grants 9 P41 GM103622 and 8 P41 GM103426 from the National Institute of General Medical Sciences of the NIH. This research used resources of the Advanced Photon Source, a U.S. Department of Energy (DOE) Office of Science User Facility operated for the DOE Office of Science by the Argonne National Laboratory under Contract DE-AC02-06CH11357.

Unmasking Unfolded States

Advances in structural biology have yielded an abundance of high-resolution descriptions of folded states of proteins. However, atomic-level descriptions of proteins in unfolded states under folding conditions have remained elusive due to the enormous variability in the conformation of unfolded protein states and the very low population of unfolded states under folding conditions. Researchers using the APS have recently combined a series of time-resolved biophysical techniques with simulations and theory to obtain a high-resolution description of unfolded protein ensembles under folding conditions for a simple protein with a two-state folding transition. These unfolded states are characterized by discernible sequence-specific conformational preferences. These preferences are averaged over by conformational fluctuations, giving rise to ensemble-averaged properties consistent with those of random coils—polymer conformation where monomer subunits are oriented randomly. These findings increase the understanding of functional and pathological interactions involving unfolded forms of proteins, which can be relevant to human pathology and biotechnology applications.

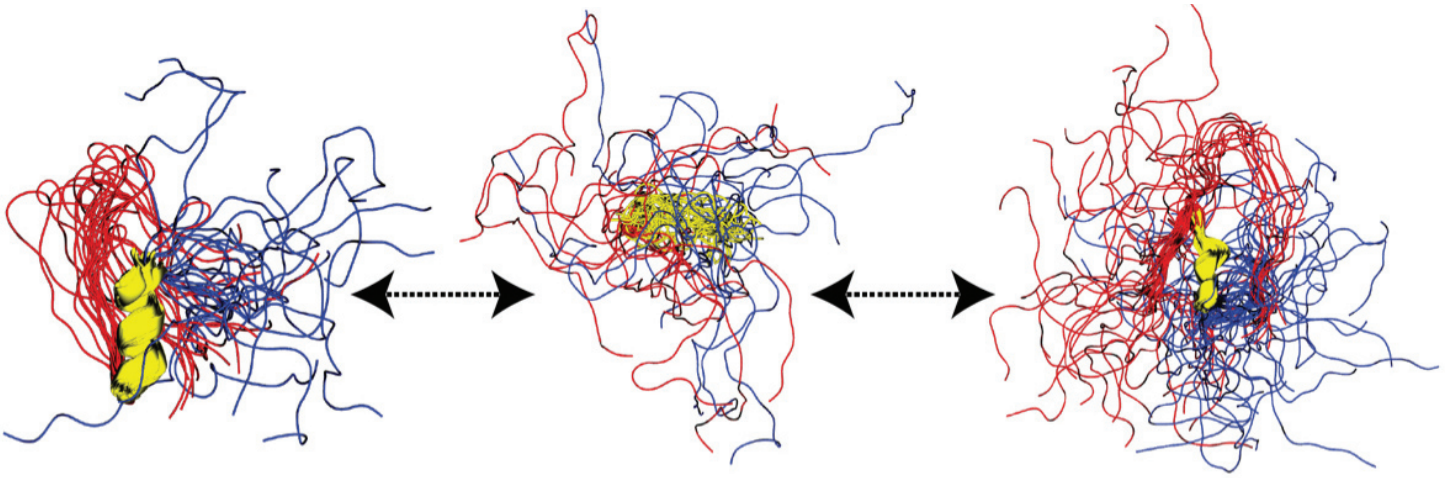

Fig. 1. In this study, time-resolved FRET, time-resolved SAXS, and all-atom simulations provided insights into the structural ensemble of the unfolded state of the L9 protein under folding conditions. These three sequences depict the different portions—N-terminal (blue), central (yellow) and C-terminal (red) domains—of the L9 protein in three random unfolded states.

Proteins fluctuate between folded and unfolded states. Nearly all high-resolution descriptions of proteins have been derived when they are in their folded states. Fluctuations into and out of unfolded states under folding conditions have been demonstrated using single-molecule spectroscopies, such as single-molecule Förster resonance energy transfer (FRET) and optical tweezer pulling experiments. The interactions within and between unfolded proteins are of functional relevance. As an example, it is now well established that the properties of unfolded states influence the tendencies of proteins to aggregate, and this has important implications for human disease and biotechnology.

Recently, there has been substantial progress in characterizing folding pathways using a combination of novel experimental approaches and improved computational methods. However, the initial stages of protein folding, specifically the nature of unfolded states under folding

conditions, remain a source of controversy, even for simple single-domain globular proteins that undergo an apparent two-state folding transition. A better understanding of unfolded states under folding conditions would shed light on the mechanisms of protein folding and interactions involving unfolded proteins in cellular settings.

The folded states of globular proteins are typically compact. Upon dilution from high concentrations of denaturant into native conditions, a foldable yet unfolded and expanded protein must undergo a collapse transition to progress to its compact and folded (native) state. Rapid contraction or collapse upon dilution has been observed in refolding experiments for some, but not all proteins. Determining the position of the collapse transition and characterizing the conformational properties of unfolded ensembles before and following this collapse are essential steps toward deciphering folding mechanisms and for developing a clear understanding of how a given protein's amino acid sequence determines its behavior in solution.

Unfolded states are accessible via spontaneous, albeit low-likelihood, fluctuations. Characterizing the resultant low-likelihood states requires the use of methods with high temporal resolution that can "catch" these short-lived transitions (Fig. 1). The combination of rapid mixing techniques and spectroscopic measurements such small-angle x-ray scattering (SAXS) has allowed the direct interrogation of unfolded states under near-native conditions in the absence of strongly destabilizing mutations.

However, SAXS has its limitations: It offers limited structural resolution, requires high protein concentrations, and can be insensitive to the presence of low-likelihood, long-range contacts and local structure. These limitations are of particular importance when characterizing unfolded proteins under low concentrations of denaturant in equilibrium experiments. FRET experiments, meanwhile, have suggested that contraction of the unfolded state can occur before the folding transition. Single-molecule fluorescence experiments provide the clearest evidence for some proteins undergoing continuous contraction of their unfolded states as a function of decreasing denaturant concentration, but require the use of bulky fluorescent labels, which have been suggested to promote contraction.

Researchers from Stony Brook University, Washington University in St. Louis, the University of Massachusetts Medical School, and University College London (UK) used a combination of time-resolved FRET, unnatural amino acids, time-resolved SAXS carried out at the Bio-CAT 18-ID beamline of the APS, all-atom simulations, and polymer theory to obtain a high-resolution description of unfolded states under refolding conditions for the N-terminal domain of the L9 protein (NTL9). NTL9 is 56 residues long and is one of the simplest examples of a common two-state, α–β fold.

The combination of multiple time-resolved FRET, time-resolved SAXS, and computational results shows that the unfolded state of NTL9 under folding conditions is conformationally heterogeneous; certain regions of the protein undergo significant collapse while others remain relatively expanded.

Finally, simulations reveal that for NTL9 modest contraction occurs rapidly, on a timescale that is faster than that of folding. The global ensemble-averaged dimensions of the chain are consistent with those of a random coil, i.e., a flexible polymer that assumes all possible conformations randomly.

These findings are in agreement with theoretical predictions based on coarse-grained models and inferences drawn from single-molecule experiments regarding the sequence-specific scaling behavior of unfolded proteins under folding conditions.

In summary, this study uncovers atomistic descriptions of unfolded ensembles under folding conditions, opening the door to designing features into unfolded states without impacting the properties of folded states to interrogate the effects of such designs on folding, function, and cellular phenotypes. — Chris Palmer

See: Ivan Peran[1], Alex S. Holehouse[2], Isaac S. Carrico[1], Rohit V. Pappu[3]*, Osman Bilsel[4]**, and Daniel P. Raleigh[1,4]***, "Unfolded states under folding conditions accommodate sequence-specific conformational preferences with random coil-like dimensions," Proc. Natl. Acad. Sci. U.S.A. **116**(25), 12301 (June 18 2019). DOI: 10.1073/pnas.1818206116
Author affiliations: [1]Stony Brook University, [2]Washington University in St. Louis, [3]University of Massachusetts Medical School, [4]University College London
Correspondence: * pappu@wustl.edu,
** osman.bilsel@umassmed.edu,
*** d.raleigh@ucl.ac.uk

This work was supported by Wellcome Trust Grant 107927/Z/15/Z (to D.P.R.), the U.S. National Science Foundation (NSF) Grants IDBR 1353942 and MCB 0721312 (to O.B.) and MCB-1614766 (to R.V.P.), and the Human Frontiers Science Program Grant RGP0034/2017 (to R.V.P.). I.P. was supported in part by NSF Grant MCB-1330259 (to D.P.R.). O.B., R.V.P., and D.P.R. are members of the protein-folding consortium that is supported by the NSF through Grant MCB 1051344. Bio-CAT is supported by Grant 9 P41 GM103622 from the National Institute of General Medical Sciences of the National Institutes of Health. This research used resources of the Advanced Photon Source, a U.S. Department of Energy (DOE) Office of Science User Facility operated for the DOE Office of Science by Argonne National Laboratory under Contract DE-AC02-06CH11357.

APS Users by Employment Level FY2019

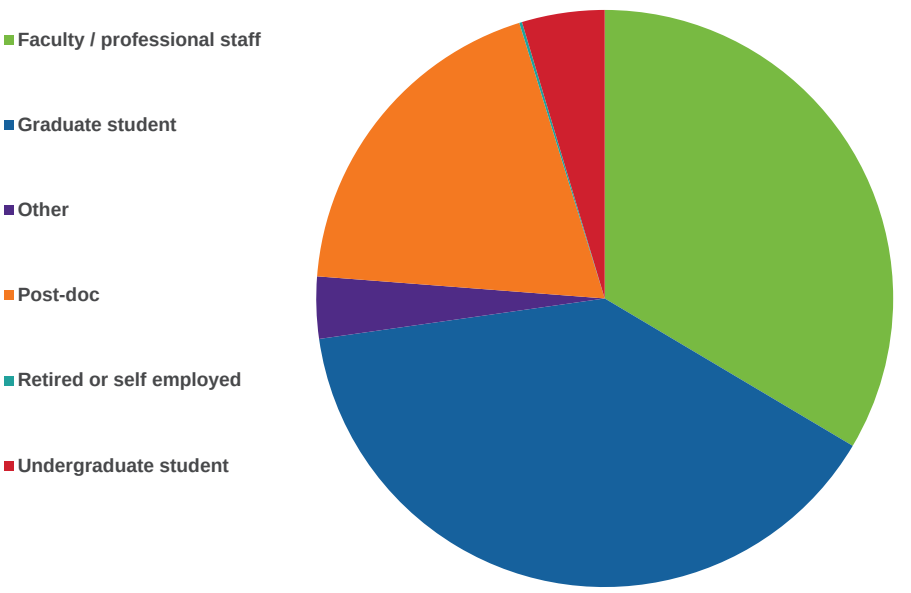

APS User Institutions by Institution Type FY2019

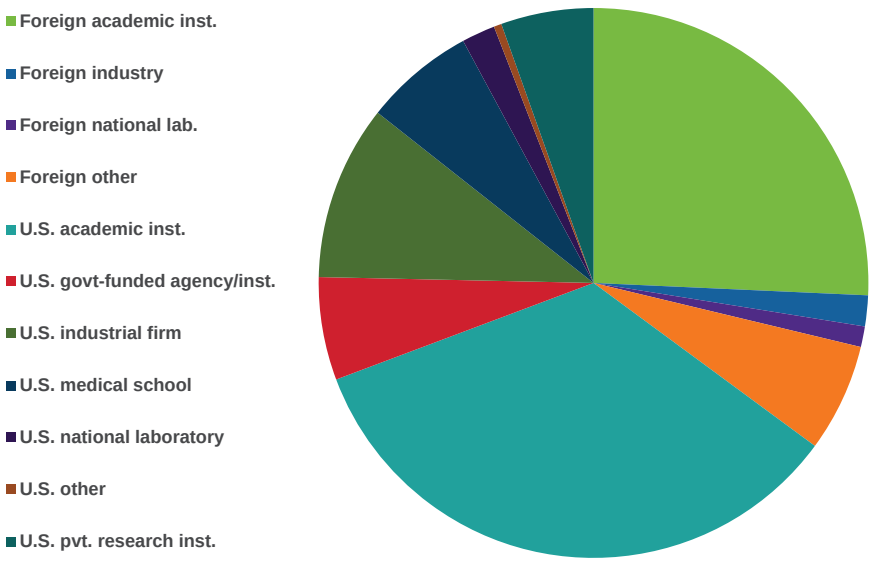

Structural Biology

New Findings in the Quest for the Elusive HIV Vaccine

Despite significant advances in the treatment of HIV in recent decades, the ability of the virus to evade the humoral immune system has challenged scientists in their quest to develop a workable HIV vaccine. In a new study, which involved collecting x-ray diffraction data at the APS, researchers aimed to improve our understanding of how broadly neutralizing antibodies (bNAbs) are elicited by the HIV-1 fusion peptide, a critical component of the HIV cell-entry machinery. The results of this study will guide follow-up research to help define mechanisms for the elicitation of bNAbs against HIV and other diverse pathogens, and will also help to inform clinical trials for HIV.

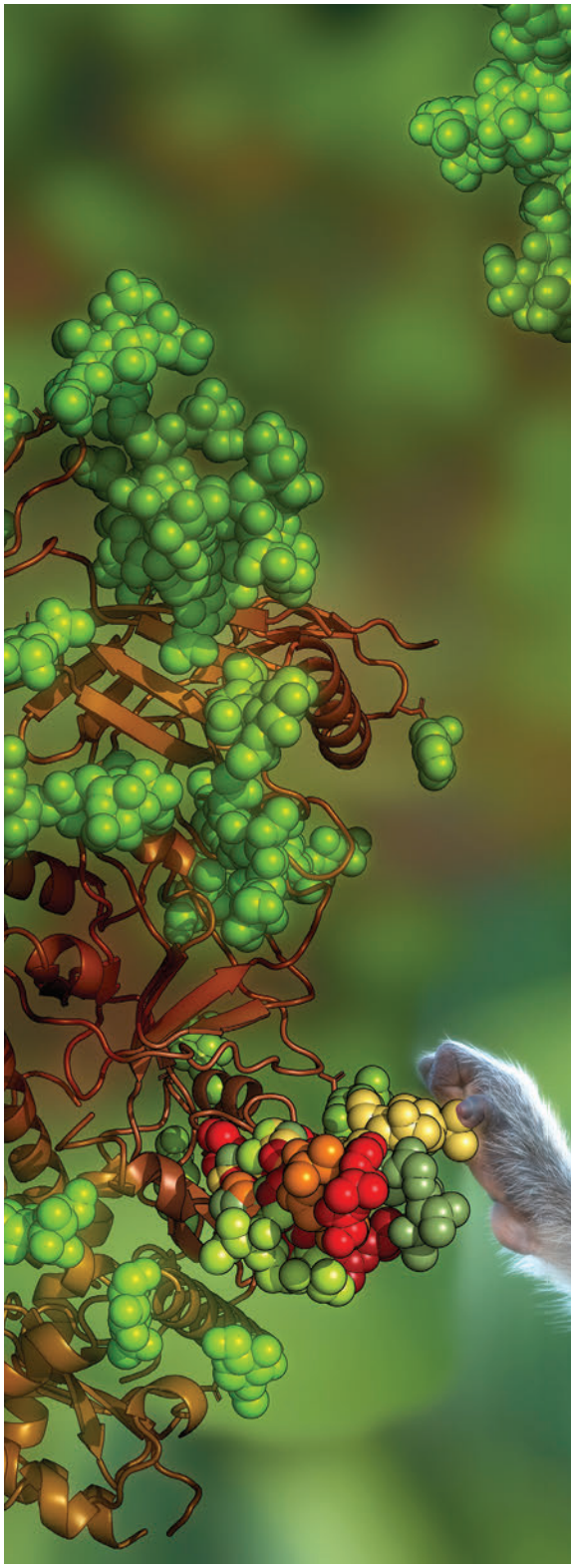

Developing an effective vaccine against HIV has been a long-sought research goal. However, achieving this goal has proven difficult because the virus can rapidly mutate and avoid the immune system with both glycan shielding and conformational masking. The circulating diversity of HIV is therefore extraordinarily high, and the virus is extremely neutralization resistant, with the critical envelope glycoprotein (Env) protected by an evolving glycan shield and extensive conformational masking. Although HIV-infected patients typically develop type-specific antibodies, these are not effective against the diverse circulating strains of the virus that typify HIV infection. However, some patients with HIV infection could—often after a decade or more of high viral loads—naturally produce bNAbs that can target and neutralize many strains of the virus. As such, bNAbs have become a key focus in the field of HIV prevention science in recent years. However, elicitation of bNAbs by vaccination, not by infection, has been a tough challenge.

A multi-national, multi-institution team, led by researchers from the National Institutes of Health, found that the N terminus of the HIV-1 fusion peptide is a promising vaccine target [1]. By focusing the vaccine-induced immune response on the N-terminus of the fusion peptide, they elicited antibodies capable of neutralizing up to about 30% of HIV strains. It required priming immunizations with the N-terminal residues coupled to a carrier protein, followed by boosting immunization with Env trimer.

Although antibodies could be elicited with promising neutralizing breadth, both their potency and consistency needed to be improved. It also took almost a year to elicit the desired fusion peptide-directed antibodies in macaques, which are prized for their ability to predict human response. During much of the initial six months of immunization, serum neutralization was, for the most part, too weak to be measured. And lastly, the mechanism for elicitation was unclear: why did fusion peptide-priming elicit antibodies of such high breadth, when trimer-only immunization did not?

To better understand how bNAbs could be elicited, the group performed a follow-up study in which they investigated the development of five lineages of fusion peptide-directed HIV-1 neutralizing antibodies from vaccinated macaques. They conducted genetic and structural analyses of the antibodies, collecting x-ray diffraction data at the SER-CAT beamline 22-ID-D at APS.

Their new study revealed developmental details, with each of the lineages initiated by fusion peptide-carrier immunizations by week 10 and matured with Env trimer immunization. Moreover, these detailed analyses indicated that priming with fusion peptide had induced an antigen-binding hotspot focused on fusion peptide, with increased somatic hypermutation in the region of antibody contact with fusion peptide.

These findings have thus provided important new insights in the field of HIV vaccine research. In addition to identifying vaccine-induced antibodies capable of neutralizing up to 59% of HIV-1 strains, the findings also improve understanding of the mechanism by which fusion peptide-directed antibodies of high neutralization breadth can be induced.

In addition to guiding follow-up research to help define mechanisms for the elicitation of bNAbs against HIV and other diverse pathogens, the results of this study will also help to inform clinical trials for HIV. — Nicola Parry

A nonhuman primate reaching for and grabbing the diverse conformations taken by the fusion peptide, just as elicited antibodies do. Image credit, Jonathan Stuckey and Kai Xu, VRC, NIAID, NIH.

Reference

[1] K. Xu et al., "Epitope-based vaccine design yields fusion peptide-directed antibodies that neutralize diverse strains of HIV-1," Nat. Med. 24(6), 857 (2018 June). DOI: 10.1038/s41591-018-0042-6

See: Rui Kong[1], Hongying Duan[1], Zizhang Sheng[2], Kai Xu[1], Priyamvada Acharya[1,3,4], Xuejun Chen[1], Cheng Cheng[1], Adam S. Dingens[5,6], Jason Gorman[1,3], Mallika Sastry[1], Chen-Hsiang Shen[1], Baoshan Zhang[1], Tongqing Zhou[1], Gwo-Yu Chuang[1], Cara W. Chao[1], Ying Gu[1], Alexander J. Jafari[1], Mark K. Louder[1], Sijy O'Dell[1], Ariana P. Rowshan[1], Elise G. Viox[1], Yiran Wang[1], Chang W. Choi[1], Martin M. Corcoran[7], Angela R. Corrigan[1], Venkata P. Dandey[3], Edward T. Eng[3], Hui Geng[1], Kathryn E. Foulds[1], Yicheng Guo[2], Young D. Kwon[1], Bob Lin[1], Kevin Liu[1], Rosemarie D. Mason[1], Martha C. Nason[8], Tiffany Y. Ohr[1], Li Ou[1], Reda Rawi[1], Edward K. Sarfo[1], Arne Schön[9], John P. Todd[1], Shuishu Wang[1], Hui Wei[3], Winston Wu[1], NISC Comparative Sequencing Program[10], James C. Mullikin[10], Robert T. Bailer[1], Nicole A. Doria-Rose[1], Gunilla B. Karlsson Hedestam[7], Diana G. Scorpio[1], Julie Overbaugh[6], Jesse D. Bloom[5,11], Bridget Carragher[3], Clinton S. Potter[3], Lawrence Shapiro[1,2], Peter D. Kwong[1,2]*, and John R. Mascola[1]**, "Antibody Lineages with Vaccine-Induced Antigen-Binding Hotspots Develop Broad HIV Neutralization," Cell **178**, 567 (July 25, 2019). DOI: 10.1016/j.cell.2019.06.030
Author affiliations: [1]National Institute of Allergy and Infectious Diseases, [2]Columbia University, [3]Simons Electron Microscopy Center, [4]Duke University School of Medicine, [5]Fred Hutchinson Cancer Research Center, [6]University of Washington, [7]Karolinska Institutet, [8]National Institute of Allergy and Infectious Diseases, [9]Johns Hopkins University, [10]National Human Genome Research Institute, [11]Howard Hughes Medical Institute,
Correspondence: * pdkwong@nih.gov, ** jmascola@nih.gov

Support for this work was provided by the Intramural Research Program of the Vaccine Research Center, National Institute of Allergy and Infectious Diseases; the National Human Genome Research Institute; Bill and Melinda Gates Foundation (OPP1162123 to T.Z.); National Institutes of Health (R21 1R21AI138024-01A1 to Z.S., R01AI140891 to J.D.B., DA039543 and R01AI120961 to J.O.); and the International AIDS Vaccine Initiative's Neutralizing Antibody Consortium. J.D.B. is an Investigator of the Howard Hughes Medical Institute, A.S.D. was supported by an National Science Foundation Graduate Research Fellowship (DGE-1256082), and M.M.C. and G.B.K.H. were supported by the Swedish Research Council. SER-CAT is supported by its member institutions (see www.ser-cat.org/members.html), and equipment grants (S10_RR25528 and S10_RR028976) from the National Institutes of Health. This research used resources of the Advanced Photon Source, a U.S. Department of Energy (DOE) Office of Science User Facility operated for the DOE Office of Science by Argonne National Laboratory under Contract DE-AC02-06CH11357.

Mapping the Receptor that Raises Your Blood Pressure

The hormone angiotensin II (AngII), a G-protein-coupled receptor (GPCR), is best known for controlling blood pressure and kidney function. It binds to the angiotensin II type 1 receptor (AT1R), resulting in blood vessel constriction and salt retention by the kidneys, thus raising blood pressure, which makes it an important therapeutic target. About 5% of adults in the United States take angiotensin receptor blockers to lower their blood pressure, treat heart failure, or prevent kidney failure or stroke. Despite the receptor's critical physiological roles and its importance as a drug target, technological limitations have kept researchers from knowing what it looks like when it is activated. By stabilizing the receptor with a single-domain antibody fragment, called a "nanobody," which was discovered using a large library of proteins displayed on the surface of yeast cells, researchers using high-brightness x-rays at the APS were able to determine the three-dimensional (3-D) crystal structure of active-state human AT1R bound to an AngII analog. Their findings offer clues about how next-generation drugs might be developed that activate, rather than block, the angiotensin II receptor in highly controlled ways.

An intriguing aspect of GPCR activation is that most agonists (activators) cause GPCRs to turn on several pathways inside the cell (e.g., pathways initiated by G proteins and pathways initiated by other β-arrestin proteins), but certain "biased agonists" can selectively turn on particular pathways. This is notable because instead of increasing blood pressure, β-arrestin pathways downstream of the AT1R have positive effects on heart cells, particularly in that they increase the strength of heart muscle contractions and prevent cell death. Researchers believe these differences make β-arrestin-biased AT1R agonists—which would improve heart function without raising blood pressure—potentially superior alternatives to angiotensin receptor blockers for certain heart failure patients. Understanding why biased agonists allow the AT1R to turn on β-arrestin pathways without turning on G protein pathways requires characterizing the structure of the receptor when it's bound by said agonists.

Like many receptors that span the cell membrane, AT1R takes on different shapes depending on whether it is inactive or whether it is bound to one of its interaction partners. Typically, researchers wanting to study such a receptor while it's in a specific shape, or conformation, try to create an antibody with a complementary shape that will hold the receptor in place. When the receptor is held steady, it can be bound by an agonist and then crystallized and bombarded with x-rays. The resulting images can be translated into a highly detailed 3-D atomic structure of the agonist-bound receptor.

Currently, the only 3-D atomic structures of AT1R that have been reported are those of an inactive conformation of the receptor bound to small-molecule angiotensin receptor blockers, which engage the receptor in a fundamentally different way than AngII or other peptide "biased agonists" that could become next-generation drugs.

Despite years of effort to generate an antibody by immunizing llamas, the Duke University Medical Center researchers in this study could not find an antibody that would keep the AT1R still. However, using yeast instead of llamas, scientists at the Harvard Medical School generated a library of 500 million artificial nanobodies, one of which (AT110) was able to bind to AT1R and keep it in a stable active configuration. The Duke and Harvard researchers then used the GM/CA-XSD beamline 23 ID-B at the APS to determine the 2.9-Å resolution crystal structure of active state AT1R bound to the nanobody and S1I8, a peptide analog of AngII (Fig. 1).

Capturing the receptor's intricate crystal structure revealed how S1I8 binds to the cavity on the AT1R that faces outside of the cell. By engaging the AT1R through an extensive interface, S1I8 dramatically alters the shape of this cavity compared to when the receptor is bound to angiotensin receptor blockers. This rearrangement triggers a cascade of changes through the middle of the receptor, and finally results in the opening of the part of the AT1R that faces inside the cell. The AT110 nanobody binds in this intracellular region to stabilize this open conformation of the AT1R. Interestingly, the researchers found that the

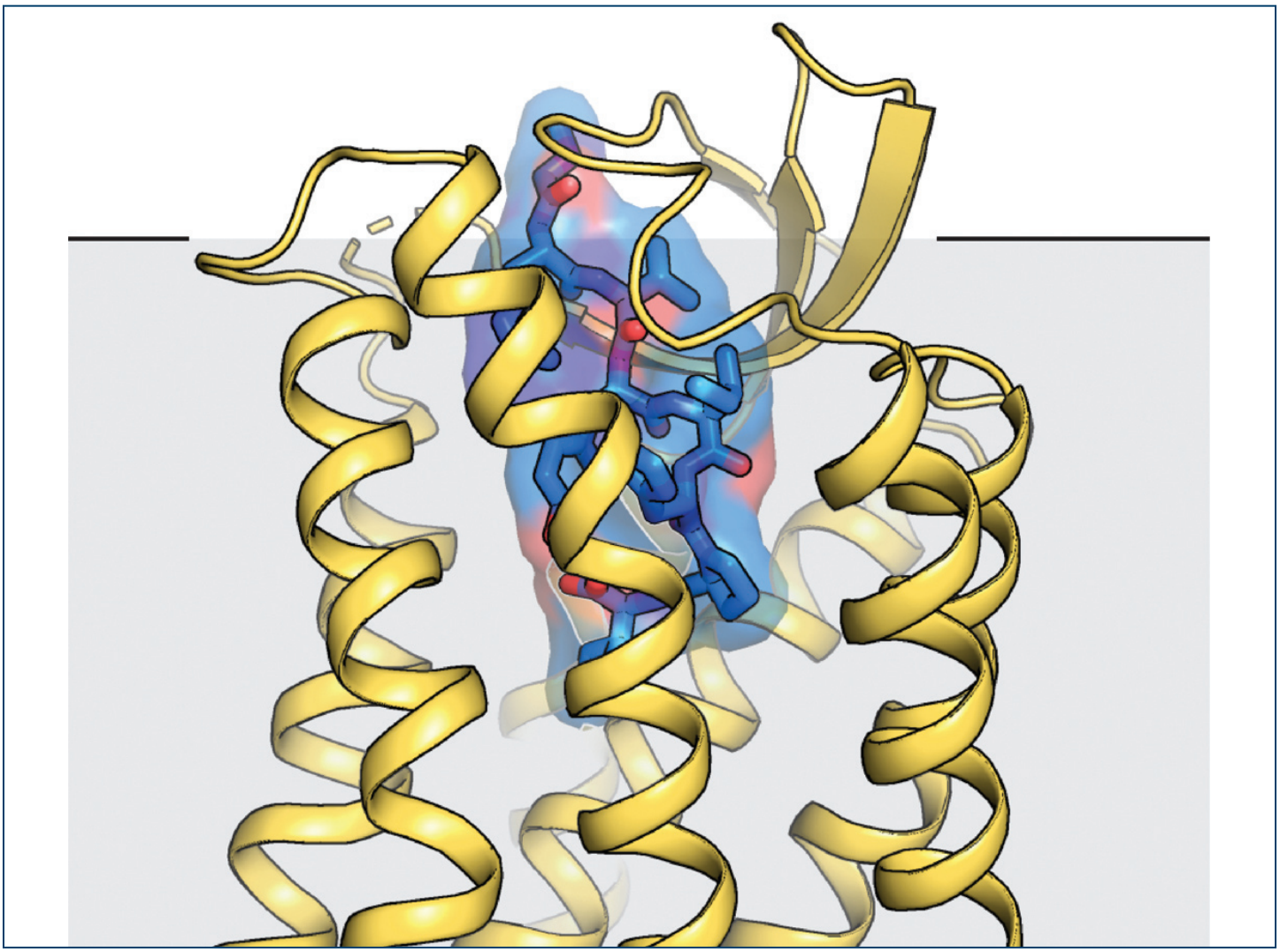

Fig 1. The angiotensin II type 1 receptor (yellow) bound to a nanobody (AT110) and S1I8 (blue), a peptide analog of the endogenous angiotensin II hormone. The gray shading in the background is the approximate location of the cell membrane.

mechanism used to propagate conformational changes through middle of the receptor is different from other GPCRs at several key sites.

The researchers hope their findings will shed light on the mechanisms underlying biased agonism, the phenomenon in which a protein that binds to a receptor activates one pathway (G-protein or β-arrestin) preferentially, rather than activating two or more pathways equally. They also believe their novel approach to develop nanobody stabilizers will be useful in determining structures of other GPCRs in specific conformations.

Finally, the new crystal structure of active AT1R may point researchers to the development of new classes of medications to treat hypertension and heart failure.

— Chris Palmer

See: Laura M. Wingler[1], Conor McMahon[2], Dean P. Staus[1], Robert J. Lefkowitz[1]*, and Andrew C. Kruse[2]*, "Distinctive Activation Mechanism for Angiotensin Receptor Revealed by a Synthetic Nanobody," Cell **176**, 479 (January 24, 2019).
DOI: 10.1016/j.cell.2018.12.006
Author affiliations: [1]Duke University Medical Center and Howard Hughes Medical Institute, [2]Harvard Medical School
Correspondence: * lefko001@receptor-biol.duke.edu,
* andrew_kruse@hms.harvard.edu

Funding was provided by National Institutes of Health grants R01HL16037 (R.J.L.) and DP5OD021345 (A.C.K.), the Mandel Center for Hypertension and Atherosclerosis at Duke (R.J.L.), the Vallee Foundation (A.C.K.), and the Smith Family Foundation (A.C.K.). R.J.L. is an investigator with the Howard Hughes Medical Institute. This research used resources of the Advanced Photon Source, a U.S. Department of Energy (DOE) Office of Science User Facility operated for the DOE Office of Science by Argonne National Laboratory under Contract DE-AC02-06CH11357.

Using Spider Toxin to Study a Sodium Channel Involved in Pain Perception

Voltage-gated sodium (Nav) channels initiate and propagate action potentials in excitable cells such as nerves and muscles. Dysfunction of these channels leads to numerous maladies ranging from epilepsy to chronic pain, so Nav channels are attractive targets for therapeutic drugs. Among the nine subtypes of human Nav channels (Nav1.1 to 1.9, each of which has somewhat distinct expression patterns, structures, and physiological roles), Nav1.7, which is highly expressed in peripheral sensory neurons, plays a critical role in pain sensation. Mutations in Nav1.7 are found in many pain syndromes, including both extreme pain disorder and indifference to pain. Knowing the detailed structure of Nav1.7 in complex with potent toxins would facilitate drug discovery for this promising target. However, efforts to obtain such structures have been hindered by challenges related to producing channels like human Nav1.7 for co-structure determination via techniques such as x-ray crystallography. Despite recent advances, the structural basis of the important functions voltage sensing, electromechanical coupling, and toxin modulation remains ill-defined. Now, researchers using two U.S. Department of Energy x-ray light sources, including the APS, determined the structure of Protoxin-II (ProTx2) from the Peruvian green velvet tarantula (*Thrixopelma pruriens*) in complex with a voltage-sensor domain (VSD) of Nav1.7 using x-ray crystallography and cryo-electron microscopy (cryo-EM). Their results may inform the future design of selective Nav channel antagonists.

Spider and scorpion venom contain toxins that target voltage-gated sodium channels by either clogging the ion channel or by modulating channel opening by binding at allosteric sites within the voltage sensing domains (VSDs). Using the latter mechanism, toxins, which are called gating modifier toxins (GMTs), have been used to probe Nav channels' complex gating properties. GMTs that bind to the VSDs of different domains exhibit different functional impacts on gating.

Researchers from Genentech created a chimera in which the VSD of the NavAb channel from the bacterium *Arcobacter butzleri* was replaced with the VSD2 from human Nav1.7. They then used x-ray crystallography at two synchrotron x-ray beamlines: the IMCA-CAT 17-ID-B beamline at the APS, and the Stanford Synchrotron Radiation Lightsource (SSRL) beamline 12-2 to determine the crystal structure of ProTx2 bound to their VSD2-NavAb chimera (Fig. 1). ProTx2 is a selective antagonist of the human Nav1.7 channel from *Thrixopelma pruriens*. ProTx2 was thought to trap VSD2 in a deactivated state, and therefore stabilize the closed channel.

The crystal structure obtained by the researchers revealed that ProTx2 targets the electronegative S3–S4 loop of VSD2. Unexpectedly, ProTx2 was found to bind VSD2 in an activated state, and electrophysiological studies confirmed ProTx2 appears to remain bound to Nav1.7 during channel opening and closing.

The researchers also performed cryo-electron microscopy (EM) analysis and obtained resolutions of ~5 Å around the VSD2 binding site. This analysis revealed ProTx2 bound to VSD2 in the deactivated state, where the S4 helix had translated 10 Å downward, which was found to push the S4–S5 linker inward to tightly close the S6 activation gate. The cryo-EM result also independently validated the structural model derived from crystallographic analysis.

Among other things, the x-ray crystal structure helps to explain why inhibitory GMTs such as ProTx2 can bind to

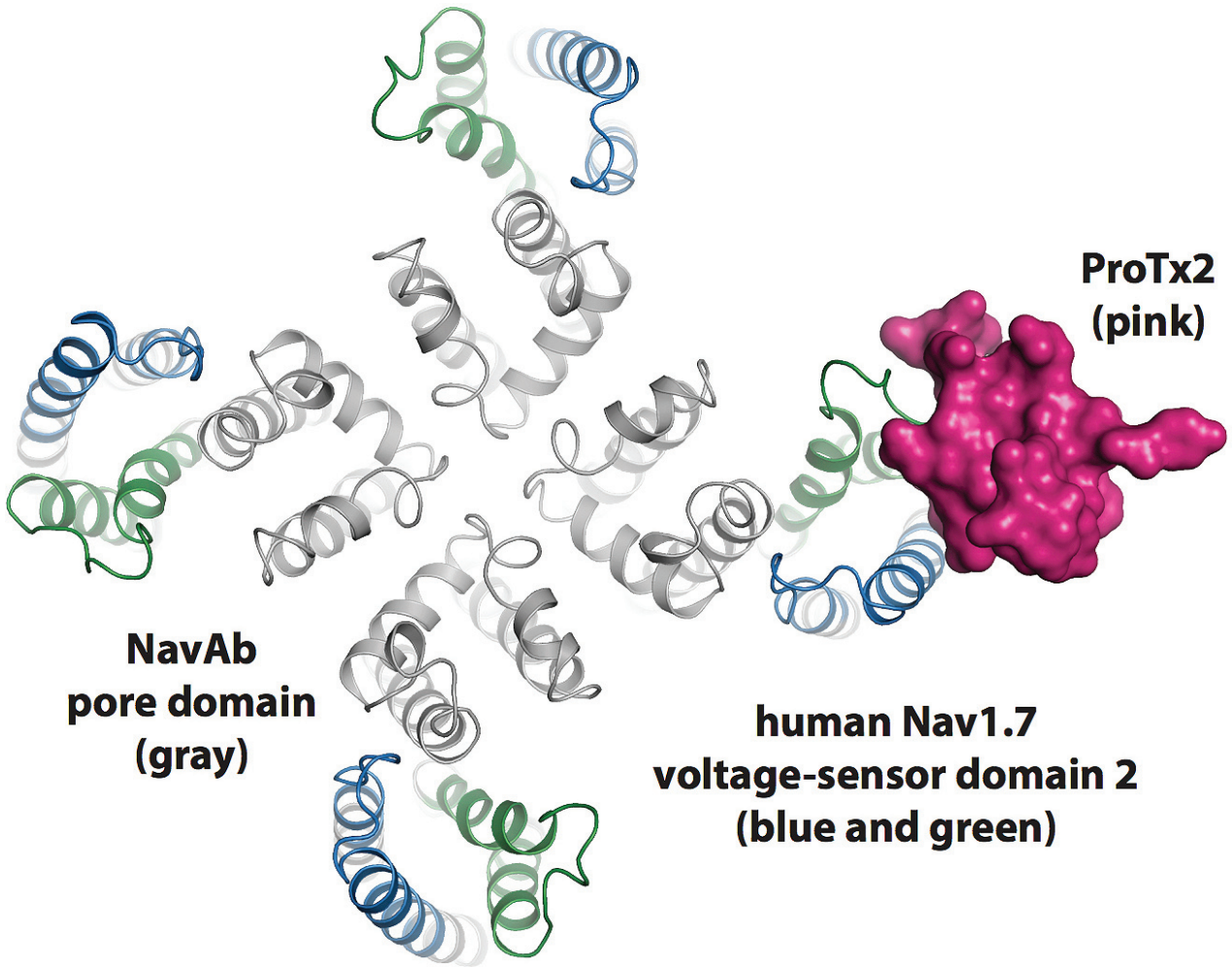

Fig. 1. Structure of the ProTx2 toxin from the Peruvian green velvet tarantula in complex with a chimeric human voltage-sensor domain 2-NavAb channel.

the resting VSD with extremely high affinity and to the activated VSD with relatively lower affinity, which underlies their inhibitory effects. The structure also explains the high selectivity of ProTx2 for Nav1.7. Finally, the researchers' observations indicate how new modulators might be designed to bind VSD2 during Nav channel gating to exert an inhibitory effect to silence hyperexcitability, even during instances of high frequency episodes, such as during epileptic seizures or chronic pain flares.

The results of this study reveal unprecedented insights into voltage sensing and electromechanical coupling within Nav channels and establish a new path for designing the next generation of Nav channel antagonists that are selective for the channels' various subtypes.

— Chris Palmer

See: Hui Xu, Tianbo Li*, Alexis Rohou**, Christopher P. Arthur, Foteini Tzakoniati‡, Evera Wong, Alberto Estevez, Christine Kuge, Yvonne Franke, Jun Chen, Claudio Ciferri, David H. Hackos***, Christopher M. Koth****, and Jian Payandeh*****, "Structural Basis of Nav1.7 Inhibition by a Gating-Modifier Spider Toxin," Cell **176**, 702 (February 7, 2019). DOI: 10.1016/j.cell.2018.12.018
Author affiliation: Genentech ‡Present address: Imperial College London
Correspondence: * li.tianbo@gene.com, ** rohou.alexis@gene.com, *** hackos.david@gene.com, **** koth.christopher@gene.com, ***** payandeh.jian@gene.com

F.T. acknowledges support from the Medical Research Council (Proximity to Discovery Award, MC_PC_14128). SSRL is supported by the U.S. Department of Energy (DOE) Office of Biological and Environmental Research, the National Institutes of Health, and the National Institute of General Medical Sciences. IMCA-CAT is supported by the companies of the Industrial Macromolecular Crystallography Association through a contract with Hauptman-Woodward Medical Research Institute, This research used resources of the Advanced Photon Source, a U.S. DOE Office of Science User Facility operated for the DOE Office of Science by Argonne National Laboratory under Contract No. DE-AC02-06CH11357.

Unraveling the Secrets of Streptozotocin's Synthesis

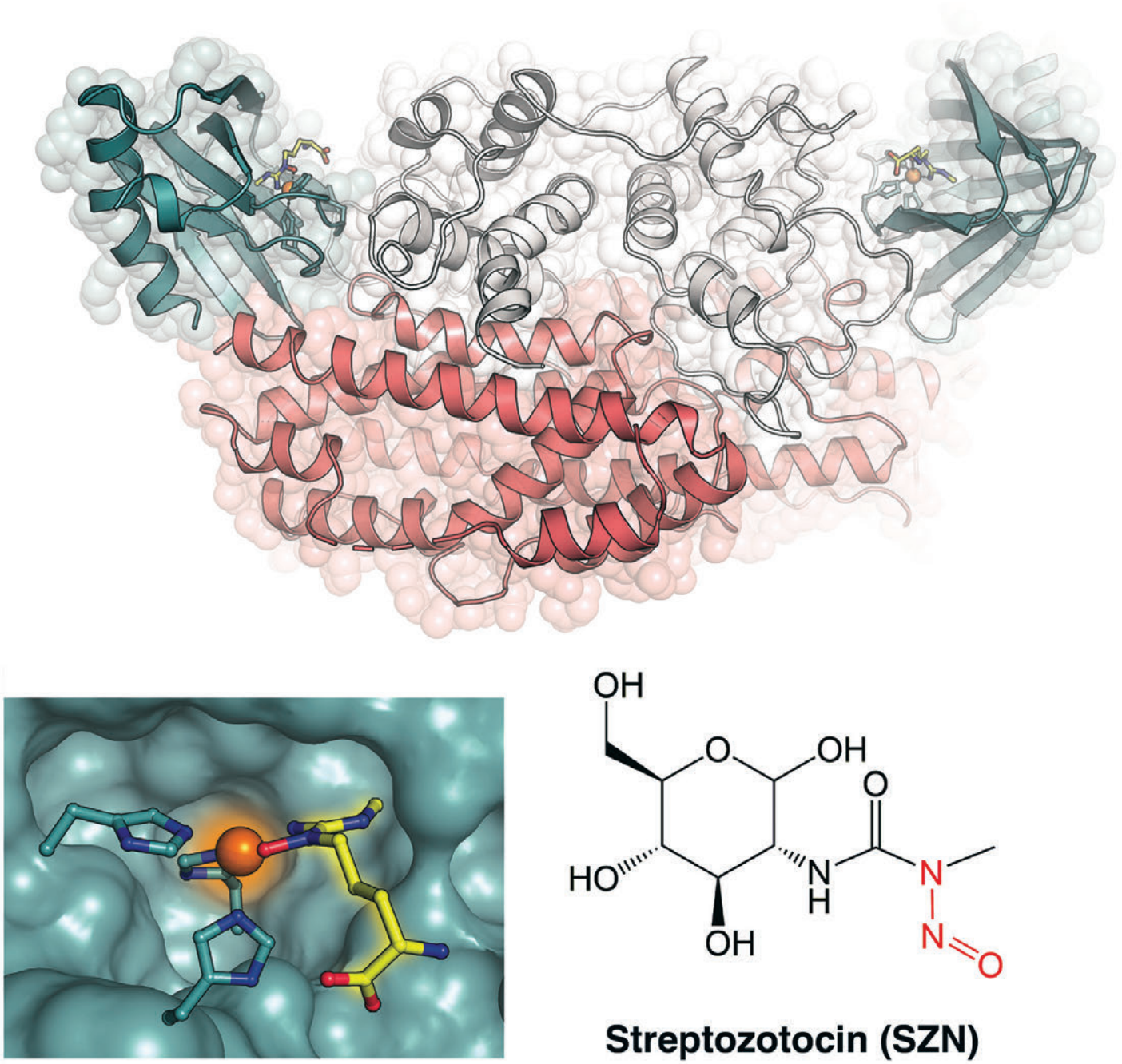

Fig. 1. A structure of the streptozotocin biosynthesis enzyme, SznF (top), reveals two different iron-containing catalytic domains (blue and pink). Bottom left: A substrate analog (yellow) binds to the iron cofactor (orange) in one of the active sites, facilitating rearrangement into the *N*-nitrosourea functional group (red) of streptozotocin (bottom right).

Soil bacteria produce streptozotocin, a natural product approved to fight cancer in humans, but for a long time, no one knew how the bacteria made this important molecule. Streptozotocin is part of a class of molecules that include an *N*-nitroso group; many of these chemicals have implications for human health as both carcinogens and medications. In this tour-de-force of a study, researchers from Harvard University identified the enzyme (SznF) that generates an *N*-nitrosourea product in the biosynthesis of streptozotocin. To help figure out how the enzyme works, colleagues from Pennsylvania State University solved the structure of the enzyme using x-ray diffraction data collected at the APS.

Streptozotocin, like other *N*-nitrosoureas, kills cancer cells by generating agents that damage DNA, including electrophilic alkylating agents and nitric oxide. It's reasonable to think that the bacteria that produce streptozotocin must have some way to protect their own DNA from these harmful effects. To track down the enzymes responsible for synthesizing the *N*-nitrosourea in streptozotocin, the researchers sequenced the genome of an organism that produces the compound and searched for gene clusters that might give the bacteria resistance to streptozotocin's DNA-alkylating effects. They were successful, identifying a block of genes that also contained an enzyme known as SznF, which, at the time, was of unknown function.

In a series of subsequent experiments, the researchers strategically interrogated the function of SznF as well as the role of the other genes in the streptozotocin biosynthetic gene cluster. Knocking out the gene for SznF in the organism eliminated the production of streptozotocin. The mutant also showed an accumulation of *N*-methyl-L-arginine (L-NMA), suggesting that molecule may be the substrate for SznF. Indeed, the researchers observed an SznF-dependent production of nitrite and nitric oxide from L-NMA, confirming that the enzyme performs *N*-oxygenation. Bit by bit, the team accumulated enough evidence to sketch out the reaction pathway for the multistep production of streptozotocin. SznF plays a critical role, performing an unusual oxidative rearrangement of L-NMA to generate the *N*-nitrosourea product.

As a next step, the team took a closer look at the unusual chemistry of SznF by solving crystal structures of the enzyme (Fig. 1). The structures, solved at the GM/CA-XSD 23-ID beamline and at the LS-CAT 21-ID x-ray beamline, both at the APS, combined with other evidence, revealed an unprecedented catalytic mechanism involving two iron-containing active sites. Furthermore, the researchers found similar enzymes in many different bacteria, including human pathogens, suggesting *N*-nitroso metabolites may be more important than previously suspected.

The structures showed two active sites: a C-terminal site that housed a mononuclear iron cofactor as well as a second iron-binding site in the center of the enzyme. Further investigation into the reactivity of each site revealed that the two metallocofactors are functionally distinct, catalyzing different steps in *N*-nitrosurea production. The C-terminal domain performs the final oxidative rearrangement reaction. A structure with a substrate analog showed that the precursor to the N-nitrosourea product binds directly to the C-terminal domain's iron cofactor. This binding mode would allow SznF to control the complicated bond-breaking and bond-forming steps that are needed to construct the N-nitroso functional group in streptozotocin.

SznF represents the first non-heme-iron-dependent enzyme of known structure that can form N-N bonds. The wide distribution of similar enzymes suggests the existence of a previously unknown universe of biologically important N-nitroso-containing compounds.

— Erika Gebel Berg

See: Tai L. Ng[1], Roman Rohac[2], Andrew J. Mitchell[2], Amie K. Boal[2]*, and Emily P. Balskus[1]**, "An *N*-nitrosating metalloenzyme constructs the pharmacophore of streptozotocin," Nature **566**, 94 (7 February 2019). DOI: 10.1038/s41586-019-0894-z
Author affiliations: [1]Harvard University, [2]Pennsylvania State University
Correspondence: * akb20@psu.edu,
** balskus@chemistry.harvard.edu

We acknowledge support from the National Institutes of Health (NIH) (DP2 GM105434 to E.P.B. and GM119707 to A.K.B.), a Cottrell Scholar Award (to E.P.B.), a Camille Dreyfus Teacher-Scholar Award (to E.P.B.), the Searle Scholars Program (to A.K.B.), and Harvard University. GM/CA-XSD has been funded in whole or in part with Federal funds from the National Cancer Institute (ACB-12002) and the National Institute of General Medical Sciences (AGM-12006). The Eiger 16M detector was funded by an NIH–Office of Research Infrastructure Programs, High-End Instrumentation Grant (1S10OD012289-01A1). Use of the LS-CAT was supported by the Michigan Economic Development Corporation and the Michigan Technology Tri-Corridor (grant 085P1000817). This research used resources of the Advanced Photon Source, a U.S. Department of Energy (DOE) Office of Science User Facility operated for the DOE Office of Science by Argonne National Laboratory under contract no. DE-AC02-06CH11357.

Progress in Understanding Triglyceride Metabolism

Triglycerides are one of the health markers that, along with cholesterol, are tested on a regular basis by doctors. They are an indicator of the level of triglyceride-rich lipoproteins in the blood; high levels are associated with cardiovascular disease. Due to the fact that many people have high levels of triglycerides, they are viewed as an important target for intervention, so a great deal of biomedical research is focused on how triglyceride levels are regulated by the body and the role of lipid-binding proteins in this regulation. However, proteins that move lipids around the body are notoriously difficult to work with due to their hydrophobic tendencies, and the protein that regulates triglyceride levels, lipoprotein lipase (LPL), is no different. Due to the propensity of LPL to unfold and aggregate, until recently only similarity models of its structure were possible. Advances in our understanding of the basic biology of LPL have made it possible for researchers using the APS to obtain a complete structure for LPL.

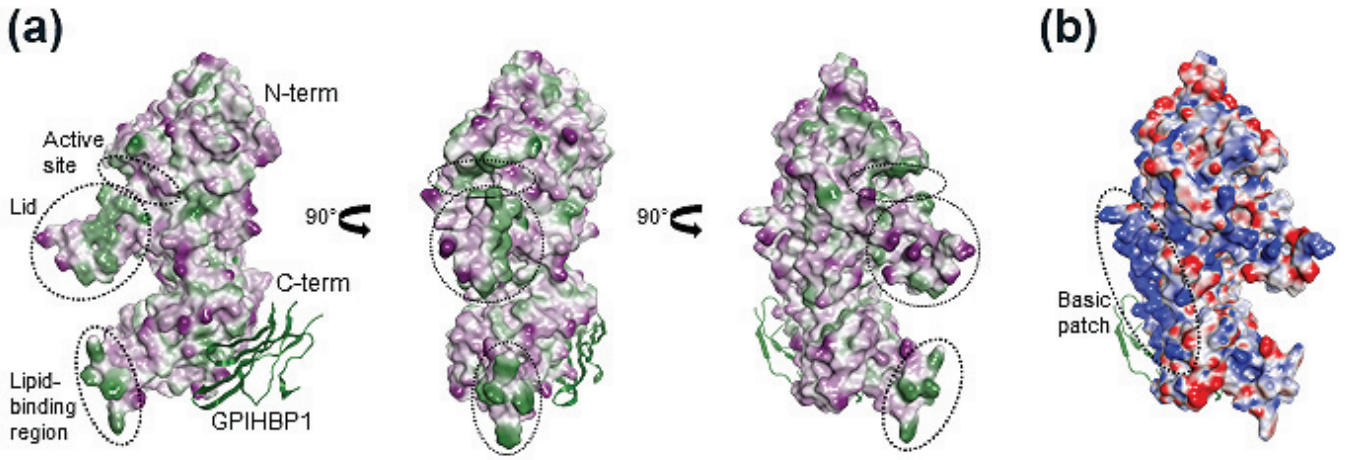

Fig. 1. Surface representations of LPL in the LPL-2/sGPIHBP1 structure (compound 2 is not shown). (a) LPL lipophilicity surface. Green, violet, and white shadings represent hydrophobic, hydrophilic, and neutral surfaces, respectively. (b) LPL electrostatic surface. Red, blue, and white shadings represent acidic (negative), basic (positive), and neutral surfaces, respectively. From R. Arora et al., Proc. Natl. Acad. Sci. U.S.A **116**(21), 10360 (May 21, 2019). © 2019 National Academy of Sciences

Genetic data have highlighted the importance of LPL in the regulation of triglyceride levels in blood through the identification of people with LPL gene variations. Those with variants that increase LPL activity or increase the amount of LPL that is secreted, for example, have lower levels of triglycerides and reduced risk of coronary artery disease. Similarly, loss of function in two of the proteins that are responsible for the correct folding and localization of LPL–LMF1 and GPIHBP1–also leads to high triglycerides. Taking these facts together, it is clear that drugs used to increase the activity of LPL could be useful therapeutics for people with high triglyceride levels. Drug design can be aided by a solid understanding of the three-dimensional structure of LPL but, until recently, LPL resisted attempts to determine its structure. With this background in mind, a team from the Novartis Institute for Biomedical Research took on the challenge of solving the crystal structure of LPL.

A key step that ultimately enabled determination of the LPL crystal structure was expressing LPL in conjunction with a soluble variant of GPIHBP1, the protein that transports LPL to its active location within tissues. The hypothesis was that GPIHBP1 would stabilize LPL and keep it from aggregating. This worked, but the complex of LPL with GPIHBP1 was obtained in low yield. The team then tried expressing LPL with GPIHBP1 and another protein, LMF1, that acts as a chaperone for LPL. Chaperones assist in the folding of proteins, and, since aggregation after unfolding was a part of the problem, it seemed as if LMF1 might do the trick. It did. With good yields of the active,

"Metabolism" cont'd. on page 80

How Essential Membrane Lipids Interact to Regulate Cellular Processes

The regulation of many cellular processes relies on interactions between sphingomyelin and cholesterol, two essential lipids in the cell's plasma membrane. Collecting diffraction data at the APS, researchers examined the three-dimensional molecular interaction between the lipid-binding protein Ostreolysin A and sphingomyelin/cholesterol complexes. The results of this study improved current understanding of how these lipids interact to carry out their regulatory functions and will instruct further research in this area.

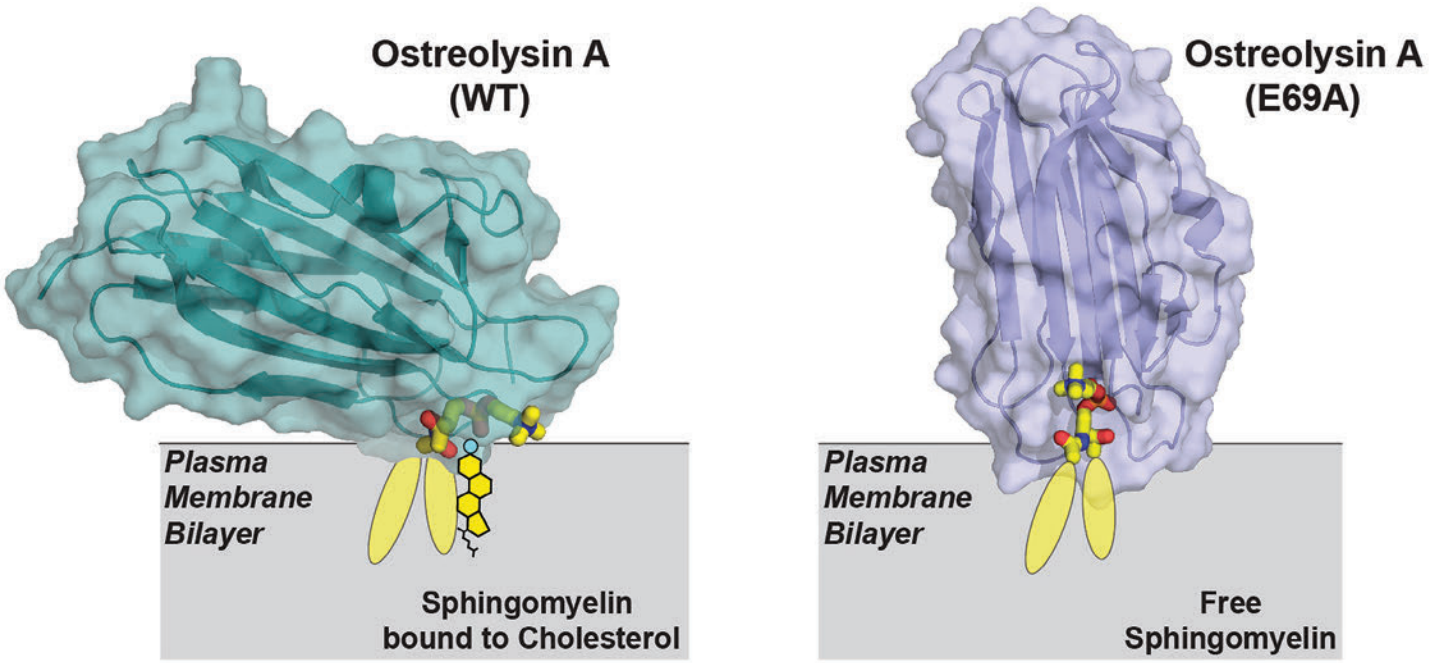

Fig. 1. Two protein sensors for two conformations of sphingomyelin in membranes, as determined at SBC-XSD at the APS.

Cholesterol and sphingomyelin are present at high concentrations in the plasma membranes of animal cells. The interaction between these two lipids at this location is vital for controlling many signaling processes within the cell. One of these key processes is regulation of the synthesis and uptake of cholesterol to control its levels in cells. This is important because the stability and integrity of the plasma membrane depends on proper levels of cholesterol. However, the exact mechanism by which these two essential lipids interact at the structural level remains poorly understood.

This lack of understanding relates, at least in part, to the fact that the plasma membrane's lipid bilayer region is a liquid and liquids do not have defined structures, which makes the interaction between lipids difficult to study. Therefore, scientists investigating this interaction need to find some way to trap lipids in states in which they may be bound to each other—for example in a sphingomyelin/cholesterol complex.

With this in mind, researchers team from the University of Texas Southwestern Medical Center performed a study, hoping to gain further insights about this interaction. They aimed to find a protein that would specifically bind to sphingomyelin/cholesterol complexes. First, they screened many candidate proteins and found one called Ostreolysin A that binds to sphingomyelin when sphingomyelin is bound to cholesterol, but not when it is free from cholesterol. *"Lipids" cont'd. on page 80*

"Metabolism" cont'd. from page 79

stable complex of LPL with GPIHBP1, the researchers were able to generate crystals for which they were able to obtain data at the IMCA-CAT 17-ID-B x-ray beamline at the APS. The structure (Fig. 1) was similar to another lipase enzyme, human pancreatic lipase, and to one for the LPL-GPIHBP1 complex recently solved by another research group.

However, as was the case for the other group's structure, the data lacked important density for a disordered "lid" region overlapping the active site and for the lipid binding domain. The Novartis team screened for compounds that bind to the LPL-GPIHBP1 complex and identified a novel inhibitor. They were able to solve another structure with the inhibitor that showed the density of the disordered regions, providing for the first time a complete structure for LPL. The lid region was shown to be in an open conformation that did not occlude the active site, and the lid and lipid binding regions were shown to create hydrophobic patches on the surface of the protein (Fig. 1), which helped illuminate how these regions of the LPL facilitate substrate recognition. For many years, LPL was believed to be active only as a homodimer. It was therefore interesting that, although the crystal structure showed two molecules of LPL in a head-to-tail arrangement as in a previous study, the electron density data did not really show any major contacts between the two molecules. After some further biochemical testing, the team feels confident that LPL actually works as a monomer, not a homodimer, an important finding that is in agreement with a recently published study from another group. — Sandy Field

See: Rishi Arora, Amitabh V. Nimonkar, Daniel Baird, Chunhua Wang, Chun-Hao Chiu, Patricia A. Horton, Susan Hanrahan, Rose Cubbon, Stephen Weldon, William R. Tschantz, Sascha Mueller, Reto Brunner, Philipp Lehr, Peter Meier, Johannes Ottl, Andrei Voznesensky, Pramod Pandey, Thomas M. Smith, Aleksandar Stojanovic, Alec Flyer, Timothy E. Benson, Michael J. Romanowski*, and John W. Trauger**, "Structure of lipoprotein lipase in complex with GPIHBP1," Proc. Natl. Acad. Sci. U.S.A **116**(21), 10360 (May 21, 2019). DOI: 10.1073/pnas.1820171116
Author affiliation: Novartis Institutes for Biomedical Research
Correspondence: * michael.romanowski@novartis.com,
** john.trauger@novartis.com

Use of the IMCA-CAT beamline was supported by the companies of the Industrial Macromolecular Crystallography Association through a contract with Hauptman-Woodward Medical Research Institute. This research used resources of the Advanced Photon Source, a U.S. Department of Energy (DOE) Office of Science User Facility operated for the DOE Office of Science by Argonne National Laboratory under Contract DE-AC02-06CH11357.

"Lipids" cont'd. from page 79

Next, the researchers used diffraction data collected at the SBC-XSD beamline 19-ID-D at the APS to solve the structure of Ostreolysin A when it was bound to the lipids (Fig. 1). Their analyses demonstrated how the protein's binding surface recognizes sphingomyelin when sphingomyelin is bound to cholesterol, but not when it is free of cholesterol.

This new information about the structure of the Ostreolysin A binding surface allowed the researchers to then model how the lipids must be arranged in the membrane. In this way, they were able to develop more understanding of the liquid membrane. They also showed that the conformation of sphingomyelin in the plasma membrane changes between two forms (Fig. 1), depending on whether it is bound to cholesterol or free of it.

Indeed, a critical point in their study was discovering a mutation in Ostreolysin A that eliminated its ability to discriminate between the two forms of sphingomyelin. The researchers solved the structure of this mutant and were able to determine how the binding surface on Ostreolysin A changed, which therefore informed them about how sphingomyelin adopted its two different conformations.

One interesting implication of these findings is that lipids can adopt different conformations in the cell's plasma membrane. More typically, we think of proteins as having different conformations. But lipids can also exist in different states, and proteins can specifically recognize one lipid state but not another.

Overall, the results of this study will help guide further research into how essential lipids interact to regulate key intracellular signalling processes. — Nicola Parry

See: Shreya Endapally, Donna Frias, Magdalena Grzemska, Austin Gay, Diana R. Tomchick, and Arun Radhakrishnan*, "Molecular Discrimination between Two Conformations of Sphingomyelin in Plasma Membranes," Cell **176**(5), 1040 (February 21, 2019). DOI: 10.1016/j.cell.2018.12.042
Author affiliation: University of Texas Southwestern Medical Center
Correspondence: * arun.radhakrishnan@utsouthwestern.edu

This work was supported by the Welch Foundation (I-1793), the American Heart Association (12SDG12040267), and the National Institutes of Health (HL20948). SBC-XSD is operated by UChicago Argonne, LLC, for the U.S. Department of Energy (DOE)-Biological and Environmental Research under contract DE-AC02-06CH11357. This research used resources of the Advanced Photon Source, a U.S. Department of Energy (DOE) Office of Science User Facility operated for the DOE Office of Science by Argonne National Laboratory under Contract DE-AC02-06CH11357.

Insight into Metabolic Pathways Important for Pathogenesis

The bacterium *Mycobacterium tuberculosis* (Mtb) is the causative agent of tuberculosis, an infection responsible for approximately 1.3 million deaths worldwide in 2018. Recent research carried out at the APS revealed how the Mtb protein Rv2498c is able to dissimilate and inactivate a human antimicrobial metabolite, itaconate, and use byproducts of the dissimilation as an energy source. X-ray diffraction data and complementary biochemical analysis and *in vivo* work by researchers from The Francis Crick Institute (UK) and the Albert Einstein College of Medicine revealed that Rv2498c is important not only for itaconate dissimilation and metabolism, but for a step in the leucine metabolic pathway as well. Together, these findings improve our understanding of this important pathogen and pave the way for development of novel antimicrobial agents.

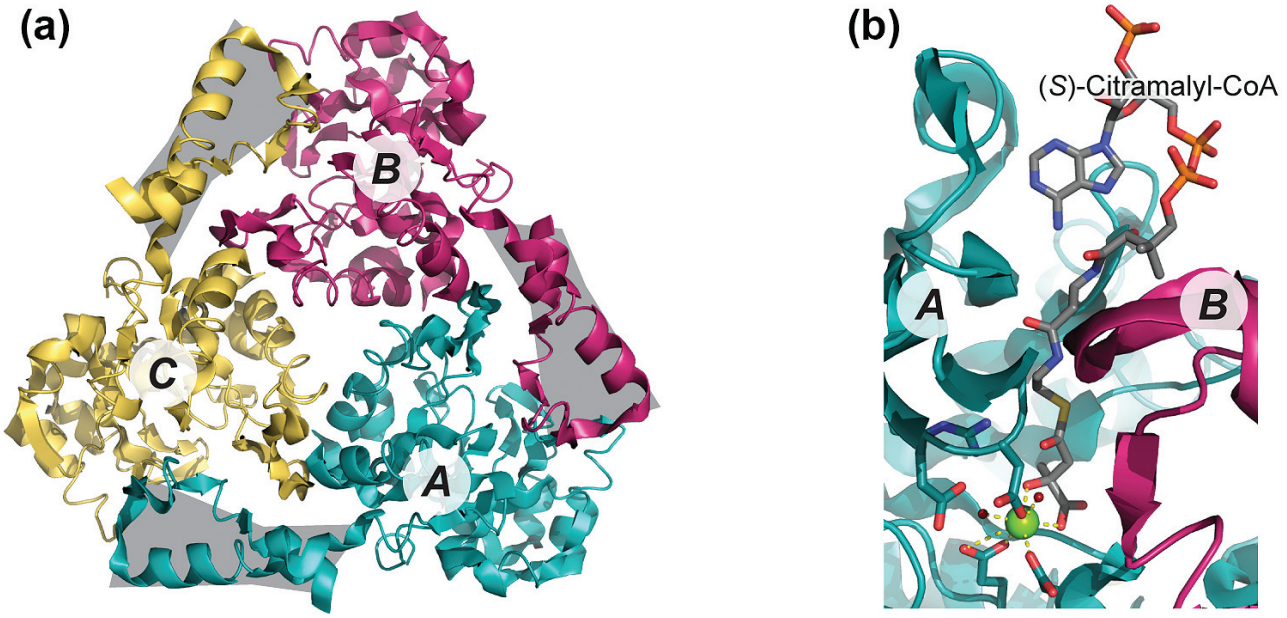

Fig. 1. Crystal structures of Rv2498c with C-terminal domain and (S)-Citramamyl-CoA. (a) Ribbon representation of trimeric Rv2498c with protomers A, B, and C (PDB: 6CJ4). The structured C-terminal domain is highlighted in grey. (b) Ribbon and stick representation of Rv2498c bound to (S)-citramalyl-CoA.

Mtb is a complex microorganism known for its ability to persist in humans in spite of host defenses and currently available antimicrobial therapies. To defend against bacterial infections in general, the body produces a number of antimicrobial chemicals. One of these metabolites, itaconate, is produced by macrophages during inflammation. Even though Mtb is known to induce very high physiologic concentrations of itaconate, it is able to avoid destruction by this otherwise bactericidal molecule.

Within the Mtb genome, there are a number of proteins with unknown function. Though many are assigned potential functions based on bioinformatic analysis, this method is an incomplete assessment of protein activity, and often results in misclassification of proteins. One Mtb protein, Rv2498c was originally thought to be a subunit (CitE) of an enzymatic complex called the citrate lyase complex. However, other required subunits are absent in the Mtb genome, making the ascribed role unlikely. Initial biochemical analysis of the Rv2498c protein revealed that it is unable to cleave the CitE substrate (S)-citryl-CoA. Rather, Rv2498c acts on the carbon–carbon bond of an-

"Pathways" cont'd. on page 83

Searching for Unusual Bonds Using a Very Bright Light

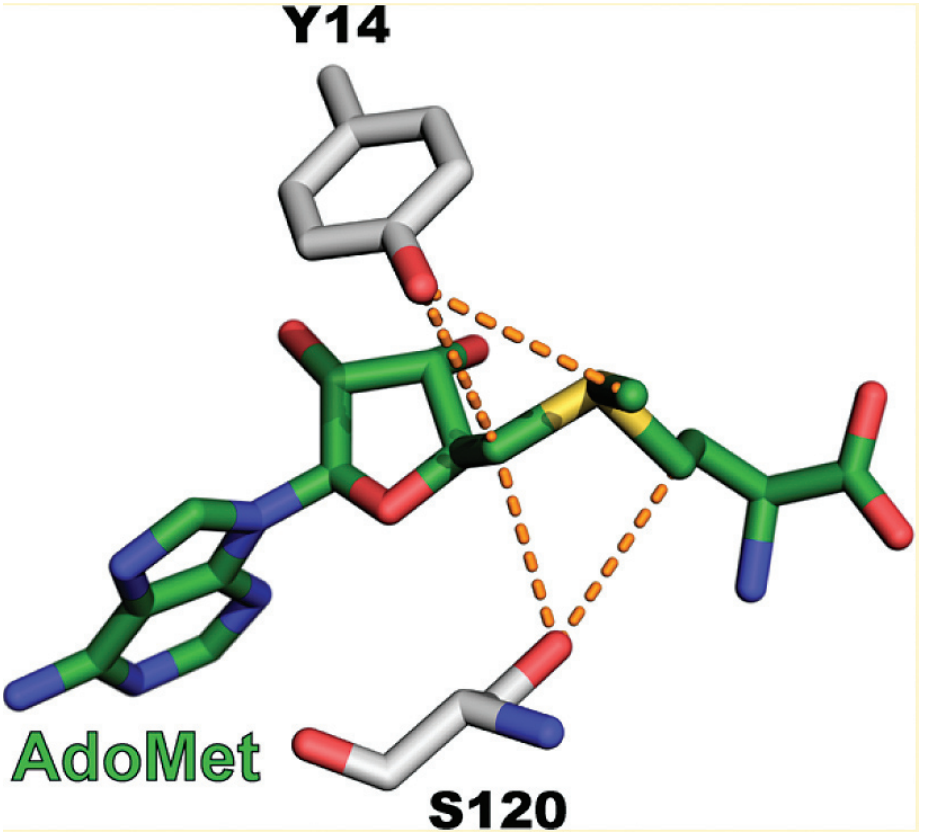

Fig. 1. The structure of TylM1 bound to the methyl donor S-adenosylmethionine (AdoMet). Researchers generated Tyrosine-14 to phenylalanine (Y14F) and Serine-120 to alanine (S120A) mutations to selectively ablate the CH···O hydrogen bonding (orange dashes) to AdoMet.

Methyltransferases are a class of proteins that catalyze the addition of a methyl group to a variety of substrates. These enzymes are classified according to their structure and target substrate. The methylation that they catalyze is involved in many biochemical pathways, including the synthesis of the antibiotic Tylosin. The N-methyltransferase that is responsible for the final step in the production of one component of this antibiotic is called "TylM1." Previous studies suggested that this enzyme may engage in an unconventional type of interaction with the methyl-donating substrate S-adenosylmethionine (AdoMet), which is termed carbon-oxygen (CH···O) hydrogen bonding. Researchers predicted that this unusual type of hydrogen bonding may be important for the enzyme's recognition of the AdoMet substrate and even in catalysis. A research team working at the APS set out to investigate the functions of CH···O hydrogen bonding in the active site of TylM1, which is suspected of employing these unusual interactions to promote methyl transfer during catalysis. The scientists performed x-ray diffraction studies in an attempt to pin down the source of these atypical hydrogen bonds, which have helped paint a clearer picture of these interactions in this important class of enzymes.

The team of scientists from the University of Michigan, Duke University, Oregon State University, and Utah State University conducted a series of experiments to reveal details about the role of the CH···O hydrogen bonds in the enzyme's activity. They probed the active site of TylM1 using a technique called "site-directed mutagenesis," which allowed the experimenters to individually change specific amino acids within the protein active site. They then utilized the resulting mutated versions of the protein in enzyme kinetics studies, where they monitored the impact that each change had on the rate of the reaction. They characterized

"Bonds" cont'd. on next page

"Bonds" cont'd. from previous page

the substrate binding patterns using nuclear magnetic resonance spectroscopy.

Once all of the mutated versions of TylM1 were purified, crystals were formed using very specific conditions, all in the presence of the AdoMet, in order to illustrate how the substrate and enzyme were interacting. Droplets containing the crystals were flash-frozen in liquid nitrogen. Using the LS-CAT 21-ID-G beamline at the APS, the researchers collected x-ray diffraction data of the enzyme-substrate complex crystals. The resulting diffraction patterns were analyzed using special software that allows for the development of a three-dimensional rendering of the protein-substrate complex. Figure 1 displays the structure of the active site of TylM1 bound to AdoMet, illustrating the CH···O hydrogen bonds between the substrate and the amino acids Tyrosine-14 (Y14) and Serine-120 (S120) in the enzyme.

The team was able to determine the functional role of these amino acids by mutating Tyrosine-14 to phenylalanine (Y14F) and Serine-120 to alanine (S120A) in TylM1 and then analyzing the kinetic properties of these mutants. By comparing the kinetic data and crystal structures of the TylM1 mutants to the native enzyme, the researchers concluded that Tyrosine-14 helps to position the methyl group of AdoMet for transfer to the sugar substrate. They also proposed that Serine-120 has an impact on substrate recognition and turnover. Finally, the researchers observed that any substitutions within the enzyme that eliminated CH···O hydrogen bonding between the active site and the AdoMet methyl group diminished catalysis, thus reinforcing the presence and importance of these interactions in methyl transfer by TylM1.

— Alicia Surrao

See: Robert J. Fick[1], Scott Horowitz[2], Brandon G. McDole[1], Mary C. Clay[3], Ryan A. Mehl[4], Hashim M. Al-Hashimi[3], Steve Scheiner[5], and Raymond C. Trievel[1]*, "Structural and Functional Characterization of Sulfonium Carbon–Oxygen Hydrogen Bonding in the Deoxyamino Sugar Methyltransferase TylM1," Biochemistry-US **58**, 2152 (2019). DOI: 10.1021/acs.biochem.8b01141
Author affiliations: [1]University of Michigan, [2]University of Denver, [3]Duke University, [4]Oregon State University, [5]Utah State University
Correspondence: * rtrievel@umich.edu

These studies were supported by National Science Foundation Grant CHE-1508492 to H.M.A.-H. and R.C.T. Use of the LS-CAT was supported by the Michigan Economic Development Corp. and the Michigan Technology Tri-Corridor (Grant 085P1000817). This research used resources of the Advanced Photon Source, a U.S. Department of Energy (DOE) Office of Science User Facility operated for the DOE Office of Science by Argonne National Laboratory under Contract DE-AC02-06CH11357.

"Pathways" cont'd. from page 81

other cellular metabolite, (S)-citramalyl-CoA, a known metabolic intermediate of the itaconate dissimilation pathway, to form pyruvate and Ac-CoA (molecules used as an energy source by the cell). Thus, Rv2498c is not a citrate lyase, but an (S)-Citramalyl-CoA Lyase. To understand the basis for this specificity, researchers captured atomic-level snapshots of Rv2498c bound to (S)-citramalyl-CoA using x-ray crystallography data collected by the staff of the LRL-CAT beamline 31-ID-D at the APS. By looking at the structure of the protein bound to its substrate, researchers were able to identify areas of the protein most important for substrate specificity and catalytic activity (Fig. 1).

Additional phylogenetic analysis, which compares the evolutionary relationships between proteins, prompted further exploration of Rv2498c's ability to process other metabolites. This analysis revealed that Rv2498 is able to metabolize (R)-HMG-CoA, an intermediate of leucine metabolism. This mode of leucine metabolism is entirely unique, and is an important finding for understanding how Mtb is able to survive in the host.

Together, these activities make Rv2498c a bifunctional enzyme. Importantly, an Mtb strain lacking Rv2498c is unable to reproduce in a mouse model of infection to the same degree as normal Mtb, supporting the hypothesis that Rv2498c is critical for Mtb infection. Identification of the true function of Rv2498c, together with structural information paves the way for development of antimicrobial agents and builds basic understanding of a significant human pathogen. — Emma Nichols

See: Hua Wang[1], Alexander A. Fedorov[2], Elena V. Fedorov[2], Debbie M. Hunt[1], Angela Rodgers[1], Holly L. Douglas[1], Acely Garza-Garcia[1], Jeffrey B. Bonanno[2], Steven C. Almo[2], and Luiz Pedro Sório de Carvalho[1]*, "An essential bifunctional enzyme in Mycobacterium tuberculosis for itaconate dissimilation and leucine catabolism," Proc. Natl. Acad. Sci. U.S.A. **116**(32), 15907 (August 6, 2019). DOI: 10.1073/pnas.1906606116
Author affiliations: [1]The Francis Crick Institute, [2]Albert Einstein College of Medicine
Correspondence: * luiz.carvalho@crick.ac.uk

Work in L.P.S.d.C.'s laboratory is supported by the Francis Crick Institute, which receives core funding from Cancer Research UK Grant FC001060, UK MRC Grant FC001060, and Wellcome Trust Grant FC001060. L.P.S.d.C.'s laboratory also acknowledges funds from Wellcome Trust New Investigator Award 104785/B/14/Z. S.C.A. acknowledges U.S. National Institutes of Health Grant P01 GM118303. Hua Wang can be reached at his laboratory, the Institute of Infection, Immunity & Inflammation. Use of the LRL-CAT beamline awas provided by Eli Lilly Company, which operates the facility. This research used resources of the Advanced Photon Source, a U.S. Department of Energy (DOE) Office of Science User Facility operated for the DOE Office of Science by Argonne National Laboratory under Contract DE-AC02-06CH11357.

Changing Shapes in Fruit Fly Cryptochromes Dictate Circadian Rhythms

Our circadian clock allows us to predict changes in our environment based on the day-night cycle. But rather than gears and springs, circadian clocks are composed specifically of chemical processes that alter the shapes of molecules. To begin to tease apart the details of these molecular events, an international team of researchers has turned to *Drosophila melanogaster*, the fruit fly, and that fly's light-activated proteins, called cryptochromes, which play a crucial part in setting and keeping the fly entrained with the light-dark cycle. Recent scientific results obtained at the APS show for the first time the series of shapes taken by an animal cryptochrome when activated by light, which in turn have the potential to help us make sense of the activities of human cryptochromes.

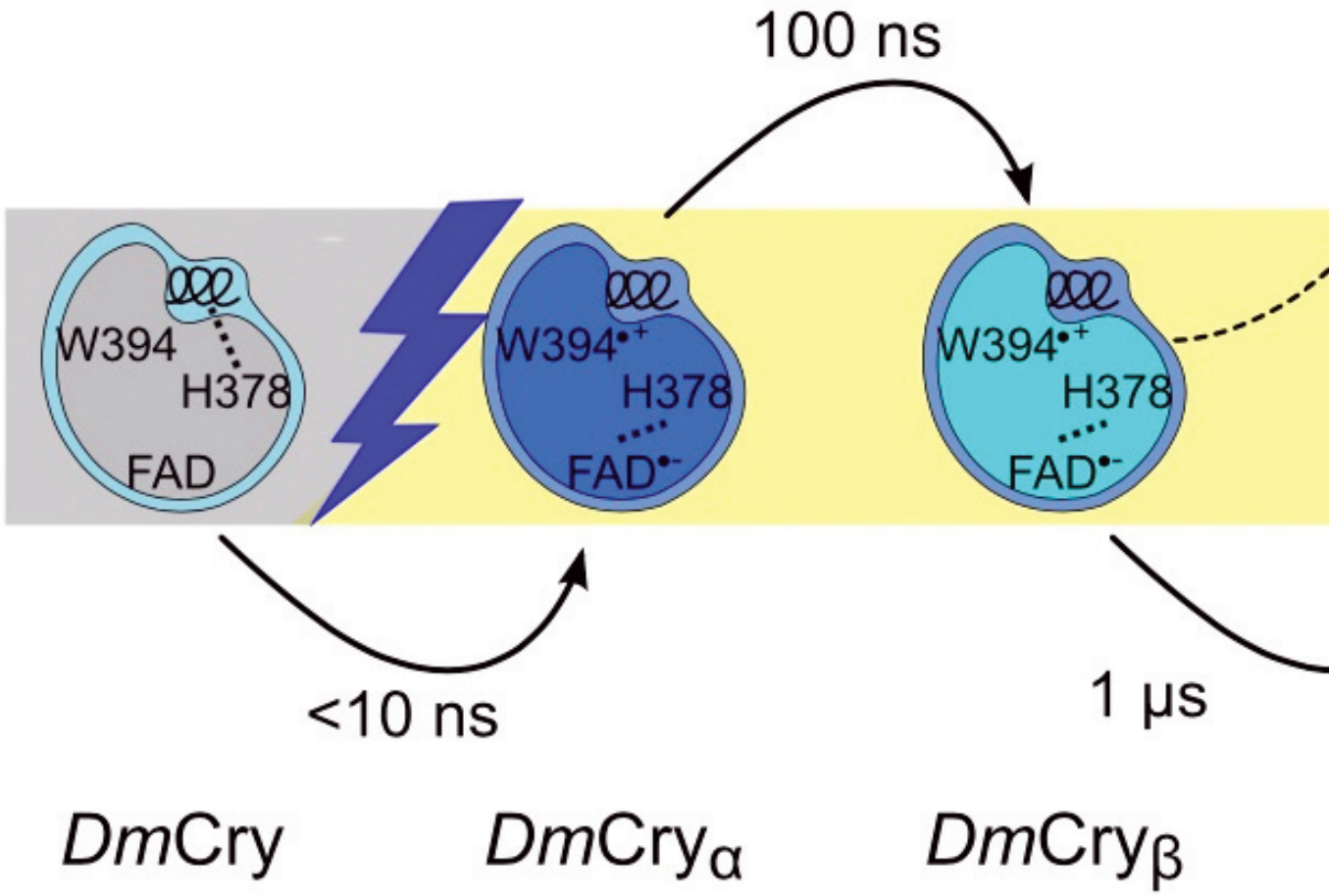

Fig. 1. Shape change of *Dm*Cry as a function of time after light activation, indicating different species and signaling conformation.

Within the cell, it is the shape of the molecule, called its conformation, that allows it to interact with those around it. Molecules in the cell change shape in response to their environment–such as light and dark–and also as part of signaling transduction. Signaling transduction occurs as a sequence of chemical reactions and can cause transcription of genes. A protein's signaling state conformation is of special interest because it reveals how its signals may be passed on to other proteins in the cell.

The single type I insect cryptochrome in the fruit fly, abbreviated *Dm*Cry, binds with the TIMELESS protein as part of the process that entrains the cell to a day-light cycle. The cryptochrome is light activated but its interactions are a function of its shape, specifically its C-terminal

tail (which refers to the portion of the molecule which ends in a free carboxyl group). Previous investigations into the role of *Dm*Cry were performed at photoequilibrium and thus gave little insight into the full sequence of shape changes that occur due to light activation. Scientists from the University of Gothenburg (Sweden), Lund University (Sweden), Albert-Ludwigs-Universität Freiburg (Germany), and the University of Jyväskylä (Finland) collaborated to image the cryptochrome and determine the series of shapes it takes, including specifying which is the signaling state conformation.

The team members imaged the conformations of multiple sample molecules as a function of time after light excitation, at nanosecond and millisecond intervals (Fig. 1). Their samples included a wild-type *Dm*Cry cryptochrome from a fruit fly; a mutant fruit fly cryptochrome (with a histidine 378 to alanine exchange to inhibit signal relay); and a control molecule, a 6-4 photolyse molecule from the African clawed frog *Xenopus laevis* (which behaves similarly to the fruit fly cryptochrome under light conditions but lacks a C-terminal tail). Together with colleagues from The University of Chicago the team measured the sample molecules' shapes using time-resolved x-ray solution scattering at the BioCARS 14-D-B x-ray beamline at the APS.

The team found that the cryptochromes' shapes changed as a function of time. The best fit for their data assumed the wild-type *Dm*Cry cryptochrome went through five different conformations. Their measurements implied changes in shape to the C-terminal tail of both the wild-type and mutant cryptochromes. As additional support for this argument, they found no such x-ray response from the control molecule that lacked a C-terminal tail. Their measurements of the difference pair distance distribution indicated two other changes. One, the cryptochromes become extended after light activation and detach their

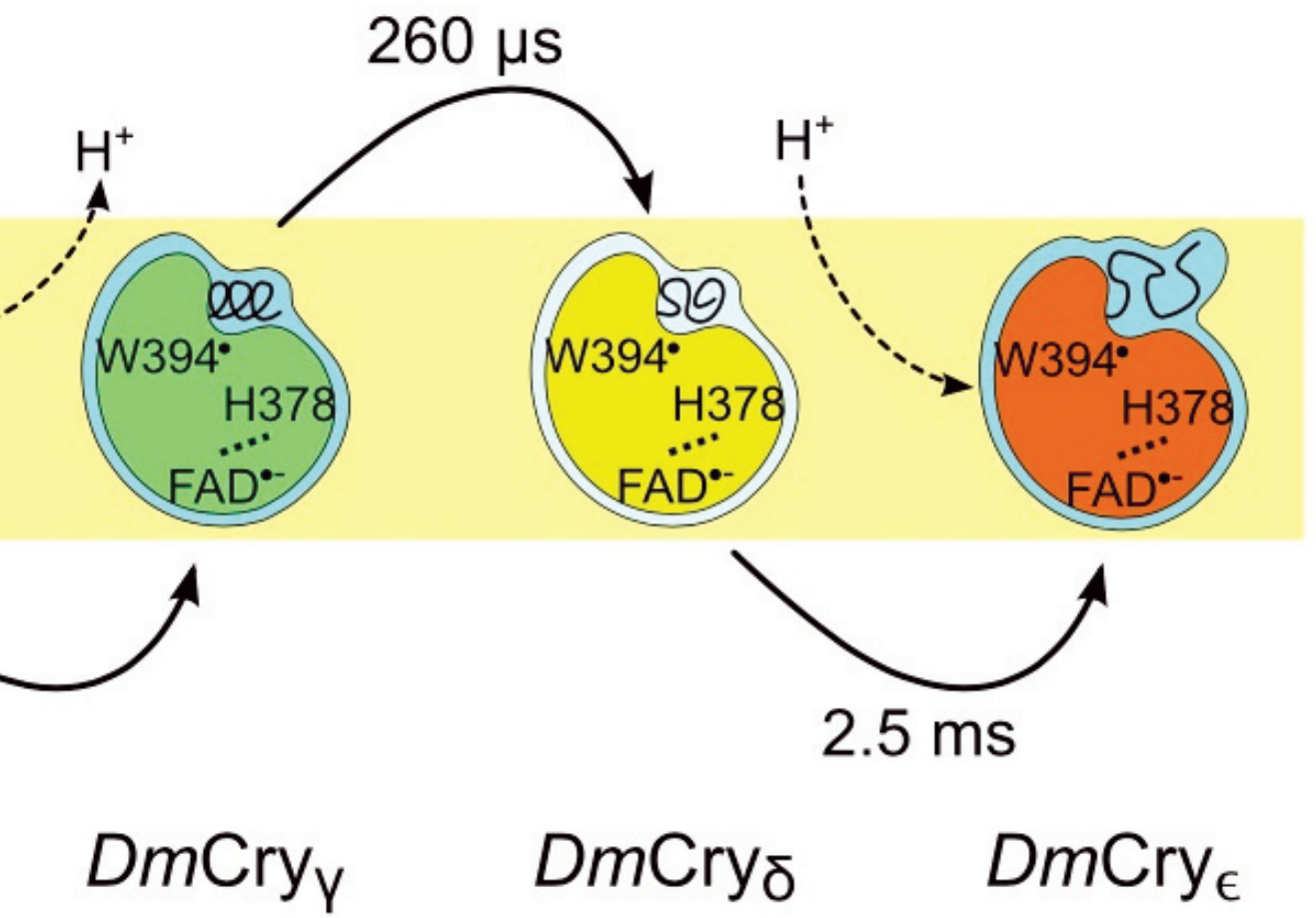

"Circadian" cont'd. on page 87

A Therapeutic Target for Parkinson's Disease

Parkinson's disease (PD) is a neurodegenerative disorder that affects about 7 million people worldwide, including 1 million in the U.S. Though the causes of PD remain unknown, the leucine-rich repeat kinase 2 (LRRK2) protein is a known contributor to both sporadic and inherited disease. Importantly, the C-terminal of LRRK2, the WD40 domain, is required for LRRK2 neurotoxicity. To better understand the biological functions of LRRK2 and the impact that PD-associated mutations have on protein function, researchers used anomalous diffraction phasing at the APS to solve the structure of the WD40 domain of human LRRK2 to a resolution of 2.6 Å. This structure allowed researchers to map known disease-associated mutations and to use complimentary biochemical analysis to explore the functional effects of pathogenic mutations on LRRK2 dimerization. Together, these findings provide support for development of LRRK2-targeting therapies for PD.

"Parkinson's" cont'd. on next page

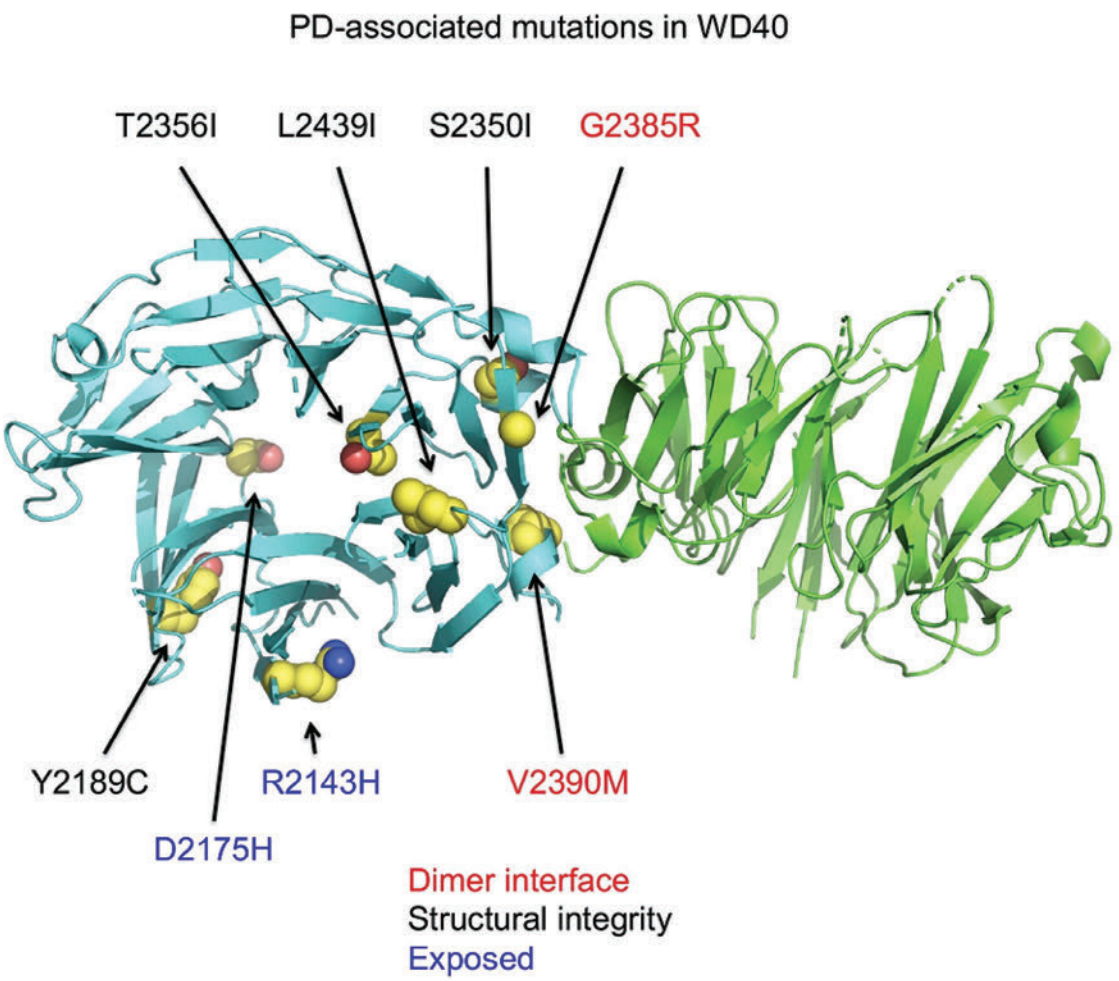

Fig. 1. Crystal structure of the WD40 domain of LRRK2 showing locations of PD-associated mutations. Carbon atoms are shown in yellow, nitrogen atoms in blue, and oxygen atoms in red. Red type indicates mutations found along the dimer interface, and blue type indicates amino acids that are surface-exposed. Black type indicates amino acids important for maintaining the structural integrity of the domain.

"Parkinson's" cont'd. from previous page

There are a number of genetic and environmental factors associated with development of Parkinson's disease. For example, the incidence of PD increases with age, and there are a number of mutations within a range of genes that have been associated with PD. Though mutations in some of these genes are present in a small subset of PD patients, like those responsible for familial PD, others, like the protein LRRK2, are major contributors to hereditary and sporadic PD.

Though the exact function of LRRK2 is unclear, as is the exact nature of its contribution to PD, it is known that the C-terminal WD40 structural domain is required for LRRK2-indiced neurotoxicity. In the current work, the researchers from Harvard Medical School, Boston Children's Hospital, the University of Dundee (UK), and the University of California, San Diego, crystalized WD40 and used x-ray diffraction data obtained at the NE-CAT 24-ID-C beamline at the APS to build a model of the protein to a resolution of 2.6 Å. With the structure of WD40 in hand, the researchers were able to map mutations known to contribute to PD onto the three-dimensional structure (Fig. 1). Using complementary biochemical analysis, the team confirmed that LRRK2 exists in solution as a concentration-dependent dimer, resolving ambiguity in the field surrounding the functional state of the protein. Importantly, several mutations at the dimerization interface were shown to increase LRRK2 activity, lending support to the hypothesis that LRRK2 pathogenicity in PD is due to hyperactivation of the protein.

That PD mutations contribute to hyperactivation is an important finding, as this supports LRRK2 as a drug target for novel anti-PD therapies. Future research will be aimed at a deeper understanding of the complexities of LRRK2 biology, including the factors which influence the imperfect correlation between LRRK2 dimerization and activity, and the effect of pathogenic mutations on the activity of the full-length protein. — Emma Nichols

See: Pengfei Zhang[1,2], Ying Fan[3], Heng Ru[1,2], Li Wang[1,2], Venkat Giri Magupalli[1,2], Susan S. Taylor[4], Dario R. Alessi[3], and Hao Wu[1,2]*, "Crystal structure of the WD40 domain dimer of LRRK2," Proc. Natl. Acad. Sci. U.S.A. **116**(5), 1579 (January 29, 2019). DOI: 10.1073/pnas.1817889116
Author affiliations: [1]Harvard Medical School, [2]Boston Children's Hospital, [3]University of Dundee, [4]University of California, San Diego
Correspondence: * wu@crystal.harvard.edu

This work was supported by The Michael J. Fox Foundation for Parkinson's Research [Grants 11211 (to H.W.) and 6986 (to D.R.A.)] and by the Medical Research Council [Grant MC_UU_12016/2 (to D.R.A.)]. The NE-CAT beamlines are funded by the National Institute of General Medical Sciences from National Institutes of Health (NIH) Grant P30 GM124165. The Pilatus 6M detector on the 24-ID-C beamline is funded by a NIH-Office of Research Infrastructure Programs High-End Instrumentation Grant S10 RR029205. This research used resources of the Advanced Photon Source, a U.S. Department of Energy (DOE) Office of Science User Facility operated for the DOE Office of Science by Argonne National Laboratory under Contract DE-AC02-06CH11357.

"Circadian" cont'd. from page 85

C-terminal tail. Two, there is a change to the density of the solvent layer surrounding the cryptochromes, which they confirmed through modeling.

They used small-angle x-ray scattering at the BM29 beamline of the European Synchrotron Radiation Facility (France) to determine which shape was the signaling state conformation. They found that histidine 378 is not solely responsible for signal relay as the signaling state conformation is also formed in the mutant cryptochrome lacking the histidine. The team probed the *Dm*Cry cryptochrome conformations at different pH levels, concluding that the signaling state shape is a function of pH.

Through this new understanding of cryptochrome conformation, including identification of the signaling state conformation, the research team begins to illuminate the first moments of signal transduction in the circadian clock of the fruit fly, an initial step in shedding light on understanding human circadian rhythms.

— Mary Alexandra Agner

See: Oskar Berntsson[1,2]*, Ryan Rodriguez[3]*, Léocadie Henry[1], Matthijs R. Panman[1], Ashley J. Hughes[1], Christopher Einholz[3], Stefan Weber[3], Janne A. Ihalainen[4], Robert Henning[5], Irina Kosheleva[5], Erik Schleicher[3]**, Sebastian Westenhoff[1]*, "Photoactivation of Drosophila melanogaster cryptochrome through sequential conformational transitions," Sci. Adv. **5**, eaaw1531 (17 July 2019). DOI: 10.1126/sciadv.aaw1531
Author affiliations: [1]University of Gothenburg, [2]Lund University, [3]Albert-Ludwigs-Universität Freiburg, [4]University of Jyväskylä, [5]The University of Chicago
Correspondence: * westenho@chem.gu.se,
** erik.schleicher@physchem.uni-freiburg.de

S. Wes. acknowledges funding from the Swedish Foundation for International Cooperation in Research and Higher Education, the European Research Council (725642), and the Foundation of Strategic Research, Sweden. E.S. and S. Web. thank the DFG (235777276/GRK1976) for financial support. J.A.I. acknowledges a grant from the Academy of Finland (296135) and the Jane and Aatos Erkko Foundation. BioCARS is supported by the National Institute of General Medical Sciences of the National Institutes of Health under grant R24GM111072. The time-resolved x-ray diffraction setup at Sector 14 was funded, in part, through a collaboration with P. Anfinrud (NIH/NIDDK). This research used resources of the Advanced Photon Source, a U.S. Department of Energy (DOE) Office of Science User Facility operated for the DOE Office of Science by Argonne National Laboratory under contract no. DE-AC02-06CH11357.

A Novel Inhibitor Provides a Boost for Chemotherapy

Cancer is caused by uncontrolled cellular replication. Of course, there can be no cellular replication without DNA replication. Doctors have been using DNA-damaging drugs to kill cancer for decades, but often malignant cells overcome the DNA damage and continue to replicate, leading to poor health outcomes. A key to the cancer cells' resilience is a special class of polymerases—enzymes that catalyze DNA replication—that can essentially ignore DNA damage and copy the DNA, whatever shape it's in, even if it means creating new malignant cells with faulty DNA. Depending on the nature of the DNA damage, sometimes this process can trigger secondary malignancies. Recently, researchers discovered JH-RE-06, a small-molecule inhibitor of one of these special polymerases. To understand how the inhibitor works, a multi-institution team of researchers collected x-ray diffraction data at the APS, in the process uncovering an unusual inhibition mechanism. Combining JH-RE-06 with existing chemotherapies may offer doctors a new tool to kill even the most obstinate cancers.

DNA replication is the very essence of life, allowing hereditary information to be transferred from cell to cell and from generation to generation. The cell has an entire machinery dedicated to the preservation and maintenance of DNA, yet sometimes, to save a life, the cell must replicate its DNA in spite of damage. In these cases, the cell engages a process known as "translesion synthesis" (TLS), which deploys TLS DNA polymerases to replicate DNA in spite of mutations. Cancer cells that exploit TLS to overcome mutations caused by DNA-damaging medications are said to have chemotherapeutic resistance.

TLS is a two-step process involving an initiation TLS polymerase and an elongation TLS polymerase. Scientists looking for inhibitors of TLS polymerases have been hampered due to similarities between these enzymes and the polymerases that replicate normal DNA. An inhibitor that blocked both TLS polymerases and normal polymerases would not be a good drug, as it would lead to the death of normal healthy cells. Zhou's team found a way around this by targeting a specific protein-protein interaction between an insertion TLS polymerase and an elongation TLS polymerase that doesn't exist in the standard polymerases. The researchers performed an ELISA assay screen of around 10,000 structurally diverse compounds in search of inhibitors of this interaction, and were rewarded with a hit: JH-RE-06.

As a next step, Zhou's the team probed the atomic details of inhibition by crystallizing a fragment of the polymerase along with JH-RE-06. Using data from studies at the SER-CAT beamline 22-ID-D the APS, the researchers solved a 1.50-Å-resolution crystal structure of the inhibitor-polymerase complex (Fig. 1). That's when they got a surprise. The inhibitor bound on a relatively featureless side of the polymerase, inducing dimerization that prevented the interaction of the insertion polymerase with the elongation polymerase.

The big test was whether JH-RE-06 had an impact on living cells. Cisplatin is a chemotherapy that works by damaging DNA, and cisplatin resistance is not uncommon. To test JH-RE-06, the researchers performed experiments on the effects of cisplatin with and without the inhibitor in a series of human cancer cell lines, including fibrosarcoma, melanoma, and prostate adenocarcinoma, as well as mouse lung adenocarcinoma cells. The researchers also tested the combination in non-cancer human and mouse cells. The researchers found that JH-RE-06 enhanced the cytotoxicity of cisplatin in cancer cell lines, but not in normal cell lines, as they hoped. The researchers

also combined JH-RE-06 with other agents that damage DNA beyond cisplatin and found similar results. The most encouraging results came from a xenograft mouse model of human melanoma; those mice treated with a combination of JH-RE-06 and cisplatin survived longer than those treated with saline or either agent alone.

By improving chemotherapy, JH-RE-06 represents a novel class of adjuvants and may perhaps someday become a standard strategy for fighting cancer. — Erika Gebel Berg

See: Jessica L. Wojtaszek[1‡], Nimrat Chatterjee[2], Javaria Najeeb[1], Azucena Ramos[2], Minhee Lee[3], Ke Bian[4], Jenny Y. Xue[3‡‡], Benjamin A. Fenton[1], Hyeri Park[3], Deyu Li[5], Michael T. Hemann[2*], Jiyong Hong[1,3**], Graham C. Walker[2***], and Pei Zhou[1*], "A Small Molecule Targeting Mutagenic Translesion Synthesis Improves Chemotherapy," Cell **178**, 152 (June 27, 2019).
DOI: 10.1016/j.cell.2019.05.028
Author affiliations: [1]Duke University Medical Center, [2]Massachusetts Institute of Technology, [3]Duke University, [4]University of Rhode Island Present address: ‡National Institute of Environmental Health Sciences, ‡‡Weill Cornell/Rockefeller/Sloan Kettering Tri-Institutional M.D.-Ph.D. Program
Correspondence: * hemann@mit.edu,
** jiyong.hong@duke.edu,
*** gwalker@mit.edu,
**** peizhou@biochem.duke.edu

This work was supported in part by grants from the National Cancer Institute (CA191448 to P.Z. and J.H.; CA213042 to D.L.), the Alexander and Margaret Stewart Trust (to P.Z.), the National Institute of Environmental Health Sciences (ES028303 to G.C.W.; ES028865 to D.L.), Duke University (to J.H.), and the Center for Precision Cancer Medicine at MIT (to M.T.H.). G.C.W. is an American Cancer Society Professor. SER-CAT is supported by its member institutions and equipment grants (S10_RR25528 and S10_RR028976) from the National Institutes of Health. This research used resources of the Advanced Photon Source, a U.S. Department of Energy (DOE) Office of Science User Facility operated for the DOE Office of Science by Argonne National Laboratory under Contract DE-AC02-06CH11357.

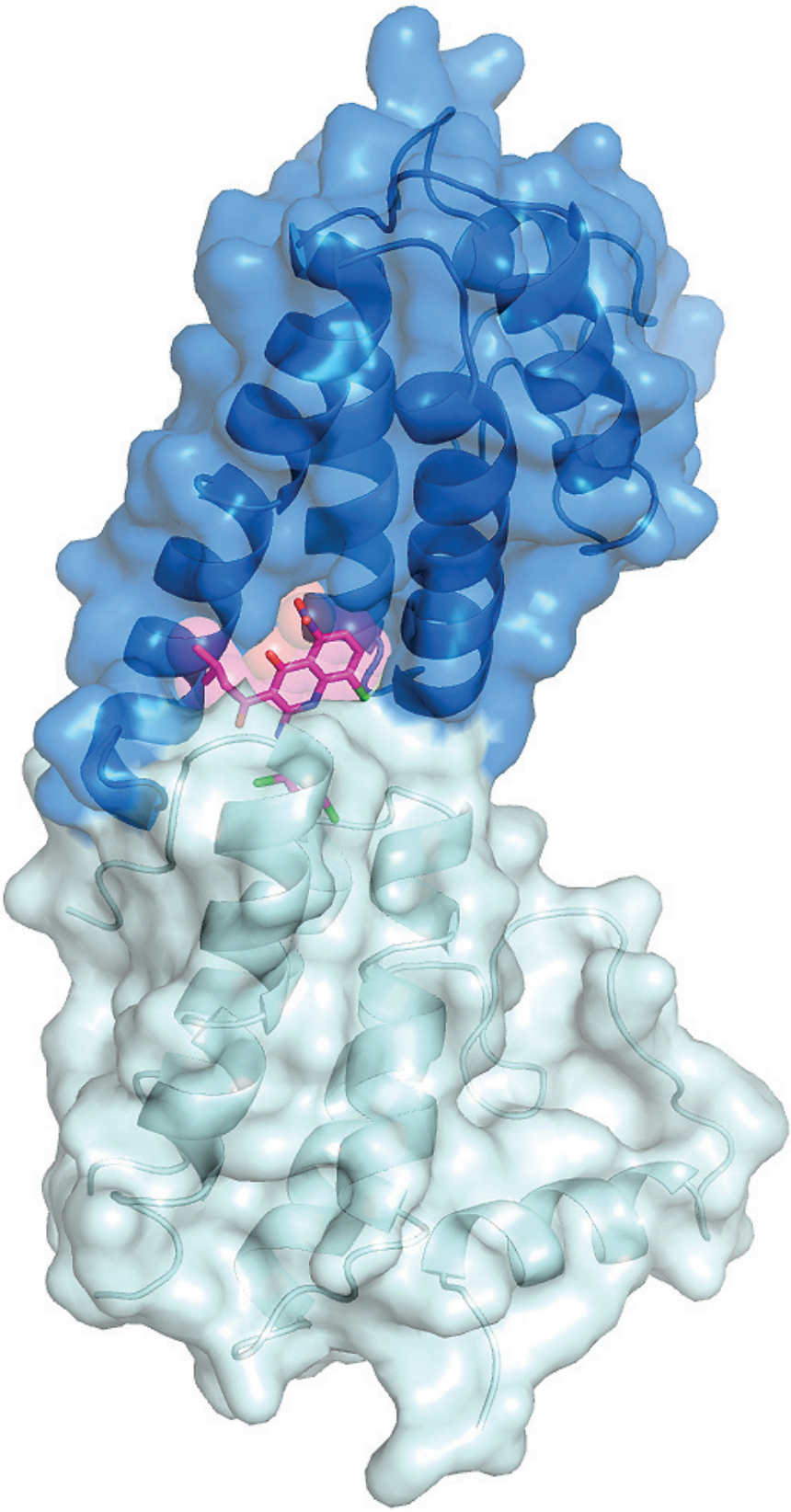

Fig. 1. Surface representation of the TLS polymerase fragments (blue and white) and JH-RE-06 (pink) complex showing the formation of a large ligand cavity at the dimeric interface and the near encapsulation of the inhibitor within the cavity.

How Poxviruses Evade the Sting of Our Basic Immune Defenses

One way that the innate immune system, our first line of defense against microbes, detects viruses is to detect viral DNA in our cells. Of course, we all have DNA in our cells, but it is neatly packaged into our nuclei and mitochondria. So, if DNA is detected outside of these areas, that is a reason for sounding the alarm. The way our cells do that is to have a messenger system that detects the viral DNA through an enzyme called cyclic GMP-AMP synthase (cGAS) that makes the small messenger molecule 2'3'-cGMP-AMP (cGAMP) carry the signal to the innate immune system through the receptor STING. This elegant system provides a way to activate immune responses to viral intruders, but also may present a target that viruses can exploit to evade our defenses by silencing the alarm. In fact, this idea was the basis for recent work in which researchers hypothesized that evolution would favor viruses that could disrupt the cGAS-STING signaling pathway and, thus, evade detection. The work, supported by research at the APS, identified a novel class of viral proteins and has implications for a wide variety of fields from vaccination and gene therapy to cancer therapeutics.

The first step in the project, conducted by researchers from the Harvard Medical School, Harvard University, the Dana Farber Cancer Institute, and the Dana-Farber/Brigham and Women's Cancer Center, was to develop an assay to detect viral evasion. cGAMP is extremely stable, making it both a good messenger and a good target for the assay. Reasoning that the best way to stop the message is to kill the messenger, the team developed a way to detect the degradation of cGAMP in cell lines that were infected with different viruses. After screening 24 different types of viruses, they had a candidate, vaccinia virus (VACV), a type of poxvirus. They named the viral factor poxvirus immune nuclease or poxin and discovered it was the product of the vaccinia B2R gene. Expression of the protein allowed them to purify and characterize the poxin biochemically. The VACV poxin is specific for cGAMP and acts to degrade this cyclic messenger molecule to a linear form of the molecule that is no longer recognized by STING, effectively blocking the signal. *In vivo*, they found that if they removed the poxin gene from vaccinia virus and then infected mice with it, it was attenuated by 40-fold compared to the wild-type virus.

In an effort to understand more about the molecular mechanism of the poxin protein, the researchers solved three crystal structures using data collected at the NE-CAT 24-ID-C beamline at the APS and at the Advanced Light Source beamline 8.2.1. They solved the structures for the unbound form, a pre-reactive form of the poxin bound to a non-hydrolyzable cGAMP analog, and a post-reactive form with natural cGAMP that showed the linear enzymatic product. The structures showed that the poxin protein forms a V-shaped homodimer in which two active sites are formed at the interface of the N-terminal protease-like domain and the C-terminal domain of opposing monomers (Fig. 1). The cGAMP lodges in a deep pocket between the N-terminus and C-terminus of the two monomers, and part of the C-terminal domain then recognizes the cGAMP substrate and forms a clamp that holds it in place while also moving into the active site the bond to be cut. The structures clearly show how the product aligns in the enzymatic pocket and how three specific amino acids perform the reaction.

These poxin genes appear to be conserved among viruses in the orthopoxvirus genus, but a search for proteins with similar structures did not identify any more distantly related poxin homologs in the structure database. To look for poxins in other organisms, the researchers utilized the Position-Specific Iterative Basic Local Alignment Search Tool, which can detect distant relationships between proteins. Interestingly, they found that insect viruses and some types of insects, including moths and

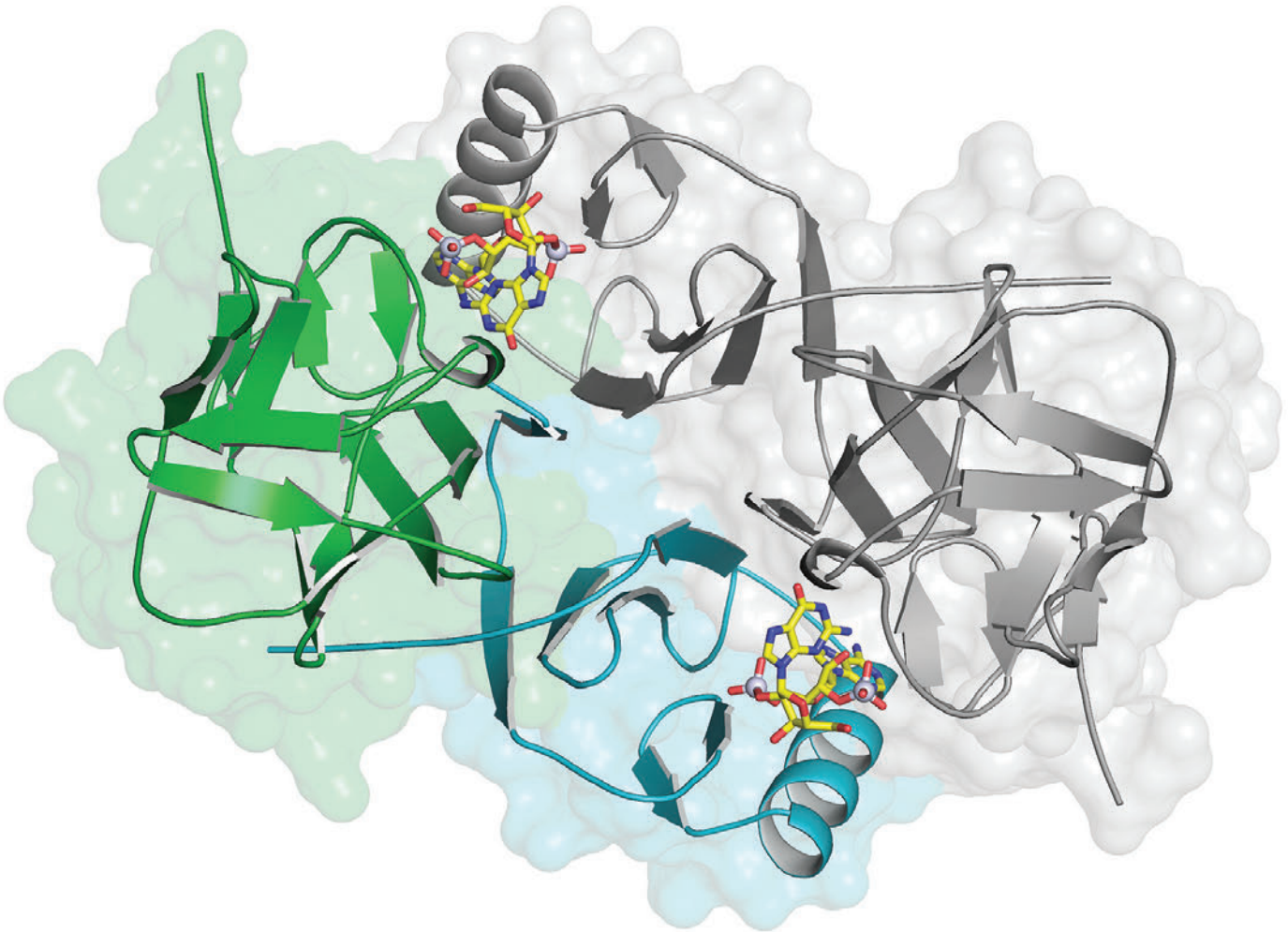

Fig. 1. Crystal structure of the VACV poxin. This protein is a homodimer with two active sites for binding cGAMP (shown in stick representation) between the N-terminal domain of one monomer (N-terminal domain in green, C-terminal domain in cyan) and the C-terminal domain of the other monomer (shown in gray).

butterflies, contain similar genes, suggesting an ancient origin for these poxin enzymes.

For the present, the team hopes their discovery will provide valuable new information that may impact the work of others who use poxviruses in a wide array of medical applications and for researchers who study the fascinating world of immune detection and evasion.

— Sandy Field

See: James B. Eaglesham[1,2,3], Youdong Pan[1], Thomas S. Kupper[1,4], and Philip J. Kranzusch[1,2,3]*, "Viral and metazoan poxins are cGAMP-specific nucleases that restrict cGAS–STING signalling," Nature **566**, 259 (14 February 2019).
DOI: 10.1038/s41586-019-0928-6
Author affiliations: [1]Harvard Medical School, [2]Dana-Farber Cancer Institute, [3]Harvard University, [4]Dana-Farber/Brigham and Women's Cancer Center
Correspondence: * philip_kranzusch@dfci.harvard.edu

The work was funded by the Claudia Adams Barr Program for Innovative Cancer Research (P.J.K.), Richard and Susan Smith Family Foundation (P.J.K.), Charles H. Hood Foundation (P.J.K.), a Cancer Research Institute CLIP grant (P.J.K.), funding from the Parker Institute for Cancer Immunotherapy (P.J.K.), National Institutes of Health (NIH) grants R01 AI127654 and R01 AR062807 (T.S.K.) and support through a NIH T32 Training grant AI007245 (J.B.E.). NE-CAT is funded by the National Institute of General Medical Sciences from the NIH (P30 GM124165). The Pilatus 6M detector on the 24-ID-C beamline is funded by a NIH-ORIP HEI grant (S10 RR029205). Use of beamline 8.2.1 of the Advanced Light Source, a U.S. Department of Energy (DOE) Office of Science User Facility under Contract No. DE-AC02-05CH11231, is supported in part by the ALS-ENABLE program funded by the National Institutes of Health, National Institute of General Medical Sciences, grant P30 GM124169-01. This research used resources of the Advanced Photon Source, a U.S. DOE Office of Science User Facility operated for the DOE Office of Science by Argonne National Laboratory under Contract No. DE-AC02-06CH11357.

Helix Cracking Represents a Novel Form of Biofilm-Formation Regulation

Bacterial signaling kinases (enzymes that add phosphate groups to other molecules) have recently been shown to engage in unexpected regulatory crosstalk. Yet the underlying molecular mechanisms remain largely unknown. Researchers at Virginia Polytechnic Institute and State University explored these mechanisms in RetS, which regulates the GacS two-component system signaling pathway of the bacterium *Pseudomonas aeruginosa*. Their crystallographic studies, carried out at two U.S. Department of Energy x-ray light sources including the APS, have uncovered structurally dynamic features within the RetS kinase region, suggesting that RetS uses the reversible unfolding of a helix, a phenomenon called "helix cracking," to regulate the biofilm-forming activities of GacS. These findings may suggest new ways to combat bacterial infections and lay a foundation for understanding an emerging form of bacterial signaling regulation.

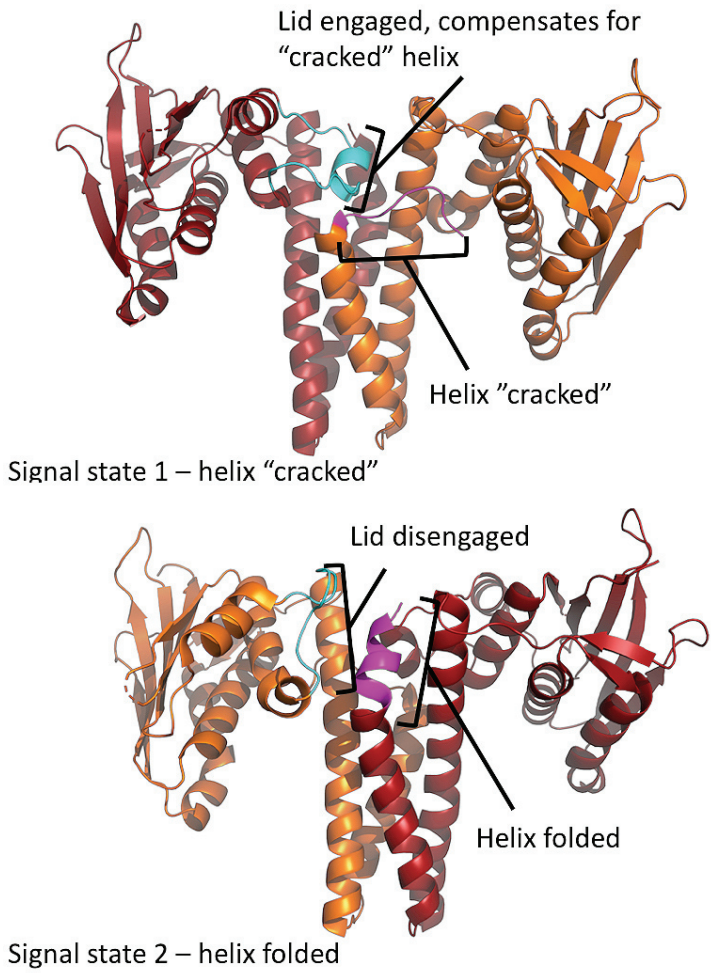

Fig. 1. In the bacterium *Pseudomonas aeruginosa*, the kinase RetS (pictured here) uses helix cracking,to regulate the biofilm-forming activities of GacS. In signal state 1 (top), the helix is cracked. To compensate for the cracking of the helix, a small loop region called the ATP lid becomes engaged. These movements are thought to cause the release of GacS to facilitate biofilm formation. In signal state 2 (bottom), the helix flips back to a folded configuration and the ATP lid disengages.

Two-component system (TCS) signaling pathways are a major signaling mechanism in bacteria and archaea (single-celled organisms) and are also found in simple eukaryota and higher plants. Bacteria use TCS pathways to monitor critical external and internal stimuli—including nutrient levels, ion and gas concentration, temperature, redox states, and cell density—and translate these signals into appropriate responses. Classical TCS pathways share a conserved core architecture: a histidine kinase (HK) protein domain (the "sensor") coupled mechanistically to a receiver domain (the "response regulator").

Pseudomonas aeruginosa is an opportunistic pathogen that causes serious acute or chronic infections in humans. Acute infections are characterized by severe cytotoxicity caused by secretion of effector proteins via a protein appendage called the Type III secretion system (T3SS). Pseudomonas aeruginosa employs more than 60 sensor kinases and uses several, including the kinases GacS and RetS, to orchestrate its adaptive responses, such as regulating the production of virulence factors involved in the development of acute or chronic infections. GacS upregulates biofilm-associated processes and downregulates mechanisms associated with acute infections. To effectively modulate these cell-wide responses, GacS signaling is inhibited by RetS and enhanced by the kinase LadS.

Previously, it had been assumed that evolution selects against such crosstalk to maintain signaling specificity. However, mounting evidence suggests that networked interactions between signaling kinases may be quite common. The GacS system constitutes an ideal model for examining unexplored mechanisms of regulation as the enzyme is subject to both positive and negative regulation by LadS and RetS, respectively. The interactions between RetS and GacS were recently shown to involve three distinct mechanisms; the least understood mechanism is nonenzymatic and involves tight, direct binding interactions between the HK regions of the two proteins. This binding inhibits GacS autophosphorylation and enhances the efficiency of the other two mechanisms.

In the present study, researchers from Virginia Polytechnic Institute and State University sought to examine the molecular basis for this nontraditional direct binding interactions between the HK regions of RetS and GacS that inhibit GacS autophosphorylation. They collected synchrotron x-ray diffraction data for crystals containing the native protein using the LRL-CAT beamline 31-ID-D at the APS; and they performed synchrotron x-ray diffraction on slightly modified RetSHK crystals using beamline 17-ID-1 (AMX) of the National Synchrotron Light Source (NSLS II) at Brookhaven National Laboratory.

The RetSHK crystal structures revealed that a structurally dynamic region within the catalytic core of RetS is critical for GacS binding and possibly plays a key role in the regulation of the interaction. Specifically, the crystal structures suggest the RetS-GacS interaction is modulated by the reversible unfolding (i.e., "helix cracking") of a short helical region in the catalytic core of RetS (Fig. 1). The equilibrium between the folded and unfolded states of this region appears to be modulated by the conformational plasticity of a loop region (called the ATP lid) in RetS, which typically mediates ATP binding in canonical HKs. These movements may cause the release of GacS to facilitate biofilm formation. This knowledge could be useful in developing methods for combating bacterial infections, but first researchers will need to identify an effective ligand of the RetS sensory domain, which is thought to control the timing for reliving the inhibition of GacS signaling through RetS

In addition, the implications of this work extend beyond the RetS/GacS system because the helix cracking occurs right next to a highly conserved catalytic residue, suggesting this model could represent a new general model for the regulation of canonical HKs. — Chris Palmer

See: Jordan M. Mancl‡, William K. Ray, Rich F. Helm, and Florian D. Schubot*, "Helix Cracking Regulates the Critical Interaction between RetS and GacS in Pseudomonas aeruginosa," Structure **27**, 785 (May 7, 2019). DOI: 10.1016/j.str.2019.02.006
Author affiliation: Virginia Polytechnic Institute and State University ‡Present address: The University of Chicago
Correspondence: * fschubot@vt.edu

This study was supported by National Institutes of Health (NIH) grant R21AI128255-01A1 to F.D.S. and R.F.H. Use of the LRL-CAT beamline was provided by Eli Lilly Company, which operates the facility. This research used resources of the NSLS II, a U.S. Department of Energy (DOE) Office of Science User Facility operated for the DOE Office of Science by Brookhaven National Laboratory under Contract No. DE-SC0012704. The Life Science Biomedical Technology Research resource is primarily supported by the NIH, National Institute of General Medical Sciences through a Biomedical Technology Research Resource P41 grant (P41GM111244), and by the DOE Office of Biological and Environmental Research (KP1605010). This research used resources of the Advanced Photon Source, a U.S. DOE Office of Science User Facility operated for the DOE Office of Science by Argonne National Laboratory under Contract DE-AC02-06CH11357.

Harnessing a Protein Activity to Treat Neurodegenerative Disease

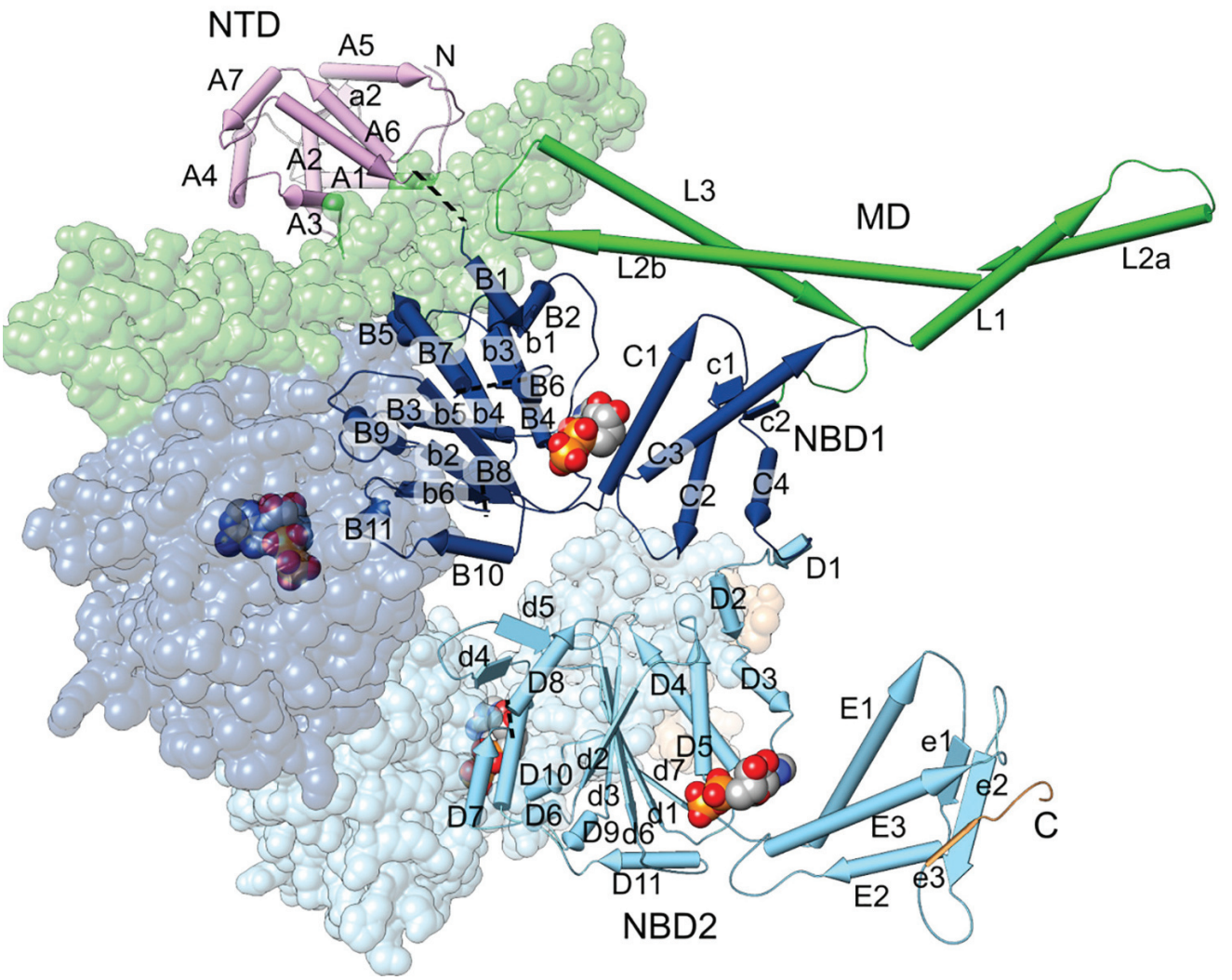

Fig. 1. The crystal structure of CtHsp104. From K. Michalska et al., Structure **27**, 449 (March 5, 2019). © 2019 Published by Elsevier Ltd.

A number of neurodegenerative disorders, including Parkinson's and Huntington's diseases, result from damage caused by neurotoxic protein aggregates. Protein disaggregases (any enzyme that breaks up protein aggregates), such as Hsp104, are able to unfold and release misfolded and aggregated proteins, thereby reducing the presence of amyloid plaques. Disagreggases are present throughout all the kingdoms of life and are thought to have evolved to have different specificities and, thus, may represent a valuable untapped resource for treating fatal neurodegenerative diseases caused by aggregation of specific proteins. In order to understand the structural basis for Hsp104 activity, researchers using the APS crystalized Hsp104 and collected x-ray diffraction data to solve its structure. The structure revealed the most complete view of Hsp104 to date and complementary analysis showed that unlike other related Hsps, Hsp104 is able to specifically degrade pathogenic misfolded proteins relevant to human disease.

In a healthy cell, proteins fold into structures that are stable and soluble in cellular conditions. During stress conditions (whether environmental or disease induced) proteins may misfold and form clumps (or aggregates) that damage the cell. In many neurodegenerative diseases, including Parkinson's disease, Huntington's disease, and spinocerebellar ataxias, these amyloid aggregates are major contributors to neuron death and disease progression. The protein deagreggase Hsp104 is an amyloid-remodeling protein present in all nonmetazoan eubacteria. Across this wide range of organisms, Hsps have a range of activities: some more efficiently remodel amyloid than others, and have different specificities in terms of the proteins they are able to act upon.

In the current study by researchers from Argonne, The University of Chicago, Stanford University, and the University of Pennsylvania, high-resolution x-ray crystallography data obtained at the SBC-XSD beamline 19-ID-D at the APS allowed the team to produce a model of Hsp104 from a fungus, *Calcarisporiella thermophilia*, to a resolution of 2.70 Å (Fig. 1). At this resolution, many details of the interactions critical for function are clear and the relative positions of structural domains within the complex are seen. The model shows a six-member, ring-like protein complex with a large channel through which aggregate protein substrate can be translocated. When compared to a cryo-EM structure, the CtHSP104 crystal structure has a higher helical rise, the domains of each hexamer are oriented differently, and the channel width is narrower. These differences likely represent the natural range of movement within this dynamic protein. This type of flexibility is important for unfolding a range of different proteins.

Importantly, the enzymatic activity of CtHsp104 is able to specifically target and efficiently degrade amyloid made from a diverse set of proteins, each of which gives rise to neurodegenerative disease (TDP-43, α-Syn, and 103Q), thereby reducing their toxicity.

This finding is particularly exciting, as it highlights the potential for evolutionarily divergent Hsps to be modified for therapeutic purposes. Understanding the differences between related Hsps may allow for future research to clarify the structural determinants of substrate specificity and enzyme efficacy, paving the way for development of treatments for neurodegenerative diseases for which there are currently no effective medications for stopping or reversing disease. — Emma Nichols

See: Karolina Michalska[1,2], Kaiming Zhang[3], Zachary M. March[4], Catherine Hatzos-Skintges[1,2], Grigore Pintilie[3], Lance Bigelow[1], Laura M. Castellano[4], Leann J. Miles[5,6], Meredith E. Jackrel[5], Edward Chuang[5,7], Robert Jedrzejczak[1,3], James Shorter[4]*, Wah Chiu[3]**, and Andrzej Joachimiak[1,2]***, "Structure of Calcarisporiella thermophila Hsp104 Disaggregase that Antagonizes Diverse Proteotoxic Misfolding Events," Structure **27**, 449 (March 5, 2019). DOI: 10.1016/j.str.2018.11.001
Author affiliations: [1]Argonne National Laboratory, [2]The University of Chicago, [3]Stanford University, [4]University of Pennsylvania
Correspondence: * jshorter@pennmedicine.upenn.edu,
** wahc@stanford.edu, *** andrzejj@anl.gov

This work was supported by National Institutes of Health (NIH) grants R01GM099836 (to J.S.), GM094585 and GM115586 (to A.J.), P41GM103832, R01GM079429, U54GM103297 and S10OD021600 (to W.C.), National Institute of Allergy and Infectious Diseases contracts HHSN272201200026C and HHSN272201700060C to the Center of Structural Genomics of Infectious Diseases (to A.J.), and NIH training grants T32GM071399 and F31NS101807 (to Z.M.M.). J.S. was also supported by a Muscular Dystrophy Association Research Award (MDA277268), the Life Extension Foundation, the Packard Center for ALS Research at Johns Hopkins University, and Target ALS. L.M.C. was supported by a National Science Foundation Graduate Research Fellowship DGE-0822. M.E.J. was supported by a Target ALS Springboard Fellowship. E.C. was supported by a Blavatnik Family Fellowship. SBC-XSD is supported by the U.S. Department of Energy (DOE) Office of Biological and Environmental Research contract DE-AC02-06CH11357. This research used resources of the Advanced Photon Source, a U.S. DOE Office of Science User Facility operated for the DOE Office of Science by Argonne National Laboratory under Contract No. DE-AC02-06CH11357.

Figuring Out How Gut Microbes Feast on Fiber

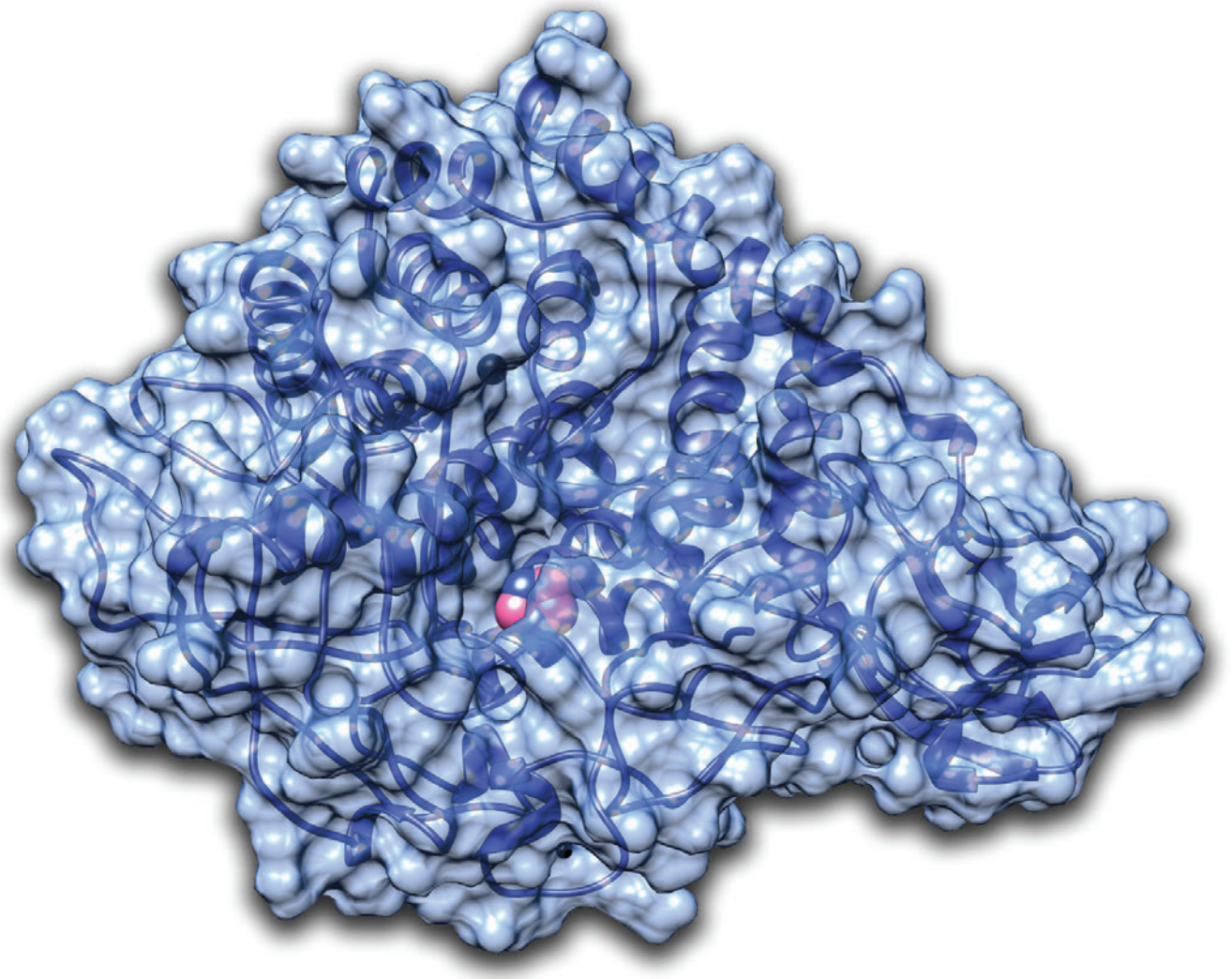

Fig. 1. A rendering of the crystal structure of the glycoside hydrolase BoGH9, solved with data collected at a LS-CAT beamline at the APS. The structure was solved with imidazole in the active site, shown in blue/pink spheres.

The human gut is host to multitudes of microorganisms, many that are critical to human health. These symbionts are believed to play a number of roles, including the breakdown of fiber molecules that human enzymes are incapable of digesting. This fiber nourishes the vast microbial community in the gut. The gut symbiont *Bacteroides ovatus*—a representative member of the Bacteroidetes phylum, ubiquitous and dominant human gut dwellers—dedicates 20% of its genome to carbohydrate catabolism. To better understand human gut health, researchers took a closer look at the carbohydrate digestion machinery in *Bacteroides ovatus*. Using data collected at the APS and at the Diamond Light Source (England), the team solved the structures of bacterial proteins involved in carbohydrate digestion. The insights from these structures, as well as biochemical analyses, may someday support the development of novel therapeutics targeted at gut microbes.

For gut bacteria to utilize carbohydrates, they must first capture the nutrients from the surrounding milieu. Bacteroidetes have multiple cell surface proteins that are on the polysaccharide hunt, identifying and harvesting the tasty molecules. These proteins are encoded within polysaccharide utilization loci (PUL), gene clusters that encode glycoside hydrolases and surface glycan-binding proteins. Glycoside hydrolases are enzymes that catalyze the hydrolysis of certain bonds in carbohydrates, while surface glycan-binding proteins play an essential role in saccharide capture at the outer membrane of bacteria. While the function many PUL proteins has been studied on an individual basis, little is known about how these proteins work together to coordinate carbohydrate capture and uptake.

To gain insight into the interplay between PUL proteins, researchers from the University of Michigan Medical School, the University of British Columbia (Canada), and the University of York (UK) focused on a few players from a specific PUL: the xyloglucan utilization locus (XyGUL) from *Bacteroides ovatus*. Xyloglucans are polysaccharides that are prominent in the cell walls of some beloved fruits and vegetables, including tomatoes, lettuce, and peppers. About 92% of human microbiomes contain homologues to XyGUL, underscoring the importance of xyloglucans to the diet of gut microbes. The XyGUL has 12 genes, each with a role in the capture, import, and degradation of xyloglucans, and scientists have characterized most of these players, creating a useful model system for the study of carbohydrate catabolism in gut microbes. This research team focused on the interactions between three members of the XyGUL: a glycoside hydrolase called "BoGH9," which can perform the initial cleavage of the xyloglucan backbone, and two xyloglucan-specific surface glycan-binding proteins, SGBP-A and SGBP-B.

The researchers teased out some key features for how these proteins work together and independently to metabolize xyloglucan. For example, BoGH9 in isolation shows weak reactivity with xyloglucans, yet is required in a strain of bacteria that expresses a non-binding version of SGBP-A. Insights were gained from the crystal structure of BoGH9 (Fig. 1), solved with data collected at the LS-CAT 21-ID-F x-ray beamline at the APS, such as why BoGH9 is highly active against a mixed-linkage beta glucan compared to xyloglucan. In other studies at the Diamond Light Source, crystals of the GH9-MR protein were imaged.

Overall, the data supports that the transport of xyloglucan is dependent on SGBP-A binding xyloglucan, but that this transport is also dependent on BoGH9 and SGBP-A. This suggests that a multiprotein complex forms at the cell surface to facilitate and modulate carbohydrate capture. — Erika Gebel Berg

See: Matthew H. Foley[1], Guillaume Déjean[2], Glyn R. Hemsworth[3], Gideon J. Davies[3], Harry Brumer[2], and Nicole M. Koropatkin[1]*, "A Cell-Surface GH9 Endo-Glucanase Coordinates with Surface Glycan-Binding Proteins to Mediate Xyloglucan Uptake in the Gut Symbiont *Bacteroides ovatus*," J. Mol. Biol. **431**, 981 (2019). DOI: 10.1016/j.jmb.2019.01.008
Author affiliations: [1]University of Michigan Medical School, [2]University of British Columbia, [3]University of York
Correspondence: * nkoropat@umich.edu

M.H.F. was partially supported by a predoctoral fellowship from the Cellular Biotechnology Training Program (T32GM008353). G.J.D. is funded by the Royal Society through the Royal Society Ken Murray Professorship. G.J.D. and G.R.H. were supported by the Biotechnology and Biological Sciences Research Council (Grants BB/L021633/1 and BB/I014802/1). Use of LS-CAT was supported by the Michigan Economic Development Corporation and the Michigan Technology Tri-Corridor (Grant 085P1000817). This research used resources of the Advanced Photon Source, a U.S. Department of Energy (DOE) Office of Science User Facility operated for the DOE Office of Science by Argonne National Laboratory under Contract No. DE-AC02-06CH11357.

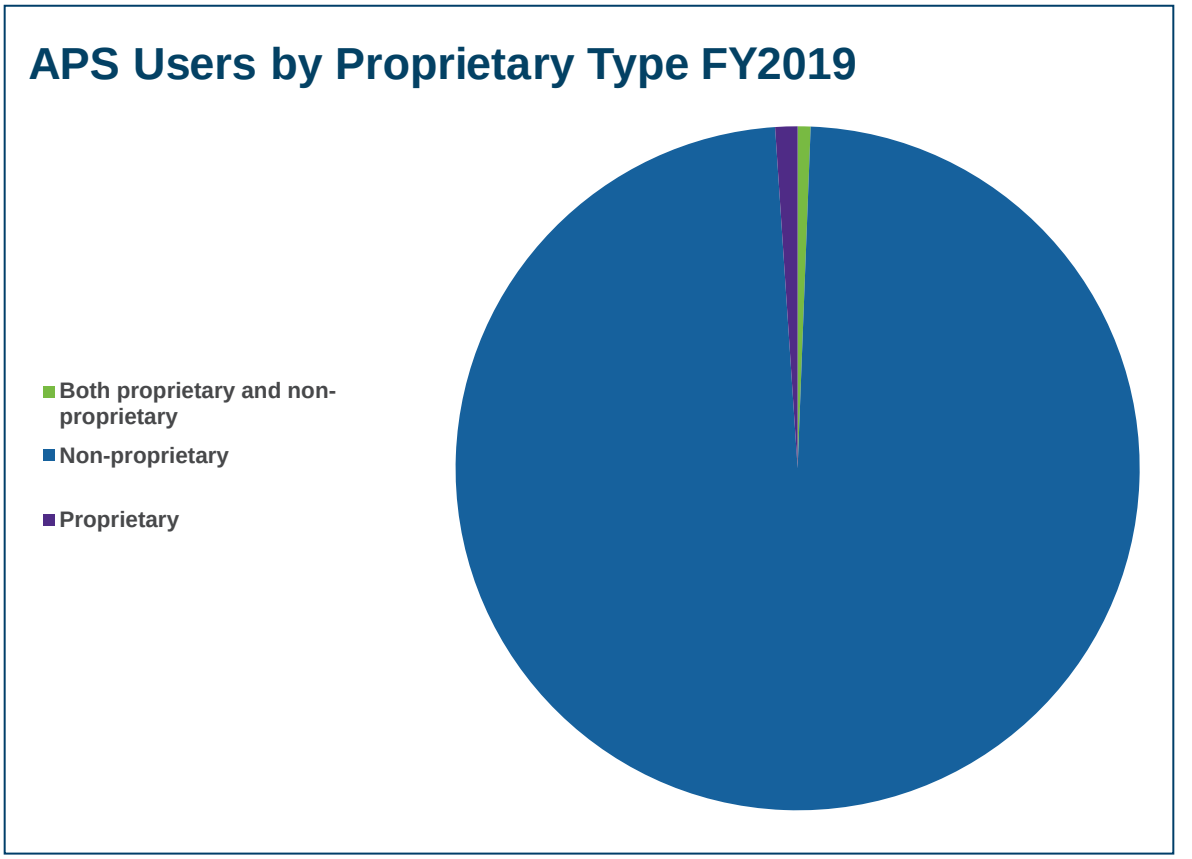
APS Users by Proprietary Type FY2019
Both proprietary and non-proprietary
Non-proprietary
Proprietary

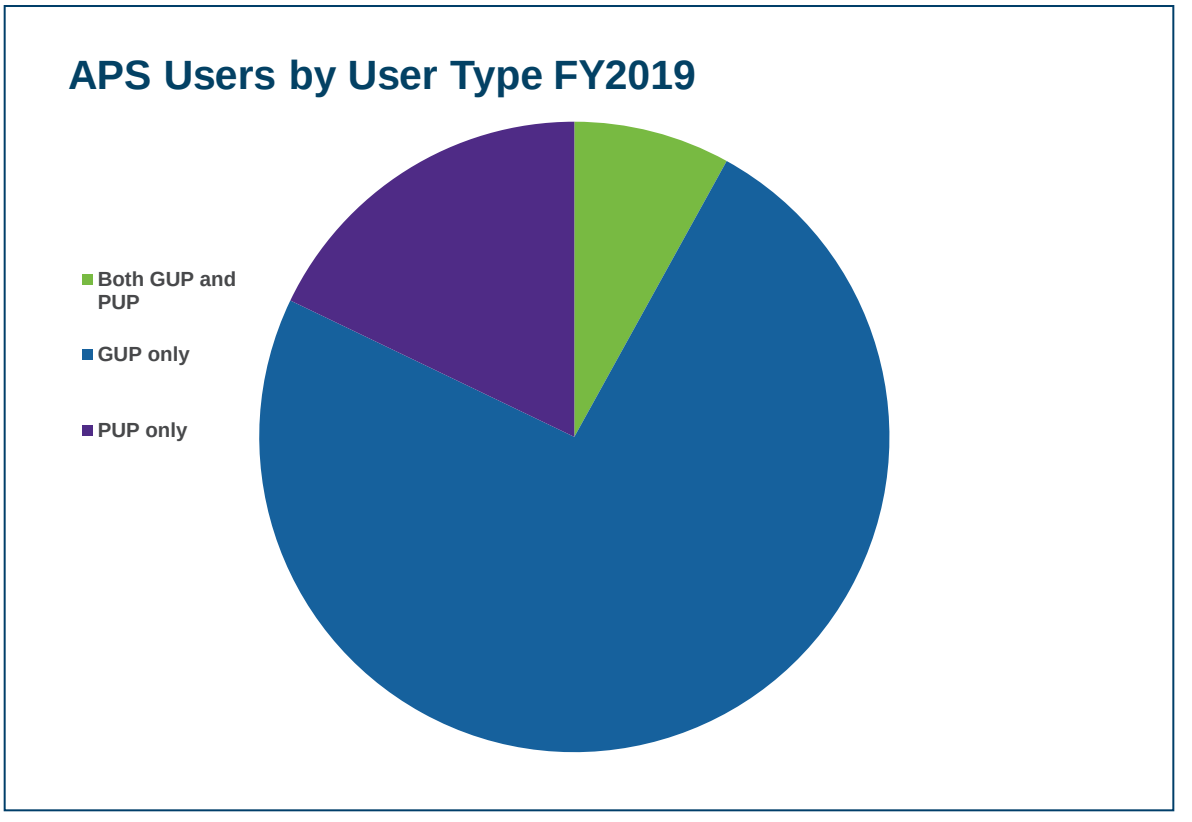
APS Users by User Type FY2019
Both GUP and PUP
GUP only
PUP only

Environmental, Geological, and Planetary Science

Brittle Failure Linked to Eclogitization of the Lower Continental Crust

Understanding the changes in chemical and mechanical states deep within the Earth requires information from field observations, geophysical data, and laboratory experiments. Experimental studies predict that granulite rocks with specific characteristics at lower continental crustal conditions deform plastically. By contrast, field observations on Norwegian granulites reveal that eclogitization (the breakdown of plagioclase in the presence of a hydrous fluid) produces brittle seismic failure in the metastable lower continental crust, where seismicity, fluid infiltration, and eclogitization are strongly coupled. To understand the rheology of the lower continental crust, researchers using the APS monitored acoustic emissions taken during experimental deformation of plagioclase-rich samples under eclogite-facies conditions. When eclogitization was fast relative to the imposed strain rate, deformation was ductile. When eclogitization was slow, deformation was accompanied by high acoustic-emission activity—a proxy for brittle deformation (Fig. 1). In nature, these transformations can bring about earthquakes.

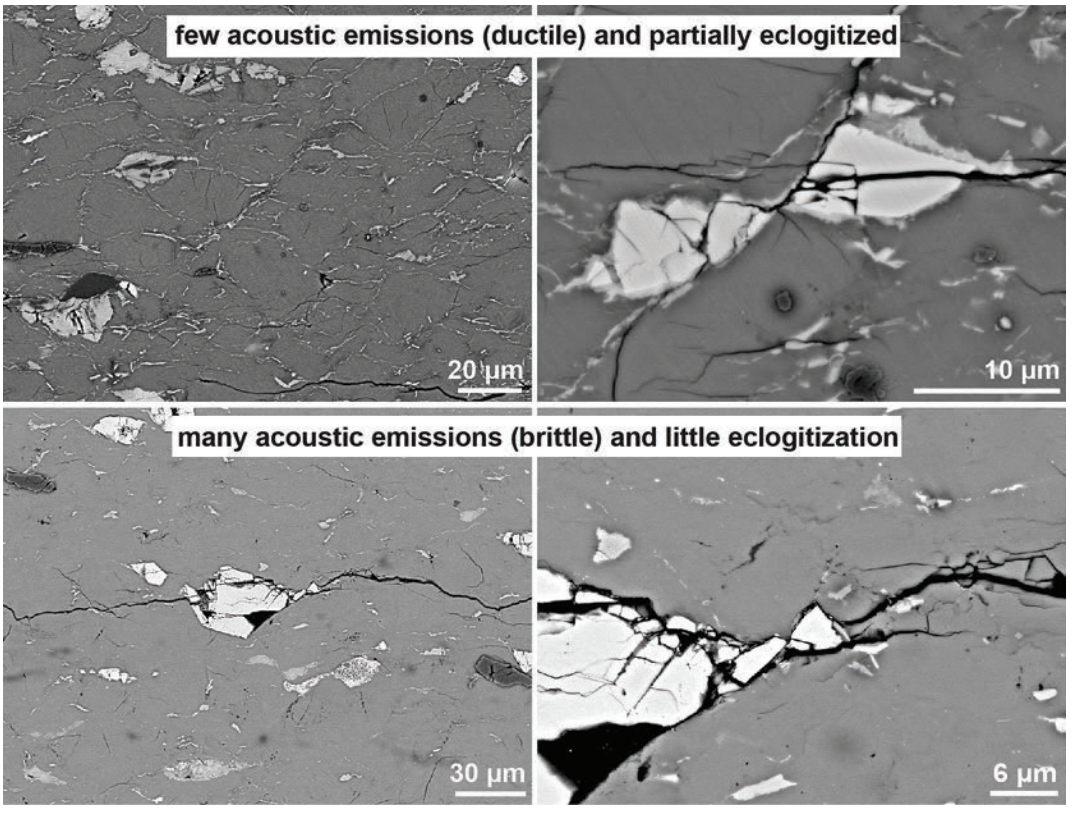

Fig. 1. Ductile and brittle rheologies seen in granulite microstructures from Norway.

This work by researchers from the University of Oslo (Norway), the PSL Research University (France), the Sorbonne Université (France), Université Lille (France), Freie Universität Berlin (Germany), The University of Chicago, and Université Grenoble Alpes and Université Savoie Mont Blanc (France) shows the results of experimental deformation in four plagioclase-rich samples in the presence of a hydrous fluid. It uses acoustic emissions to link changes in rock rheology, seen in Norwegian granulite samples during metamorphism, with the kinetics of eclogitization reactions. The deformation experiments used the D-DIA apparatus to study acoustic emissions, a deformation multi-anvil press at the GSECARS beamline 13-BM-D of the APS. To monitor the strain and differential stress of the samples at eclogite-facies pressure-temperature conditions outside the plagioclase stability field, the researchers ran synchrotron x-ray radiographs every five minutes, as well as powder diffraction patterns.

The acoustic emissions revealed different mechanical behaviors. Low acoustic emissions signified that deformation was ductile. This occurred under two sets of conditions: when there was no reaction and when net eclogitization was fast compared to the imposed strain rate. High acoustic emissions meant that deformation was brittle. This occurred when eclogitization reaction rates were slow. In this instance, plagioclase broke down into partially eclogitized nanocrystalline reaction products.

After the experiments, each sample exhibited two main microstructural features—bright bands and dark areas—that originated at the onset of eclogitization. Dark areas in the plagioclase matrix indicated higher sodium and lower calcium, mineral compositions closer to albite or jadeite. Bright bands adjacent to the plagioclase matrix came from plagioclase breakdown. Zoisite was the first of these crystals to nucleate and grow. Kyanite and quartz only appeared in the sample that had undergone the most eclogitization.

The minerals that are present after eclogitization occupy a small volume fraction of the samples, are strain free, and are nano-crystalline. The growth of strain-free nano-crystalline material causes a local decrease in strength and the negative volume change, which concentrates stress at the tips of the transformed regions, leading to brittle failure. The materials at micro and nanometer scales contain eclogite bands filled with crystals that are oriented to enable sliding during further deformation. These features generate self-localizing transform faults. In nature, eclogitization takes place at lower strain rates and temperatures; the rheological behavior of the sample is controlled by soft eclogite. In rocks located in Holsnøy, Norway, weak and deformed eclogite is found within unreacted and undeformed strong granulite blocks.

If the observed embrittlement is controlled by plagioclase breakdown relative to the imposed strain rate, researchers can scale their lab conditions to match those of natural systems. In the lab, eclogitic reactions reduce grain-size and a negative change in volume causes the sample to release heat and further enhances the brittle behavior. The researchers conclude that this is the same mechanism that causes embrittlement in the lower crust, or even in the intermediate or deep mantle, as long as fluids are present. — Dana Desonie

See: Sarah Incel[1,2]*, Loïc Labrousse[3], Nadège Hilairet[4], Timm John[5], Julien Gasc[2], Feng Shi[6], Yanbin Wang[6], Torgeir B. Andersen[1], François Renard[1,7], Bjørn Jamtveit[1], and Alexandre Schubnel[2], "Reaction-induced embrittlement of the lower continental crust," Geology **47**, 235 (29 January 2019).
DOI: 10.1130/G45527.1
Author affiliations: [1]University of Oslo, [2]PSL Research University, [3]Sorbonne Université, [4]Université Lille, [5]Freie Universität Berlin, [6]University of Chicago, [7]Université Grenoble Alpes, Université Savoie Mont Blanc
Correspondence: * s.h.m.incel@geo.uio.no

The study received funding from the Alexander von Humboldt-Foundation (Feodor Lynen Research Fellowship to S. Incel). Further funding came from the People Program (Marie Curie Actions) of the European Union's Seventh Framework Program FP7/2017–2013/and Horizon 2020 under REA grant agreements 604713 (to Schubnel) and 669972 (to Jamtveit), National Research Foundation Centre of Excellence grant 223272 (to Andersen), and National Science Foundation grant EAR-1661489 for the development of acoustic emission experiments (to Wang). GSECARS is supported by the National Science Foundation-Earth Sciences (EAR-1634415) and Department of Energy (DOE)-Geo-Sciences (DE-FG02-94ER14466). This research used resources of the Advanced Photon Source, a U.S. DOE Office of Science User Facility operated for the DOE Office of Science by Argonne National Laboratory under Contract No. DE-AC02-06CH11357.

Peeling Back Details about Strontium-Bearing Barite Using Organic Films

The formation of the mineral barite is essential to the global cycles of organic carbon, sulfate, and oxygen. Incorporation of the Earth metal strontium (Sr) into marine barite may accurately reflect oceanic conditions as well as the evolution of geochemical environments. But two unresolved paradoxes have existed regarding barite. Although the seawater column and marine sediments harbor extensive amounts of this mineral, the global oceans exhibit a comparative undersaturation of barite. In addition, the widespread presence of Sr-rich barite is enigmatic because the incorporation of strontium into this mineral is thermodynamically unfavorable. Now, research carried out at the APS has resolved both of these paradoxes. Using *in situ* grazing incidence small-angle x-ray scattering (GISAXS), a research team discovered that organic films increase ion supersaturation and promote the formation of strontium-rich barite. These findings have important implications for biomineralization processes, industrial strontium removal, and local paleoenvironments.

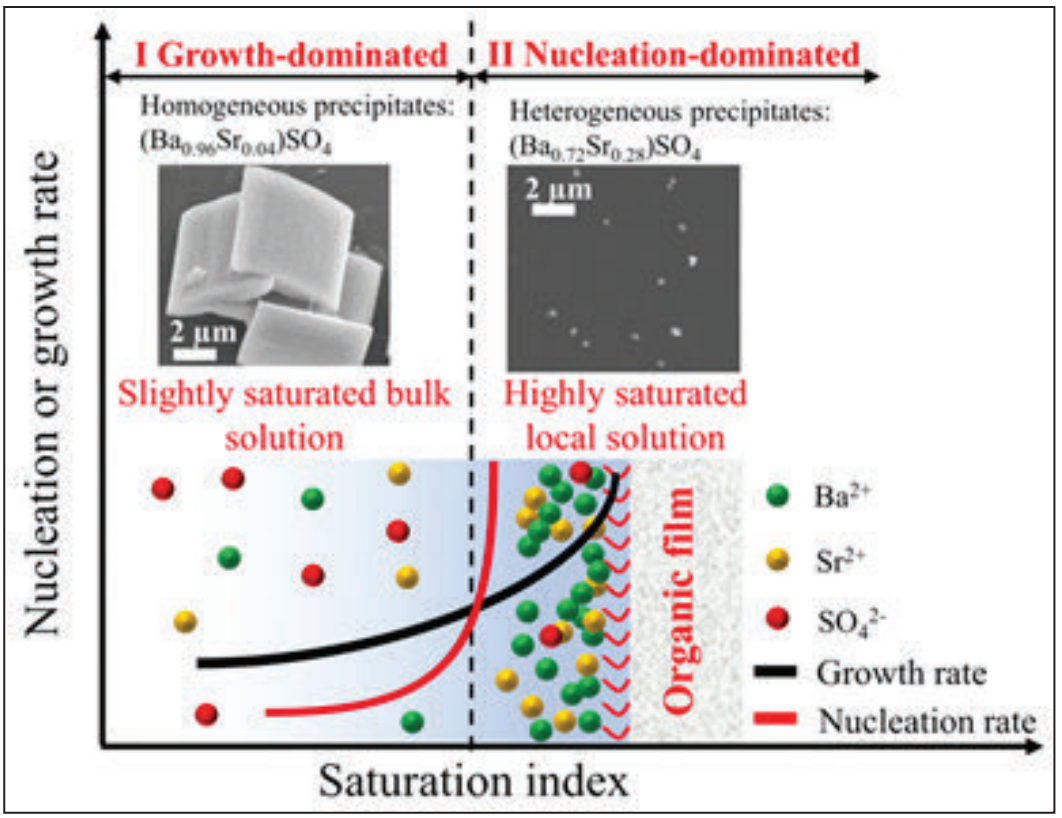

Fig. 1. Schematic displaying cation enrichment at organic-water interfaces and the correlations of nucleation (red line) and growth (black line) rates with saturation indicies.

This study, performed by scientists from the University of Houston, tOak Ridge National Laboratory, Pacific Northwest National Laboratory, and the University of Washington investigated two major, existing paradoxes regarding the mineral barite. The first of these paradoxes has to do with the distribution and concentration of barite. While the global oceans show an overall under-saturation of barite, this mineral is respectively oversaturated in marine sediments, which are comprised of insoluble materials that accumulate on the ocean floor. Barite is also over-represented in certain seawater columns, which represent a volume of water (i.e., from the water's surface to the bottom sediment) of a given area. The precise mystery is why barite exhibits a unique, oceanic localization.

The second paradox involves thermodynamic favorability. Compared to barite alone, which consists of barium sulfate ($BaSO_4$), the solubility of strontium sulfate ($SrSO_4$) is 3 orders of magnitude higher, meaning that the incorporation of strontium into barite is not thermodynamically favorable and is something that is energetically discouraged. Therefore, the existence of strontium-rich barite suggests that a separate variable is promoting its formation.

To resolve these paradoxes, the authors first utilized the advanced x-ray scattering technique GISAXS at a high-energy synchrotron. This technique, which allows for nanoscopic measurements of *in situ* nanoparticle nucleation and growth on organic films in solution, was performed at the XSD beamline 12-ID-B of the APS. Measurements were performed under different conditions where the saturation of ions (i.e., barium and strontium) was varied and an organic film substrate was either present or absent. Figure 1 displays the cation enrichment at organic-water interfaces and the correlations of nucleation and growth rates.

In Stage I, under slightly supersaturated bulk solutions, precipitation was growth-dominated and therefore barite precipitated in bulk solution (SEM image, left inset) grew quickly to micrometer-sized, Sr-poor crystals. Stage II indicates a nucleation-dominated precipitation process at a highly supersaturated solution, which was achieved near the organic-water interfaces due to significant cation enrichment. The right inset image displays results from *ex situ* scanning transmission electron microscopy coupled with energy-dispersive x-ray spectroscopy, and shows nanometer-sized, Sr-rich heterogeneous precipitates formed on organic films.

It was discovered that organic films (i.e., films either containing living matter or materials derived from living matter) promote an enrichment of both barium and strontium ions around organic-water interfaces. This leads to a saturation of these ions and ultimately to the creation of strontium-barite. Hence, strontium-rich barite is generated via the help of organic films. Conversely, strontium-poor barite is generated in bulk solutions. Strontium-rich barites formed on organic films were found to be controlled by a nucleation-dominant process overgrowth compared to strontium-poor barites formed in bulk solution.

These data are impactful for four significant reasons. First and foremost, they resolve both of the previously unsolved paradoxes regarding strontium and barite. Despite it being thermodynamically undesirable, the uptake of strontium into barite occurs due to the help of organic films. The influence of organics also helps to explain why strontium barite is more concentrated in certain regions such as organic-rich marine sediments, but not in others.

Secondly, the mechanism by which strontium is incorporated into barite and the rate of this incorporation allows for insights into local paleoenvironments. More specifically, the percentage of strontium present in barite could theoretically serve as a signature for a particular oceanographic era.

The third reason is relevant to industrial processes that utilize strontium. The finding that the enrichment of strontium in barite is enhanced by organic films allows for potential novel strategies aimed at strontium removal.

A fourth reason is that the elucidated role of organic films increases our understanding of biomineralization processes and suggests a broader, larger role of organics in mineral formation.

More generally, this study also demonstrates the utility of GISAXS and how this powerful synchrotron x-ray research technique can be used to solve complex scientific questions. — Alicia Surrao

See: Ning Deng[1], Andrew G. Stack[2], Juliane Weber[2], Bo Cao[1], James J. De Yoreo[3,4], and Yandi Hu[1]*, "Organic–mineral interfacial chemistry drives heterogeneous nucleation of Sr-rich $(Ba_x,Sr_{1-x})SO_4$ from undersaturated solution," Proc. Natl. Acad. Sci. U.S.A. **116**(27), 13221 (July 2, 2019).
DOI: 10.1073/pnas.1821065116
Author affiliations: [1]University of Houston, [2]Oak Ridge National Laboratory, [3]Pacific Northwest National Laboratory, [4]University of Washington
Correspondence: * yhu12@Central.UH.EDU

This work supported by the U.S. Department of Energy (DOE) Office of Science-Basic Energy Sciences, Chemical Sciences, Geosciences, and Biosciences Division. STEM/EDX characterization was conducted at the Center for Nanophase Materials, a U.S. DOE user facility. This research used resources of the Advanced Photon Source, a U.S. DOE Office of Science User Facility operated for the DOE Office of Science by Argonne National Laboratory under Contract No. DE-AC02-06CH11357.

How Magnetite Does Its Trick

The interactions between groundwater and minerals in the soil control many things, from whether radioactive waste spills can contaminate drinking water to how fast creatures at the base of the food chain can grow. Magnetite, an iron oxide, is a common mineral that plays an important role in these interactions. It acts as a geochemical battery, donating and accepting electrons in response to environmental conditions. But exactly how magnetite does this is not well-understood. Researchers used the APS to reveal how a tiny particle of magnetite accepts and expels an oxygen atom and its accompanying electrons, and the resulting strains that develop in the particle. Their findings illuminate both the inner working of magnetite as a geochemical battery, and how these reactions may contribute to how the rocks we see every day weather and break down.

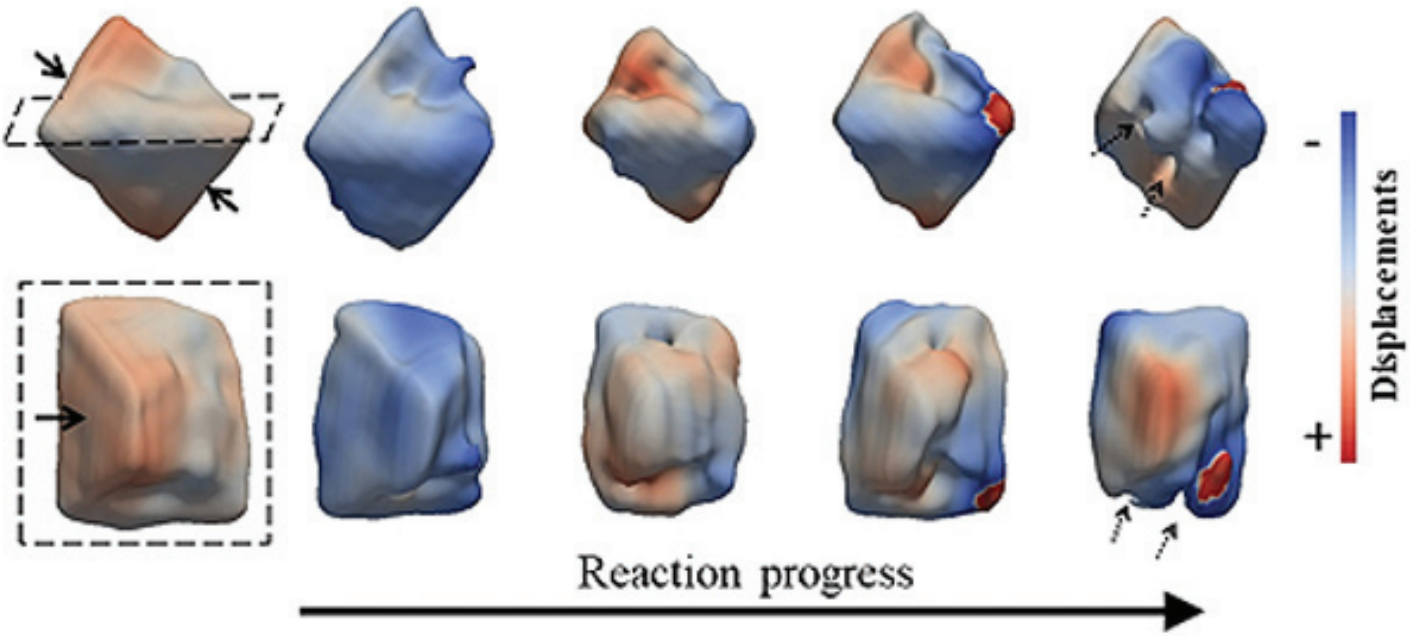

Fig. 1. Two views of the same particle of magnetite. The upper row shows the particle from the side; the lower row shows a top down view. The far left shows the pristine particle; it strains and suffers spatially variable displacements as the oxidation reaction progresses (successive images to the right.)

When it comes to rocks, size and shape matter a great deal—and we're not talking just boulders and pebbles. Size and shape matter even at the level of particles a few hundred nanometers in size interacting with water molecules. Researchers from Argonne, the University of Delaware, and Sogang University (Korea) were interested in how adding or subtracting an oxygen atom introduces strain or relaxation inside a magnetite particle. Called oxidation when oxygen is added, and reduction when oxygen is subtracted, it's a common chemical reaction essential to life and happens in the mineral magnetite all over our planet, in many different geologies and environments.

The standard understanding of oxidation/reduction in magnetite particles describes it as starting at the surface of a particle. Once the whole surface is oxidized, the reaction happens in the next layer down, creating a shell of oxidized material around an unreacted mineral core.

The researchers used the XSD beamline 34-ID-C at the APS to check if that scenario was true. The beamline's instrumentation is some of the best in the world for illuminating individual particles. It can shape the powerful x-rays into a fine beam of coherent light that stays perfectly fixed on the particle as it rotates during the measurement (not an easy task). Coherent x-ray light, which is x-rays with a fixed phase relationship with each other, allowed the researchers to resolve very fine details in the structure

across a single particle of magnetite, rather than just the average structure of all particles.

To see how the particle changed with oxidization, the team employed Bragg coherent diffraction imaging technique which is a powerful tool enabling the researchers to look at fine structure inside the sample. First, they collected coherent x-ray diffraction patterns on the pristine particle. After oxidizing the particle in an acid bath for a period of time, they measured the coherent diffraction patterns again, repeating the cycle several times. They analyzed these data to create images of the same particle as the oxidation reaction took place so they could view how the particle's shape and structure evolved.

What they saw was strain build-up within the particle. The reaction didn't take place just at the surface; strain and crystal defects began building up in the interior of the particle as well as the exterior. In effect, the particle was stretching in some places, compressing in other places, and eventually breaking bonds in the form of a dislocation (Fig. 1.) That shows that the idea of concentric shells of reaction that gradually take up more and more of the body of the particle is inaccurate. That is, even though the reaction might occur on the particle surface, it has ramifications throughout the particle that lead to strain and structural changes.

The next steps in this research will look at how the size and shape of minerals influence a wide array of geochemical reactions. The researchers are particularly excited about the planned upgrade to the APS, which will increase the flux and intensity of coherent x-rays and make it possible to watch how chemical reactions take place in real time. — Kim Krieger

See: Ke Yuan[1]*, Sang Soo Lee[1], Wonsuk Cha[1], Andrew Ulvestad[1], Hyunjung Kim[2], Bektur Abdilla[3], Neil C. Sturchio[3], and Paul Fenter[1]**, "Oxidation induced strain and defects in magnetite crystals," Nat. Commun. **10**, 703 (2019).
DOI: 1038/s41467-019-08470-0
Author affiliations: [1]Argonne National Laboratory, [2]Sogang University, [3]University of Delaware
Correspondence: * keyuan@umich.edu, ** fenter@anl.gov

This work was supported by the U.S. Department of Energy (DOE) Office of Science-Basic Energy Sciences, Chemical Sciences, Geosciences, and Biosciences Division under Contract DE-AC02-06CH11357 to UChicago Argonne, LLC, operator of Argonne National Laboratory. Use of the Center for Nanoscale Materials, an Office of Science user facility, was supported by the U.S. DOE Office of Science-Basic Energy Sciences, under Contract no. DE-AC02-06CH11357. H.K. thanks the support by the National Research Foundation of Korea (NRF-2014R1A2A1A10052454 and 2015R1A5A1009962). This research used resources of the Advanced Photon Source, a U.S. DOE Office of Science User Facility operated for the DOE Office of Science by Argonne National Laboratory under Contract No. DE-AC02-06CH11357.

More about Magnetite

From trade routes to conquest, the pageant of human history would have been very different without the magnetic properties of magnetite (below), a nondescript black mineral. Many people assume that magnetite's name is derived from its magnetic properties, but the term magnet actually comes from the mineral. Magnetite was named after the Magnesia region of Thessaly, Greece, the home of the Magnetes and an important center of iron production. The historical importance of this region's mineral deposits is reflected by two elements, magnesium and manganese, which were also named for this region.

One of only a few naturally occurring magnetic materials, magnetite fascinated early civilizations and set many on a path toward the modern compass.

Consequently, open-sea navigation, commerce, and warfare are to a great degree part of magnetite's legacy. A relatively common metallic mineral, magnetite is also one of modern society's most important iron ores. In our modern Earth, magnetite seldom forms in sedimentary environments. Back in the Early Proterozoic (2.5 to 1.6 billion years ago) large deposits of magnetite precipitated directly from seawater, as it was a time when the world's oceans and atmosphere had not yet become as oxygen-rich as they now are.

Magnetite is opaque and leaves a black streak when rubbed across a hard, rough surface. It is one of the most abundant metal oxides, and its crystal structure contains both the ferrous (Fe^{2+}) and ferric (Fe^{3+}) forms of iron ions. A complex pattern of electrons between the two forms of iron is the source of its magnetic nature. Although other metallic minerals may mimic magnetite's color, luster, hardness and specific gravity, magnetite is the only common mineral that is magnetic.

Magnetite crystals usually only occur when magma cools slowly enough for crystals to form and settle out of the magma. These crystals are typically octahedrons to dodecahedrons (8-sided to 12-sided shapes) that may exhibit fine lines (known as "striations") on some surfaces. More often, magnetite occurs in its massive form, commonly called "lodestone." This variety has a much more pronounced magnetic character, and large deposits of massive magnetite can play havoc with compasses. Lodestone's magnetic attraction, however, is never strong enough to pull nails from ships as early sailing tales claimed!

Source: Department of Geology at the University of Minnesota, www.esci.umn.edu/courses/1001/minerals/magnetite.shtml. Image: Ra'ike, https://bit.ly/2ZIU433

Uncovering the Interfacial Behavior of Hematite Far from Equilibrium

Iron oxides and oxyhydroxides come in dozens of distinct varieties and are involved in many biological, geological, and technological processes. They serve as the sources of catalytic activity for a variety of enzymes and assist micro-organisms in producing methane from decomposing organic matter. They further serve to bind and sequester a variety of toxic and heavy metals. While these processes have existed since the dawn of time, humans have recently found uses for their properties in everything from cosmetics to biological sensing to drug delivery. But, given how recent these applications are, it follows that many of the reaction pathways involving iron oxides are not fully understood. Of particular interest is the working of hematite, Fe_2O_3, an iron oxide mineral commonly found in rocks and ores around the world—even in rocks on Mars. In hematite, the flux of Fe^{2+}/Fe^{3+} between aqueous ions and hematite crystals have been studied extensively but within a relatively narrow window of environmental conditions. Researchers aimed to crack this window open a bit further by using the APS to study the exchange between Fe^{2+}/Fe^{3+} on hematite surfaces at low pH, a condition that will more closely imitate what might occur in some natural and technological settings. The details that they uncovered shed light on the Fe^{2+}/Fe^{3+} redox cycle and provide a better understanding of the complex geochemical behaviors of iron (oxyhydr)oxides.

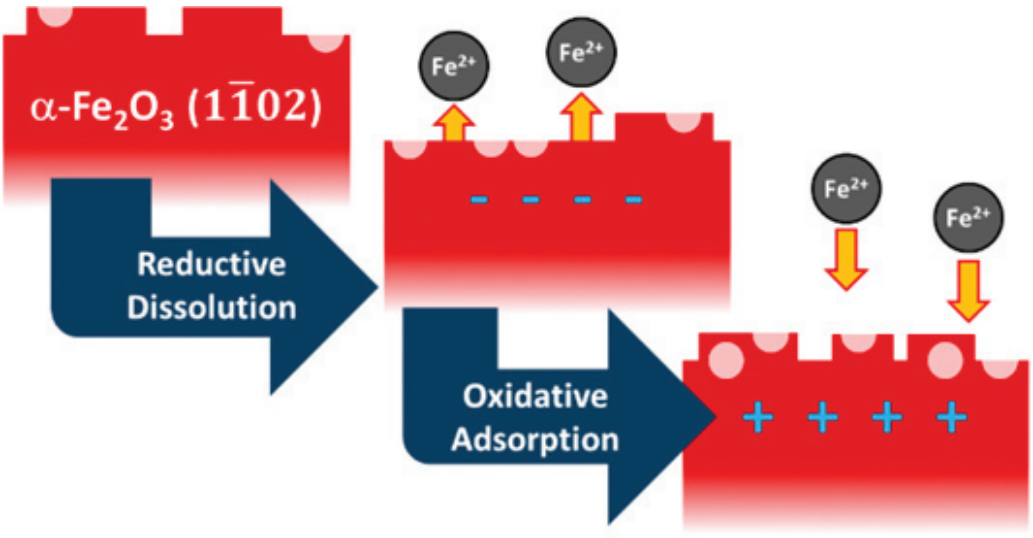

Fig. 1. Atomic-scale illustration of iron oxide surfaces under fluctuating electrochemical conditions showing the dissolution and reprecipitation of Fe as cathodic bias is applied and removed. Figures from M.E. McBriarty et al., J. Phys. Chem, C **123**, 8077 (2019). Copyright © 2019 American Chemical Society

A naturally-conductive hematite crystal from Brazil was cut to a uniform shape and the surface cleaned and polished to prevent any unwanted interactions from contaminants. Crystal truncation rod analysis (CTR) was used to resolve the crystal-solution interface, so that coordinated and free iron could be distinguished and monitored. CTR is a surface-sensitive diffraction technique. By using a computer program to fit an atomic-scale structure model to the data, scientists can determine the locations of atoms at crystal surfaces and interfaces with exquisite precision. The researchers, from the Pacific Northwest National Laboratory and colleagues from The University of Chicago, were also able to apply varying electric potentials across the crystal surface using a novel electrochemical cell. These interface-sensitive x-ray scattering experiments were conducted at the GSECARS beamline 13-ID-C at the APS.

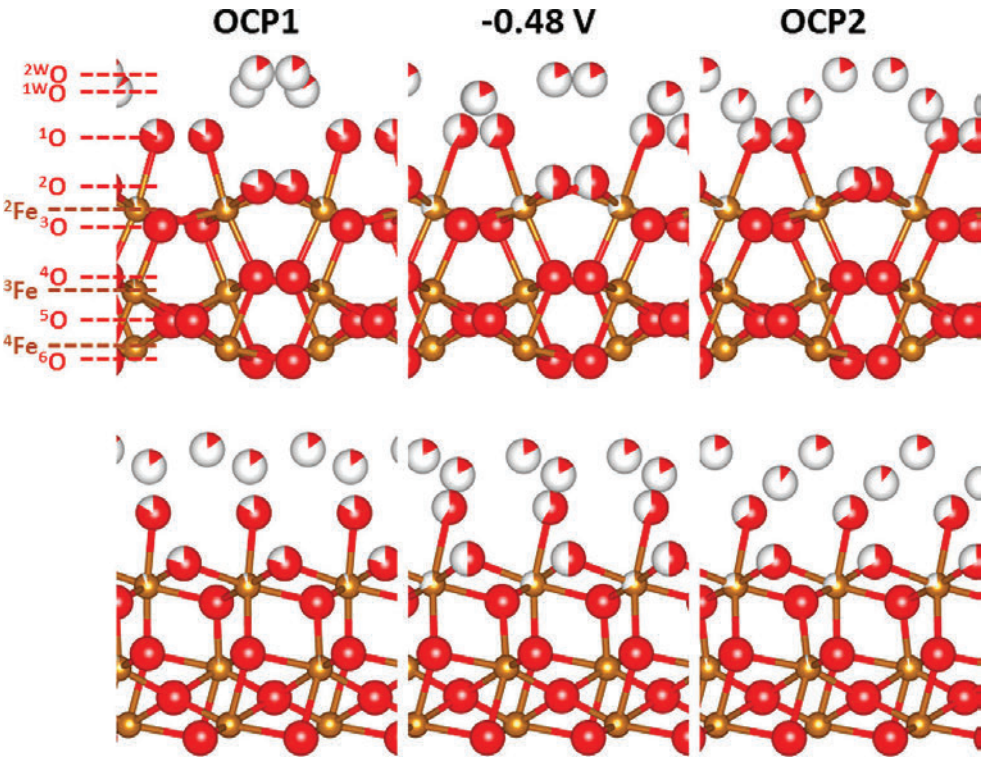

Fig. 2. Ball-and-stick models of interface structures from CTR fits. Larger red balls represent oxygen (O); smaller gold balls represent iron (Fe). The shaded fraction of each ball represents the fractional occupancy of the site. No hydrogen (H) atoms are included because CTR measurements are insensitive to H positions. Each column corresponds to one electrochemical state. The top (bottom) row is viewed along the b (a) axis of the orthorhombic surface unit cell.

The researchers' CTR experiments confirmed that a noticeable change on the surface of the hematite occurs when the pH is shifted downward and potential is applied (Fig. 2). When the surface electric potential was adjusted toward a cathodic bias, high energy interfacial atoms dissolve, producing a surface similar to the one formed by annealing at high temperatures in air, resulting in a very smooth crystal surface. Turning off the bias resulted in disordered reprecipitation of iron. This partial re-adsorption of atoms onto the crystal surface appeared to increase the roughness of the surface. Figure 1 displays the researchers' proposed mechanism for iron oxide surfaces under fluctuating electrochemical conditions. The illustration shows the dissolution and reprecipitation of iron as cathodic bias is applied and removed.

In summary, this research team successfully made atomic-scale, *in situ* observations of the unique mineral-electrolyte interfaces of hematite at conditions far from equilibrium, which can be quite different from those that take place at equilibrium. The CTR experiments enhanced the researchers' molecular-scale view of the structures at the electrode-electrolyte interfaces. This suite of experiments serves as a compelling case study in how CTR measurements can complement and confirm the highly detailed structural and chemical data offered by molecular dynamics simulations. — Alicia Surrao

See: Martin E. McBriarty[1‡], Joanne E. Stubbs[2], Peter J. Eng[2], and Kevin M. Rosso[1*], "Reductive Dissolution Mechanisms at the Hematite-Electrolyte Interface Probed by *In Situ* X-ray Scattering," J. Phys. Chem. C **123**, 8077 (2019).
DOI: 10.1021/acs.jpcc.8b07413
Author affiliations: [1]Pacific Northwest National Laboratory [2]The University of Chicago [‡]Present address: Intermolecular, Inc.
Correspondence: * kevin.rosso@pnnl.gov

This material is based upon work supported by the U.S. Department of Energy (DOE) Office of Science-Basic Energy Sciences, Chemical Sciences, Geosciences, and Biosciences Division through its Geosciences program at Pacific Northwest National Laboratory (PNNL). PNNL is a multiprogram national laboratory operated by Battelle Memorial Institute under Contract No. DE-AC05-76RL01830 for the U.S. DOE. The research was performed in part using the Cascade supercomputer at the Environmental and Molecular Sciences Laboratory, a DOE Office of Science User Facility sponsored by the Office of Biological and Environmental Research. GeoSoilEnviroCARS is supported by the National Science Foundation–Earth Sciences (Grant EAR-1634415) and DOE–Geosciences (Grant DE-FG02-94ER14466). This research used resources of the Advanced Photon Source, a U.S. Department of Energy (DOE) Office of Science User Facility operated for the DOE Office of Science by Argonne National Laboratory under Contract No. DE-AC02-06CH11357.

How Biochar Sorbs and Reduces Chromium

Biochar, created by partially burning organic waste to turn it into a charcoal-like material, is widely used as a soil amendment. Among its properties is the ability to sequester pollutants such as mercury, selenium, and chromium. Using a combination of x-ray fluorescence (XRF) and spectroscopy methods incorporating confocal imaging that allows specific depths within a material to be assayed, researchers working at the APS mapped the distribution of different oxidation states of chromium that has been absorbed into biochar. The technique will also work on other elements, and provides new insights into the chemical changes that enable biochar to capture and immobilize pollutants.

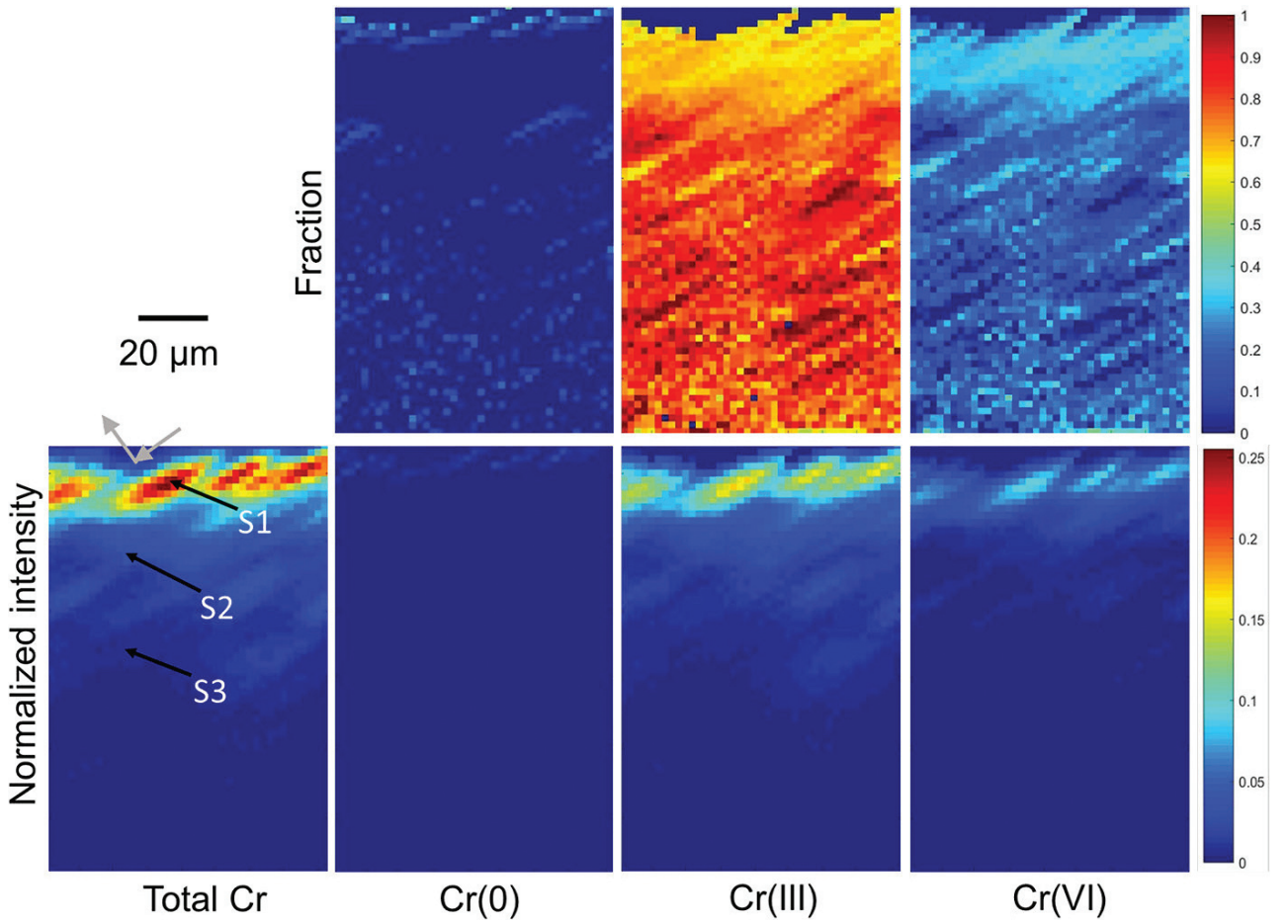

Fig. 1. Redox maps of an interior slice through the particle. Fraction (top row) and absorbance (bottom row) of Cr(0), Cr(III), and Cr(VI) in each pixel of the area after data processing for redox mapping in MATLAB. The total Cr absorbance distribution is presented in the left map. The gray arrow indicates incident beam and emitted XRF, as well as the particle surface. The scale is the fractional distribution of Cr at the three oxidation states (0–1; top right) and the absorbance distribution of total Cr and different Cr species (0–0.25; bottom right). From P. Liu et al., Anal. Chem. **91**, 5142 (March 20, 2019).

X-ray fluorescence reveals the presence of a chosen element, while XANES (x-ray absorption near-edge structure) spectra can distinguish oxidation states. However, because XANES requires data collection times of several minutes or more, it can only be used at a limited number of locations in a sample, and can itself cause chemical changes. A more general technique, applicable to thin-film samples, combines full-field XANES scans at several different energies with a data analysis method known as "linear combination fitting" to create a best-fit map of the distribution of chemical states. But slicing through a material to expose its interior often causes unwanted changes in redox states.

Researchers from the University of Waterloo (Canada), the China University of Geosciences, Argonne, and the Canadian Light Source, Inc., added a further ingredient to this mix of techniques: confocal imaging, which can be used in conjunction with x-ray fluorescence (XRF) and XANES to obtain data from specific depths within the interior of a sample.

The research team obtained samples of commercially made oak biochar and soaked small pieces in an aqueous solution of potassium dichromate, $K_2Cr_2O_7$. After 24 h they removed the biochar and analyzed the remaining solution to see how much chromium the biochar had taken up. Their goal was to find out how the absorbed chromium was distributed within the biochar and what oxidation state or states it was in. In potassium dichromate, chromium is in the oxidation state Cr(VI), which is mobile and known to have negative health consequences. Cr(III), by contrast, is immobile in aqueous environments at near neutral pH and is an essential mineral needed by humans at low levels.

Working at XSD x-ray beamline 20-ID-B,C at the APS, the team first performed a confocal x-ray fluorescence scan, at a single beam energy, on a piece of chromium-spiked biochar measuring about 1 mm x 1.8 mm x 0.8 mm. They explored a slice into the sample's interior by scanning across a line 250-µm long in 5-µm steps, then repeatedly moving the confocal probe deeper into the particle and rescanning until they reached a depth of 400 µm. Each of the 4000 volume elements of the scan measured 2 µm x 2 µm x 2 µm, and the total scan time was 17 min. The resulting map showed that most of the chromium was at or near the surface of the biochar, but that some had penetrated within.

The researchers then chose three locations, one at the surface and two in the interior, and performed micro-XANES analyses, also at beamline 20-ID-B,C, to determine the redox state of the chromium (Fig. 1). At the surface, they found about 35% Cr(VI) and 64% Cr(III), while at the deepest location those proportions were 13% and 86% respectively.

The researchers then scanned a smaller part of the previous slice, measuring 80-µm across and 140-µm deep, with a step size of 2 µm and at a total of 33 different x-ray energies. This process took about 5 h. The 33 energies, including important features of the XANES spectra as well as other dramatic absorption features, were selected by means of Monte Carlo simulations to get the best statistical fit using linear combination fitting.

The team thus determined a map of chromium redox states for each pixel of the interior slice. Most of the adsorbed chromium was found at the surface of the particle, where about 60% of it is reduced to Cr(III). The redox map shows that little chromium is absorbed into the particle's interior, but that more of it is reduced to Cr(III). The results agreed with the spot checks from the three micro-XANES observations but give a broader picture of how chromium is absorbed by biochar.

The researchers say that the method can be applied to other elements, although for species that exist in a larger number of oxidation states, more x-ray data would be required and the data analysis would be more demanding. Still, the technique is a noninvasive way of exploring absorption and chemical change within solid particles that could be useful in numerous environmental and engineering contexts. — David Lindley

See: Peng Liu[1,2], Carol J. Ptacek[2]*, David W. Blowes[2], Y. Zou Finfrock[3,4], Mark Steinepreis‡, and Filip Budimir[2], "A Method for Redox Mapping by Confocal Micro-X-ray Fluorescence Imaging: Using Chromium Species in a Biochar Particle as an Example," Anal. Chem. **91**, 5142 (March 20, 2019).
DOI: 10.1021/acs.analchem.8b05718
Author affiliations: [1]China University of Geosciences, [2]University of Waterloo, [3]Argonne National Laboratory, [4]Canadian Light Source, Inc. ‡Present address: Stantec Consulting, Ltd.
Correspondence: * ptacek@uwaterloo.ca

This research was funded by the Natural Sciences and Engineering Research Council of Canada (NSERC), and the National Natural Science Foundation of China (Nos. 41521001 and 41877478), the 111 Program (State Administration of Foreign Experts Affairs & the Ministry of Education of China, No. B18049), and Program of Geological Processes, Resources and Environment in the Yangtze Basin (No. CUGCJ1702). This research used resources of the Advanced Photon Source, an Office of Science User Facility operated for the U.S. Department of Energy (DOE) Office of Science by Argonne National Laboratory, and was supported by the U.S. DOE under Contract No. DE-AC02-06CH11357, and the Canadian Light Source and its funding partners.

APS Users by Institutional Geographic Distribution (FY 2019)

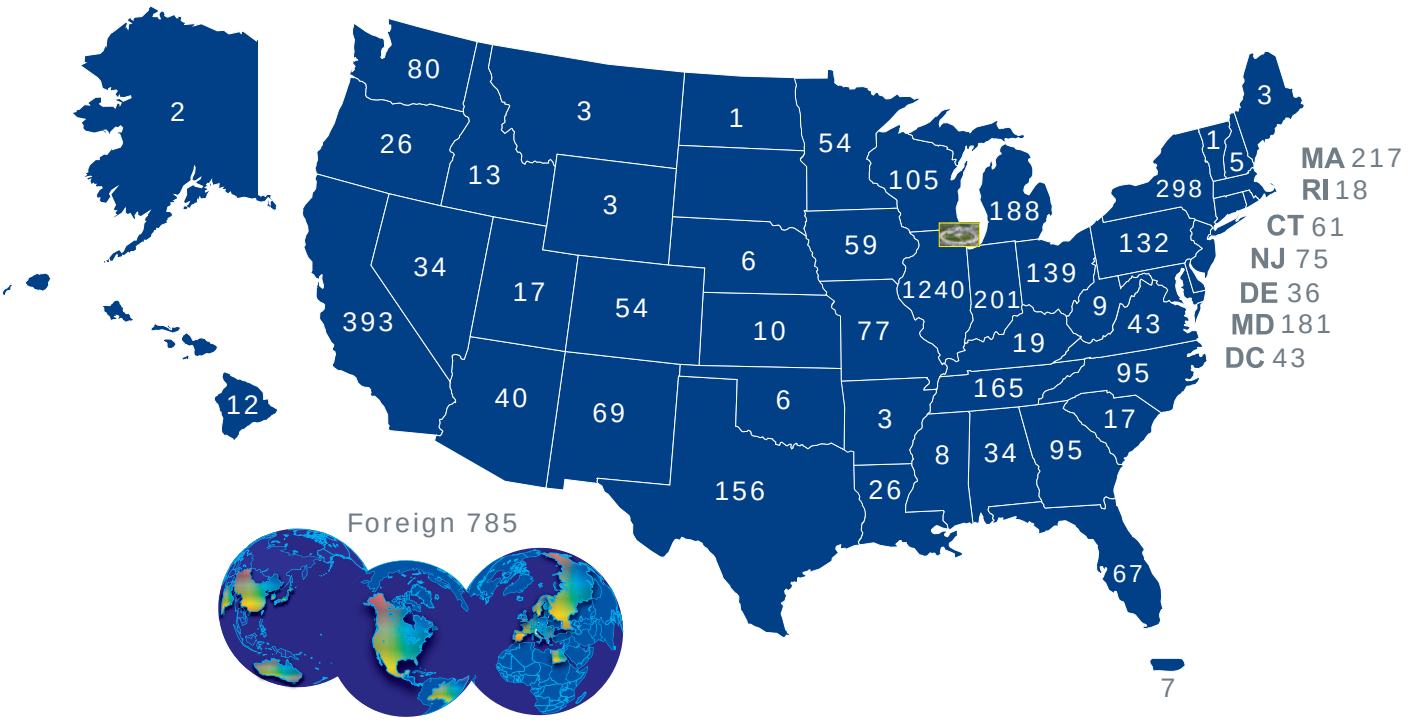

A new algorithm has been applied so that only 1 unique user is associated with mail-in and remote proposals.

APS Funding (FY 2006-FY 2019)

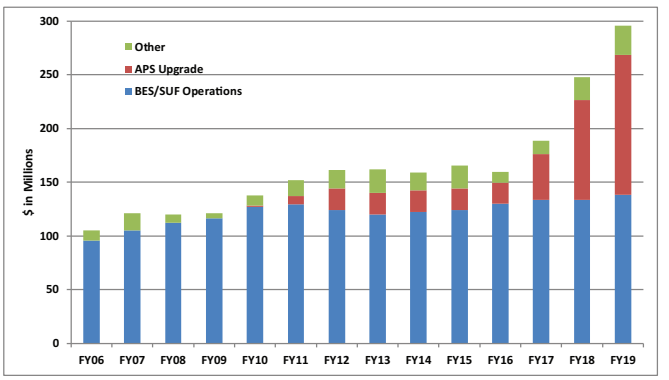

APS Staffing (FY 2007-FY 2019)

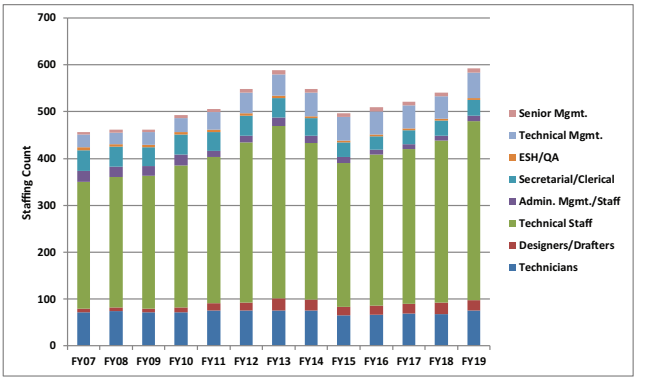

Nanoscience

Closing in on the Holy Grail of Targeted Drug Delivery

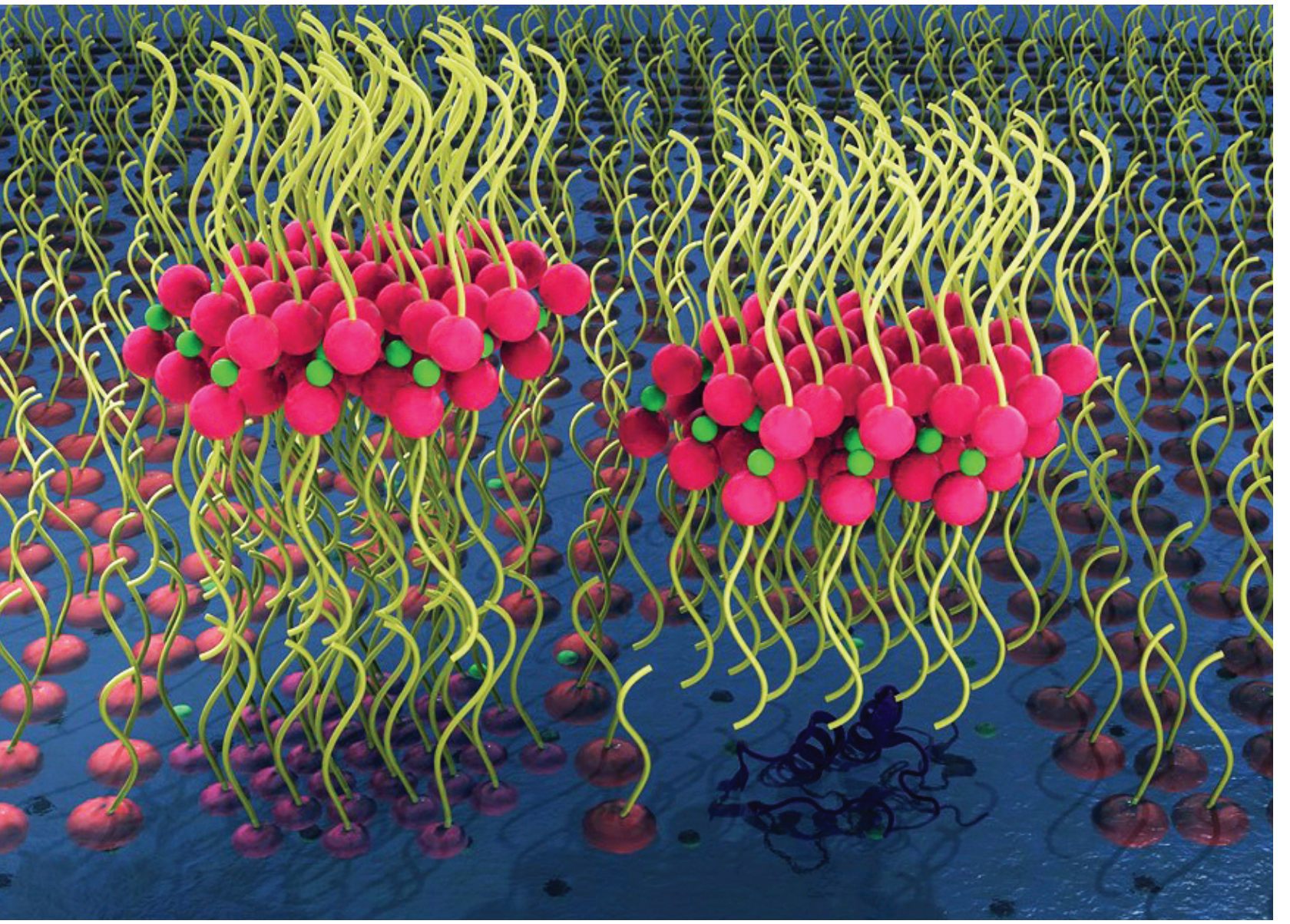

Fig. 1. Artist's rendering of highly ordered, self-assembled inverted bilayer and trilayer structures after enzyme-catalyzed degradation of saturated phospholipids, fatty acids together with divalent cations.

Advances in the evolving field of nanomedicine are helping scientists to design drug delivery systems that specifically target diseased tissues without harming healthy tissues. These include phospholipid-based drug delivery systems (PDDSs), which are particularly useful because scientists can modify the makeup of these systems to change their functions to meet specific treatment needs. Collecting data at the APS, researchers used x-ray reflectivity and grazing incidence x-ray diffraction to examine the three-dimensional molecular interaction between phospholipids and enzymes that leads to the release of drugs from these delivery systems. The results of this study will inform future research in PDDS designed to optimize nanomedicine composition for drugs targeting diseased tissue sites.

The ability to specifically target a drug to diseased cells without affecting healthy ones is considered the Holy Grail for the treatment of complex diseases. Nanomedicine is a relatively new and developing science that combines nanotechnology with biomedical and pharmaceutical sciences. Over the past two decades, several types of nanomedicines have shown promise in achieving the dream of delivering drugs to specific targeted sites.

Exploiting the overexpression of the enzyme secretory phospholipase A2 (sPLA2) in various tumors and inflammatory diseases represents one strategy for enzyme-triggered release of liposomal drug carriers selectively at a target tissue. Among current systems of nanomedicines, PDDSs have gained extensive attention as carriers for a wide range of drugs. This is because PDDSs, containing substances that occur naturally in biological membranes, are both nontoxic and biodegradable. For this reason, a few liposomal-vesicle-based nanomedicines were approved by the U.S. Food and Drug Administration for clinical uses.

Scientists at the University of Illinois at Chicago recently performed a study to develop "smart" liposomal nanoparticles for targeting delivery of biologically active payloads to diseased tissues. They aimed to optimize the composition of the liposomal vesicles based on understanding of the molecular interactions that take place between enzymes and polymer-phospholipids.

According to the researchers, changing the composition of the PDDS (with respect to its lipids, polymer conjugation, and membrane proteins) can alter its nanostructures, physicochemical characteristics, and biomedical functionalities. This flexibility allows scientists to change the design of these systems and modify liposome behavior *in vivo* according to specific therapeutic needs. However, because of the enormous number of possible modifications, optimizing the PDDS structure is not feasible by empirical trials. Systematic understanding of the molecular interactions between polymer-phospholipids and enzymes is therefore necessary but challenging.

Hoping to gain insight into these molecular interactions, the researchers, along with colleagues from The University of Chicago, used high-brightness x-rays at ChemMatCARS beamline 15-ID-C of the APS. They investigated the molecular packing, interaction, and degradation of phospholipids catalysed by enzymes, using a model phospholipid known as DPPC, and the enzyme sPLA2.

The researchers found that after sPLA2 degraded the phospholipid DPPC, fatty acids and divalent calcium ions came together to form highly-ordered, inverted bilayer and tri-layer structures (Fig. 1). This provides a molecular-level explanation of how the enzyme activity damages the phospholipid structure and leads to bursting of the liposomes and drug release.

The results of this study will be critical in helping to guide the design of PDDSs that are stable as they circulate in the bloodstream, but can quickly dissemble at the site of disease such as inflammation or cancer in the presence of an increased amount of enzyme. — Nicola Parry

See: Pin Zhang[1], Veronica Villanueva[1], Joseph Kalkowski[1], Chang Liu[1], Alexander J. Donovan[1], Wei Bu[2], Mark L. Schlossman[1], Binhua Lin[2], and Ying Liu[1]*, "Molecular interactions of phospholipid monolayers with a model phospholipase," Soft Matter **15**, 4068 (2019). DOI: 10.1039/c8sm01154k
Author affiliations: [1]University of Illinois at Chicago, [2]The University of Chicago
Correspondence: * liuying@uic.edu

The study is supported by the National Science Foundation (NSF) Nanomanufacturing Program (NSF CAREER #1350731). ChemMatCARS Sector 15 is principally supported by the Divisions of Chemistry (CHE) and Materials Research (DMR), NSF, under grant number NSF/CHE-1834750. This research used resources of the Advanced Photon Source, a U.S. Department of Energy (DOE) Office of Science User Facility operated for the DOE Office of Science by Argonne National Laboratory under Contract DE-AC02-06CH11357.

How Nanoparticles Can Pretend to Be Electrons

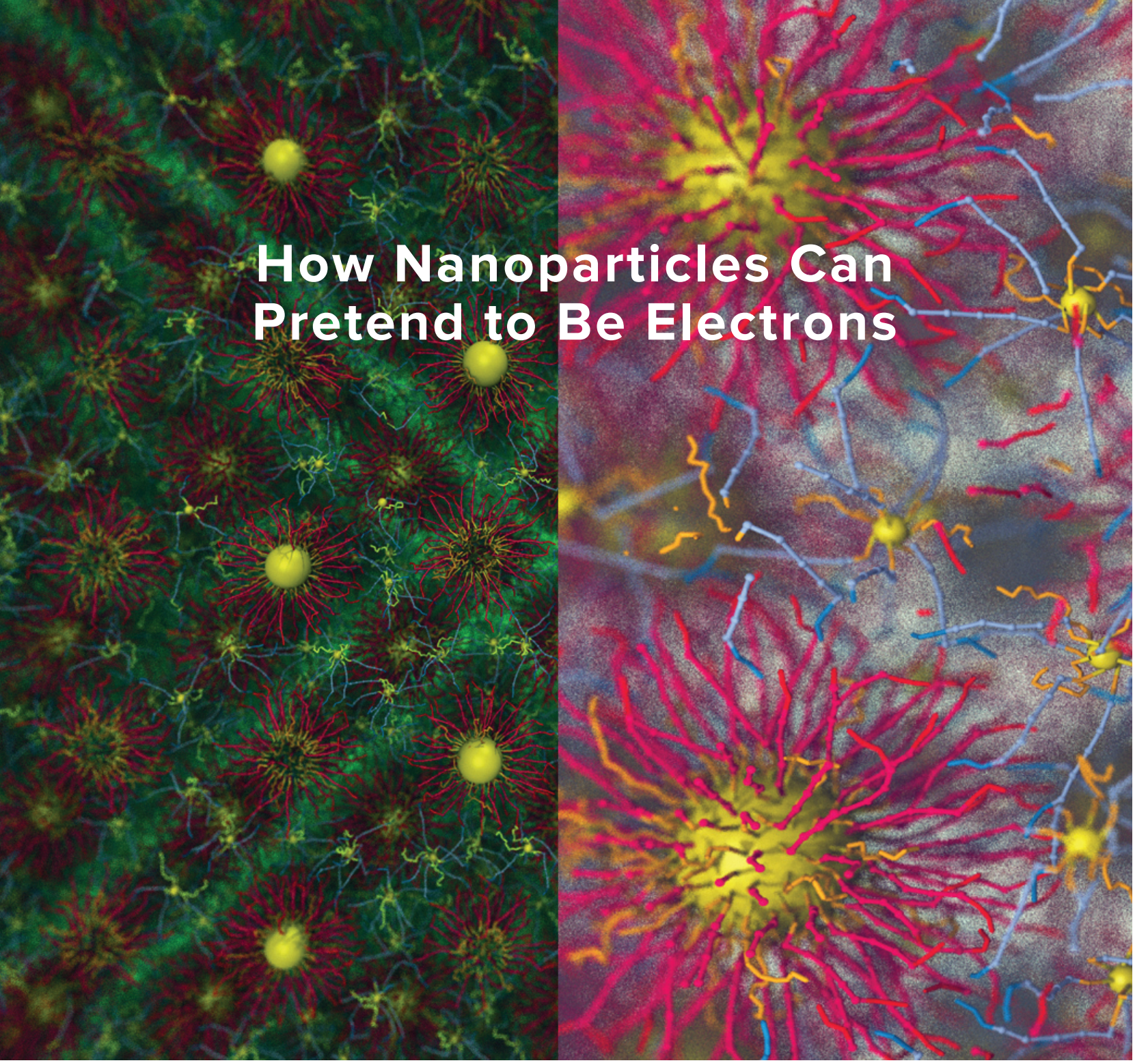

Fig. 1. Snapshots of the molecular dynamics simulation of larger DNA functionalized nanoparticles (NPs) with 150 DNA linkers per NP held in crystal positions by smaller particles (electron equivalents) with only eight DNA linkers per NP; the ratio of smaller to larger NPs in the mixture is 6 to 1. Image: Martin Girard.

In the past couple of decades, colloid science has provided chemists and material scientists with a versatile and convenient means to experiment with crystal structure, allowing them to design and synthesize nanoscale materials with various properties and possibly useful applications. One powerful technique involves using DNA as ligands to bind together nanoparticles (NPs), creating programmable atom equivalents (PAEs). But while such structures can work as atomic analogs, an important piece has been missing: no equivalent of the electron has yet been seen in colloidal crystals. Now, a team of researchers from Northwestern University and Argonne using the APS has finally confirmed such an elusive phenomenon, and with it a new property of colloidal crystals analogous to electron behavior in metals. The identification of this unusual behavior opens up wholly new avenues of research in colloidal crystals, while also offering fresh possibilities for using them to design and create new materials for a range of practical applications, such as photonic crystals.

One of the team members, Chad Mirkin from Northwestern, originally developed the techniques for using DNA strands to construct colloidal crystals as a means of more precisely engineering their structure. Hundreds of DNA strands coating nanoparticles can direct and bind them together to form crystal lattices in customized configurations; the nanoparticles attaching only to others with complementary DNA. In the present experiments, the investigators assembled DNA-functionalized gold NPs of varying sizes, 10, 5, 2, and 1.4 nm in diameter, and observed the results using small-angle x-ray scattering (SAXS) at the DND-CAT beamline 5-ID-B,C,D of the APS, as well as electron microscopy. Molecular dynamics simulations and theoretical analysis were carried out based on the SAXS data.

The smaller NPs are functionalized with fewer numbers of DNA strands, and thus they share a limited number of bonds than the larger NPs, which are functionalized with a greater number of DNA strands. So, the links between the smaller and larger particles are often more tenuous than those between the larger particles. The combinations of the first three NP groups (10 nm + 10 nm, 10 nm + 5 nm, 10 nm + 2 nm) form regular crystal lattices in expected configurations. But combining 10-nm nanoparticles with their 1.4-nm counterparts led to a surprising result never before seen in colloidal crystals, but predicted by the simulations of the Olvera de la Cruz group (Fig. 1). Because of the extremely small size of the 1.4-nm NPs, they hold only 4 to 8 DNA strands that can link with other NPs. Instead of bonding with other particles in the lattice, the 1.4-nm NPs freely roamed through it, making only loose connections with various larger particles and then moving on. The team showed that the smaller NPs were acting as electron equivalents (EEs), moving freely similar to how electrons do in metals (that allows them to conduct electricity) and holding the larger NPs in their crystal positions. The research team describes this behavior in colloidal crystals with the term "metallicity' or M_{cc}.

When the team attempted to modify this behavior, both by increasing the number of DNA linkers on the 1.4-nm NPs and by decreasing temperature, the EEs ceased their roaming and instead nestled in fixed locations within the lattice, as predicted by the simulations. This phenomenon, they observe, is similar to the phase transition from a conductor to an insulator seen in metals under certain conditions. By adjusting the ratio of EEs to PAEs and the number of DNA strands of the EEs, the investigators were able to realize three separate crystal phases in the lattice: body-centered cubic, face-centered cubic, and Frank-Kasper A15.

The research team notes that this discovery might also imply the existence of other exotic behaviors that might arise from the metallicity and phase transition phenomena. More experimental and theoretical work based on these findings is likely to lead to even more interesting possibilities and insights. — Mark Wolverton

See: Martin Girard[1], Shunzhi Wang[1], Jingshan S. Du[1], Anindita Das[1], Ziyin Huang[1], Vinayak P. Dravid[1], Byeongdu Lee[2], Chad A. Mirkin[1]*, and Monica Olvera de la Cruz[1]**, "Particle analogs of electrons in colloidal crystals," Science **364**, 1174 (21 June 2019). DOI: 10.1126/science.aaw8237
Author affiliations: [1]Northwestern University, [2]Argonne National Laboratory
Correspondence: * chadnano@northwestern.edu,
** m-olvera@northwestern.edu

This material is based on work supported by the Center for Bio-Inspired Energy Science (CBES), an Energy Frontier Research Center funded by the U.S. Department of Energy (DOE) Office of Sciences-Basic Energy Sciences (DE-SC0000989, for computational studies), the Air Force Office of Scientific Research (FA9550-17-1-0348, for synthesis, spectroscopy, and electron microscopy), the Vannevar Bush Faculty Fellowship program sponsored by the Basic Research Office of the Assistant Secretary of Defense for Research and Engineering and funded by the Office of Naval Research (N00014-15-1-0043), the Sherman Fairchild Foundation (for electron microscopy and computational support), and the Biotechnology Training Program of NU (for cryo-TEM). This work made use of facilities at the NUANCE Center at NU (NSF ECCS-1542205 and NSF DMR-1720139), the Structural Biology Facility at NU (NCI CCSG P30 CA060553). DND-CAT is supported by Northwestern University, The Dow Chemical Company, and DuPont de Nemours, Inc. This research used resources of the Advanced Photon Source, a U.S. DOE Office of Science User Facility operated for the DOE Office of Science by Argonne National Laboratory under Contract No. DE-AC02-06CH11357.

Watching Catalysts at Work Inside Fuel Cells

To satisfy growing energy demands worldwide and reduce reliance on fossil fuels, researchers are increasingly investigating the feasibility of alternate ways to generate power, such as fuel cells. One of the most popular types is the proton exchange membrane fuel cell (PEMFC), which generates power using the oxygen reduction reaction (ORR). This reaction takes place at the cathode, where oxygen molecules adsorbed and reduced there react with protons supplied by the cell's anode to form water. But although these fuel cells have enormous potential, they aren't on the mass market yet, mostly due to the lack of efficient catalysts to facilitate this sluggish reaction. One class of promising catalysts is nanoalloys of platinum (Pt) with 3d-transition metals (TMs). These are less expensive and more catalytically active than pure Pt. Unfortunately, despite their potential, these nanoalloy catalysts have not performed as well as predicted by theory. This is because under operating conditions, the catalyst particles undergo various structural changes ranging from sub-angstrom atomic fluctuations and sharp nanophase transitions to a gradual strain relaxation and growth, which inflict significant losses on their electrocatalytic activity. Researchers used the APS to study dynamic structural changes in Pt and 3d-TM nanoalloy particles functioning as catalysts for ORR at the cathode of an operating PEMFC and how their electrocatalytic activity evolves with these changes. The insights gained from these studies may help researchers design better catalysts for fuel cells that capitalize on the most productive transient nanostructures.

Research has shown that a variety of factors can help improve the performance of Pt and 3d-TM nanoalloy catalysts, including high-temperature annealing, chemical etching to remove unalloyed TM species, or creating TM core-Pt shell or Pt-frame type nanostructures. These efforts have typically been evaluated by experiments on model nanoalloy systems conducted under controlled laboratory conditions. However, few studies have investigated the atomic-level changes experienced by these nanoalloy particles under actual working conditions in a fuel cell and how these changes affect their performance in real time.

Toward that end, researchers from Central Michigan University and the State University of New York at Binghamton synthetized several different types of Pt-TM nanoalloy nanoparticles with a broad range of compositions, some including one type of TM, others including two. Microscopy revealed that these nanoparticles were all approximately 8.7 nanometers in diameter and rounded in shape. Once incorporated into a PEMFC, the researchers, together with colleagues from Argonne, used the XSD 1-ID-B,C,E beamline at the APS (Fig. 1) to study their behavior under operating conditions by combined x-ray spectroscopy and pair distribution function analysis. Studies revealed simultaneous changes in the atomic-level structure and ORR activity of the catalyst nanoparticles as they functioned at the device's cathode—a harsh and highly corrosive environment with interfacial acidity, high humidity, elevated temperature, and voltage excursions. The team took these measurements using a focused beam of 85-keV x-rays while the PEMFC was cycled between 0.6 V and 1.0 V for about 5 to 6 h, corresponding to about 1600 potential cycles.

As their results show, the composition and atomic structure of the nanoalloys changed profoundly, from the initial state to the active form and further along the cell operation. In particular, right at the beginning of potential cycling, the Pt-TM alloy nanoparticles experienced a significant drop in ORR activity, which appears to be linked to leaching of TM species from the nanoparticles and a fast decrease of the atomic-level strain. As cycling continued, further losses in electrocatalytic efficiency arose putatively from the exchange of dissolved atomic species between nearby particles. Transient structure states exhibiting enhanced ORR activity were also observed.

Their research also shows that the rate and magnitude of the dynamic changes can be rationalized through deviations from Vegard's law, which approximates the lattice parameter of crystalline alloys and its relationship to electrochemical activity and stability. In addition, factors

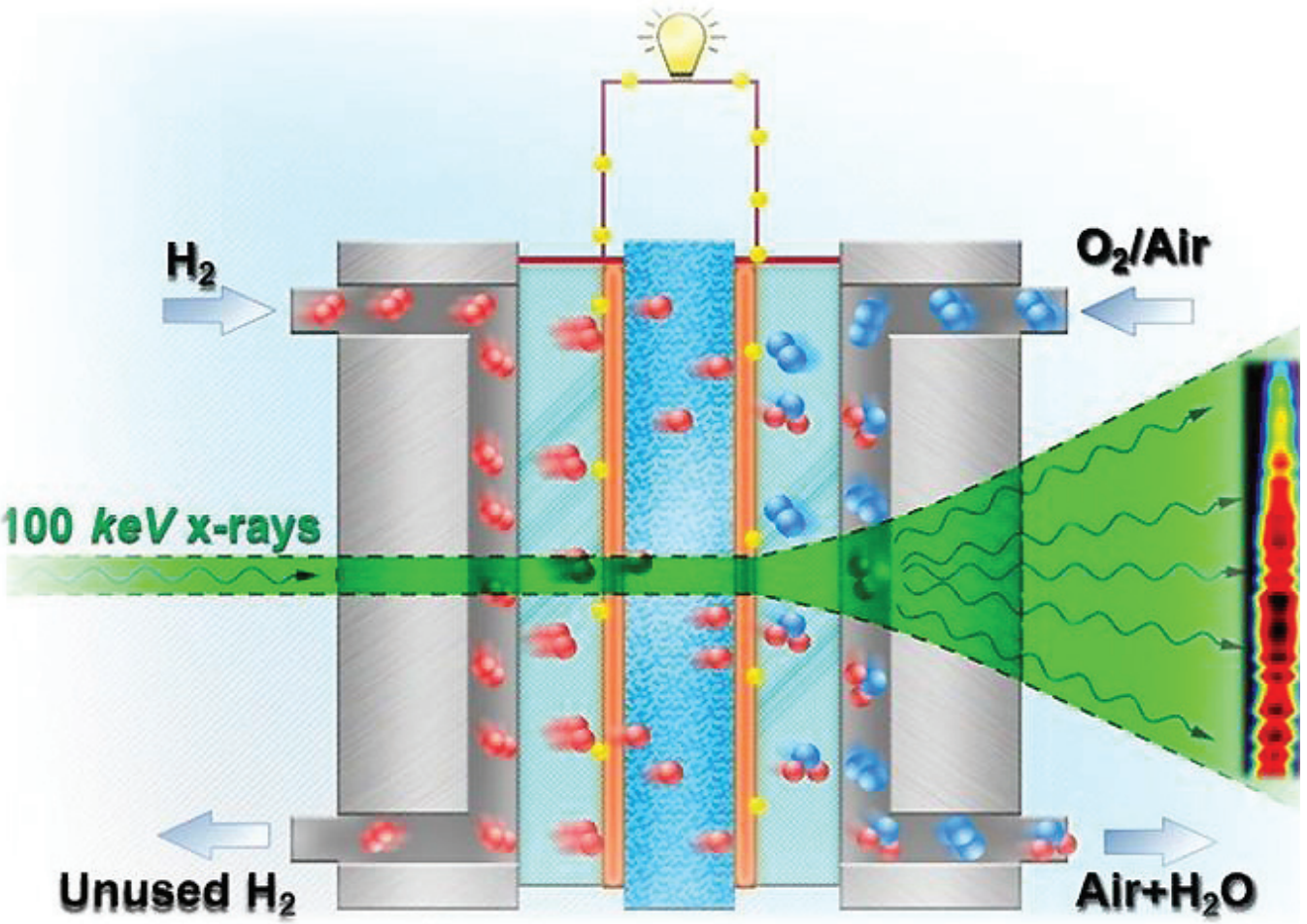

Fig. 1. Schematic of an *in operando*, high-energy x-ray diffraction experiment on Pt and 3d-TM electrocatalysts for ORR at the cathode of a PEMFC (left) revealing non-uniform changes in Pt-Pt bonding distances during 5 hours of potential cycling (oscillating pattern on the right).

that contribute to the remarkable performance of these nanoalloys as electrocatalysts (such as the large surface-to-volume ration and difference in sizes of Pt and TM atoms) can also contribute to their instability under operating conditions.

The authors suggest that, to be successful, studies on improving the performance of ORR catalysts further must recognize that as-synthesized Pt and 3d-TM nanoalloys are merely pre-catalysts, and actual catalysts are formed under operating conditions. It is essential to study the dynamic behavior of nanoalloy catalysts under operating conditions and derive meaningful relationships between relative changes in their composition, structure and electrocatalytic activity with respect to the initial state, and not to resort indiscriminately to approximations borrowed from metallurgy, such as Vegard's law. These findings may help researchers identify ways to improve electrocatalysts for ORR, bringing fuel cell technologies a step closer to commercialization. — Christen Brownlee

See: Valeri Petkov[1]*, Yazan Maswadeh[1], Jorge A. Vargas[1], Yazan Maswadeh[1], Jorge A. Vargas[1], Shiyao Shan[2], Haval Kareem[2], Zhi-Peng Wu[2], Jin Luo[2], Chuan-Jian Zhong[2], Sarvjit Shastri[3], and Peter Kenesei[3], "Deviations from Vegard's law and evolution of the electrocatalytic activity and stability of Pt-based nanoalloys inside fuel cells by *in operando* X-ray spectroscopy and total scattering," Nanoscale **11**, 551 (2019). DOI: 10.1039/c9nr01069f
Author affiliations: [1]Central Michigan University, [2]State University of New York at Binghamton, [3]Argonne National Laboratory
Correspondence: * petko1vg@cmich.edu

This work was supported by the U.S. Department of Energy (DOE) Office of Science-Basic Energy Sciences Grant DE-SC0006877. This research used resources of the Advanced Photon Source, a U.S. DOE Office of Science User Facility operated for the DOE Office of Science by Argonne National Laboratory under Contract DE-AC02-06CH11357.

X-ray Availability and Reliability

In fiscal year 2019*, the APS x-ray source continued to function as a highly reliable delivery system for synchrotron x-ray beams for research. Several factors support the overall growth in both the APS user community and the number of experiments carried out by that community. But there is a direct correlation between the number of x-ray hours available to users; the success of the APS experiment program; and the physicists, engineers, and technicians responsible for achieving and maintaining optimum x-ray source performance. Below are definitions of important measures for the delivery of x-ray beam to users (latest data shown graphically).

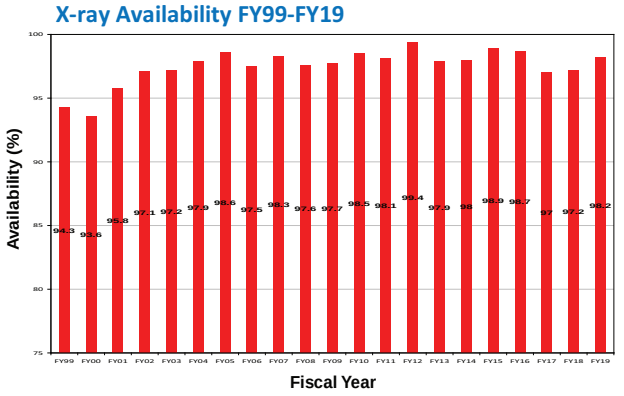

X-ray Availability: The number of hours that beam is available to users divided by the number of hours of scheduled beam delivery prior to the beginning of a run. The specific definition of available beam is that the APS main control room has granted permission to users to open shutters, and there is more than 50-mA stored beam in the storage ring.

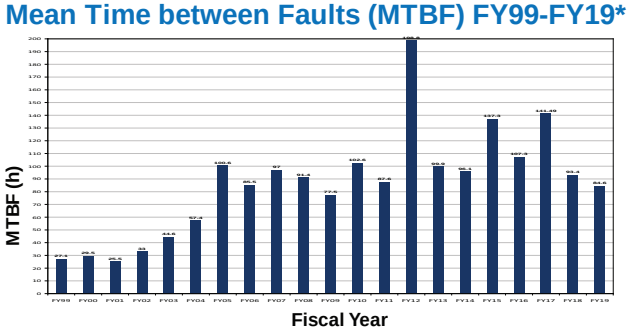

Storage Ring Reliability: A measure of the mean time between beam losses (faults), or MTBF, calculated by taking the delivered beam and dividing by the total number of faults. The APS targets, and routinely exceeds, 70 h MTBF. A fault is defined as complete unavailability of beam either via beam loss or removal of shutter permit not related to weather. A fault also occurs when beam has decayed to the point where stability and orbit can no longer be considered reliable (50 mA).

* While the highlights in, and title of, this report cover calendar year 2019, data on accelerator performance and user statistics are measured on the basis of fiscal years.

Typical APS Machine Parameters

Linac

Output energy	425 MeV
Output beam charge	0.3–3 nC
Normalized emittance	5–20 mm-mrad
Frequency	2.856 GHz
Modulator pulse rep rate	30 Hz
Gun rep rate	2–26 Hz
(1-13 pulses, 33.3 ms apart every 0.5 s)	
Beam pulse length	8–15 ns
Bunch length	1–10 ps FWHM

Particle Accumulator Ring

Nominal energy	425 MeV
Circumference	30.66 m
Cycle time	0.5 s or 1 s
Fundamental radio frequency (RF1)	9.77 MHz
12th harmonic RF frequency (RF12)	117.3 MHz
RMS bunch length	0.34 ns
(after compression)	

Injector Synchrotron (Booster)

Nominal extraction energy	7.0 GeV
Injection energy	425 MeV
Circumference	368.0 m
Ramping rep rate	2 Hz or 1 Hz
Natural emittance	132 nm-rad (nominal)
	87 nm-rad (actual)
Booster RMS bunch length	100 ps
Radio frequency	351.935 MHz

Storage Ring System

Nominal energy	7.0 GeV
Circumference	1104 m
Number of sectors	40
Length available for insertion device	5.0 m
Nominal circulating current, multibunch	100 mA
Natural emittance	2.5 nm-rad
RMS momentum spread	0.096%
Effective emittance	3.1 nm-rad
Vertical emittance	0.040 nm-rad
Coupling (operating)	1.5%
Revolution frequency	271.555 kHz
Radio frequency	351.935 MHz
Operating number of bunches	24 to 324
RMS bunch lengths	33 ps to 25 ps
RMS bunch length of 16 mA in hybrid mode	50 ps

Novel Accelerator and X-ray Techniques and Instrumentation

A New Tool for Laser Shock Physics

Sometimes the only way to find out how a material responds under extreme conditions is to examine it under such conditions. It is not an easy proposition when considering what happens at near-instantaneous time scales coupled with high temperatures and intense pressures, particularly when we want to examine such events in real time instead of merely settling for sifting through the aftermath. Although it is possible to model such phenomena mathematically, the models still cannot actually show what is happening in the moment, a crucial part of fully understanding the event. The Dynamic Compression Sector (DCS) at Sector 35 of the APS provides a unique way to do just that. One of the stations of the DCS specializes in laser shock-induced phenomena that occur when materials are shock compressed by bursts of high-energy photons.

The heart of the Laser Shock Station (Fig. 1) is the combination of the high-energy, tunable x-ray beams of the third-generation APS synchrotron and an ultraprecise 100-J, 5-17-ns, 351-nm-frequency tripled Nd:glass laser with programmable pulse shaping. Because of the mechanical design of the interaction chamber and laser transport optics, the angle between the x-ray beam and the laser beam can be varied by up to 135°, so constant realignment of the optical setup between different shots is not necessary. The chamber can translate vertically and laterally to take advantage of both the broadband "white" APS x-ray beam and the monochromatic "pink" beam as needed. The Laser Shock Station itself is divided into five separate areas, comprising a laser room, a gowning room, the laser control room, an area containing the x-ray beam, an interaction chamber and related equipment, and a user area.

The sample holder within the interaction chamber can accommodate exposures of up to 14 separate samples while maintaining the necessary vacuum conditions for laser interaction experiments. Samples are assembled in three layers—including a thin lithium fluoride window, the sample material, and a Kapton® ablator—and are mounted on aluminum bars, which are then attached to a holder wheel. After x-ray shots on all 14 samples on one wheel have been completed, the wheel can be quickly replaced with another already-prepared sample holder.

Such design features of the Laser Shock Station equipment allow for a great deal of flexibility in experimental design, an advantage also enhanced by the 90-psec temporal resolution of the APS x-ray beam as well as the wide variety of laser pulse shapes available. These pulses can be delivered to the sample at shot energies at increments of 10% from 10 to 100 J without affecting the pulse shape or focal profile. The laser does require an interval of about 30 min between shots to allow for cooling of the optics, recharging, and data storage.

As a demonstration of the capabilities of the Laser Shock Station, a series of x-ray diffraction experiments was conducted on tantalum sample foils. Using the facility's VISAR (Velocity Interferometer System for Any Reflector) diagnostics to verify the shape of the shock wave along with its arrival time and peak amplitude, 31 experiments were completed at two different laser energies, with several repeated in order to demonstrate reproducibility of the results. The experimental series gave excellent shocked and unshocked x-ray diffraction data, including an indication of sample melting at the highest stresses. The exceptional reproducibility of the laser shock pulse permits precise time correlation of x-ray data from different experiments.

With this experimental confirmation of its capabilities, the DCS team has declared that the Laser Shock Station is fully operational and ready for users. As a state-of-the-art experimental facility in the highly specialized field of shock physics, coupled with the proven capabilities of the APS, the Laser Shock Station and the other stations of the DCS promise some startling discoveries to come.

— Mark Wolverton

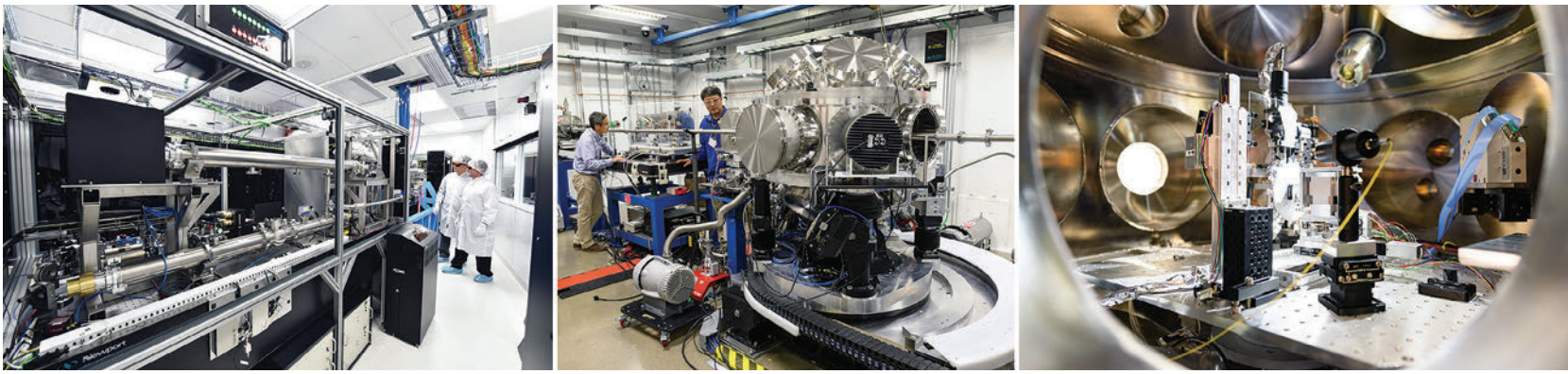

Fig. 1. The DCS Laser Shock Station. Above, left to right: the 100-J laser system, the highly flexible interactive chamber with translation stage and 135° rotation, and the sample holder and optics for x-ray and optical diagnostics inside the interactive chamber. Below: A schematic of the Laser Shock Station. From X. Wang et al., Rev. Sci. Instrum. **90**, 053901 (2019). Published under license by AIP Publishing

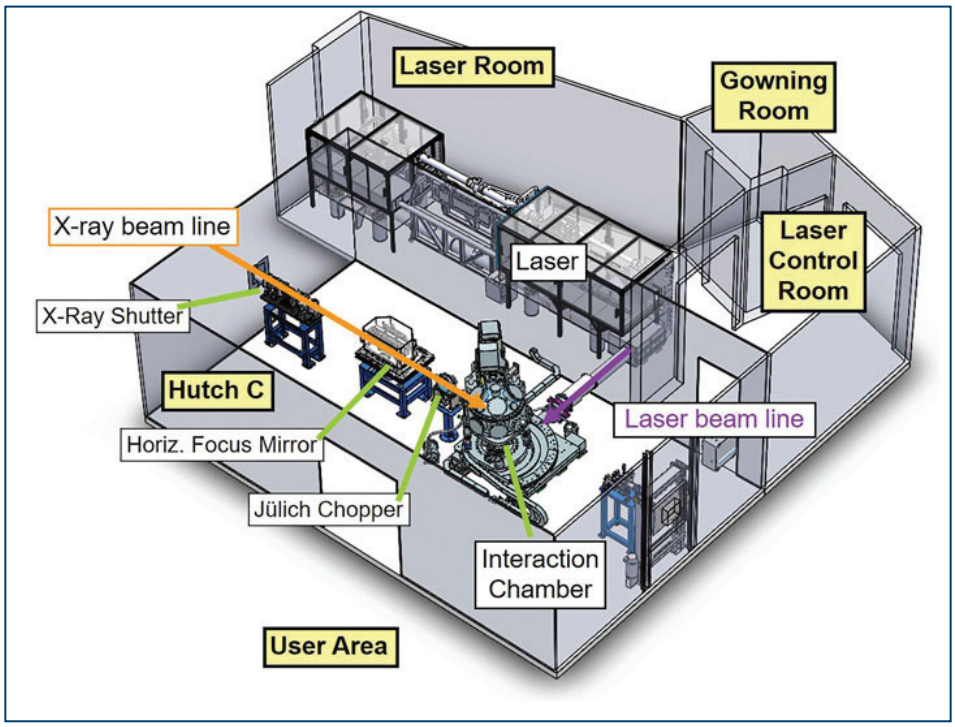

See: Xiaoming Wang[1], Paulo Rigg[1], John Sethian[1], Nicholas Sinclair[1], Nicholas Weir[1], Brendan Williams[1], Jun Zhang[1], James Hawreliak[1], Yoshimasa Toyoda[1], Yogendra Gupta[1]*, Yuelin Li[1,2], Douglas Broege[3], Jake Bromage[3], Robert Earley[3], Dale Guy[3], and Jonathan Zuegel[3], "The laser shock station in the dynamic compression sector. I," Rev. Sci. Instrum. **90**, 053901 (2019).
DOI: 10.1063/1.5088367
Author affiliations: [1]Washington State University, [2]Argonne National Laboratory, [3]University of Rochester
Correspondence: * ymgupta@wsu.edu

The journal article is based upon experimental activities for the Dynamic Compression Sector, which is operated by Washington State University under the U.S. Department of Energy (DOE) National Nuclear Security Administration Award No. DE-NA0002442. In addition to the support through Washington State University as noted above, this work was also supported by the University of Rochester and the New York State Energy Research and Development Authority. This research used resources of the Advanced Photon Source, a U.S. DOE Office of Science User Facility operated for the DOE Office of Science by the Argonne National Laboratory under Contract No. DE-AC02-06CH11357.

High-Speed and High-Resolution X-ray Imaging with the Velociprobe

A team of researchers from Argonne has developed a new device for quickly acquiring high-resolution x-ray images over large sample areas. Dubbed the "Velociprobe," the new instrument utilizes a technique called "x-ray ptychography." Installed at the APS, the Velociprobe demonstrated its imaging capabilities in a series of tests. One test showed the device's capability to locate an x-ray beam on a sample to an accuracy of 2 nm. Another test involved rapidly scanning an integrated circuit to reveal details with sub-10-nm resolution. Although these are impressive results, the true imaging capabilities of the Velociprobe will be realized with the upcoming APS Upgrade, which will increase the coherent x-ray flux by more than 100 times. This dramatic increase in flux density will allow the Velociprobe to usher in the next generation of fast scanning of materials at high spatial resolution.

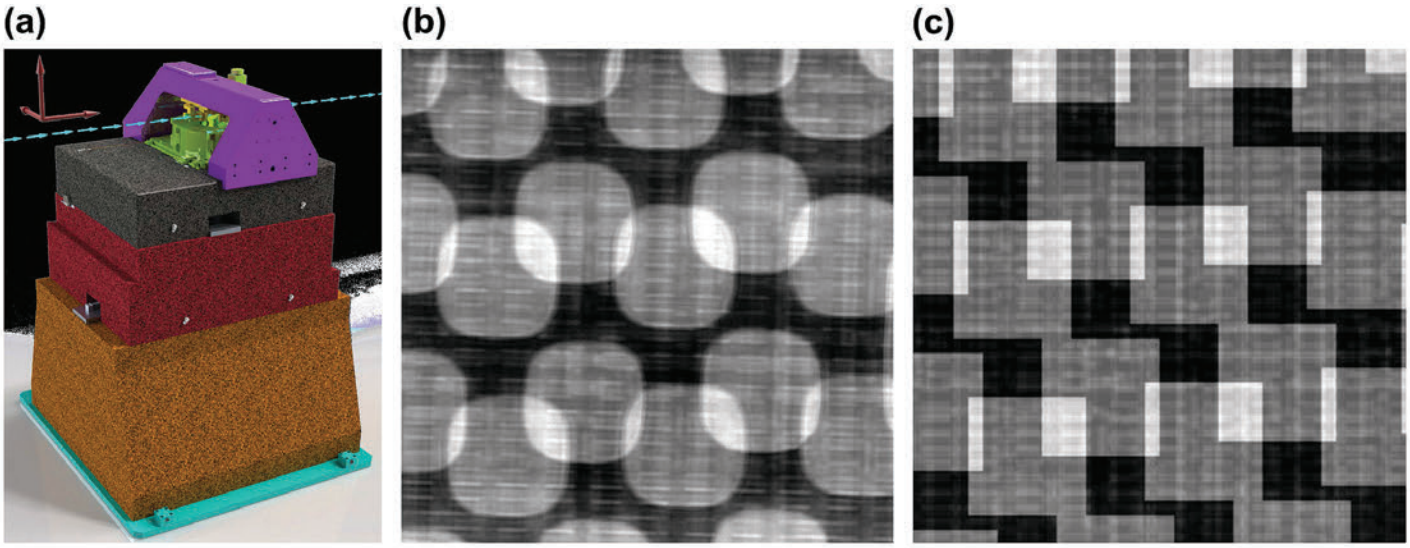

Fig. 1. Panel (a) highlights the major components of the Velociprobe. It rests upon a steel plate (cyan-colored component at bottom). Middle sections consist of precisely-shaped granite blocks that move relative to one another on a cushion of air. When the air is removed, the blocks meet and form a highly stable platform. A gantry atop the Velociprobe holds its optical components and the sample. Cyan arrows indicate the x-ray path. Panel (b) is a high-resolution micrograph of an integrated circuit imaged by the Velociprobe in 1.2 sec. Individual square-shaped features are 720 nm across. Panel (c) simulates the expected features based upon engineering diagrams. The rounded corners of the 'squares' in (b) are attributed to the manufacturing process.

X-ray ptychography involves shining a coherent x-ray beam at many closely-spaced points on a sample, producing a collection of x-ray diffraction patterns. Computer algorithms then reconstruct the sample image from the recorded patterns.

Although the principles behind x-ray ptychography are well understood, scientists have invariably encountered difficulties when building practical instruments incorporating the technique. Even slight vibrations or thermal fluctuations can introduce errors in positioning the x-ray beam, which blurs the image. Another limitation involves how the x-ray beam is moved, or scanned, over the sample. X-ray ptychography instruments have traditionally used the step scan approach to obtain the diffraction patterns. In the step scan mode, after one diffraction pattern

is recorded the x-ray beam (or the sample itself) is moved a tiny amount, the new position is confirmed, and then another diffraction pattern is produced and recorded. This intermittent procedure means that most of the incoming x-ray photons are wasted.

The Velociprobe was engineered to address many of these limitations while also taking full advantage of the dramatically higher x-ray flux anticipated from the APS Upgrade. The basic design philosophy was to improve upon each aspect of earlier ptychographic instruments in order to achieve faster imaging at higher resolutions. The left side of Fig. 1 depicts the Velociprobe. Both the sample and the optics used to focus the x-ray beam are mounted near the top of the device. The incoming x-ray beam is indicated by the line of arrows.

The bulk of the Velociprobe consists of several sizable granite blocks, which together weigh nearly 8000 lbs (approximately 3600 kg). These massive granite components provide stability and help isolate the sample and optics package from vibrations. Coarse horizontal and vertical movement of the system is accomplished by innovative (and patent-pending) ultra-stable mechanical drivers mounted between the granite blocks. Air pumped between the smooth granite blocks facilitates movement. When the movement is complete, the air dissipates to form a rigid, granite-on-granite structure.

The sample is held within the sample stage stack, which can be moved independently of the granite blocks. The optics stage stack hangs on the gantry just above the sample stack. The optics stack holds the zone plate (reminiscent of a bullseye) that focuses the x-ray beam onto the sample. Ultra-fine motion of the zone plate is measured via three laser interferometers. These measurements are fed into a sophisticated closed-loop feedback system, which commands sensitive piezoelectric devices. This ultra-precise-and-stable movement system demonstrated a position accuracy of 2 nm.

The researchers also used recently-developed techniques to dramatically reduce imaging time. In place of the intermittent step scan procedure, a fly-scan approach was adopted. This technique continuously creates diffraction patterns by directing the x-ray beam to follow a spiral or other pattern across the sample. Such continuous-scanning methods greatly reduce overall imaging time.

Using the advanced fly-scan approach at the XSD 2-ID-D beamline at the APS, the Velociprobe produced a series of two-dimensional images from various samples. For instance, a gold test pattern was imaged at a spatial resolution of just under 9 nm. A fast scan was also used to quickly image an integrated circuit, as shown in Fig. 1 (middle panel). The entire scan required only 1.2 sec.

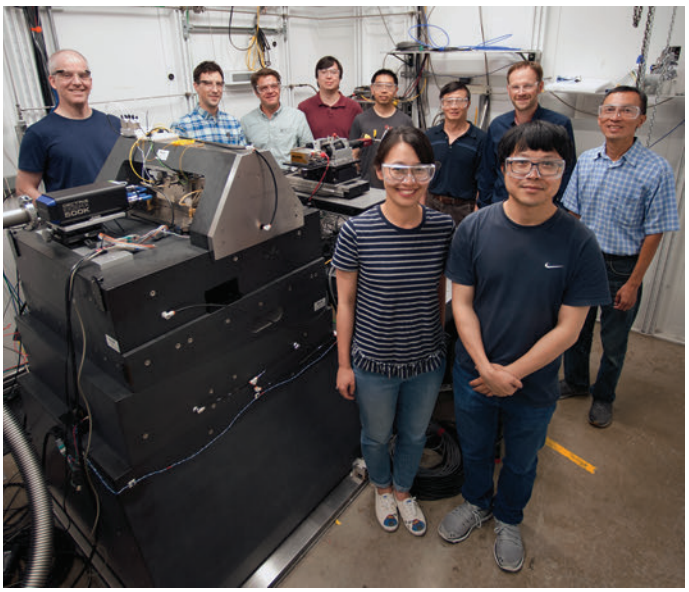

Argonne members of the Velociprobe development team from XSD, in the APS 2-ID-D enclosure. Left to right, first row: Yudong Yao, Junjing Deng. Left to right, second row: Christian Roehrig, Jeffrey Klug, Curt Preissner, Michael Wojcik, Yi Jiang, Zhonghou Cai, Stefan Vogt, and Barry Lai. The Velociprobe is at left.

Further development of the Velociprobe is under way. While the images produced in this study were two-dimensional, an upgrade will permit high-resolution three-dimensional imaging. Additionally, the planned installation of a fluorescence detector will allow the Velociprobe to perform both ptychographic and fluorescence x-ray imaging.

— Philip Koth

See: Junjing Deng[1]*, Curt Preissner[1], Jeff A. Klug[1], Sheikh Mashrafi[1], Christian Roehrig[1], Yi Jiang[1], Yudong Yao[1], Michael Wojcik[1], Max D. Wyman[1], David Vine[1], Ke Yue[1], Si Chen[1], Tim Mooney[1], Maoyu Wang[2], Zhenxing Feng[2], Dafei Jin[1], Zhonghou Cai[1], Barry Lai[1], and Stefan Vogt[1], "The Velociprobe: an ultrafast X-ray nanoprobe for high-resolution ptychographic imaging," Rev. Sci. Instrum. **90**, 083701 (2019). DOI: 10.1063/1.5103173
Author affiliations: [1]Argonne National Laboratory, [2]Oregon State University
Correspondence: * junjingdeng@anl.gov

The authors would like to thank Joseph Arko, Bruce Hoster, and the staff of the Argonne Central Shops for their assistance with manufacturing and modifying various components. The Velociprobe was supported by Argonne Laboratory Directed Research & Development 2015-153-N0. This work is partially supported by the Office of the Director of National Intelligence, Intelligence Advanced Research Projects Activity. This research used resources of the Advanced Photon Source and the Center for Nanoscale Materials, U.S. Department of Energy (DOE) Office of Science User Facilities operated for the DOE Office of Science by Argonne National Laboratory under Contract No. DE-AC02-06CH11357.

Achieving Picosecond Control of Hard X-rays with MEMS Optics

Things happen fast at the nanoscale. The spatiotemporal study of important materials-related processes such as structural change, phase transition, diffusion, ionic transport, fluid flow, strain propagation, and many others is crucial for understanding structure and function at the nanoscale and mesoscale, but requires experiments using the pulsed nature of synchrotron-based x-ray sources. The ultrafast, time-resolved, hard x-ray imaging, scattering, and spectroscopy techniques often employed in such investigations can be limited by the temporal resolution and timing patterns of the sources. Achieving temporal manipulation at the pulse length or 100-psec time scales at the synchrotron x-ray facilities is possible only with difficult and expensive modifications to the facility technologies that can compromise other capabilities of the x-ray source. A team of researchers from the APS and the Argonne Center for Nanoscale Materials developed another way of accessing ultrafast time scales by using microelectromechanical system (MEMS)-based photonic devices to achieve dynamic control of the hard x-ray pulses.

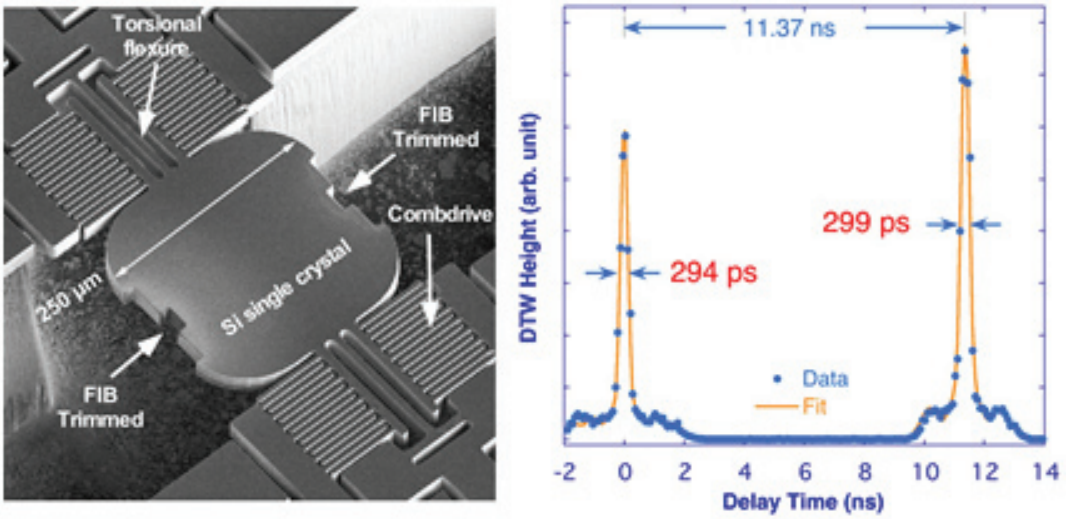

Fig. 1. MEMS oscillator tuned to the APS storage ring frequency for manipulating hard x-ray pulses at 300 psec. Left: scanning electron microscopy images of the MEMS device after multiple rounds of micromachining using a focused ion beam. Right: Demonstration of 300-ps diffractive time window in a delay scan covering two consecutive pulses in the APS 324-bunch mode where the two x-ray pulses are 11.37 ns apart. This scan was done with a MEMS device oscillating at 271.555 kHz, the exact APS storage-ring frequency. For detail, see P. Chen. et al., Nat. Commun. **10**, 1158 (2019). doi.org/10.1038/s41467-019-09077-1

Most previous work on MEMS photonic devices has concentrated on communication and imaging applications in visible and infrared wavelengths, with only limited exploration of the potential of x-ray devices, despite some demonstration of their possibilities by this same group of researchers. Here, the team created two groups of MEMS resonators of different resonant frequencies, consisting of thin silicon crystal chips (Fig. 1) that diffract or transmit x-rays by changing the orientation relative to the x-ray beam and carried out the time-resolved x-ray measurements at the XSD 7-ID-C beamline at the APS.

As the device oscillates around the Bragg angle θ_B, a diffractive time window (DTW) opens, and the timing between the DTW and the x-ray pulse can be manipulated. When the DTW is wider than the x-ray pulse, the MEMS device can act as a pulse-picking chopper; when narrower, it will create x-ray pulses shorter than the incident pulses, enabling higher temporal resolution. If the DTW is close to the x-ray pulse in width, x-ray streaking can be obtained, making sub-pulse-resolution possible in experiments of single-pulse duration.

To function as a practical dynamic x-ray optical device, the MEMS device must be tuned to the x-ray storage-ring frequency, which is accomplished by using a focused ion beam to trim mass from the crystal until its resonance frequency matches the frequency of the synchrotron source or one of the source's harmonics. One set of devices (designated as P0/2) was tuned to a resonance frequency of 135.777 kHz, which is half the APS operating frequency of P0 = 271.555 kHz; the second set was tuned to the full APS frequency and designated as P0 devices.

Adjusting the DTW to time scales in the sub-nanosecond range was done by applying higher excitation voltages to the MEMS oscillator to increase its oscillation amplitude. With the P0/2 devices, varying the excitation voltage from 50 V to 100 V caused a steady decrease in the DTW, from several nanoseconds to just below 0.5 nsec. Shorter time scales are impractical because voltages above ~100 V would make the oscillation approaching the mechanical limit of the MEMS devices. With the higher-frequency P0 MEMS devices, the researchers found that higher excitation voltages were necessary to obtain the same oscillation amplitudes when the devices were operated in air at a normal pressure of about 100 kPa because of fluid dynamic damping effects. Operating the devices in a vacuum environment, however, significantly reduced the necessary excitation voltage to achieve reduced DTW values.

With a P0 device at a pressure of 1.32 kPa and an excitation voltage of 50 V, a DTW of approximately 300 psec was achieved. Currently, this is limited somewhat by noise and physical factors such as the achievable amplitude of the device, but a higher frequency may be able to overcome this to demonstrate dispersing/streaking behavior, providing a means of performing time-domain research beyond the pulse-length limitation without the need for storage ring modifications.

The ultrafast MEMS-based x-ray optics demonstrated in this work opens a variety of exciting new possibilities to manipulate and control single hard x-ray pulses. The MEMS devices can operate in pulse-picking modes with extremely fine spatiotemporal resolution at typical high-energy synchrotron light sources such as the APS, promising a suite of new research opportunities at current and especially upgraded low-emittance sources such as the APS Upgrade Project. — Mark Wolverton

See: Pice Chen, Il Woong Jung, Donald A. Walko, Zhilong Li, Ya Gao, Gopal K. Shenoy, Daniel López, and Jin Wang*, "Ultrafast photonic micro-systems to manipulate hard x-rays at 300 picoseconds," Nat. Commun. **10**, 1158 (2019).
DOI: 10.1038/s41467-019-09077-1
Author affiliation: Argonne National Laboratory
Correspondence: * wangj@aps.anl.gov

Critical technical support from Tim Mooney and Michael Hu of the APS are gratefully acknowledged. This research is supported by the Accelerator and Detector Research Program of the U.S. Department of Energy (DOE) Office of Science-Basic Energy Sciences. The use of the Center for Nanoscale Materials and Advanced Photon Source was supported by the U.S. DOE Office of Science-Basic Energy Sciences under Contract No. DE-AC02-06CH11357.

MEMS the Word

Micro-electro-mechanical systems, or MEMS, is a technology that in its most general form can be defined as miniaturized mechanical and electro-mechanical elements (i.e., devices and structures) that are made using the techniques of microfabrication. The critical physical dimensions of MEMS devices can vary from well below one micron on the lower end of the dimensional spectrum, all the way to several millimeters. Likewise, the types of MEMS devices can vary from relatively simple structures having no moving elements, to extremely complex electromechanical systems with multiple moving elements under the control of integrated microelectronics. The one main criterion of MEMS is that there are at least some elements having some sort of mechanical functionality whether or not these elements can move. The term used to define MEMS varies in different parts of the world. In the United States they are predominantly called MEMS, while in some other parts of the world they are called "microsystems technology" or "micromachined devices."

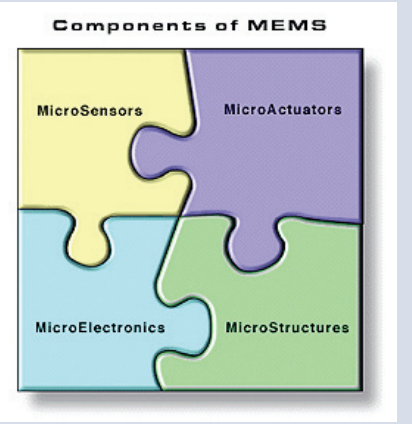

Source: https://bit.ly/2S3tn79

The Future is Pink for Molecular Movies

For many years, investigators who decipher the mysteries of protein structure have sought a way to move from the static environment of protein crystals to a more dynamic method for determining the structures of proteins in action. Protein conformational changes have been approximated by taking "snapshots" of protein crystals with and without different substrates or inhibitors and then comparing the two structures. But what if it was possible to capture many snapshots of different small crystals in random orientations at different time points and piece together the data to see time-resolved changes? This could provide data about a protein's structure and its movement through possible conformations, creating a series of images that could be turned into a kind of movie. Now, the first proof-of-concept experiments using high-viscosity sample injection combined with pink-beam serial crystallography (SX) have offered a glimpse into the possibilities of molecular moving pictures.

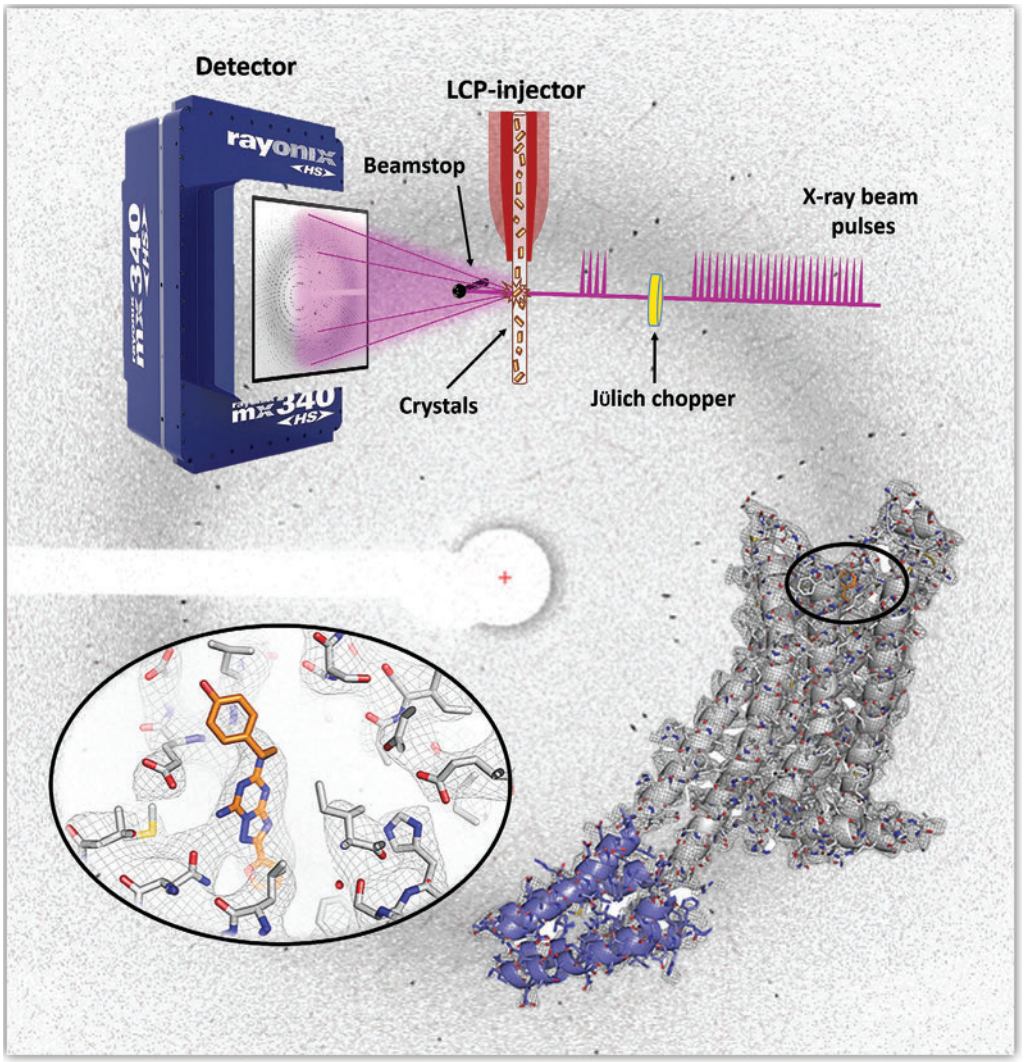

Fig. 1. Experimental set-up for data collection from pink-beam radiation with high-viscosity sample injection at BioCARS 14-ID-B (top) and quality of the electron-density map of the A2AAR structure with difference electron density map shown as inset (bottom).

The work builds on recent technological breakthroughs in structural biology. These include advances in the development of high-brightness photon sources (e.g., x-ray free-electron lasers [XFELs]), fast read-out detectors, and novel sample delivery methods (e.g., high-viscosity injectors) that have solved technical challenges in the field. For example, using XFELs to collect data on thousands of nano- or microcrystals in serial femto-second crystallography (SFX) experiments overcomes problems associated with the need to generate large crystals for structure determination and, because it uses ultrashort duration XFEL pulses, it outruns the radiation damage associated with long x-ray radiation exposures.

However, there are only five XFEL facilities worldwide, limiting investigator access to this breakthrough technology. Recently, investigators have been testing the idea that SX experiments using polychromatic x-ray beam radiation (the so-called "pink beam") generated from

third-generation synchrotron sources, such as APS, could overcome this limitation. Pink-beam radiation is suitable for these experiments because it provides a higher photon flux (100 times higher than monochromatic beams) that allows detection of much shorter time scales than standard synchrotron beams.

The research team in this study, from Arizona State University, Argonne, The University of Chicago, and the University of Southern California hypothesized that combining this high-brightness photon source with the latest high-viscosity injection technology to deliver thousands of nano- or microcrystals to the beam could generate a complete dataset in a shorter time with a smaller sample volume, providing time-resolved data without damaging radiation exposures (Fig. 1). The work demonstrates the feasibility of using a synchrotron radiation source to capture time-resolved protein structure data using this novel system.

To test their hypothesis, the team chose two proteins for which structures have already been determined: an enzyme, proteinase K (PK), and a G-protein coupled receptor, the human A2A adenosine receptor (A2AAR). They were able to solve the structure of PK with the new method at 1.8-Å resolution using the BioCARS 14-ID-B x-ray beamline at the APS. The crystals were 10-15 µm in size and were exposed to about 460 psec of radiation for each crystal, about 30 kGy of radiation. The structure aligned well with previous structures solved through conventional methods and another recent pink-beam SX structure solved at BioCARS. When they tested the structure for radiation damage by evaluating the integrity of two disulfide bonds in the structure that are particularly susceptible to radiation damage, they found no site-specific radiation damage.

The structure for A2AAR was a bit more complicated because the crystals were very small (~5 µm) and only weak and sparse diffraction data of low resolution were observed under the data collection conditions used for PK. Therefore, the team increased the consecutive pulses of pink-beam radiation to 24 (from 4 for PK, 3.5-µs total exposure) and obtained data that enabled them to resolve the structure at 4.2 Å with a total radiation dose of 210 kGy per crystal. Although some alterations to the standard Laue data processing strategy were required due to the low resolution of the data, the final data set was of high quality and the structure aligned well with previous structures (Fig. 1). Finally, a check for radiation damage also revealed no site-specific radiation damage at the four disulfide bonds in A2AAR.

With this positive proof-of-concept experiment for the use of pink-beam radiation with high viscosity injection of the sample, the researchers believe that molecular movies may soon be coming to a theater near you. — Sandy Field

See: Jose M. Martin-Garcia[1], Lan Zhu[1], Derek Mendez[1], Ming-Yue Lee[1], Eugene Chun[1], Chufeng Li[1], Hao Hu[1], Ganesh Subramanian[1], David Kissick[2], Craig Ogata[2], Robert Henning[3], Andrii Ishchenko[4], Zachary Dobson[1], Shangji Zhang[1], Uwe Weierstall[1], John C. H. Spence[1], Petra Fromme[1], Nadia A. Zatsepin[1], Robert F. Fischetti[2], Vadim Cherezov[4]*, and Wei Liu[1]**, "High-viscosity injector-based pink-beam serial crystallography of microcrystals at a synchrotron radiation source," IUCrJ **6**, 412 (2019). DOI: 10.1107/S205225251900263X
Author affiliations: [1]Arizona State University, [2]Argonne National Laboratory, [3]The University of Chicago, [4]University of Southern California
Correspondence: * cherezov@usc.edu, ** w.liu@asu.edu

We thank Vukica Šrajer (BioCARS) for processing PK data with Precognition, for discussions regarding Laue data processing, and for carefully checking the manuscript before submission. This work was supported by the Centre for Applied Structural Discovery at the Biodesign Institute at Arizona State University (W. Liu, P. Fromme, U. Weierstall, J. C. H. Spence, J. M. Martin-Garcia, N. A. Zatsepin, L. Zhu, M.-Y. Lee, E. Chun, G. Subramanian), a Mayo Clinic Arizona State University Collaborative Seed Grant Award (W. Liu), the Flinn Foundation Seed Grant (W. Liu) and No. 1991 (P. Fromme, J. C. H. Spence, and J. M. Martin-Garcia), the STC Program of the National Science Foundation (NSF) through BioXFEL (No. 1231306; W. Liu, P. Fromme, U. Weierstall, J. C. H. Spence, N. A. Zatsepin, D. Mendez, C. Li, G. Subramanian), NSF BIO ABI grant No. 1565180 (N. A. Zatsepin, D. Mendez, U. Weierstall, and J. C. H. Spence), and the National Institutes of Health (NIH) grants R21DA042298 (W. Liu), R01GM124152 (W. Liu), R01GM095583 (P. Fromme) and R35GM127086 (V. Cherezov and A. Ishchenko), ACB-12002 (R. F. Fischetti, D. Kissick, and C. Ogata) and AGM12006 (R. F. Fischetti, D. Kissick, and C. Ogata). Use of BioCARS was supported by the National Institute of General Medical Sciences of the NIH under grant number R24GM111072. The time-resolved setup at BioCARS was funded in part through a collaboration with Philip Anfinrud (NIH/NIDDK). Use of the GM/CA-XSD facility was supported by the National Cancer Institute (ACB-12002; R. F. Fischetti, D. Kissick, and C. Ogata) and the National Institute of General Medical Sciences (AGM12006; R. F. Fischetti, D. Kissick, and C. Ogata). This research used resources of the Advanced Photon Source, a U.S. Department of Energy (DOE) Office of Science User Facility operated for the DOE Office of Science by Argonne National Laboratory under Contract DE-AC02-06CH11357.

A New Method Clarifies Lithium's High-Pressure Phase Diagram

Although lithium is a simple metal under ambient conditions, it displays unexpectedly complex behaviors when driven to higher densities by increased external pressures. One of the most remarkable of these is anomalous melting. Lithium's melting temperature first increases to a maximum but then falls unexpectedly to a minimum as pressures mount. Studying the melting temperature minimum has proved problematic using diamond anvil cells (DACs) in high-pressure synchrotron x-ray experiments because lithium attacks the diamond anvils in this region of its phase diagram, causing the cells to readily fail. As a result, only two measurements of the minimum melting temperature were previously made and these produced differing results, until researchers applied a new technique that capitalized on the high x-ray flux available at the APS. The researchers found that they could make sufficient x-ray diffraction measurements on the fly as pressures were increased much more rapidly than in traditional DAC studies. The DACs still eventually failed, but only after accurate measurements were made covering the disputed region of lithium's phase diagram and beyond.

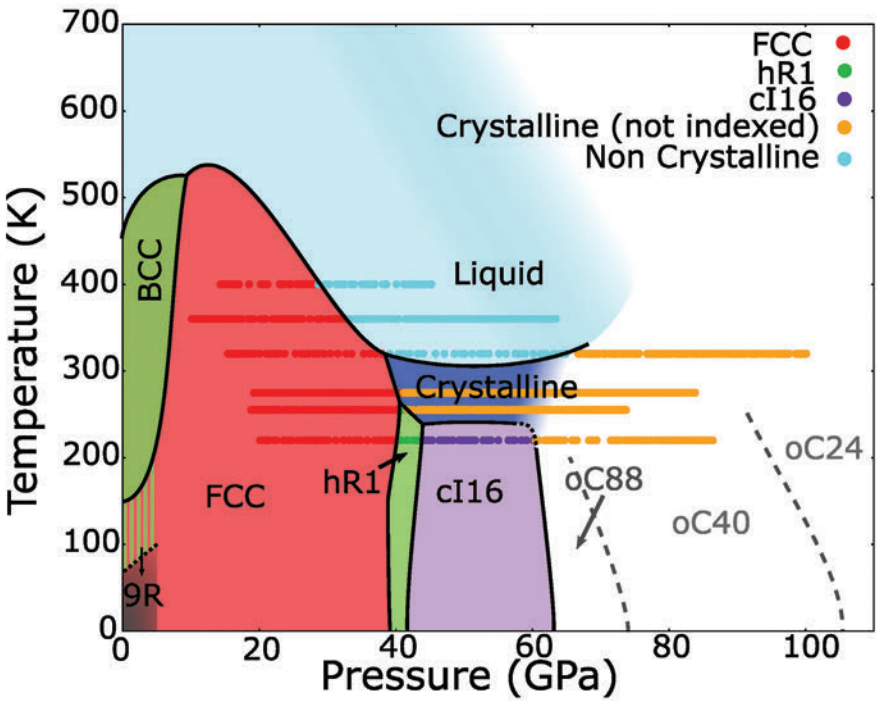

Fig. 1. Phase diagram of lithium. Circles show data points collected in this study. Phase boundaries marked with solid lines take into account data from this and other studies. The dotted boundary of *cI*16 near 60 GPa and 230 K indicates the probable location of a triple point, with an uncharacterized phase between cI16 and the melt in blue.

One previous measurement had found the minimum melting temperature to be 190 K between 40 and 60 Gpa, while another determined it to be 306 K at 44 GPa. A proposed explanation for the discrepancy was that lithium below the melting curve may be in an amorphous state. Neither result was in accord with theoretical predictions. One theoretical study found the minimum to be between 250 and 300 K at 65 GPa, while another predicted it would be at 270 K at 50 GPa. Theoretical studies also predicted that lithium would form a variety of low-coordination and low-symmetry phases under such pressures.

The researchers in this study, from the SLAC National Accelerator Laboratory, Stanford University, and Argonne investigated

the phase behavior of lithium by compressing it isothermally at a rate of 0.2 to 1 GPa/sec from about 15 GPa to diamond anvil failure at 220, 255, 275, 320, 360, and 400 K. Pressures to over 100 GPa were investigated, more than covering the disputed portion of the melting curve (Fig. 1). Melting was determined by the abrupt loss of diffraction peaks upon compression. The researchers found no evidence of melting at or below 275 K. Indeed, in the region where melting was previously reported, they found unambiguous evidence of *hR*1 and *cI*16 lithium phases, which were both stable to higher temperatures than previously reported. The minimum melting temperature of lithium was found to be between 275 and 320 K at about 50 GPa, below which the solid was determined to be crystalline. Analysis of the stability of the *cI*16 and *oC*88 phases that were found suggested the existence of a triple point between these and an undetermined solid phase at 60 GPa between 220 and 255 K. The success of the rapid compression approach in overcoming lithium degradation of the diamond anvils allowed x-ray diffraction data to be collected at the HPCAT-XSD 16-ID-B beamline of the APS at higher pressures and temperatures than was possible with traditional methods.

The advent of x-ray free electron lasers offers particular promise for this technique, as their greater flux and pulsed nature are ideally suited to attaining even higher compression rates. By this route, it may prove possible to explore the lithium melting curve and high-temperature phases in the megabar regime. It also seems likely that this method will be useful in the study of other materials that damage diamond anvils under extreme conditions.

— Vic Comello

See: Mungo Frost[1], Jongjin B. Kim[1], Emma E. McBride[1], J. Ryan Peterson[1,3], Jesse S. Smith[2]*, Peihao Sun[1,3], and Siegfried H. Glenzer[1], "High-Pressure Melt Curve and Phase Diagram of Lithium," Phys. Rev. Lett. **123**, 065701 (2019).
DOI: 10.1103/PhysRevLett.123.065701
Author affiliations: [1]SLAC National Accelerator Laboratory, [2]Argonne National Laboratory, [3]Stanford University
Correspondence: * jssmith@anl.gov

This work was supported by the U.S. Department of Energy (DOE) Office of Fusion Energy Sciences under funding No. FWP100182. Equipment support from the Stanford Synchrotron Radiation Lightsource (SSRL) was provided by the DOE Office of Basic Energy Sciences under Contract No. DE-AC02-76SF00515. HPCAT-XSD operations are supported by DOE-National Nuclear Security Adiminstration's Office of Experimental Sciences. This research used resources of the Advanced Photon Source, a U.S. DOE Office of Science User Facility operated for the DOE Office of Science by Argonne National Laboratory under Contract DE-AC02-06CH11357.

About Lithium

From an article by Elizabeth Miller at "Mental Floss"

Lithium, one of the smallest, simplest, and oldest elements, is a key ingredient in the batteries that power smartphones, laptops, and electric cars. It is also one of the most effective treatments for bipolar disorder, and research may make lithium the key to unlocking the causes of that illness.

In 1800, Brazilian naturalist José Bonifácio de Andrada e Silva discovered petalite (left), a rare, gem-quality mineral found in granite, on the island of Utö, Sweden. He found that the rock had a strange quality: when thrown into a fire, it created intense crimson flames. In 1817, a 25-year-old Swedish aristocrat-turned-chemist named Johan August Arfvedson discovered lithium while analyzing petalite. Having recognized most of the mineral's content as silica and aluminum, he deduced that a new alkali metal made up the remaining share. It was Arfvedson's only recorded discovery; he soon retired from chemistry to manage his inherited fortune.

Hydrogen, helium, and lithium, the first three elements in the periodic table, were all created in the Big Bang, but the first two elements are abundant, and lithium is not. Astrophysicists had a theory that novae, or stellar explosions, were responsible for lithium's scant distribution in the universe, but they didn't have data for how that worked until Nova Centauri's December 2013 explosion—visible to the naked eye, if your eyes were in the southern hemisphere. Researchers witnessed the dying star ejecting lithium into space.

More than half of the world's lithium supply comes from high-altitude lakes and salt flats in the "lithium triangle" in Bolivia, Chile, and Argentina, where it's mined in a grid of brine pools. Lithium doesn't range freely through nature, but must be isolated from other minerals, such as petalite. It's found in traces in almost all igneous rocks and in many mineral springs. Those who swim in lithium-infused hot springs are often told that it has curative powers, including improved brain function and elevated mood—though there's no evidence of this.

Lithium has several advantages that make it the go-to for power: It's the lightest known metal and can store power without adding a lot of weight to devices. Lithium-ion batteries have some of the highest energy densities of any current battery technology; they deliver three times the voltage of nickel-based batteries, according to the University of Washington's Clean Energy Institute.

Source: https://bit.ly/38KwkiW Photo: Eurico Zimbres, Wikimedia Commons // CC BY-SA 2.5

E. Ercan Alp (XSD) received the International Board of Applications of Mössbauer Effect Science Award in recognition of his outstanding contributions to the development of synchrotron radiation techniques and their scientific applications based on the Mössbauer effect; and was named an Argonne Distinguished Fellow, the highest scientific and engineering rank at the Laboratory, which is reserved for Argonne staff who have made internationally recognized achievements in science or engineering relevant to Argonne's core mission, or have provided critical technical leadership of major complex projects that impacted the future directions of the Laboratory.

Mark A. Beno (XSD) was elected posthumously to American Association for the Advancement of Science Fellowship in honor of his invaluable contributions to science and technology.

John P. Connolly, IV (APS Engineering Support Division) was selected for the 4th Cohort of the Oppenheimer Science and Energy Leadership Program .

Daniel Haskel (XSD) was appointed a Fellow of the Northwestern University Institute of Science and Engineering; and received the UChicago Argonne Board of Governors Distinguished Performance Award for his work on developing and leading world-class instrumentation, research, and user programs for x-ray studies of quantum matter and magnetism at extreme pressure conditions.

Andrew N. Johnson (Accelerator Systems Division, ASD) received the International Conference on Accelerator and Large Experimental Physics Control Systems (ICALEPCS) Leadership in Mentoring Award for his contribution to inspiring countless control system engineers working within the international Experimental Physics and Industrial Control System collaboration.

Kwang-Je Kim (ASD) was named an Argonne Emeritus Scientist, granted only to the most distinguished contributors to the Laboratory.

Cunming Liu and **Niranjan D. Parab** (XSD) received the Argonne Postdoctoral Performance Award, Liu for uncovering fundamental mechanistic details on the electronic and structural response of photoexcited perovskite materials, and Parab for pioneering work in the field of additive manufacturing.

Alex H. Lumpkin (Advanced Photon Source Upgrade Project) received The FEL Prize for his seminal, time-resolved measurements of dynamics in free-electron laser (FEL) oscillators and the elucidation of microbunching in relativistic electron beams and self-amplified spontaneous emission FELs.

Mark Rivers (The University of Chicago and the Center for Advanced Radiation Sources) received the 2019 ICALEPCS Lifetime Achievement Award for developing software that saved other developers untold hours of work by providing reliable performance and a high level of portability, and for freely sharing his expertise and providing expert support to the many users of his software.

Guoyin Shen (HPCAT-XSD) was named a Fellow of the Mineralogical Society of America in light of the high regard colleagues have for his scientific activities; he joins a distinguished group of individuals who have been recognized for their outstanding contributions to the fields of mineralogy, crystallography, geochemistry, and petrology.

Richard A. Spence (XSD) received the Argonne Director's Award for significantly exceeding the normal requirements of his position, project assignment, and individual situation by convincing others to reuse or repurpose their stored equipment, and actively supervising the riggers, hoists, and pulleys that are used to move heavy machinery at the APS.

Marion M. White (AES) was named a Fellow of the American Physical Society for her tireless efforts to increase the participation of women and minorities in physics, especially through one-on-one mentoring and educating minorities from elementary school through college about opportunities in the field.

Kamila M. Wiaderek (XSD), along with four co-authors of the paper, published in *Nature*, "Niobium Tungsten Oxides for High-rate Lithium-ion Energy Storage," received the Charles Hatchett Award for originality and technical excellence and the best paper on the science and technology of niobium-based materials.

Ashley Weiland (APS user, University of Texas at Dallas) was one of 70 graduate students chosen nationwide to participate in the U.S. Department of Energy Office of Science Graduate Student Research Program.

Raymond S. Ziegler (XSD) received the UChicago Argonne Board of Governors Outstanding Service Award for his contributions to a high-throughput x-ray scattering chamber; leading the rebuild of an APS beamline equipment protection system and the higher-x-ray-energy reconfiguration of another beamline; and streamlining the infrastructure of an APS experiment station, as well as a demonstrable and continued commitment to safety and quality.

Photon Sciences Directorate Organization Chart

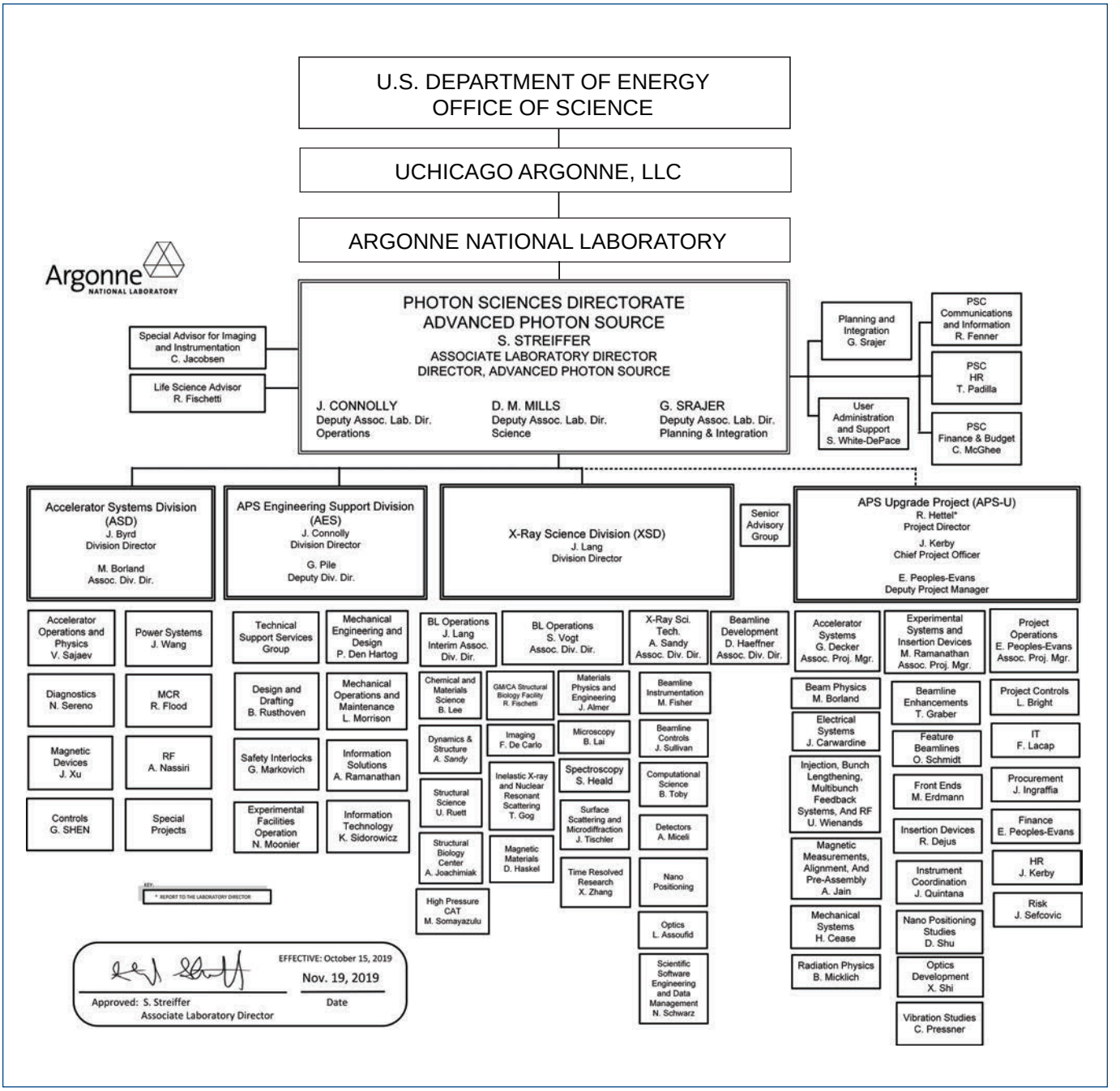

APS Source Parameters

Undulator A (31 insertion devices [IDs] in 25 sectors)

Period: 3.30 cm
Length: 2.1 m in sectors 16, 21, 23, 24, 28, 34; 2.3 m in Sector 6; 2.4 m in sectors 1, 2, 5, 7, 8, 9, 10, 11, 15, 17, 18, 19, 20, 22, 26, 28, 31, 32, 33
Minimum gap: 10.5 mm
B_{max}/K_{max}: 0.892 T/2.75 (effective; at minimum gap)
Tuning range: 3.0–13.0 keV (1st harmonic)
3.0–45.0 keV (1st–5th harmonic)
On-axis brilliance at 7 keV (ph/s/mrad^2/mm^2/0.1%bw):
4.1 x 10^{19} (2.4 m), 4.0 x 10^{19} (2.3 m), 3.3 x 10^{19} (2.1 m)
Source size and divergence at 8 keV:
Σ_x: 276 μm Σ_y: 11 μm
$\Sigma_{x'}$: 12.7 μrad (2.4 m), 12.8 μrad (2.3 m), 12.9 μrad (2.1 m)
$\Sigma_{y'}$: 6.7 μrad (2.4 m), 6.8 μrad (2.3 m), 7.1 μrad (2.1 m)

2.30-cm Undulator (2 IDs in sectors 11, 14)

Period: 2.30 cm Length: 2.4 m
Minimum gap: 10.5 mm
B_{max}/K_{max}: 0.558 T/1.20 (effective; at minimum gap)
Tuning range: 11.8–20.0 keV (1st harmonic)
11.8–70.0 keV (1st-5th harmonic, non-contiguous)
On-axis brilliance at 12 keV (ph/s/mrad^2/mm^2/0.1%bw): 6.9 x 10^{19}
Source size and divergence at 12 keV:
Σ_x: 276 μm Σ_y: 11 μm
$\Sigma_{x'}$: 12.3 μrad $\Sigma_{y'}$: 5.9 μrad

2.70-cm Undulator (5 IDs in sectors 3, 12, 14, 35)

Period: 2.70 cm
Length: 2.1 m in Sector 12; 2.4 m in sectors 3, 14, and 35
Minimum gap: 10.5 mm
B_{max}/K_{max}: 0.698 T/1.76 (effective; at minimum gap)
Tuning range: 6.7–16.0 keV (1st harmonic)
6.7–60.0 keV (1st-5th harmonic, non-contiguous)
On-axis brilliance at 8.5 keV (ph/s/mrad^2/mm^2/0.1%bw):
5.7 x 10^{19} (2.4 m), 4.7 x 10^{19} (2.1 m)
Source size and divergence at 8 keV:
Σ_x: 276 μm Σ_y: 11 μm
$\Sigma_{x'}$: 12.7 μrad (2.4 m), 12.9 μrad (2.1 m)
$\Sigma_{y'}$: 6.7 μrad (2.4 m), 7.1 μrad (2.1 m)

3.00-cm Undulator (8 IDs in sectors 12, 13, 16, 21, 23, 27, 34)

Period: 3.00 cm
Length: 2.1 m in sectors 12, 13, 16, 21, 23, 34; 2.4 m in Sector 27
Minimum gap: 10.5 mm
B_{max}/K_{max}: 0.787 T/2.20 (effective; at minimum gap)
Tuning range: 4.6–14.5 keV (1st harmonic)
4.6–50.0 keV (1st-5th harmonic)
On-axis brilliance at 8 keV (ph/s/mrad^2/mm^2/0.1%bw):
4.8 x 10^{19} (2.4 m), 3.9 x 10^{19} (2.1 m)
Source size and divergence at 8 keV:
Σ_x: 276 μm Σ_y: 11 μm
$\Sigma_{x'}$: 12.7 μrad (2.4 m), 12.9 μrad (2.1 m)
$\Sigma_{y'}$: 6.7 μrad (2.4 m), 7.1 μrad (2.1 m)

3.50-cm SmCo Undulator (Sector 4)

Period: 3.50 cm Length: 2.4 m
Minimum gap: 9.75 mm
B_{max}/K_{max}: 0.918 T/3.00 (effective; at minimum gap)
Tuning range: 2.4–12.5 keV (1st harmonic)
2.4–42.0 keV (1st-5th harmonic)
On-axis brilliance at 7 keV (ph/s/mrad^2/mm^2/0.1%bw): 3.7 x 10^{19}
Source size and divergence at 8 keV:
Σ_x: 276 μm Σ_y: 11 μm
$\Sigma_{x'}$: 12.7 μrad $\Sigma_{y'}$: 6.7 μrad

3.60-cm Undulator (Sector 13)

Period: 3.60 cm
Length: 2.1 m
Minimum gap: 11.0 mm
B_{max}/K_{max}: 0.936 T/3.15 (effective; at minimum gap)
Tuning range: 2.2–11.8 keV (1st harmonic)
2.2–40.0 keV (1st-5th harmonic)
On-axis brilliance at 6.5 keV (ph/s/mrad^2/mm^2/0.1%bw): 2.8 x 10^{19}
Source size and divergence at 8 keV:
Σ_x: 276 μm Σ_y: 11 μm
$\Sigma_{x'}$: 12.9 μrad $\Sigma_{y'}$: 7.1 μrad

1.72-cm Undulator (3 IDs in sectors 30, 35)

Period: 1.72 cm
Length: 4.8 m (2 x 2.4 m) in Sector 30; 2.4 m in Sector 35
Minimum gap: 10.6 mm
B_{max}/K_{max}: 0.330 T/0.53 (effective; at minimum gap)
Tuning range: 23.7–26.3 keV (1st harmonic)
On-axis brilliance at 23.7 keV (ph/s/mrad^2/mm^2/0.1%bw):
1.0 x 10^{20} (4.8 m), 4.4 x 10^{19} (2.4 m)
Source size and divergence at 23.7 keV:
Σ_x: 276 μm Σ_y: 11 μm
$\Sigma_{x'}$: 11.6 μrad (4.8 m) 11.9 μrad (2.4 m)
$\Sigma_{y'}$: 4.3 μrad (4.8 m), 4.9 μrad (2.4 m)

1.80-cm Undulator (Sector 32)

Period: 1.80 cm
Length: 2.4 m
Minimum gap: 11.0 mm
B_{max}/K_{max}: 0.244 T/0.41 (effective; at minimum gap)
Tuning range: 23.8 - 25.3 keV (1st harmonic)
71.4 - 75.9 keV (3rd harmonic)
On-axis brilliance at 23.8 keV (ph/s/mrad^2/mm^2/0.1%bw): 2.8 x 10^{19}
Source size and divergence at 23.8 keV:
Σ_x: 276 um Σ_y: 11 um
$\Sigma_{x'}$: 11.9 urad $\Sigma_{y'}$: 4.9 urad

IEX 12.5-cm Quasi-Periodic Polarizing Undulator (Sector 29)

Period: 12.5 cm
Length: 4.8 m
Circular polarization mode:
Max. currents: horizontal coils 34.4 A, vertical coils 20.7 A
K_{max}: 2.73 (effective; at max. currents)
B_{max}: 0.27 T (peak; at max. currents)
Tuning range: 0.44–3.5 keV (1st harmonic)
On-axis brilliance at 1.8 keV (ph/s/mrad^2/mm^2/0.1%bw): 1.4 x 10^{19}
Linear horizontal polarization mode:
Max. current: vertical coils 47.6 A
K_{max}: 5.39 (effective; at max. current
B_{max}: 0.54 T (peak; at max. current)
Tuning range: 0.24–3.5 keV (1st harmonic)
0.24–11.0 keV (1st–5th harmonic)
On-axis brilliance at 2.1 keV (ph/s/mrad^2/mm^2/0.1%bw): 1.1 x 10^{19}
Linear vertical polarization mode:
Max. current: horizontal coils 50.3 A
K_{max}: 3.86 (effective; at max. current)
B_{max}: 0.37 T (peak; at max. current)
Tuning range: 0.44–3.5 keV (1st harmonic)
0.44–11.0 keV (1st–5th harmonic)
On-axis brilliance at 2.1 keV (ph/s/mrad^2/mm^2/0.1%bw): 1.1 x 10^{19}
Fast polarization switching not required
Source size and divergence at 2 keV:
Σ_x: 276 μm Σ_y: 13 μm
$\Sigma_{x'}$: 13.9 μrad $\Sigma_{y'}$: 8.8 μrad

12.8-cm Circularly Polarizing Undulator (Sector 4)

Period: 12.8 cm
Length: 2.1 m
Circular polarization mode:
Max. currents: horizontal coils 1.34 kA, vertical coils 0.40 kA
K_{max}: 2.85 (effective; at max. currents)
B_{max}: 0.30 T (peak; at max. currents)
Tuning range: 0.4–3.0 keV (1st harmonic)
On-axis brilliance at 1.8 keV (ph/s/mrad^2/mm^2/0.1%bw): 3.1 x 10^{18}
Linear horizontal polarization mode:
Max. current: vertical coils 0.40 kA
K_{max}: 2.85 (effective; at max. current)
B_{max}: 0.30 T (peak; at max. current)
Tuning range: 0.72–3.0 keV (1st harmonic)
0.72–10.0 keV (1st–5th harmonic)
On-axis brilliance at 2.1 keV (ph/s/mrad^2/mm^2/0.1%bw): 2.3 x 10^{18}
Linear vertical polarization mode:
Max. current: horizontal coils 1.60 kA
K_{max}: 3.23 (effective; at max. current)
B_{max}: 0.34 T (peak; at max. current)
Tuning range: 0.58–3.0 keV (1st harmonic)
0.58–10.0 keV (1st–5th harmonic)
On-axis brilliance at 2.1 keV (ph/s/mrad^2/mm^2/0.1%bw): 2.3 x 10^{18}
Switching frequency (limited by storage ring operation): 0–0.5 Hz
Switching rise time: 50 ms
Source size and divergence at 2 keV:
Σ_x: 276 μm Σ_y: 12 μm
$\Sigma_{x'}$: 16.7 μrad $\Sigma_{y'}$: 12.7 μrad

1.80-cm Superconducting Undulator (2 IDs in Sectors 1, 6)

Period: 1.80 cm
Length: 1.1 m
Gap: 9.5 mm (fixed)
Max. current: 450 A
B_{max}/K_{max}: 0.962 T/1.61 (effective; at maximum current)
Tuning range: 11.2–24.7 keV (1st harmonic)
11.2–150.0 keV (1st-13th harmonic, non-contiguous)
On-axis brilliance at 13 keV (ph/s/mrad^2/mm^2/0.1%bw): 3.2 x 10^{19}
Source size and divergence at 13 keV:
Σ_x: 276 μm Σ_y: 11 μm
$\Sigma_{x'}$: 13.2 μrad $\Sigma_{y'}$: 7.5 μrad

3.15-cm Helical Superconducting Undulator (Sector 7)

Period: 3.15 cm
Length: 1.2 m
Coil winding diameter: 31.0 mm
Max. current: 450 A
B_{max}/K_{max}: 0.413 T/1.213 (B_x=B_y effective; at maximum current)
Tuning range: 6.0-13.0 keV (1st harmonic)
On-axis brilliance at 6.0 keV (ph/s/mrad^2/mm^2/0.1%bw): 2.2 x 10^{19}
Source size and divergence at 6 keV:
Σ_x: 276 μm Σ_y: 11 μm
$\Sigma_{x'}$: 14.7 μrad $\Sigma_{y'}$: 10.0 μrad

APS Bending Magnet

Critical energy: 19.51 keV
Energy range: 1–100 keV
On-axis brilliance at 16 keV (ph/s/mrad^2/mm^2/0.1%bw): 5.4 x 10^{15}
On-axis angular flux density at 16 keV (ph/s/mrad^2/0.1%bw): 9.6 x 10^{13}
Horizontal angular flux density at 6 keV (ph/s/mradh/0.1%bw): 1.6 x 10^{13}
Source size and divergence at the critical energy:
Σ_x: 92 μm Σ_y: 31 μm
$\Sigma_{x'}$: 6 mrad $\Sigma_{y'}$: 47 μrad

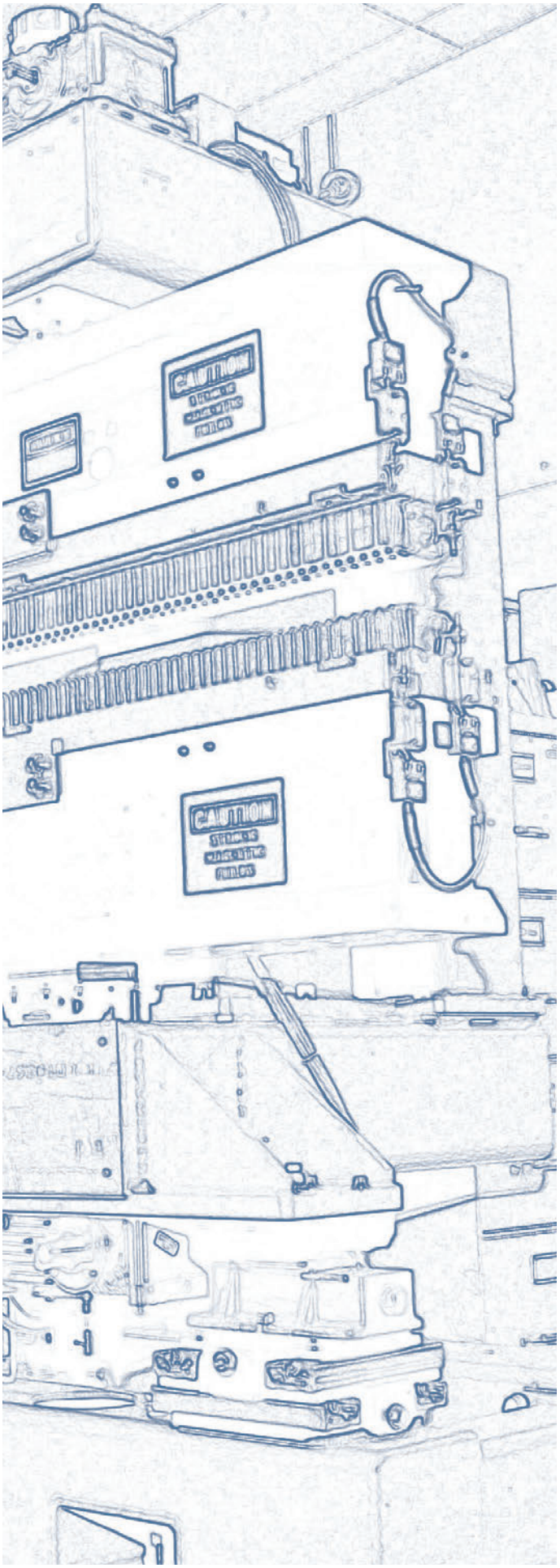

Acknowledgments

APS Science 2019 Editorial Board:

John Byrd (ANL-ASD), John Connolly (ANL-AES), Robert Fischetti (ANL-PSC), Robert Hettel (ANL-PSC), Jim Kerby (ANL-PSC), Jonathan Lang (ANL-XSD), Dennis Mills, (ANL-PSC), George Srajer (ANL-PSC), Stephen Streiffer (ANL-PSC), Stefan Vogt (ANL-XSD)

Reviewers:

Vukica Srajer (BioCARS); Thomas Irving (Bio-CAT); Binhau Lin (ChemMatCARS); Yogendra Gupta, Sheila Heyns, and Paulo Rigg (DCS), Denis Keane (DND-CAT); Michael Becker, Robert Fischetti, and Janet Smith (GMCA-XSD); Mark Rivers, Vitali Prakapenka, Steve Sutton, and Yanbin Wang (GSECARS); Maddury (Zulu) Somayazulu (HPCAT-XSD); Lisa Keefe (IMCA-CAT); Jordi Benach (LRL-CAT); Keith Brister (LS-CAT); Bruce Bunker and Carlo Segre (MR-CAT); Kay Perry (NE-CAT); Andrzej Joachimiak (SBC-XSD); John Rose and Bi-Cheng Wang (SER-CAT); Ahmet Alatas, Jonathan Almer, Francesco De Carlo, Wonsuk Cha, Zou Finfrock, Thomas Gog, Daniel Haskel, Steve Heald, Barry Lai, Byeongdu Lee, Uta Ruett, Jon Tischler, Alec Sandy, Shastri and Xiaoyi Zhang (XSD)

Unless otherwise noted, the research highlights in this report were written by:

Mary Alexandra Agner (marymary@alum.mit.edu)
Christen Brownlee (christenbrownlee@gmail.com)
Erika Gebel Berg (erikagebel@gmail.com)
David Bradley (david@sciencebase.com)
Vic Comello ANL-CPA - retired (vcomello@anl.gov)
Dana Desonie (desonie@cox.net)
Sandy Field (sfield@fieldscientific.com)
Emma Nichols (emma@nascentmc.com)
Philip Koth (philkoth@comcast.net)
Kim Krieger (mskrieger@gmail.com)
David Lindley (dxlindley@gmail.com)
Tien Nguyen (tmnguyen5@gmail.com)
Chris Palmer (crpalmer2009@gmail.com)
Nicola Parry (nicola@parrymedicalwriting.com)
Neil Savage (neil@stefan.com)
Alicia Surrao (alicia@untoldcontent.com)
Mark Wolverton (exetermw@earthlink.net)

Photography: Wes P. Agresta, Mark L. Lopez (both ANL-CPA)
Aerial photograph of the APS: John Hill (Tigerhill Studio, http://www.tigerhillstudio.com)
Publications, contracts, rights and permissions, circulation: Jessie L. Skwarek (ANL-PSC)
Printing oversight: Gary R. Weidner (ANL-CPA)
Editorial, project coordination, design, photography: Richard B. Fenner (ANL-PSC)

Our thanks to the corresponding authors and others who assisted in the preparation of the research highlights, to the users and APS personnel who wrote articles for the report, and our apologies to anyone inadvertently left off this list. To all: your contributions are appreciated.

U.S. DEPARTMENT OF
ENERGY

Office of Science

Advanced Photon Source
Argonne National Laboratory
9700 S. Cass Ave.
Lemont, IL 60439 USA
www.anl.gov • www.aps.anl.gov